Molecular Characterisation of the Human Macula

Michael Barry Powner

UCL

Thesis submitted in fulfilment of the requirements for the degree of

Doctor of Philosophy

Supervised by Dr. Marcus Fruttiger

2011

I, Michael Barry Powner confirm that the work presented in this thesis is my own. Where information has been derived from other sources, I confirm that this has been indicated in the thesis.

Acknowledgements:

I would like to thank my supervisor Marcus Fruttiger for all his guidance, persistence and patience over the last 4 years.

Many thanks also go to Glen Jeffery and Ant Vugler for advice and help during this project. And to all the people at the institute that have been around to make the time fly by, especially to Natalie, Charlie, Andrew and Shalini.

I would also like to thank all those that have helped me with the technical aspects to this project. Our collaborators, Mark Gillies, Meidong Zhu and Alice Len who helped with the processing of the MacTel type 2 sample used and provision of all the adult human tissue used. Also a special thanks to Alice, who helped extensively with the processing of tissue for proteomic analysis. Thanks to Greg Hageman and the members of his lab for the provision of the MacTel type 2 sample and the embedding of tissue from this sample for electron microscopy. Thanks also to Peter Munro and Robin Howes for the embedding and sectioning of tissue for electron microscopy and to members of Dianne Girrelli's team at the London HDBR for provision of and staging of human foetal eye tissue.

I would like to thank the Lowy Medical Research Institute for generously funding the project.

Finally I would like to give the biggest thanks to my family for helping me through to get to this point in my life; thanks to my parents who have always encouraged, supported and guided me to get the most out of what I do, to my sisters for their continual support and also huge thanks to Vanessa, who has given me so much support and advice since we've been together.

Abstract:

The human macula is essential for high acuity vision but its biochemical and cellular properties are poorly understood.

A disease that specifically affects the macula, Macular Telangiectasia (MacTel) type2 was investigated by studying postmortem tissue from a single donor. This revealed Müller cell loss specifically in the macula, which might be responsible for the vascular changes and photoreceptor degeneration typical of this disease. To establish whether the disease has subclinical vascular changes outside the macula, the peripheral retina was studied. This showed that contrary to previous reports, abnormal looking capillaries are not disease-specific but a normal ageing phenotype in humans.

Proteomics and immunohistochemistry was used to characterise maculae in healthy donors. Comparative proteomics identified differentially expressed proteins and immunohistochemistry confirmed the distribution of selected proteins. This led to the discovery of several Müller cell markers, lactate dehydrogenase (LDHB), glial fibrillary acidic protein (GFAP),αB crystallin (CRYAB) and αA crystallin (CRYAA), which are expressed at higher levels in the macula, demonstrating that Müller cells can take on different differentiation phenotypes depending on retinal area. Furthermore, the spatial expression pattern of LDHB, GFAP and CRYAB was found to correlate with the size/shape of the area that is affected in MacTel type2, providing a possible explanation why the disease affects only the macula.

Embryonic development of the macula was investigated in eye tissue obtained from abortions by using immunohistochemistry and gene expression analysis (qPCR and differential gene display). Müller cell markers, CRYAA, CD44 and CRALBP were found to be specifically expressed in the presumptive macula, starting at 7 gestation weeks (CS20), prior to ganglion cell and photoreceptor differentiation. Genomic comparison between this region and peripheral retina revealed further differentially expressed genes and led to the identification of a morphogen, Retinoic acid, which might play a role in macula development in the human retina.

Contents

List of tables

List of figures

Abbreviations:

2D LC MS/MS	two dimensional liquid chromatography tandem mass spectrometry
AABA	α-amino butyric acid
ACN	acetonitrile
ACP	annealing control primer
AMD	age related macular degeneration
APS	ammonium persulphate
AQP	aquaporin
BSA	bovine serum albumin
COX2	cytochrome *c* oxidase 2
CRABP1	cellular retinoic acid binding protein 1
CRALBP	cellular retinaldehyde binding protein 1 (aka. RLBP1)
CRYAA	alpha A crystallin
CRYAB	alpha B crystallin
CYP26A1	cytochrome P450 family 26, subfamily A, polypeptide1
CYP26C1	cytochrome P450 family 26, subfamily C, polypeptide1
DAB	3,3'-diaminobenzidine
DEG	differentially expressed gene
ENO1	enolase 1
FGF	fibroblast growth factor
GA	geographic atrophy
GCL	ganglion cell layer
GFAP	glial fibrillary acidic protein
GS	glutamine synthetase
H&E	haematoxylin and eosin
HFL	Henlé fibre layer
HRP	horse radish peroxidise
Iba1	ionised calcium binding adapter molecule 1
INL	inner nuclear layer
IPL	inner plexiform layer
iTRAQ	isobaric tags for relative and absolute quantitation
Kir	potassium inward rectifying
LC MALDI MS/MS	liquid chromatography matrix assisted laser desorption ionisation tandem mass spectrometry
LDHB	lactate dehydrogenase B

LS	less soluble
MacTel	macular telangiectasia
MALDI	matrix-assisted laser desorption/ionisation
MMTS	*s*-methylmethanethiosulfonate
MS	mass-spectroscopy
NFL	nerve fibre layer
NV	neovascular
OCT	optical coherence tomography
ONL	outer nuclear layer
OPL	outer plexiform layer
PBS	phosphate buffered saline
PBT	PBS + 0.5% tween20
PCR	polymerase chain reaction
PFA	paraformaldehyde
qPCR	quantitative polymerase chain reaction
RAR	retinoic acid receptor
RGC	retinal ganglion cell
RLBP1	cellular retinaldehyde binding protein 1 (aka. CRALBP)
RP nano-LC ESI MS/MS	reverse phase nano liquid chromatography tandem mass spectrometry
RPE	retinal pigment epithelium
RXR	retinoid X receptor
S	soluble
SDS	sodium dodecyl sulphate
SPR	surface plasmon resonance
TCEP	tris(2-carboxyethyl)phosphine
TEM	transmission electron microscopy
TEMED	tetramethylethylenediamine
TFA	trifluroacetic acid
v/v	volume per volume
w/v	weight per volume

1. General introduction

1.1 Visual acuity and retinal specialisation

The region of high acuity vision is a morphological specialisation found in the central retina. Humans, old and new world monkeys all have this region of specialisation, but the nocturnal primates, such as the owl monkey (*Aotes*) do not.[1] The region of specialisation is known as the macula, and the central most point termed the fovea. This region of the retina is highly specialised, it has a high concentration of cone photoreceptors, a low concentration of rod photoreceptors and the number of signal transduction neurons is also significantly increased. The fovea (like its literal meaning in Latin) is a pit in the retina.

Peripheral retina has a common structure found among all mammals; it has a laminated structure of three nuclear layers and two layers of synapses. Ganglion cell nuclei and astrocyte nuclei dominate the ganglion cell layer, while amacrine, horizontal, bipolar and Müller cell nuclei are found within the inner nuclear layer. The outer nuclear layer only consists of photoreceptor nuclei, rods and cones. The projections of the ganglion cells from the top and bipolar/amacrine cells from below form the inner plexiform layer (IPL), while the photoreceptor projections generate an outer plexiform layer (OPL) below the inner nuclear layer. Müller cells have processes that span the entire depth of the retina so can be found in both plexiform layers. The Müller cell processes form tight junctions with the photoreceptor inner segments to form the outer limiting membrane, and generate the inner limiting membrane at the vitreal face of the retina. Below the neural retina there is the sub retinal space (remainder of the optic ventricle in development) and then a monolayer of pigment epithelium (retinal pigment epithelium) (Fig. 1.1 A).

The fovea and macula differ in structure from the peripheral retina. During development ganglion cells proliferate at the prospective fovea to form a ‘mound’ in central retina. At 7 months gestation lateral displacement from the fovea occurs and all cell nuclei within the ganglion cell layer and the inner nuclear layers migrate radially forming the foveal pit (Fig. 1.1 B, C). Photoreceptors do not migrate, but their axons are elongated within the OPL, to maintain synaptic contact with their corresponding bipolar cells. Along with the elongated photoreceptor axons, outer retinal Müller cell processes elongate and the soma shifts within the inner nuclear layer, but end feet forming the outer limiting membrane remain located nearer to the fovea; this region of laterally displaced processes form what is called the Henlé fibre layer (arrow heads in Fig. 1.1 D and E). The lateral displacement generates a central pit (fovea) surrounded by a region of increased retinal thickness, the macula. The laminated

structure of the retina remains parafoveally, however at the fovea only the photoreceptors with a small number of ganglion cells remain. The foveal pit also contains a population of Müller cells, termed the Müller cell cone, but the function of these Müller cells in unclear. The macula now consists of an increased ganglion cell thickness up to a maximum of 8/9 cells deep (Fig. 1.1 E), and increased numbers of interneuron's and Müller cells. The Müller cell nuclei in peripheral retina are a single layer along the central line of the inner nuclear layer; this single layer also doubles up within the macula and is missing at the fovea. The fovea contains the highest density of cone photoreceptors, the human retina contains on average 4.6million cones, with a foveal density of 200,000 cones/mm^2.[2] The cone density at the periphery is one hundredth of that at the fovea. In peripheral retina, rod photoreceptors outnumber cones, 20:1, however at the fovea there is a 300µm diameter rod free zone, with lower ratios in the parafoveal macula.[2] Interestingly there is also a central 100µm S-cone free zone, making the fovea dominated by M and L cones.[3, 4]

The definition of the macula is currently vague. The macula, original name *macula lutea* or 'yellow spot', was defined as the name suggests; it was the region of the retina where yellow macular pigments accumulate.[5] Macular pigment consists of the xanthophyll carotenoids, Lutein and Zeathanthin.[6] These pigments are taken up through the diet and are the only carotenoids to be transported into the retina.[7] These pigments can be seen with red free or blue light fundus imaging and appear to have a higher concentration 5-6mm in diameter surrounding the fovea. The concentration of the pigments decreases with eccentricity from the fovea. Zeaxanthin has been shown to be most abundant at the fovea and the concentration decreases more rapidly, whereas lutein has a more gradual decrease towards the periphery, with a lower maximal concentration at the fovea compared to zeaxanthin (macular pigment will be described in more detail in chapter **5**). Dietary intake of lutein and zeaxanthin has a significant effect on the intensity and spread of macular pigment within central retina.[8] Therefore the region perceived as the macula differs between people.

Textbooks refer to the macula as consisting of three concentric regions in central retina, the fovea at the centre, surrounded by a parafovea and perifovea (Fig. 1.1 F), first coined by Polyak in 1941.[9] The regions can be generalised by defining the perifovea as the transition zone between the specialised central retina and the periphery, the parafovea as region with the highest ganglion cell density, and the fovea as the pit. The perifovea takes on characteristics of the periphery; such has the higher vascular density and the high rod:cone ratio.[3] However, it still has a higher ganglion cell density than the peripheral retina, although the ganglion cell nuclei decrease to a single layer[2, 10] before the proposed outer limit of the perifoveal region by Polyak.[9] The fovea does have a defined anatomical boundary; it resides

within the limits of maximum ganglion cell depth of the retina. This is the location of maximal retinal thickness, central to this the retinal thickness sharply decreases to form an inverted cone shaped pit. The foveal slope marks a decrease in ganglion cell, Müller cell and interneuron numbers and very few astrocytes are present. The foveal slope also marks the transition between rod dominated and cone dominated retina, and vascularised and avascular retina. The top of the foveal slope contains the perifoveal capillaries which anastomose towards the base of the slope and form a single vascular ring and a central foveal avascular zone.[11] The parafovea as such has a defined inner boundary, but the division between parafovea and perifovea is purely based upon an arbitrary distance from the fovea. There is no anatomical or biochemical correlates to this region (Fig. 1.1 G).

The clinical definition of the macula again differs from that proposed by Polyak[9] and from macula pigment distribution; the macula is defined as any retina between the temporal superior and inferior vascular arcades.[12] This definition does at least have an anatomical correlate, however there is no justification as to why the retina in between the vascular arcades is significantly different from that outside; there is no difference in retinal function or specialisation at this boundary point. Also this definition leaves the temporal limit of the macula again vague as the arcades do not completely encircle the fovea.

As such the fovea is the only structure of the macula that has a true definition/boundary. The macula remains a term given to central, specialised retina, and yet there is no true definition as to its limits. There is a gradual change in cell numbers and type starting at the fovea and spreading radially. The Henlé fibre layer is the only significant structural feature that changes within this region. The lateral displacement of Müller cell processes and photoreceptor axons does define an anatomical boundary point within the retina; the point at which the processes cease to run horizontally and take on the vertical orientation, perpendicular to the nuclear layers. However, no molecular link has been made to date correlating this retinal landmark with differences in retinal function or disease susceptibility of the retina.

1.2 Retinal cell types

Vision is captured by the neural retina. The retina, being part of the central nervous system contains glial cells that act as support cells to ensure neuronal survival and signal transduction back to the visual cortex of the brain.

1.2.1 Retinal neurons

The retinal neurons are not just there to signal visual perception back to the brain, a lot of vertical and horizontal pre-processing occurs within the retina and an image constructed before the signal is relayed to the visual cortex.

1.2.1.1 Photoreceptors

There are two primary types of photoreceptors in the human eye, the rods and cones. Rods are responsible for scotopic, low light vision - motion contrast and brightness, while the cones capture the photopic, high acuity, spatial resolution, colour vision.[13] There are three types of cone photoreceptor, blue (short wavelength, S cone), Green (medium wavelength, M cone) and Red (long wavelength, L cone). The trichromatic cones allow a broad spectrum of colour vision. The photoreceptors are situated to the posterior aspect of the neural retina and consist of a cell body packed full of mitochondria (inner segment) with axonal projection that synapses with bipolar cells. They also contain a modified primary cilium that has evolved to form the photoreceptive element, the outer segment, that contains stacks of membranous disks packed full of photo pigments (opsins) and signalling proteins needed to transduce photons of light into neural signals.

Visual perception begins with the photoreceptors. A captured photon isomerises the chromophore conjugated to the photopigment of photoreceptor cell. Photoisomerisation converts 11-cis retinal to all-trans retinol, via all-trans retinal. This occurs within the outer segment of the photoreceptor. All-trans-retinol exits the cell and transported to the RPE; here a series of enzymatic reactions converts it back to 11-cis-retinal. 11-cis-retinal returns to the outer segment where it regenerates the photoreceptor opsin and completes the visual cycle.[14] The excited visual pigment then triggers a signal transduction cascade that amplifies the signal, leading to closure of ion channels within the plasma membranes and the cells becoming hyperpolarised. Hyperpolarisation leads to a block of glutamate (neurotransmitter) release at the photoreceptor synapse.[15]

1.2.1.2 Processing and signal conduction neurons

The block in release of glutamate through excitation of the photoreceptor cells leads to the induction of a signal within the bipolar cells of the retina. This signal is not directly transferred into the ganglion cells to be relayed to the brain, first lateral interactions with interneurons, the amacrine and horizontal cells, modify the signal and pre-process the image. The bipolar cell nuclei are located within the inner nuclear layer; the interneurons also reside

within the inner nuclear layer; the amacrine cells primarily along the border of the inner nuclear layer and the OPL, and the horizontal cells along the border with the IPL.

1.2.1.3 Retinal ganglion cells

Retinal ganglion cells (RGCs) are the last neuron in the chain to relay the image to the brain; they receive impulses from the amacrine and bipolar cells. As such they sit in the ganglion cell layer, vitreal aspect of the IPL. The cell bodies reside here however they have processes that project back through the optic nerve to the visual cortex. The processes that run along the retina-vitreal surface form what is termed the nerve fibre layer. The RGC axons are not myelinated within the retina, signal conduction is maintained by astrocytes and Müller cell end feet that ensheath the axonal projections.

1.2.2 Retinal Glia

There are three types of glia within the vascularised retina, like that of humans and mice; the Müller Cell, Retinal astrocyte and the microglia. Avascular retinae, like that of birds, do not contain astrocytes, as explained later.

1.2.2.1 Müller Cells

The Müller cells, the principal glia of the retina span the entire depth of the retina, with a cell body in the inner nuclear layer. They have projections that span radially to form the inner and outer limiting membranes, the inner limiting membrane where they make contact with the RGCs projections and the outer limiting membrane where they form tight junctions with the inner segments of the photoreceptors. Müller cells also make contact with all retinal neurons. Müller cells play a key role in neuronal survival and processing of information.[16, 17] Müller cells are crucial to the stabilisation of the retinal structure. They create a framework around which the layered arrangement of neurons is patterned.[18]

Retinal extracellular homeostasis is maintained by the Müller cell. The plasma membrane of a Müller cell has a high density of K^+ channels, especially inwardly rectifying K^+ (Kir) channels[19-22] and tandem-pore (TASK) channels.[23] Thus allowing them to clear the extracellular K^+ released by activated neurons, they transport K^+ into Müller cells, where K^+ levels are increased during light exposure.[24] The Müller cell morphology then allows them to redistribute these ions into various sinks; the vitreous, the blood supply through direct contact with the blood vessels, and to a lesser extent into the subretinal space, [25-27] where they will be less damaging. The Müller cells are capable of redistributing the K^+ only when

they maintain a negative membrane potential (around -80 mV) [28-30] via open Kir channels.[24] Water content and extracellular pH are also maintained by Müller cells. Pathological fluxes in extracellular K^+ leads to changes in the neuronal cell and glia membrane potentials.[31] The Müller cell membranes from diseased retinas may adversely affect retinal K^+ homeostasis and other transport systems of Müller cells. Transretinal water fluxes are osmotically coupled to any osmolyte changes, as such wherever K^+ moves to; water will follow through selective channels, the aquaporins.[32] Aquaporins regulate transport of water in response to osmotic gradients and differences in hydrostatic pressure. The retina contains two known aquaporins (AQP1 and AQP4), in RPE and retinal glia, AQP4 is known to be primarily expressed in the end feet of Müller cells.[33-35]

Müller cells are also involved in waste metabolism and provision of trophic substances to neurons.[36] Glucose is metabolised into lactate which is then used in oxidative metabolism in the photoreceptors, this process occurs in Müller cells and as such Müller cells are essential for neuron survival. Müller cells are also essential in neuronal information processing; they provide the precursors of neurotransmitters and also have a fast uptake of any neurotransmitters released. Müller cells release glutamine into presynaptic terminals of the neurons; they therefore play a crucial in the Glutamate-glutamine cycle of the retina. The primary glutamate transporter of the Müller cell is L-glutamate-L-aspartate transporter (GLAST).[37, 38] Immunoreactivity against GLAST shows a localisation to the cytoplasm and all radial processes in a Müller cell.[39] Müller cells mop up extracellular glutamate rapidly, thus reducing excitoxicity and disturbances to the neuronal processing of information, for example the termination of light envoked ganglion cell activity is swiftly carried out by the rapid uptake of glutamate by the Müller cells.[40] The glutamate is degraded within Müller cells by glutamine synthetase, a Müller cell specific enzyme[41] that will degrade both ammonia and glutamate[36] GLAST and GS have both been reported to change in some ocular diseases. Decreases in both proteins in Müller cells have been shown in diabetes,[42, 43] and in ischemia in rat retina.[39]

Müller cells and retinal neurons are mutually interdependent; Müller cell processes make contact with neurons which in turn determine the formation and characteristics of those processes.[17] Müller cells respond to signals from distressed cells via the Müller cell p75 neurotrophin receptor, a pro-apoptotic receptor.[44] The receptor is found in Müller cell processes and forms three horizontal layers in the IPL and one layer in the OPL of the rat retina.

In vitro experiments indicate that Müller cells are implicated in immunoregulation; however their role in vivo has not been confirmed. Müller cells have been shown to phagocytose apoptotic neuronal cells during development,[45] and explanted cultures of Müller cells have been shown to phagcytose dying photoreceptor cells.[46] Müller cells have also been shown to phagocytose melanosomes after melanin implantation in the sub retinal space of albino rats,[47] although the data for this is speculative, what appear to be melanin granules under electron microscopy could also be lipofuscin or other lipid vesicles.

Müller cells, along with astrocytes (chapter **1.2.2.2**) aid in generating the retinal equivalent of the blood brain barrier, the blood retinal barrier. A barrier that protects the neuronal retina from exposure to ions and small molecules from the blood. A tight restriction on diffusion through the endothelial cells of vessels is established through tight junctions between endothelial cells, which are induced by the surrounding glial cells.[48-51] Müller cells associate with all vascular plexus of the retina, however astrocytes are restricted to the primary plexus.

Müller cells respond to a perturbation of the retinal homeostasis by becoming reactive. This includes photopic damage, ischemia, glaucoma, retinal detachment, trauma, retinopathy and age-related degenerations, inflammatory disease or excitotoxicity. In each case Müller cells undergo reactive gliosis, characterised by proliferation of[52] and a biochemical, morphological, (due to alterations in intermediate filament formation[53]) and physiological change of the Müller cell.[54, 55] Müller cells respond to alterations in retinal homeostasis long before the appearance of clinical features. Diabetes stimulates a rearrangement of intra and extracellular structures, including the arrangement of Kir and AQP channels of Müller cells[56] prior to initiating a series of gliotic changes.[57] Retinal injury stimulates the Müller cells to release neurotrophic factors and free radical scavengers and clear excess glutamate which protects neurons. Müller cells also have been shown to de-differentiate and take on progenitor-like properties with subsequent transdifferentiation towards a neuronal phenotype (the transdifferentiation is restricted)[58] aiding in tissue regeneration. They are also key players in facilitating neovascularisation, one means of which is to up regulate vascular endothelial growth factor (VEGF).[55, 59-61] Müller cell gliosis is not always beneficial; Müller cells have been implicated in neuronal degeneration, oedema formation and can have an adverse effect on vascular survival in diseased retina.[32, 43, 55, 59] Diabetic retinopathy is exacerbated by reactive gliosis[60-62] and Müller cell scars, which hinder the repair and transdifferentiation properties of the Müller cells. Müller cell scar formation after destruction of RPE due to a retinal detachment, (this can be recreated by sub retinal injection of sodium iodate), is caused by Müller cells migrating into the sub retinal space, as shown in rabbit eyes.[63]

Immunohistochemical markers of Müller cells

Cellular retinaldehyde binding protein (CRALBP/RLBP1) is a water soluble vitamin A binding protein specifically found in retinal Müller cells and RPE.[64] Vitamin A, essential in the visual cycle, undergoes repeated shuttling between RPE and photoreceptors as bleaching of rhodopsin occurs.[65] Vitamin A is contained within the interphotoreceptor matrix (sub retinal space), the Müller cells or the RPE, this is to resolve the problems of toxicity and limits solubility.[66] Vitamin A derivatives have specific carrier proteins within these three compartments; CRALBP in the RPE and Müller cells, and interstitial retinol-binding protein (IRBP) in the sub retinal space.[66]

Glutamine synthetase (GS) and carbonic anhydrase (CA) are both also found in Müller cells.[41] These are normally expressed by astrocytes and oligodendrocytes outside of the retina, implying shared function between the different glia.[41, 67] GS requires glial-neuron contact to remain expressed, in a purified culture of Müller cells GS is downregulated after 8 days.[44]

The type III intermediate filaments, vimentin and glial fibrillary acidic protein (GFAP) are both found in Müller cells. Vimentin is found throughout the entire Müller cell.[68] In the healthy retina, GFAP is located in some Müller cell endfeet, whereas the other primary glia, astrocytes express GFAP evenly distributed throughout their cell cytoplasm.[69] Müller cells dramatically upregulate GFAP expression in response to injury.[69] Activation markers such as GFAP in Müller cells have traditionally been used as a marker of disease progression. After laser photocoagulation, GFAP is even upregulated in Müller cells distant from the site of injury[70, 71] indicating that Müller cell activation may be driven by cell-mediated signals. Both vimentin and GFAP are increasingly expressed with age in human retina.[72, 73]

CD44 is a transmembrane glycoprotein and a cell surface receptor for hyaluronic acid (HA).[74] CD44 interacts with hyaluronic acid to stimulate Rac1 signalling leading to a cytoskeletal effect and cell migration in astrocytes.[74] Localisation of CD44 to Müller cell apical microvilli has been reported in adult rat retina.[75, 76] CD44 has also been reported in the developing mouse retina (postnatal day 1) in progenitor cells that were destined to become mature Müller cells.[77]

1.2.2.2 Astrocytes

Retinal astrocytes emerge from the optic nerve and spread radially as a proliferating cell population across the inner surface of the retina. They develop from a precursor lineage at the optic nerve, these precursor cells are positive for the transcription factor Pax2.[78, 79] They produce two lineages of astrocytes, those resident in the optic nerve and those that will

migrate into the retina. The earliest marker that distinguishes the retinal astrocytes from the resident optic nerve astrocytes is platelet derived growth factor alpha (PDGFRα). PDGFRα is expressed days before invasion into the retina.[80] Platelet derived growth factor A (PDGFRA) is the ligand for the PDGFRα and is expressed by RGCs,[81] this factor is likely to be responsible for triggering the migration of retinal astrocytes into the retina.[80] Immature astrocytes have a spindle like morphology as they migrate through the retina into the periphery,[82] once they reach the peripheral retina they proliferate further and join up to form a mesh-like network. The network of astrocytes provides a template for the developing retinal vasculature.[83, 84] There is a direct correlation between astrocytes and vasculature within the retina; in animals that do not have retinal vasculature, such as the possum, there are no astrocytes.[85] However the horse, which has a small vascularised region around the optic nerve also has a matching region of retinal astrocytes,[86] in primates and mice retinal astrocytes and vasculature cover the entire surface of the retina.[86, 87] The implication from this is that astrocytes and the developing vasculature are evolutionarily linked.[88] Retinal astrocytes release vascular endothelial growth factor (VEGF) in response to regional hypoxia,[89, 90] thought to be brought about by the developing neuronal cells.[91] VEGF is a key stimulus for angiogenesis[92] driving the vasculature to proliferate into the retina. As the vessel network expands over the astrocytes, the astrocytes begin to mature.[82] They change morphology from spindle-like to stellate and proliferation stops, glial fibrillary acidic protein (GFAP) is upregulated and vimentin and VEGF are downregulated.[78, 90]

Astrocyte function goes beyond development and driving the vascularisation of the retina. They have many functions similar to Müller cells.[93] Astrocytes also contribute to the blood-retinal barrier, in the formation of the glia limitans.[94] However as mature astrocytes are largely restricted to the ganglion cell layer and nerve fibre layer[95] they only play a role in the functioning of the primary vascular plexus. Also like Müller cells, astrocytes contain glycogen, and can provide glucose to neurons. They also regulate ion homeostasis[96] and metabolism of neurotransmitters like GABA.

1.2.2.3 Microglia

Microglia, although not technically neuroglia having originated from mesodermal origin, appear in the retina prior to the retinal blood vessels. Here they lie dormant in the IPL and OPL of the retina until activated. Retinal microglia appear in three forms; parenchymal macrophages associated with neurons, paravascular macrophages associated with blood vessels and the perivascular macrophages, found within the perivascular space.[97, 98] Microglia

originate from the bone marrow and the term encompasses both dendritiform cells (resident tissue microglia) and macrophages that express luekocyte common antigen (CD45).[97, 98, 98] Both types of microglia can be stimulated into macrophagic function as a result of trauma to the retina.

1.2.3 Retinal pigment epithelium

The retinal pigment epithelium (RPE) is composed of a monolayer of cells, with the apical side in contact with the photoreceptors of the neural retina. The RPE cells contain melanin granules, necessary to absorb excess light that passes through the retina and thus reduce scattering within the globe that would otherwise decrease visual acuity. Highest levels of pigment (melanin) are found in peripheral retina, it decreases towards the posterior pole, but then increases again towards the submacula/fovea region.[99, 100] The RPE is positioned between the Bruch's membrane basally and the interphotoreceptor matrix apically, thus it is essential in forming a selectively permeable blood-retinal barrier between the underlying choroidal vasculature and the neural retina above. RPE cells have a cobble stone morphology, polygonal in shape, cell-cell contacts contain tight junctions and they have apical microvilli.

The photoreceptors are reliant upon the RPE to maintain healthy function. The apical microvilli of RPE surround the outer segments of the photoreceptors; each day when the outer segment discs of the rods and cones are shed, they are engulfed by the RPE in which they are degraded by phagolysosomes.[101] This process occurs in diurnal cycle, with the first light of each day inducing the shedding of the outer segment tips.[102] RPE also recycle the visual pigments for the photoreceptors.[103]

1.2.4 Retinal oxygen supply

As I have previously stated, astrocytes enter the retina and lay down the framework over which the retinal vasculature grows. In the human retina, blood vessels first start to appear around the optic nerve at 14-15 weeks gestation (WG)[91, 104, 105] and then spread to the periphery, not reaching the retinal margins until 34 WG.[106] Oxygen tension of the retina is key to regulation of vascular spread and modelling.[107, 108] The retinal astrocytes respond to hypoxia in the retina and release VEGF.[89-91] The retinal vasculature initially spreads through the nerve fibre layer and the ganglion cell layer forming the primary plexus. Subsequently vessels penetrate down through the retinal layers forming a deeper plexus network with

blood vessels running along the vitreal and sclera margins of the inner nuclear layer. The photoreceptor layer does not contain any retinal vessels, and are thought to be supplied with oxygen by the choroidal vasculature; a network of vessels that lies below the RPE. The primary plexus of the human retina develops in a 'lobular' arrangement, with four lobes, each of which will form the territory of a quadratic artery in the mature retina (Fig. 1.2 A, B). As development continues the lobes begin to fuse to form the network. This occurs throughout the retina excluding the future fovea (Fig. 1.2 C). Here the lobes remain distinct and skirt around the fovea. They meet at the horizontal meridian on the temporal side of the fovea at around 25WG.[104, 109] (Fig. 1.3 A) The fovea remains avascular into mature retina and the foveal depression forms within a pre-defined foveal avascular zone[110] (FAZ, Fig. 1.3 B) whilst peripheral retina is a continuous network (Fig. 1.3 C). Fitting with the fact that astrocytes pattern the developing primary plexus, the incipient fovea also lacks astrocytes during development and into adulthood.[110]

The retina, like the brain is vascularised via angiogenesis, where proliferating endothelial cells form new blood vessels sprouts and the vascular network is formed from pre-existing vessels.[111] The other methods of vascularisation within the body in vasculogenesis, where vascular endothelial precursor cells within the tissue coalesce and form vessel lumens, not requiring existing vasculature.[111] Authors are unified in the understanding that the deeper plexus vessels form through angiogenesis, however the development of the primary plexus has the field divided. Some authors propose that this occurs through vasculogenesis,[105, 108, 112-114] however identification of free standing precursor cells distal to the developing vascular front have not been identified, human studies have identified ADPase/CD39 and CXCR4 positive cells distal to the vascular front however these are not conclusive endothelial precursor markers,[112, 115-117] a definitive marker such as VEGFR2[118-120] would need to be shown. There is more evidence that supports the theory that the primary plexus develops via angiogenesis;[82] mouse studies have shown that the cells at the leading edge of the vascular front extend numerous filopodia[121-123] suggesting that they respond to attractant and repellent gradients within the retina and direct vascular growth.[124] These sub class of endothelial cells are referred to as tip cells and their expression pattern differs to other endothelial cells. Endothelial cells have an expression pattern dependent upon position as part of a venule, artery or capillary, and location within the vascular plexus. Tip cells have an expression pattern that shows that they have the potential to differentiate into various sub classes of endothelial cell. They express delta-like 4 (Dll4), PDGFB and apelin,[125-127] along with netrin receptor Unc5b and VEGFR2.[125, 128]

The retina is highly metabolically active and actually has the highest oxygen consumption of any organ.[129] The inner segments, OPL and inner portion of the IPL demand the most oxygen.[129, 130] The retinal vascular unit consists of endothelial cells surrounded by pericytes.[131] These two cell types lay down an extracellular matrix or basement membrane which is high in Collagen IV.[132] (Fig. 1.4) This unit is then further surrounded by glial end feet processes,[133] processes from both astrocytes and Müller cells surround the primary plexus, and Müller cells only at the deeper plexus. Retinal capillary endothelial cells are not fenestrated[134] however, they contain a high number of endocytotic vesicles suggesting that they are more permeable than capillaries of the brain.[134] Each cell type contributes to the barrier properties of the blood retinal barrier.[131] Endothelial cells form tight junctions/zonula occludens between one another, apparent with electron microscopy as electron dense regions at cell-cell contacts.

1.3 Susceptibility to disease

The macula, the highly specialised region of the retina is particularly susceptible to disease. One such disease, Macular Telangiectasia type 2 only affects the macula, in a defined central region. Other diseases such as X-linked Retinoschisis and Sjögren Larsson syndrome mimic the disease locality, whilst others such as Canthaxanthin retinopathy actually spare a region in central retina during disease progression. There are also diseases that initially affect the macula, but then spread into peripheral retina with disease progression, such as Age Related Macular Degeneration (AMD) and Diabetic retinopathy.

1.3.1 Macular Telangiectasia type 2

Macular telangiectasia type 2 (MacTel type 2), also known as idiopathic juxtafoveolar telangiectasia type 2, is an uncommon retinal disease that can lead to legal blindness, it was recently discovered that its prevalence is higher than previously thought, being 0.1% of the participants in the Beaver Dam Eye study,[135] which equates to approximately 70,000 people having it in the United States.[136] Recent studies have been able to more clearly elucidate the clinical phenotype of the disease.[137-141 110-115] The predominant clinical features include loss of macular transparency,[142, 143] a reduction in macular pigment (Fig. 1.5 A),[137-139] increased macular autoflourescence[139, 140] and superficial white crystals (white arrow heads Fig 1.5 B), compared to control retina (Fig. 1.5 C and D).[142, 144] There is also progressive foveal atrophy/foveal thinning as a result of disturbances in the photoreceptor layer (asterisks Fig.

1.5 E), inner and outer retinal cavitation.[142, 145] As the disease name suggests, there is also a significant vascular component to the disease; intraretinal vascular abnormalities are seen parafoveally, including vascular telangiectasis (tortuous vessels) (arrow Fig. 1.5 F), leakage (Fig. 1.5 G), right angled venules, and intraretinal and subretinal neovascularisation with disease progression.[141, 142, 144] The deterioration in visual function is predominantly caused by foveal atrophy, hyperplasia and migration of RPE into neural retina (arrow head Fig. 1.5 F) and the development of subretinal and intraretinal neovascularisation.

The clinical phenotype of MacTel type 2 is restricted to the parafoveal retina. The morphologic and functional problems are most pronounced and normally originate just temporal to the fovea, spreading around the fovea with disease progression.[144, 146-149]

The genetics of the disease have only recently been investigated. Most of the reported cases of MacTel type 2 are sporadic, nevertheless affected sibling pairs and affected pairs of monozygotic twins have been described in the literature.[150, 151] Some relatives of MacTel type 2 patients also present with subtle signs of MacTel type 2, however they suffer no vision problems.[152] This led Rando Allikmets and colleagues in New York to believe that MacTel type 2 has a genetic cause in a significant proportion of cases.[153] Vertical transmission is reported in families, therefore an autosomal dominant model of Mendelian inheritance with reduced penetrance has been assumed by Allikmets' lab.[153] They have so far screened 27 candidate genes against a cohort of MacTel type 2 patients and their relatives. Candidate genes included those known to be causative in diseases with phenotypic similarities to MacTel type 2, including familial exudative vitreoretinopathy (FEVR) and Norrie disease,[154-158] and also genes with a genetic role in retinal vascularisation, macular pigment transport and genes of interest based on the lab's familial linkage study.[153] However this approach revealed no associated genes with any significance to MacTel type 2.[153] Allikmets and colleagues are continuing the search for the causative gene in MacTel type 2 by combining a linkage analysis and whole genome sequencing approach.

The cause of MacTel type 2 is not known, and no treatment exists to prevent the progressive loss of central vision that is often seen in this disease.

1.3.2 X-linked Retinoschisis

X-linked Retinoschisis patients present with localised macula problems similar to that seen in MacTel type 2; they have central vision loss and parafoveal oedema. A common phenotype is

retinal schisis, not found in MacTel type 2, however, this schisis is most often located to parafoveal retina, however 50% of patients also present with minimal peripheral schisis.[159]

X-linked retinoschisis is a common form of juvenile macular degeneration, primarily affecting males.[160, 161] It is characterised by splitting (schisis) of the fovea, and often bilateral, and oedema formation. The schisis can occur along any level of the retina, however it is more common to split along the inner nuclear layer.[162] Visual signal transmission is affected in X-linked retinoschisis shown by a decrease in b-wave (Müller cell/bipolar response) amplitude but a preservation of the a-wave (photoreceptor response) amplitude in a scotopic electroretinogram (negative ERG).[163] The causative gene has been identified responsible for X-linked retinoschisis using a positional candidate gene approach as retinoschisin 1 (*RS*1).[164] The gene encodes 224 amino acids, of which the N-terminal 23 amino acids are a secretory signal, and there is also a highly conserved discoidin domain comprising 75% of the processed protein. The 24kDa retinoschisin polypeptide is secreted[165] and is distributed around the surface membranes of bipolar and photoreceptor cells.[166, 167] The exact function of retinoschisin in maintaining retinal structure is unknown, however potential binding partners have been established; there is a direct interaction between retinoschisin and Na/K-ATPase.[168] The Na/K-ATPase enzyme (ATP1A3 and ATP1B2 subunits are highly abundant in retina) is essential in generating the Na^+ and K^+ gradients required for maintenance of cellular homeostasis.[169] Dysfunction of cellular homeostasis can lead to oedema formation, one of the characteristics of retinoschisis, however it doesn't explain the generalised foveal schisis. The ATP1B2 subunit of Na/K-ATPase has been shown to be an adhesion molecule on glial cells that mediates glial-neuron interactions,[170, 171] it is potentially possible that retinoschisin dysfunction alters the adhesion properties of ATP1B2 in the retina, however there is no evidence to support this.

In the retina carbonic anhydrase II is found in Müller cells and red/green cones, while the RPE and corneal epithelium contain the membrane bound form of carbonic anhydrase, carbonic anhydrase IV.[172] Carbonic anhydrase inhibitors have been shown to have beneficial clinical effects; they have been shown to modulate membrane bound carbonic anhydrase IV receptors in RPE.[173] Carbonic anhydrase inhibitors enhance the fluid transporter system present within in the RPE and improves retinal adhesiveness, thus is thought that patients with diffuse RPE disease respond better to carbonic anhydrase inhibitors in removal of cystoids macular oedema.[172]

It has been shown that resolving cystic macular oedema can improve visual acuity in patients.[174, 175] A further study in 2011 treated patients with retinitis pigmentosa and X-linked

retinoschisis, which had macular oedema with carbonic anhydrase inhibitors. The treatment decreased macular oedema periodically during treatment; however reoccurrence of cysts did occur.[176] Visual acuity did not improve at a statistically significant level, however returning the retinal anatomy to normal might prevent a more rapid decrease in vision loss.

Again there is no treatment to date for X-linked retinoschisis and the specificity and exact mechanisms behind the disease remain unknown.

1.3.3 Sjögren Larsson Syndrome

In Sjögren Larsson syndrome, retinal crystals are commonly seen, limited to the parafoveal retina, mirroring the crystals seen within MacTel type 2 patients. Sjögren Larsson syndrome also results in a reduction of macular pigment, however unlike MacTel type 2 the macular pigment loss is pan retina and not limited to central macula.

Sjögren Larsson syndrome, an autosomal recessive neurocutaneous disease, has the clinical features of spastic diplegia or tetraplegia, mental retardation, ichthyosis, and the presence of crystalline retinopathy. Sjögren Larsson syndrome patients suffer from photophobia and low visual acuity. The crystalline maculopathy develops gradually within childhood, with onset within the first decade,[177] the crystals, not seen in control patients, are restricted to a parafoveal pattern (Fig. 1.6 C) and are found within the inner retinal layers. The fovea itself is sparred from crystal deposits. However visual acuity is decreased. Optical coherence tomography (OCT) reveals that the fovea is affected by the disease; there is thinned central fovea and intrafoveal cystoid spaces.[178] OCT also made it possible to locate the inner retinal crystals more specifically; focal hyper reflectivity's, which correspond to clinically visible retinal crystals, are located within the ganglion cell layer and IPLs.[178] Sjögren Larsson syndrome is also characterised by a pan retina reduction in Macular pigment levels, unlike MacTel type 2 that has a restricted loss parafoveally.[179] (Fig. 1.6 A-D)

Sjögren Larsson syndrome is caused by defects in the fatty aldehyde dehydrogenase enzyme, ALDH3A2,[180, 181] and subsequent disruption of lipid metabolism, ALDH3A2 catalyses the oxidation of long chain aliphatic aldehydes into fatty acids.[182] Resulting in an accumulation of fatty alcohols and fatty aldehydes within the tissues of the body.[183, 184]

Fuijkschot *et al*[178] have speculated that the crystals located within the GCL and IPL, where the dendrites and axons of the ganglion cell and inner retinal neurons reside, suggests a participation of the perifoveal ganglion cells in the deposition of lipids in Sjögren Larsson

syndrome. The theory does correlate with previous studies that show ganglion cell involvement in other lipid storage diseases, such as lysosomal storage disorders. However there is no firm conclusions over this; the other possibility is that the crystals reside within the Müller cell end feet, the only other cell type found at this level of the retina.

How the build-up of intraretinal crystals and defect in ALDH3A2 directly cause foveal thinning and cystoids spaces is currently unknown, also why there is a parafoveal restriction to the crystalline phenotype, yet a pan retina phenotype of macular pigment reduction is unknown.

1.3.4 Canthaxanthin retinopathy

Interestingly Canthaxanthin retinopathy is characterised by a region in central retina that is spared from retinopathy. The region unaffected mirrors the region that is affected in MacTel type 2. This is an intriguing finding especially as Canthaxanthin retinopathy results in crystalline deposits, like that seen in MacTel type 2, yet the deposits form in adjacent regions (Fig. 1.6 E and F).

Canthaxanthin is a carotenoid pigment commonly given to patients with tumours due to its strong anti-oxidant properties.[185-187] It has also been popular in the past as a natural skin tanning agent in tablet form.[188]

Canthaxanthin intake is associated with golden yellow crystal deposits forming within the retina. These crystals develop until they reach 10-14μm in size[189-191] and they are located in a ring around the fovea between 5° and 10°.[192] Studies in animals and humans show that even small quantities consumed result in crystal deposit accumulation around the macula.[192-200] The crystals are likely to consist of a canthaxanthin-lipoprotein complex.[192] The crystal deposition has been correlated with vascular abnormalities of the retina,[192, 201] however a more recent study has demonstrated that patients were asymptomatic with no defect directly correlating to the intake of canthaxanthin.[202] Although after canthaxanthin intake has stopped, the crystals remain within the retina and can take up to 20 years to be removed completely.[202]

1.3.5 Age related macular degeneration

Age related macular degeneration (AMD) is the most common macular disease in western society. A disease that, like MacTel type 2, initially affects the macula and onset of the disease is often in 5-6th decade of life. Unlike MacTel type 2 though it spreads into peripheral retina over time with a non-uniform distribution.

Clinical presentation

AMD is a late-onset, progressive degenerative disease, characterised by loss of photoreceptors, RPE and small blood vessels from the choroid. It encompasses a wide spectrum of pathologies and clinical phenotypes however, the primary affected region is the macula and surrounding central retina. The prevalence of AMD increases with age, and typically does not manifest before the age of 55 years.[203] The clinical phenotype shows minimal visual impairment initially, with decreases in high resolution central vision as the disease progresses. There have been many classifications of AMD over the years.[204] The pathology of AMD starts initially with the appearance of drusen; lipid and protein deposits between Bruch's membrane and the RPE. There are three stages of AMD, early AMD can be categorised by the presence of small drusen, ≥63μm but <125μm in size and more than 5 present in central retina. Intermediate AMD is characterised by increased deposit size to above 125μm. Larger drusen are often accompanied by pigment changes of the RPE, hypo and hyper pigmentation has been noted. Advanced AMD has more of an impact to the vision of the patient; further lesions develop; geographic atrophy (GA), followed by neovascular (NV) AMD. These are more commonly referred to as Dry AMD and Wet AMD respectively. GA lesions are defined when a region of retina, at least 175μm in diameter with a definable border, depigment and choroidal vessels are visible through the lesion, many patients with GA are asymptomatic and unaware of the disease, however 10-15% have a rapid deterioration of the retina and suffer severe vision loss. NV AMD is the most severe disease phenotype, it accounts for 90% of central vision loss among AMD patients. NV AMD can follow GA, it manifests itself as retinal or RPE detachment, sub retinal haemorrhage, subretinal fibrous tissue and generalised RPE atrophy, with the presence of neavascularisation.[205-207] Wet AMD, if untreated can progress to the cicatricial stage, referred to as a disciform scar, a 4-8mm fibroitic scar below the macula.

Pathobiology and genetics

Biochemical analysis of drusen shows that they consist of glycoconjugates and constituents of atherosclerotic plaques including, apolipoprotein B and E, vitonectin, alpha crystallin, lipids and complement proteins.[208-210] Drusen present in two forms, hard (discrete nodules) and soft (large deposits with ill-defined boundaries).[211, 212] Soft drusen are more associated with damage to the retina, RPE and choroid and are indicators of a more severe clinical outcome; the development of GA and choroidal neovascularisation (CNV).[213] GA is characterised by abnormalities of the REP; hypertrophy and hypotrophy, hyper and hypopigmentation, loss of photoreceptors, thinning of Bruch's membrane and degeneration of the choriocapillaris.[214] In

AMD the RPE is the primary cell type affected, however the photoreceptors are also attenuated.[215] CNV is the growth of new blood vessels from the choroid, penetrating through the Bruch's membrane,[216] these can then breach the RPE and invade the sub retinal space.[217] It is this neavascularisation that often results in the severe phenotypes of AMD, leading to a) neaovascular AMD, where lipid rich fluid accumulates under the RPE and/or neural retina; b) haemorrhagic AMD, where blood breaks through the RPE into subretinal space; c) disciform AMD, where fibrous tissue, blood vessels and RPE proliferation invades and replaces the neural retina. AMD ultimately leads to loss of central vision through the death of photoreceptors at the macula.[218]

In 2005 there was a significant breakthrough in understanding AMD; a strong association between disease variants in and around the complement factor H (CFH) gene was identified. The initial reports of association were via a candidate gene approach, fine mapping of candidate loci and also the first whole-genome association study in humans[219-221] and replicated the same year.[222] This genetic link between CFH and other complement genes, including complement 2 (C2), complement factor B (CFB)[223] and complement 3[224] focused the search for the cause of the disease. Complement associated genes are not the only genetic contributors to AMD susceptibility, the ARMS2/HRA1 region has also been identified. Three potential candidate genes reside in the region of association; however, the specific gene affected is still controversial; two reports indicate HTRA1 as a target gene[225, 226] whilst other studies claim ARMS2 as the stronger candidate.[227, 228]

The question still remains why AMD affects the macula and not the peripheral retina. It has been proposed that the variations in the topography of Bruch's membrane might be the cause. Morphometric data show that the elastic lamina of the Bruch's membrane is 3-6 fold thinner at the macula and 2-5 fold less dense relative to mid-peripheral retina,[229] this might render the submacular region more susceptible to ingrowth of blood vessels from the choroidal vasculature. Also elastin degradation releases peptides that have been shown to be extremely pro-angiogenic and possess macrophage recruiting properties,[230] thus initial degradation at Bruch's membrane due to its weakness could then propagate the phenotype. The choriocapillaris may also be a cause of the macula specific location of AMD; the choriocapillaris decrease in vessel calibre in the submacular area, and the network becomes more intricate. It is known that vessel calibre decreases with increasing age[231] and the macula would therefore undergo a more significant change in perfusion with age compared to the periphery. This might lead to hypoxia or other environmental factors that promote disease progression.

1.3.6 Diabetic retinopathy

Diabetic retinopathy is characterised by proliferation and/or ischemia of the retinal blood vessels. Although MacTel type 2 has a vascular phenotype, it is not similar to that seen in diabetic retinopathy. Diabetic retinopathy does affect the macula though, often resulting in ischemia and oedema formation.

Chronic hyperglycaemia in the early stages of diabetes results in blood flow alterations and increased vascular permeability. This can be characterised by a decrease in the activity of nitric oxide, and other vasodilators, whilst at the same time over activity of vasoconstrictors such as angiotensin II and endothelin 1, and release of vascular permeabilising cytokines such as VEGF. Programmed cell death is triggered in microvessels and an overproduction of extracellular matrix proteins. This leads to progressive vascular occlusion. Hyperglycemia decreases endothelial and neuronal cell trophic factors leading to oedema, ischemia, and neovascularisation driven by localised hypoxia.[232]

In diabetic retinopathy, retinal blood flow is always seen to increase.[233] This is believed to be due to a loss of autoregulation of the arterioles and venules which are seen to elongate and dilate. This leads to an increase in effective intraluminal pressure in the following capillaries. Starling's law then states that this would lead to fluid passage from the vessel into the extracellular space surrounding.[234] In combination with vasoactive cytokine release (i.e. VEGF) breaking down the blood retinal barrier, this can then lead to accumulation of albumin outside the capillaries and oedema formation.

Diabetic maculopathy - macular oedema/ischemia

There are two forms of diabetic maculopathy; ischemic maculopathy – capillary drop out, and macular oedema – fluid exudation from retinal or choriocapillaris. Oedema can be found both extracellular and intracellular, histological studies of enucleated eyes reports Müller, bipolar, ganglion and photoreceptor cell degeneration[235] and extracellular cystic spaces.[236] Cystoid macular oedema is seen to form in only the two plexiform layers of the retina. [237] Studies show that there is no correlation between the blood flow of the retina and macular oedema, thus ischemia does not cause macular oedema. Blood retinal barrier breakdown has been linked to retinal thickening.[238]

The question again is why the macula is more prone to oedema formation. One hypothesis is based on the avascularity of the fovea. In other areas of the retina, oedema can collect but is then dissipated from extracellular space in two ways, via the choroidal vasculature- the RPE

actively 'pumps' the fluid out of the retina, or via the retinal vasculature, where nearby less affected vessels transport the extracellular fluid back into the blood flow. However the vasculature at the centre of the macula is minimal and fovea is avascular. Therefore accumulated fluid can only be removed via the RPE/choroid and this is less efficient. It is also known that in diabetes the choroidal blood flow is decreased[239] (the opposite effect to the retinal blood flow) and that this has a degenerative effect on the basement membrane, so any functions of the choroidal vasculature are likely to be decreased.

1.3.7 Conclusions

Many retinal diseases specifically affect the macula. The cell types and pathways affected in AMD and diabetic retinopathy are known, and even the genes are known in AMD, and yet the reason as to why the macula is more susceptible in these diseases still remains elusive. Furthermore an explanation behind the very localised diseases; MacTel type 2, X-linked retinoschisis, canthaxanthin retinopathy and Sjögren Larsson syndrome has not been established. There is no known anatomical or biochemical boundary in the retina that restricts diseases to this perifoveal region. Understanding why the diseases are restricted/excluded to this domain of the retina might better direct therapies towards tackling these diseases.

1.4 Why should we study the macula?

Macular diseases such as AMD is the leading cause of severe and incurable blindness in developed countries.[205] It accounts for 54% of all causes of blindness in the USA, with 1.75 million over 40 year olds affected with advanced AMD and a further 7.3 million with intermediate AMD.[240] Increased age has been linked as a major risk factor to the development of AMD[241, 242] The incidence of early AMD, large drusen and pigmentary changes in intermediate AMD, and choroidal neovascularisation (CNV) and GA in advanced AMD increase with advancing age.[240] The number of individuals with AMD is expected to increase worldwide as the population ages and treatments for preventable blindness (such as cataract) become more widely available. Diabetic retinopathy is close behind AMD as the most common disease that leads to blindness. With the number of diabetics increasing year on year, the subsequent cases of diabetic retinopathy are also increasing.

1.5 Thesis Aims

Elucidating the molecular signalling pathways that induce regional differences in the human retina will lead to a better understanding of the underlying mechanisms of macular disease and aid in the design of future treatments.

This thesis aims to gain further insight into the mature and developing macula, to be able to interpret the phenotypes of macular diseases, and to adapt therapeutic approaches.

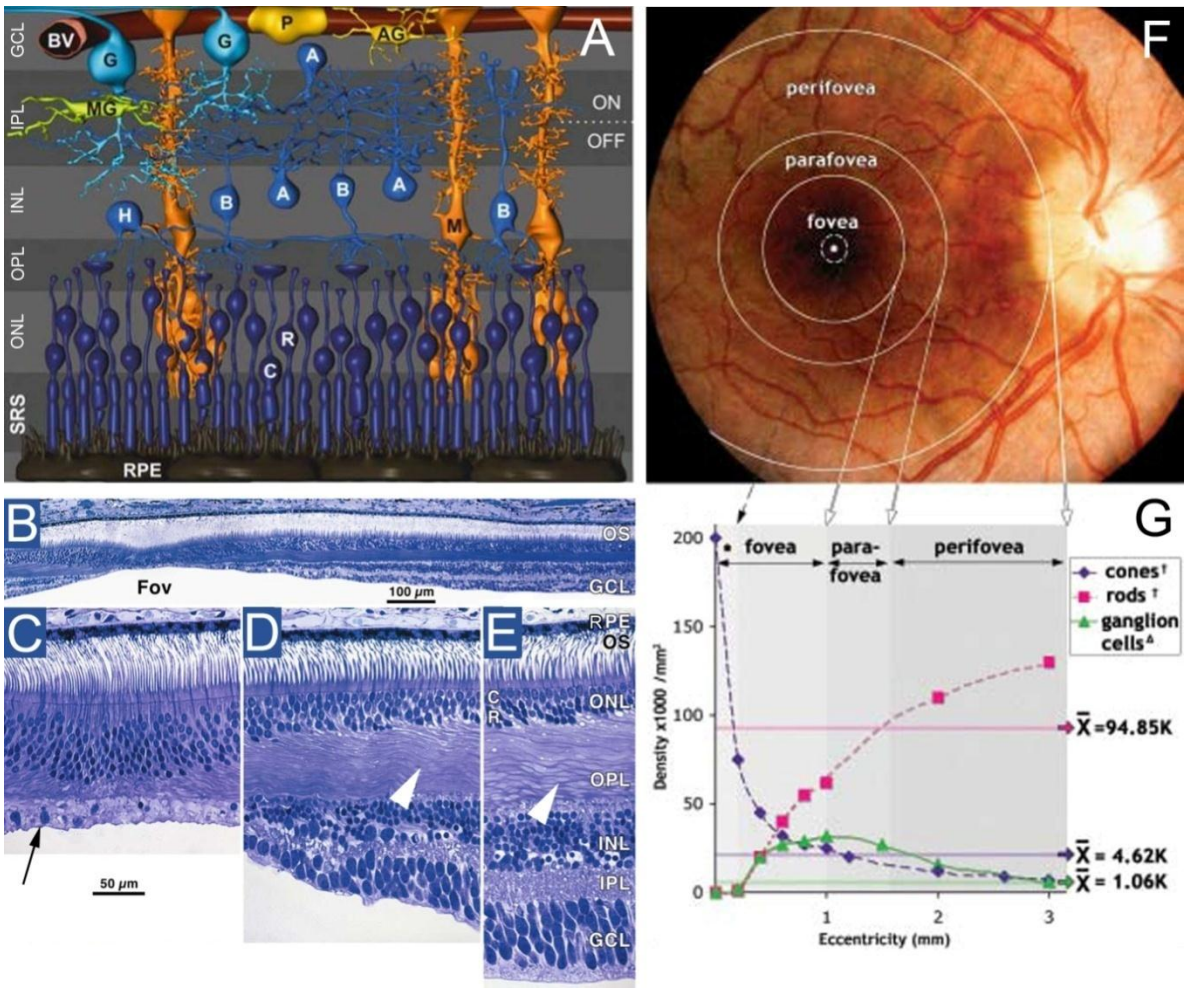

Figure 1.1. Retinal structure and macular morphology.
A: The retina has a laminated structure, consisting of the ganglion cell layer (GCL), inner plexiform layer (IPL), inner nuclear layer (INL), outer plexiform layer (OPL) and outer nuclear layer (ONL). This is then separated from the retinal pigment epithelium (RPE) by the subretinal space (SRS), the space into which the photoreceptor outer segments extend. The primary cell types of the retina are; ganglion (G), amacrine (A), bipolar (B), horizontal (H), Müller (M), astrocytes (AG), microglia (MG) and the photoreceptor cells, cones (C) and rods (R). Also there is the retinal vasculature (BV) associated with pericytes (P). (Artists impression of the retinal structure, adapted from Reichenbach and Bringmann).[243] **B-E:** Morphology of the fovea and macula in a human retina of a 72 year old (adapted from Penfold and Provis[244]), the foveal pit (**C**) contains only cone nuclei and limited numbers of ganglion cells (black arrow), at the foveal pit edge (**D**) and into parafovea (**E**), the Henlé fibre layer is present within the OPL (white arrow heads). **F** and **G**: The region defined as the macula by Polyak[9] (adapted from Provis[245]), **G** highlights the lack of anatomical correlates between the three regions defined as macula by Polyak[9].

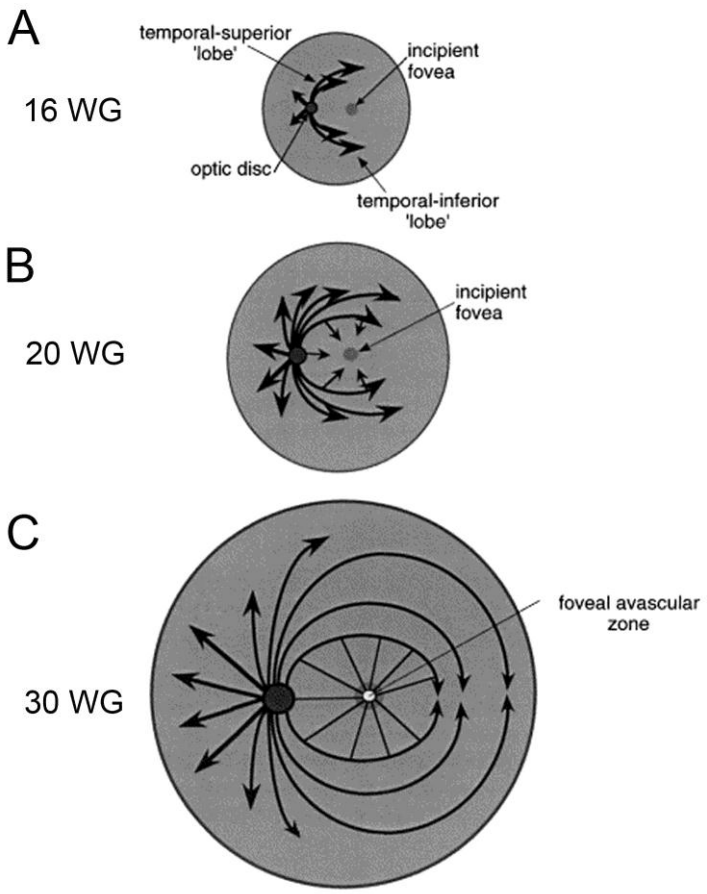

Figure 1.2. Primary plexus growth pattern of the human retinal vasculature.
The early vessels form four lobes of vasculature stemming from the optic disc (**A**). Temporal lobes skirt around the incipient fovea forming the arcades (**B**), smaller vessels branch and spread towards the fovea (**B**). Capillaries fuse surrounding the fovea, but leave an avascular zone directly above the central foveal pit (**C**). Primary vessels continue to spread outwards and towards the central meridian in temporal retina. WG; weeks gestation. Figure adapted from Provis.[246]

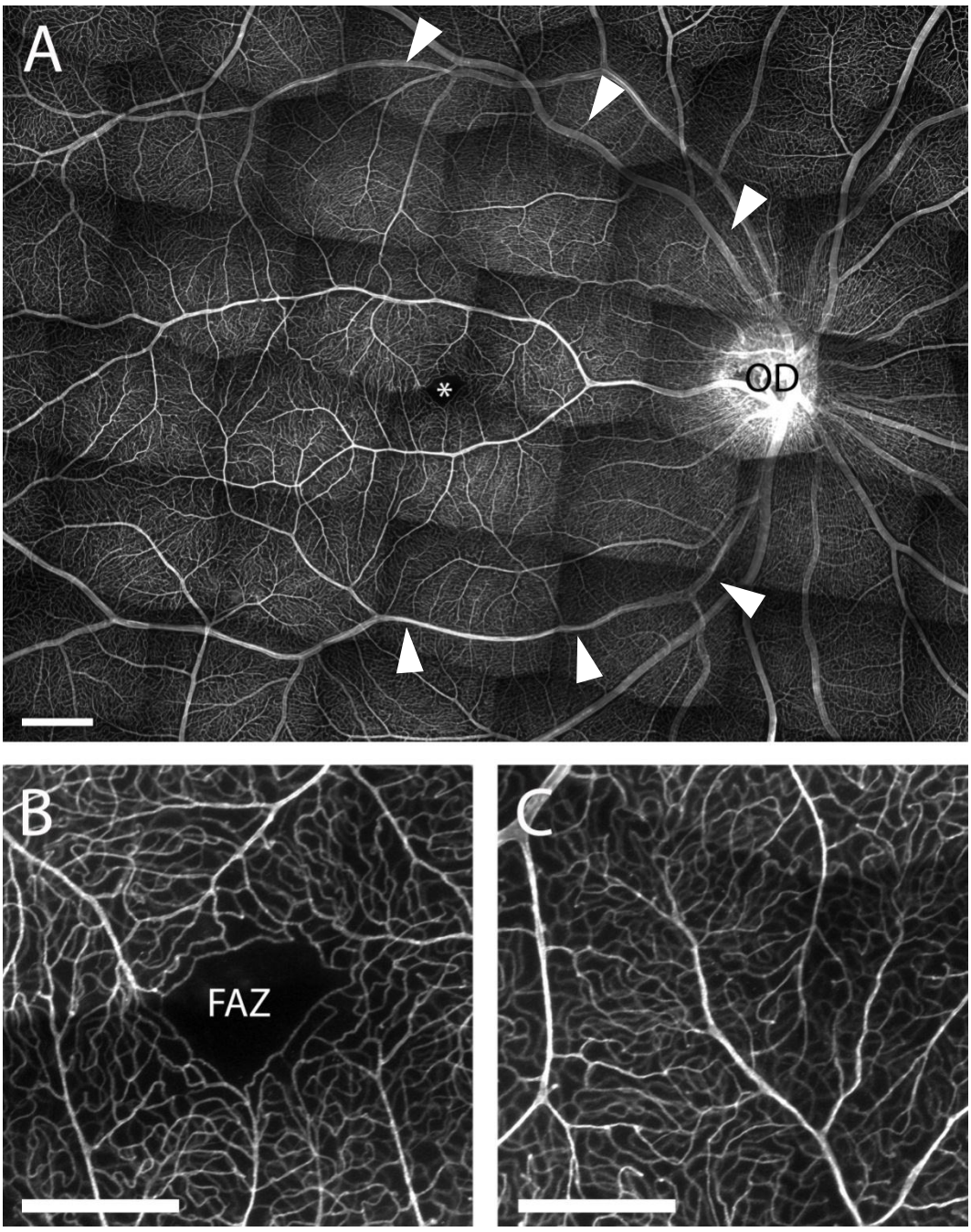

Figure 1.3. Human retinal vasculature.
Anti-collagen IV immunohistochemistry of a retina from a 75 year old donor reveals the retinal vasculature. Primary blood vessels arc around the macula/fovea (asterisk) originating at the optic disc (OD) (**A**). Arrow heads indicate temporal inferior and superior vascular arcades (**A**).The foveal pit is avascular (B) whilst the peripheral retina is a continuous network of vessels (**C**). Scale bars are 1mm in **A**, 0.5mm in **B** and **C**. Figure prepared from my own data.

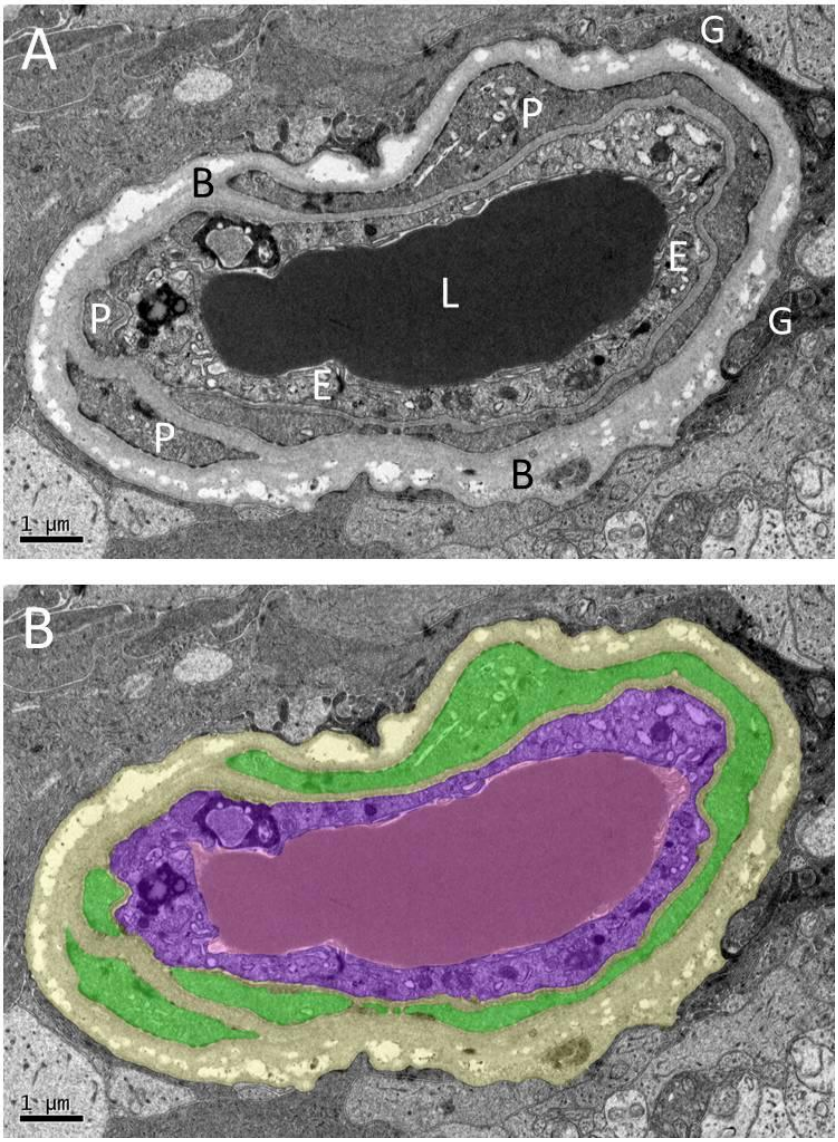

Figure 1.4. Retinal vascular unit.
Cross section through a retinal capillary seen by transmission electron microscopy. **A:** The endothelial cells (E) form a lumen (L) through which the blood vessels flow. Pericytes (P) surround the endothelial cells and both contribute to the formation of the basement membrane (B). Glial cells finish the vascular unit as their end feet surround the basement membrane (G). **B:** Highlighting the specific components reveals how the basement membrane (yellow) lies between the pericyte (green) and endothelium (purple), and borders with the glial cells. Note the lumen (pink) contains an erythrocyte. Scale bar is 1µm. Figure prepared from my own data (Chapter 3).

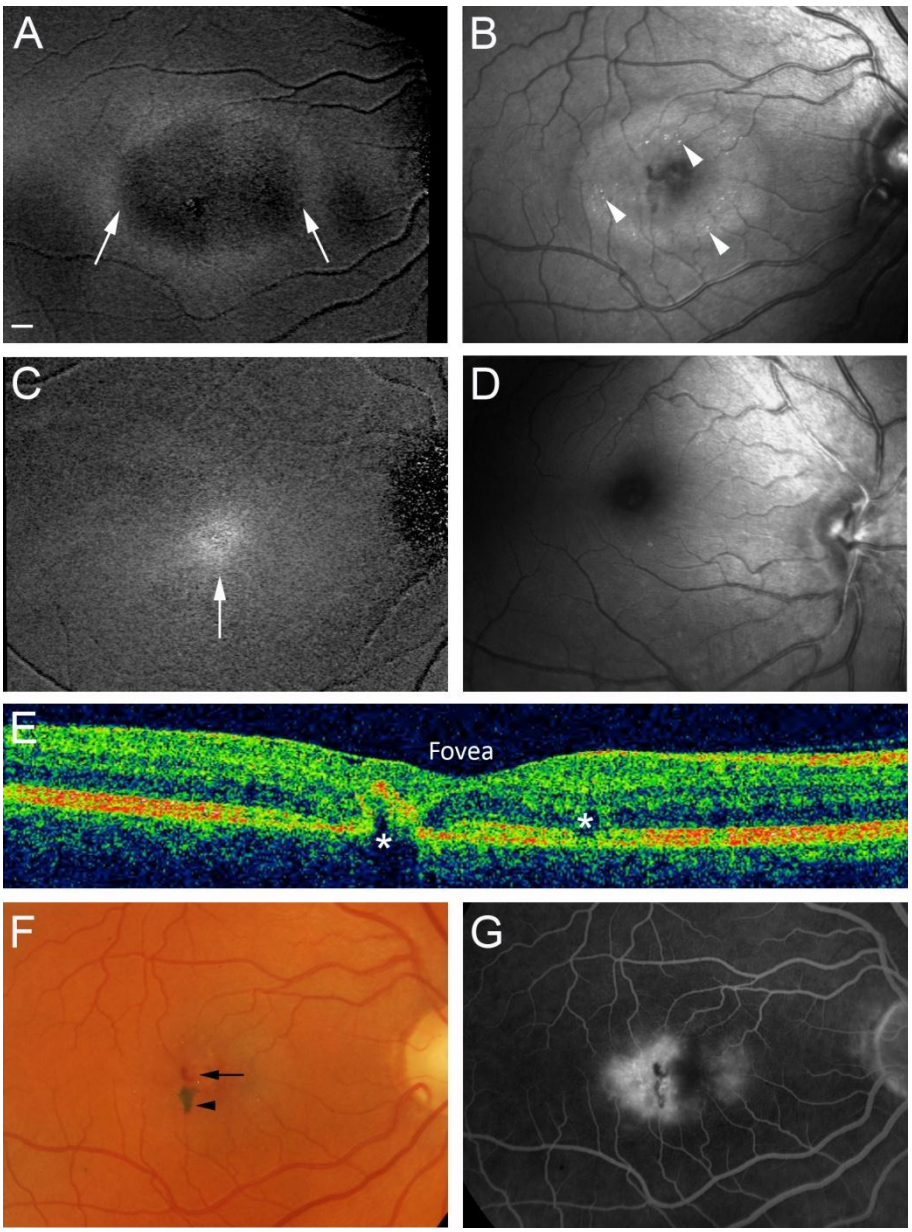

Figure 1.5. Clinical phenotype of MacTel type 2.
MacTel type 2 is characterised by a loss of parafoveal macular pigment (**A**) with a clearly demarcated ring remaining (arrows in **A**), formation of retinal crystals (arrow heads in **B**), and increased parafoveal reflectivity with confocal blue reflectance imaging; compared to control retina macular pigment distribution (**C**) and hyper reflectivity in the parafoveal retina using confocal blue reflectance (**D**). Optical coherence tomography reveals disruption to the photoreceptor layer in MacTel type 2 patients (asterisks in **E**). Telangiectatic vessels (arrow) and retinal pigment epithelium migration into the retina (arrow head) can be seen with fundus imaging (**F**). Late phase fluorescein angiograms reveal leakage from tortuous retinal vessels (G). Scale bar in A is 400µm, and is applicable for A, B, F and G. No scale available for C, D and E. Clinical images courtesy of Dr. Catherine Egan, Moorfields Eye Hospital, London, UK.

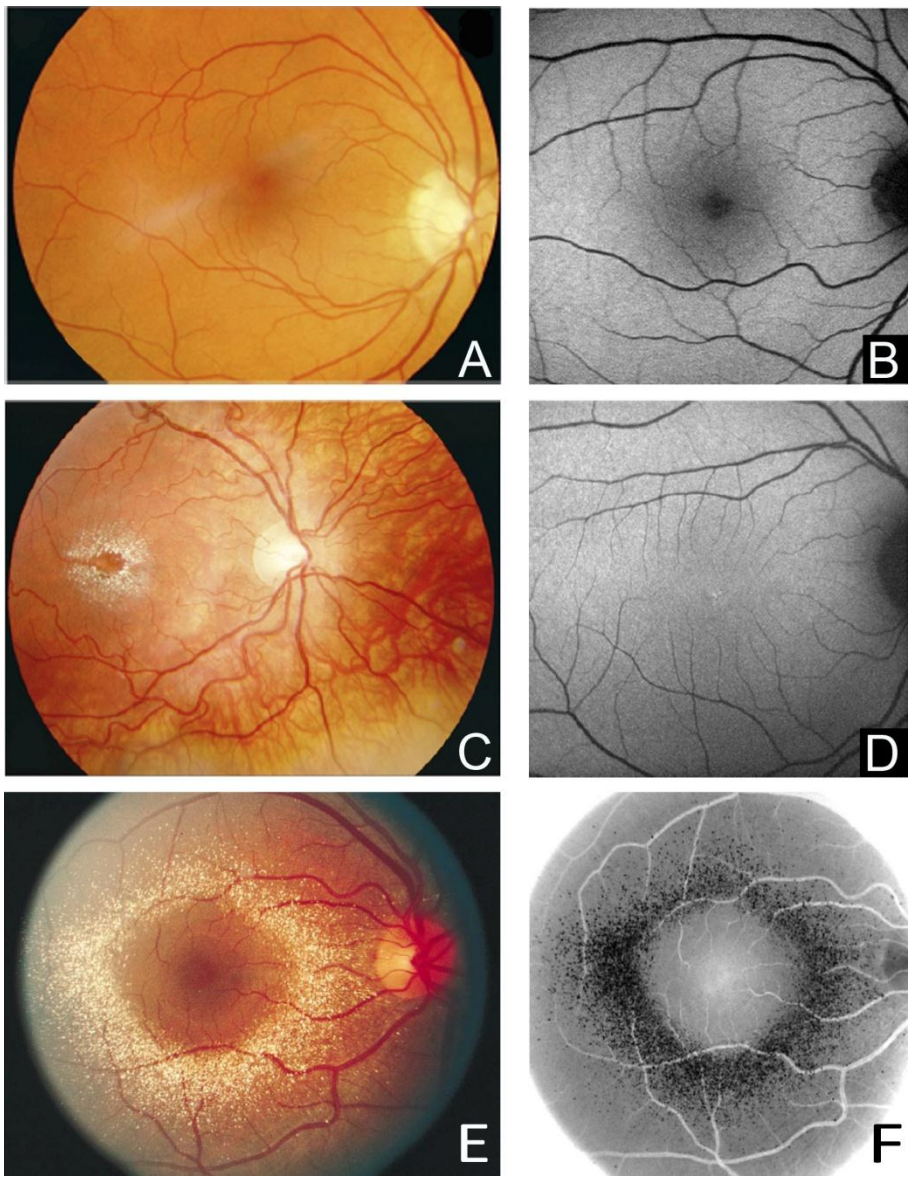

Figure 1.6. Clinical presentation of Sjögren Larsson Syndrome and Canthaxanthin retinopathy.

Retinal imaging shows no crystal deposits in a control retina (**A**) and macular pigment (dark central shadow) present at the fovea/macula (**B**). The same imaging modalities show inter retinal crystals (**C**) and pan retina loss of macular pigment in a patient with Sjögren Larsson Syndrome (**D**). Canthaxanthin retinopathy is characterised by retinal crystals, present in the macula, but excluded from the parafoveal region (**E**). Red free fundus photography (**F**) highlights the crystals better than normal fundus photography (**E**). Images adapted from van der Veen *et al.*[179] (**A**-**D**) and Espaillat *et al.*[247] (**E** and **F**).

2. Histopathology of Macular Telangiectasia type 2

The results reported in this chapter have been published in:

Powner MB, Gillies MC, Tretiach M et al. Perifoveal muller cell depletion in a case of macular telangiectasia type 2. Ophthalmology 2010;117(12):2407-2416.[248]

Len ACL, **Powner MB**, Zhu L, Hageman GS, Fruttiger M, Gillies MC. Pilot application of iTRAQ coupled with mass spectrometry to the retinal disease Macular Telangiectasia. *(in Press)*

2.1 Introduction:

Macular telangiectasia (MacTel) has been poorly understood and often misdiagnosed until recent years. Gass and Blodi[143] first proposed a classification of the disease (also known as idiopathic juxtafoveal telangiectasis) in 1993, in which they clearly distinguished type 1 from type 2. The two types were found to be distinctly different disease phenotypes; Type 1 usually occurs unilaterally and is largely restricted to males, whereas MacTel type 2 is bilateral and has no sex predilection. The clinical appearances also differ, type 1 is characterised by pronounced hyperpermeability and cystoid oedema and retinal thickening. Whereas loss of retinal transparency and small telangiectatic vessels, (identifiable only by fluorescein angiography), represent early signs of MacTel type 2. Intraretinal pigment clumping, parafoveal atrophy, and vascular membranes represented a secondary phenomenon only in type 2.

Little research was focused on the disease until about 6 years ago when a worldwide collaboration was established between clinicians and basic research scientists, to focus research efforts in understanding the clinical and pathological aspects of this disease with, of course, the end goal of a therapeutic intervention. As mentioned previously, studies on living patients have gathered a lot of new information in recent years, with the finding of macular pigment depletion from the central macula, new imaging techniques; including confocal blue reflectance and OCT allowing the disease to be diagnosed more accurately. Updated clinical criteria for the diagnosis of Macular Telangiectasia type 2 was published by Yannuzzi et al[142] in 2006. Early stage disease was classified as a patient having mild loss of transparency of the retina perimacularly, normally originating temporal to the fovea. Also early stage disease is characterised by mild leakage of perimacular capillaries in late stage fluorescein angiography, however no visible capillary dilation and telangiectasis need be visible. Late stage disease sees the progression of the loss of macular transparency to include a full ellipse surrounding

the fovea. Visible macular capillary dilation will be noted and more severe leakage seen with fluorescein angiography.[142]

However the existing knowledge about MacTel type 2 pathobiology is restricted in that it is based upon the observations from living patients. There is only one published clinico-pathological study of a confirmed MacTel type 2 case. In this case a 58 year old female with no ophthalmic complaints was found to have MacTel type 2 on routine examination before undergoing maxillectomy and orbital exenteration for squamous cell carcinoma of her left eye.[249] Light microscopic examination revealed no telangiectatic vessels, however they did observe retinal thickening, (due to marked proliferation of the basement membrane), in the inner retinal layers of the macular area. Capillaries were also noted to be present as far down as the photoreceptor layer, a region normally avascular in the retina, and this confirmed the findings from patients, where right angled venules are seen. Oedematous and cystic changes were present in the OPL that extended into the outer nuclear layer (ONL). Ultrastructural analysis of blood vessels in the clinically affected perifoveal zone revealed damaged capillaries with an almost total lack of pericytes and occasional reduced endothelial cell numbers. Furthermore, occasional loss of pericytes and multi-laminar capillary basement membrane with lipid inclusions and debris containing vacuoles was observed throughout the retina. The authors noted that these features were similar in many respects to those of diabetic retinopathy. A second case study of presumed MacTel type 2 has been carried out on a postmortem specimen from a 36 year old woman with Down's syndrome. However, this case was not clinically diagnosed as MacTel type 2. The authors described macular oedema and telangiectatic vessels with partial degeneration of endothelium and pericytes.[250] They also noted proliferation of vessels into the subretinal space, with occasional retinochoroidal vascular anastomosis and corresponding migration of RPE cells into the neural retina.[250] Neither of the two cases reported so far used immunohistochemistry to identify individual cell types in the retina. Therefore an attempt was made to obtain a further postmortem MacTel type 2 specimen by reviewing the records of the Iowa City - Lions Eye Bank, held by Gregory Hageman. This revealed one case with a definite diagnosis of MacTel type 2, based upon the clinical notes made by a retinal specialist and supported by fluorescein angiography photos. This chapter describes the histopathology of MacTel type 2 in greater detail, identifying individual cell populations and distribution patterns in comparison to matched controls.

2.2 Aim:

To gain insight into the retinal histopathological features of MacTel type 2.

2.3 Materials and Methods:

Institutional Review Board (IRB)/Ethics Committee approval for postmortem eye tissue collection and storage at the UCL Institute of Ophthalmology, Universities of Sydney and University of Iowa Department of Ophthalmology was in place.

All reagents used were from Sigma, UK, unless otherwise stated.

Technical acknowledgements: I would like to thank Greg Hageman, University of Iowa, for the provision of the clinical images used in this chapter, and also Mark Gillies, University of Sydney, for the provision of the pre-sectioned tissue of the MacTel type 2 sample.

2.3.1 Donors and tissue processing

The MacTel type 2 specimen used in this study had a postmortem time of 4 hours 12 minutes before fixation by submersion into 4% (w/v) paraformaldehyde (PFA). The right eye was fixed for histological analysis whereas the left eye had been frozen unfixed and has been used for biochemical analysis by our collaborators in Australia. Dissection removed the anterior pole of the eye after which the posterior was flattened (using four radial incisions) and photographed.

Control eyes for the macroscopic appearance and macular pigment distribution were provided by an anonymous 67 year old donor (cause of death: lung cancer, no reported ophthalmic pathology) and a 75 year old donor with a diagnosis of unilateral Coat's disease in the left eye (based on fluorescein angiogram and the presence of microaneurysms in the left macula, not shown). Control eyes for fluorescent immunohistochemistry were obtained from the right eye of a 79 year old male donor (cause of death: lung cancer) with no reported ophthalmic problems, retrieved and fixed in 2% PFA 13 hours after death. DAB immunohistochemistry was performed on the right eye of a 68 year old male donor (cause of death: intracranial haemorrhage, no reported ophthalmic problems) retrieved and fixed in 2% PFA 9 hours after death. A further control eye from a 78 year old type 2 diabetic patient without diabetic retinopathy (cause of death: stroke) was fixed 9 hours after death in 2% PFA. An additional control eye from a 71 year donor (cause of death: cerebrovascular accident) with a history of diabetic retinopathy, laser surgery and intraocular lens replacement, was fixed under 12 hours after death in 2% PFA. To test the effects of postmortem fixation delay, both eyes from a 63 year old male donor, (cause of death: prostate cancer, no reported ophthalmic pathology), were used; the right eye was taken and

fixed 8 hours postmortem, whilst the left eye was kept at room temperature in sterile PBS for 48 hours before fixation.

A region of the posterior globe that included the optic disc, fovea and a section of nasal periphery was dissected and placed into slow running water for 24 hours before paraffin wax embedding. The fixed tissue was dehydrated through graded alcohols and xylene before embedded in paraffin wax using a LEICA TP1020 automatic tissue processor (Leica, UK). Naso-temporal sections were cut at 6µm and collected onto Superfrost® plus slides (VWR, UK). Sections were deparaffinised using xylene. Sections for fluorescent immunohistochemistry or haematoxylin and eosin (H&E) staining were rehydrated through graded alcohols. Sections for DAB immunohistochemistry were first incubated in 3% H_2O_2 in glacial methanol for 30 minutes (to block endogenous peroxidases) prior to rehydration.

2.3.2 Antigen retrieval

Long periods in fixative and the wax embedding of the tissue meant that antigen retrieval methods were required prior to immunohistochemical analysis. Each antibody required slightly different retrieval conditions. Sections where antibodies directed against GS, RLBP1 and collagen IV were to be used required heating to a minimum of 125°C in 90% glycerol (molecular grade, Sigma, UK) and 10% 0.01M sodium citrate buffer pH6.0 for 20 minutes. Claudin-5 immunostaining required 129°C for 15 minutes, whereas GFAP, vimentin, ML-opsin and rhodopsin immunostaining required heating to a minimum of 120°C for 15 minutes in the same buffer. Eno1, Cox2 and LDHB immunostaining required heating to 135°C for 10 minutes in 90% glycerol (molecular grade, Sigma, UK) and 10% 0.01M sodium citrate buffer pH6.0. Iba1 immunostaining however required heating to 128°C for 10 minutes in 10% 0.1M Tris EDTA buffer (10mM Tris-Base, 1mM EDTA, 0.05% Tween20) pH9.0 in Glycerol.

2.3.3 Fluorescent labelled immunohistochemistry

All incubations were carried out in a dark humidified chamber. Following antigen retrieval, sections were briefly washed in water, incubated for 1 hour at room temperature in blocking buffer (1% BSA, 0.5% triton X-100 in PBS) and then in primary antibody (diluted in blocking buffer, Table 2.1) either at room temperature for 1 hour or overnight at 4°C. Sections were washed in washing buffer (0.1% tween20 in PBS) and incubated for 1 hour at room temperature in secondary antibodies (Invitrogen, UK, diluted 1:200 in blocking buffer).

Subsequently sections were washed in washing buffer, treated with Hoechst (10µg/ml in washing buffer) for 30 seconds, washed finally in PBS and mounted in Citifluor mounting medium (Agar Scientific, UK) or Mowiol. Images were taken using a Leica DM IRB fluorescent microscope (Leica, UK) and/or a Zeiss LSM510 UV confocal microscope (Zeiss, UK).

2.3.4 DAB Immunohistochemistry

Following endogenous peroxidase blocking and antigen retrieval, sections were briefly washed in water, incubated for 1 hour at room temperature in 100% normal serum (species dependant on secondary antibody used), then into primary antibody diluted in 100% normal serum for 1 hour at room temperature (Table 2.1 for antibody information). Sections were washed in PBS. The sections were subsequently stained using VECTASTAIN Elite ABC kits (Vector labs, UK); sections were treated as per manufacturer's guidelines from the secondary antibody incubation step. Sections were incubated for 30minutes in biotinylated secondary antibody, 1:200 in 1.5% normal serum in PBS. Sections were washed in PBS and then incubated in VECTASTAIN® Elite ABC Reagent (Vector Labs, UK) at room temperature for 30minutes. To develop the stain, slides were washed in PBS and incubated with SIGMA*FAST*™ 3,3'-Diaminobenzidine (DAB) tablets dissolved in dH_2O for 30-60seconds or until the stain darkened sufficiently. They were then mounted in glycerol and imaged.

2.3.5 Nuclei counting

Haematoxylin and eosin (H&E) stained sections were used to count the number of cell nuclei in the inner nuclear layer. Section numbers 140, 143 and 150, through the macula, superior to the fovea from the MacTel type 2 specimen were counted. As a control, three macula sections from the corresponding superior/perifoveal region from an age matched control donor were analysed. The distance between the fovea and optic disc edge was measured and split into 20 equal sized segments. The number of nuclei within the inner nuclear layer were counted in 15 segments temporal to the fovea and in 15 segments nasal to, and including the fovea. The values for each segment were averaged for the MacTel type 2 sections and the control sections, and the most nasal segment was used for normalization to 100%. Statistical analysis was performed using Student's t-test.

2.4 Results:

2.4.1 Clinical features

The 65 year old male donor, who died from a cerebrovascular accident, had a history of type 2 diabetes, hyperlipidemia and hyperthyroidism. He had a family history of age-related macular degeneration, however no features of diabetic retinopathy (DR) or macular degeneration were described in the ophthalmologist's notes, nor were there any features of DR evident in the available colour photographs and fluorescein angiograms, or evidence upon gross examination. The donor was diagnosed with MacTel type 2 by a retinal specialist 12 years prior to death. An angiogram available from that time shows typical features of MacTel type 2 (Fig. 2.1). Telangiectatic vessels were observed in the temporal perifoveal area early in the angiogram with more widespread diffuse staining of the entire perifoveal area in later images. Visual acuity was 20/25 OD, 20/40 OS. These readings were unchanged at the last recorded clinic visit, 10 years before death.

2.4.2 Macroscopic appearance of the retina

Photographs of dissected postmortem eyes (unfixed) revealed a loss of macular pigment in the MacTel type 2 retina (Fig. 2.2 A, B). Remaining macular pigment (white arrows in Fig. 2 A, B) was clearly visible as a ring around the fovea, with a sharp in inner boundary and more diffuse towards the periphery. Control retinas from an anonymous donor, with no reported ophthalmic pathology, have macular pigment concentrated as a yellow/brownish dot in the centre of the macula at the fovea (Fig. 2.2 C, D). A patient with Coat's disease in the left eye had a normal appearance of macular pigment in both eyes (Fig. 2 E, F). Depletion of macular pigment (with the most pronounced alterations in the temporal perifoveolar region) has, as I've previously stated, been described by Helb *et al* (2008) to be a specific and early clinical feature of MacTel type 2.[138, 246, 251, 252] The macular pigment depletion seen in this post-mortem case further confirms the nature of the changes to macular pigment distribution in MacTel type 2, and in combination with the fluorescein angiogram identify the MacTel type 2 sample as a definite case of MacTel type 2.

2.4.3 Retinal vasculature

Serial sections from an eye were immunolabelled with Collagen IV to reveal the vascular profiles to observe the previously noted abnormal vessels, since these are a notable characteristic of MacTel Type 2. Leakage of fluorescein from perifoveal blood vessels (arrowheads in Fig. 2.1) indicates presence of the telangiectatic vessels characteristic of the

disease. Wax sections serially cut from the right eye were used to study the nature of the telangiectatic vessels further. However the location of this region of retina first had to be established to ensure the vessels studied correlated to those seen to be permeable to fluorescein. To this end some of the sections were stained with an antibody directed against collagen IV to reveal vascular profiles (Fig. 2.3 A). The naso-temporal position of all major vessels (insets in Fig. 2.3 A) was mapped in the sections (red dots in Fig. 2.3 A) and then matched with the angiogram (Fig. 2.3 B). The specific distribution of main vessels in the naso-temporal axis allowed identification of the approximate position in the superior-inferior axis of each wax section on the angiogram (numbered scale in Fig. 2.3 B).

H&E staining of some of the sections revealed blood-filled, abnormally dilated vessels in the deeper plexus of the retinal vasculature (sections 140 and 150; Fig. 2.3 C-E). These abnormal vessels were limited to the clinically affected, perifoveal region and particularly pronounced temporal to the fovea, but were not present in the periphery. Furthermore, they were limited to the deeper plexus whilst vessels in the RGC layer were of normal diameter throughout the retina. The specimen showed a tendency to splitting in the horizontal plane throughout the macular region. Whether this is a tissue processing artefact or due to structural changes inherent in the condition is not clear, although this is unlikely as the eye was immersion fixed and the more peripheral regions are well preserved.

Collagen IV, marking vascular basement membrane, and claudin-5, marking tight junctions between retinal endothelial cells were used to further characterise these telangiectatic vessels (Fig. 2.4 A-G). Claudin-5 immunoreactivity was visible in all vessels (arrowheads Fig. 2. 4 B, D, F), despite uniform, strong autofluorescence in the lumen of many vessels. Claudin-5 is a protein involved in tight junction formation between endothelial cells, its immunoreactivity in both normal and dilated vessels indicates the presence of endothelial cells in both (stars in Fig. 2.4 D, F). However, telangiectatic vessels appeared to have reduced collagen IV staining in comparison to normal vessels within the same specimen in the unaffected peripheral retina (Fig. 2.4 D-G). This reduction in the basal lamina component collagen IV was only seen in deeper plexus vessels in the perifovea. However, other abnormalities were also noted. Small vacuoles within vascular basal lamina were noted in single confocal slices (arrows Fig. 2.4 E, G) in most macular vessels but also to some degree in the periphery (Fig. 2.4 C).

2.4.4 Microglia

In order to assess whether an inflammatory component may contribute to the vascular abnormalities characteristic of the MacTel type 2 retina, we used the microglia marker Iba1 [253] (Fig. 2.5 A-H). In a control retina from a healthy donor Iba1-positive microglia were found in the RGC layer, the IPL and the INL (Fig. 2.5 A-D). Microglia were often associated with blood vessels, consistent with previous studies.[254, 255] The distribution of Iba1-positive microglia in the MacTel type 2 retina was similar to the control and no obvious changes in microglia number or morphology were noted. Even around abnormal vessels (arrowheads Fig. 2.5 G, H) the density and morphology of macrophages appeared normal.

2.4.5 Glia

An antibody directed against glial fibrillary acidic protein (GFAP) was used to visualize retinal astrocytes. In the healthy control eye (Fig. 2.6 A-D) retinal astrocytes were found in their expected distribution in the nerve fibre layer, the RGC layer and in the IPL. The strong GFAP positive signal visible in the fovea (Fig. 2.6 C) is likely to be a manifestation of the so-called Müller cell cone [256] and not retinal astrocytes as they are normally excluded from the fovea.[86] In the nasal retina the IPL exhibited particularly pronounced astrocyte staining with prominent perpendicular processes into the retina (Fig. 2.6 D). These processes did not appear to be from Müller cells since they only extended to the boundary between the IPL and the INL. In the MacTel type 2 retina (Fig. 2.6 E-H) retinal astrocytes seemed to be distributed in a similar fashion as in the control specimen. They were associated with nerve fibres and blood vessels in the RGC layer and the IPL. There was no Müller cell cone but this may have been because the section examined did not contain the fovea.

Müller cells normally express GFAP only at very low levels and in healthy retina they are barely detectable by immunohistochemistry. Nevertheless we found a very faint stain in Henlé's fibre layer (arrow Fig. 2.6 B). However, GFAP is known to be strongly upregulated by reactive Müller cells and is therefore a popular marker to detect certain retinal pathologies.[257, 258] Remarkably, no evidence of reactive Müller cells was found in the MacTel type 2 retina (Fig. 2.6 E-H).

Müller cell distribution was then visualized with an antibody directed against vimentin (Fig. 2.7 A, B). In the control retina strong consistent staining was visible throughout the macula and peripheral retina, consistent with the expected distribution of Müller cells. However, in the MacTel type 2 specimen vimentin immunoreactivity was markedly reduced in the macula (Fig. 2.7 B). This lack of staining could either be an indication of downregulation of vimentin

or a gross loss of Müller cells. To further elucidate this two other Müller cell markers, glutamine synthetase (GS, Fig. 2.7 C) and retinaldehyde binding protein (RLBP1 also known as CRALBP, Fig. 2.7 D) were used. A clearly demarcated area in the central macula exhibited reduced staining with both antibodies, suggesting Müller cell dropout in a specific macular region in this MacTel type 2 eye.

Postmortem degenerative changes could be argued to be the cause of the loss of Müller cell staining at the macula of the MacTel type 2 eye, and therefore the finding could be an artifact. Although the MacTel type 2 eye was enucleated and fixed 4 hours after death and showed normal Müller cell staining in the periphery it cannot be entirely excluded that the macula could be particularly sensitive to postmortem artifacts, especially due to the reported higher metabolic demands in this region.[259, 260] In order to address this possibility, an enucleated postmortem eye was kept in an unfixed state for a further 48 hours at room temperature in phosphate buffered saline (PBS) after enucleation, before standard processing for immunohistochemistry was carried out. Müller cell staining was not affected in the macula of this eye (Fig. 2.7 E). Furthermore, because the MacTel type 2 donor had a history of type 2 diabetes, the distribution of the three Müller cell stains was checked in two control eyes from type 2 diabetes patients, one with and one without diabetic retinopathy, and found normal distribution of Müller cells (data not shown).

Since it became apparent that there was a clearly defined Müller cell loss from the macula, and there was also macular pigment depletion with a clearly defined inner boundary, it was logical to attempt to spatially correlate the macular pigment ring with the region of Müller cell loss. The colour photograph (from Fig. 2.2 A) was scaled and matched to the angiogram using small traces of blood in the macular region (Fig. 2.7 F-H), and then superimposed the area of macular pigment depletion onto the angiogram (green patch in Fig. 2.7 H). Since the approximate position and scale of each cross-section was already mapped within the angiogram, it was possible to show that the lack of Müller cell staining correlated with the area of macular pigment loss (Fig. 2.7 H).

In order to further test whether the disappearance of Müller cell markers represents a lack of cells in the macula, H&E stained sections were used to count the number of cell nuclei in the inner nuclear layer (Fig. 2.7 I). In a control retina we found a drop in the fovea and a slight increase of cell nuclei numbers either side of the fovea in the perifoveolar region. In the MacTel type 2 sample numbers were lower throughout the macula relative to the periphery, and when scaled to the macular pigment loss and vimentin stain, this region of decreased cell

nuclei numbers closely correlates to the region of Müller cell loss, suggesting that cells - most likely Müller cells - were missing or reduced in number.

Our collaborators Prof. Mark Gillies and Dr. Alice Len at the Save Sight Institute, University of Sydney, Australia have carried out a biochemical analysis of the fellow eye from this MacTel type 2 donor (from which the macula and peripheral samples were fresh frozen at the point of enucleation). Their comparative proteomic analysis highlighted numerous proteins from the glycolytic pathway as being downregulated in the macula biopsy when compared to the expression pattern between macula and peripheral retina seen in healthy control and diabetic retinas (data not shown). This prompted us to further investigate the distribution patterns of some of these glycolytic pathway proteins in the fellow MacTel type 2 eye from the same patient we were using. Antibody staining against two selected glycolytic enzymes (enolase 1; ENO1 and lactate dehydrogenase B; LDHB) in control tissue from a diabetic control patient and a normal donor was consistent with Müller cell specific expression, displaying strong staining of perpendicular fibres (black arrowheads in Fig. 2.8 D, E, G, H) and Henlé fibres (white arrowheads in Fig. 2.8 D, E, G, H). Furthermore, ENO1 staining was also strongly expressed in a cell population in the inner nuclear layer, the layer of Müller cell soma are located (arrows in Fig. 2.8 D, G, M, P). ENO1 and LDHB staining were both significantly depleted in the macular region of the MacTel type 2 sample (Fig. 2.8 A, B) but peripheral retina staining was persistent in the diseased eye (Fig. 2.8 J, K). In contrast, staining against COX2 (part of the oxidative phosphorylation pathway and a neuronal marker) showed no change in the diseased macula (Fig. 2.8 C, L).

2.4.6 Photoreceptors and retinal pigment epithelium (RPE)

It has been published that MacTel type 2 patients suffer from reduced retinal sensitivity and reduced visual acuity, [261-263] as such we studied the photoreceptors in our MacTel type 2 specimen to establish if any such cause of visual problems could be determined. As expected, in the control specimen anti-rhodopsin immunostaining showed rods were excluded from the fovea, but clearly visible in the macula and throughout the periphery, whereas cones were concentrated in the fovea (Fig. 2.9 A-D). The anti ML-opsin antibody from Chemicon used not only labels cone outer segments but also the entire cell, including synaptic bodies and axonal connections in the OPL and Henlé fibre layer (Fig. 2.9 C, D). In the MacTel type 2 eye the distribution of rods and cones was similar to the control eye. The presence of ML-opsin staining in Henlé fibre layer was reduced but indicated the presence of at least some cone axons in the macula (Fig. 2.9 G, H). ML-opsin staining was also strongly present in the

fovea (Fig. 2.9 H) but due to poor preservation of photoreceptors in all of our samples it was not possible to ascertain whether there was a reduction of cone numbers in the MacTel type 2 fovea.

The structural integrity and general appearance of the RPE (not shown) was checked in all sections studied from the MacTel type 2 specimen and, as observed in the previous two MacTel type 2 case studies [249, 250], no obvious abnormalities were found.

2.5 Discussion:

The results listed are limited in that they are from a single case of MacTel type 2, however they are still crucial in further understanding the disease. With no other histological case reports to date that have addressed the cell types involved, and that diagnosis of the condition relies on gathering a pattern of patient signs and symptoms that may sometimes result in an equivocal diagnosis any information gathered can advance the understanding significantly. Furthermore, lack of insight into the cause of the disease impedes the development of treatment strategies. Hence our study, though limited to one patient, is important in this field. We have extended the findings of the two previous clinicopathological reports of MacTel type 2 by performing immunohistochemical analysis on an eye derived from a clinically verified MacTel type 2 donor, thereby providing new information about the pathogenesis of this obscure condition. The most striking finding was one of depleted expression of Müller cell specific markers in the central macula compared to both peripheral retina and control samples. Expression of other markers, such as rhodopsin, ML-opsin, COX2, GFAP and others was normal in the central macula of the affected eye. This suggests that the reduction of Müller cell markers does not represent general tissue degeneration or fixation artifacts within the macular region, but instead is a specific indication of Müller cell pathology. The glycolytic pathway is known to be dominant in the glial cells of the retina, while the neurons produce their ATP primarily via oxidative phosphorylation.[264] Glycolysis in Müller cells converts glucose (derived from the blood) into lactate,[265, 266] which is then secreted by the Müller cells and preferentially taken up by photoreceptors to fuel mitochondrial oxidative metabolism and the glutamate resynthesis.[267] The absence of the glycolytic enzymes ENO1 and LDHB within central macula from the affected eye (Fig. 2.8 A, C) further supports the Müller cell loss conclusion. The decreased expression of the two enzymes is restricted to the central macula and the cell morphology seen in control samples indicates Müller cell localisation. Müller cells being the primary source of lactate for photoreceptor function and survival serves to link the pathology of the disease to the effects

on visual function seen in patients in clinics. Over time, if Müller cell death is occurring, then lactate levels for photoreceptors of the macula will decrease in localised regions, therefore potentially limiting photoreceptor function for the patient and a decrease in visual acuity.

Furthermore, we have been careful to compare findings from macular and extra macular regions of the MacTel type 2 eye with controls from healthy patients, a patient with type 2 diabetes and no retinopathy, a patient with diabetic retinopathy and a sample with a very long postmortem delay before fixation to try to ensure the specificity of changes to MacTel type2.

The apparent Müller cell loss observed in the MacTel type 2 sample is consistent with the reduced numbers of cell nuclei counted in the INL, and is also consistent with the retinal thinning observed with optical coherence tomography (OCT) in living patients.[268] In contrast, both previous MacTel type 2 histology case reports reported oedematous thickening of the macula [249, 250]. Our MacTel type 2 sample was split and abnormally thickened, particularly in the macular region. This discrepancy between in vivo and histological observations might be explained by fixation or tissue processing artifacts. It is more likely that increases in retinal thickness in vivo are masked by the cellular loss in the MacTel type 2 macula.[269]

Müller cells do not comprise a cellular entity that can be visualised upon clinical examination, however the consequences of Müller cell loss and/or dysfunction might well be detectable *in vivo*. Since Müller cells are intimately related to the retinal vasculature, it is quite possible that their dysfunction would be associated with clinically visible telangiectasis. Müller cells also interact very closely with retinal neuronal cells; for example, they recycle the toxic neurotransmitter glutamate to glutamine.[270] It is therefore also plausible to suggest that Müller cell degeneration would be accompanied by loss of neurons in MacTel type 2 as was suggested by recent findings in patients examined with OCT.[271] This might also be linked to the progressive central macular thinning observed clinically in MacTel type 2 patients.[268]

Gass drew attention to the “Müller cell cone”, a layer of Müller cells sitting above the Henlé fibre layer immediately beneath the inner limiting membrane (ILM) in the base of the foveal depression, which he further postulated to be the major location for sequestration of macular pigment.[256] Disease of the Müller cells in this case may explain the “ILM drape”, or cavities within the inner neural retina in this location that are commonly found in eyes with MacTel type 2 on optical coherence tomography,[145, 149, 272] as well as the loss of macular pigment.[138, 252]

Müller cell processes envelope retinal blood vessels in the deeper plexus of retinal vasculature and are believed to contribute to induction of blood retina barrier integrity.[51, 55] Blood vessels in the RGC layer are thought to be supported more by retinal astrocytes.[273] Thus, the observed limitation of vascular abnormalities to the deeper plexus of the retinal vasculature is consistent with a Müller cell dysfunction, supporting Gass' suggestion that the primary abnormality may reside in the perifoveolar neuronal retina or Müller cells.[274] Further research studying the effects of Müller cell loss/disruption in animals models will be key to understanding the underlying mechanisms involved in this disease.

It is noticeable that the histological findings and the macroscopic appearance of the MacTel type 2 specimen correlated well with the angiogram, which was taken 12 years prior to the donor's death. This suggests that the disease was slowly progressive in this patient, who had not developed late stage complications of MacTel type 2 such as neovascularisation and retinal pigment invasion by the time of death.[143] Abnormally dilated vessels in this patient were primarily found in the deeper plexus of the retinal vasculature, which is characteristic of the early stages of MacTel type 2. The presence of claudin-5 in these abnormal vessel segments implies the presence of at least some endothelial cells but should not be interpreted to reflect functional blood retina barrier.[275] Green et al. noted normal zonula occludens in telangiectatic vessels but also occasional endothelial cell drop out,[249] which could not be excluded in our specimen. Nevertheless, the dramatic reduction of collagen IV in telangiectatic vessels clearly indicates some form of vascular pathology which might be associated with pericyte dysfunction. Like Green *et al*., [276] we also found subtle vascular changes in the retinal periphery such as small vacuoles in the vascular basement membrane, which will be the focus of chapter **3**.

Table 2.1: Primary antibodies

Antibody	Company	Cat. #	Dilution
Glia			
Retinaldehyde binding protein (RLBP1 or CRALBP)	AffinityBioReagents, UK	MA1-813	1:200
Enolase 1 (ENO1)	Abcam, UK	ab49343	1:200
Glial fibrillary acidic protein (GFAP-Cy3)	Sigma, UK	C9205	1:200
Glutamine synthetase (GS)	Chemicon, UK	MAB302	1:200
Lactate dehydrogenase B (LDHB)	Abnova, UK	H00003945-M01	1:50
Vimentin-Cy3	Sigma, UK	C9080	1:200
Ionised calcium binding adaptor molecule 1 (Iba1)	Biocare Medical, UK	CP290A	1:200
Vasculature			
Collagen IV	AbD serotec, UK	2150-0140	1:200
Claudin-5	Molecular probes, Invitrogen, UK	35-2500	1:200
Photoreceptors			
ML-opsin	Chemicon, UK	AB5405	1:200
Rhodopsin	Chemicon, UK	MAB5356	1:200
Oxidative phosphorylation			
Cytochrome *c* oxidase 2 (COX2)	Molecular probes, Invitrogen, UK	A6404	1:200

Table 2.1. List of primary antibodies, suppliers and dilutions used.

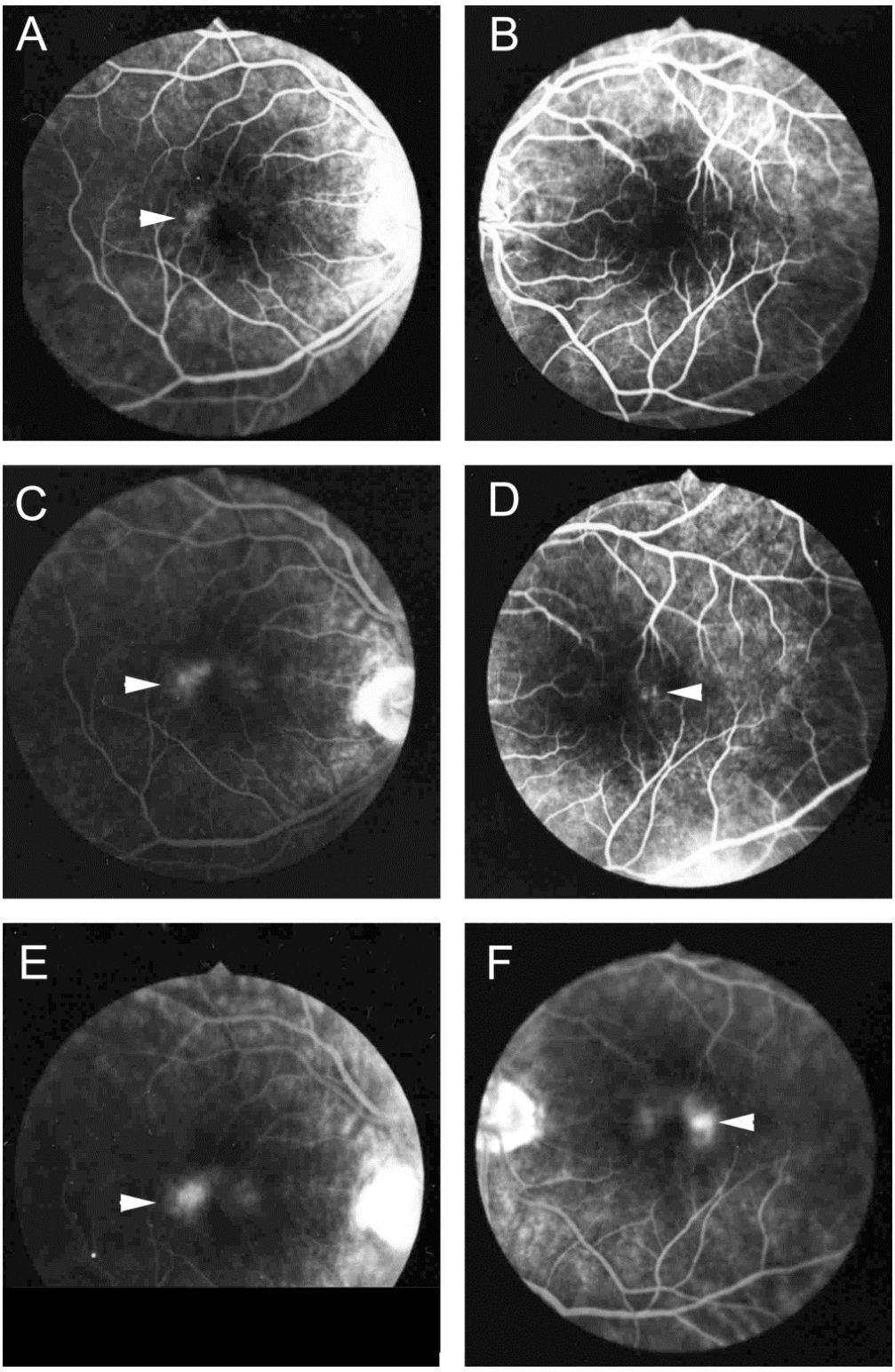

Figure 2.1. MacTel type 2 fluorescein angiograms
Angiogram of the right (**A, C, E**) and left eye (**B, D, F**) showing fluorescein leakage in the perifovea (arrowheads). The leakage is particularly prominent temporal to the fovea, which is characteristic for MacTel type 2. Images provided by Gregory S Hageman, University of Iowa.

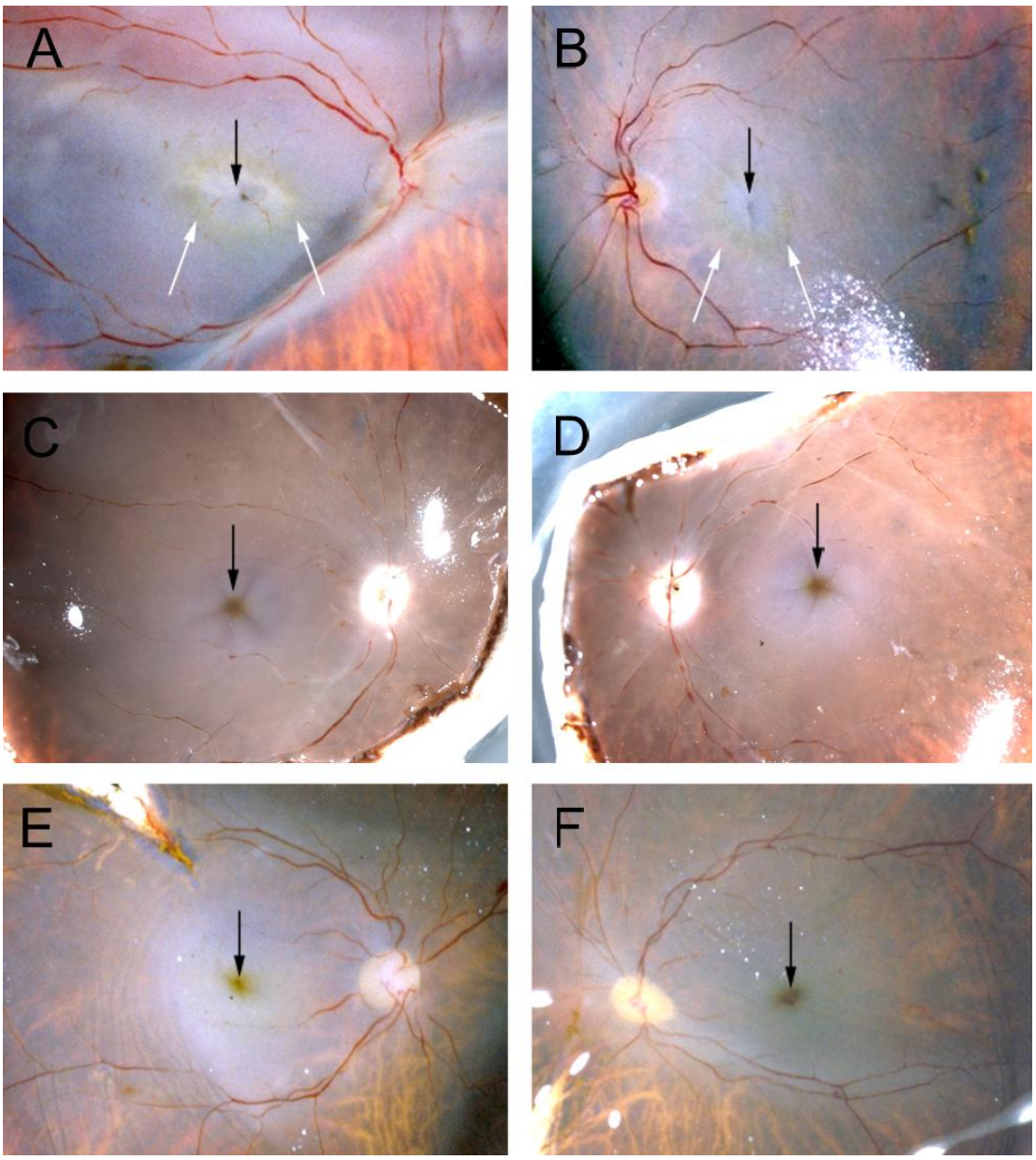

Figure 2.2. Macular pigment

Photographs of dissected eye globes from three different donors before fixation showing the distribution of macular pigment. In the MacTel type 2 patient (**A, B**) macular pigment is absent from the centre of the macula (black arrows) but faintly visible as a perifoveolar ring (white arrows). In contrast, in the two control donors (**C-F**) the highest concentration of macular pigment is found in the fovea (black arrows). Images A, B, E and F were provided by Gregory S Hageman, University of Iowa.

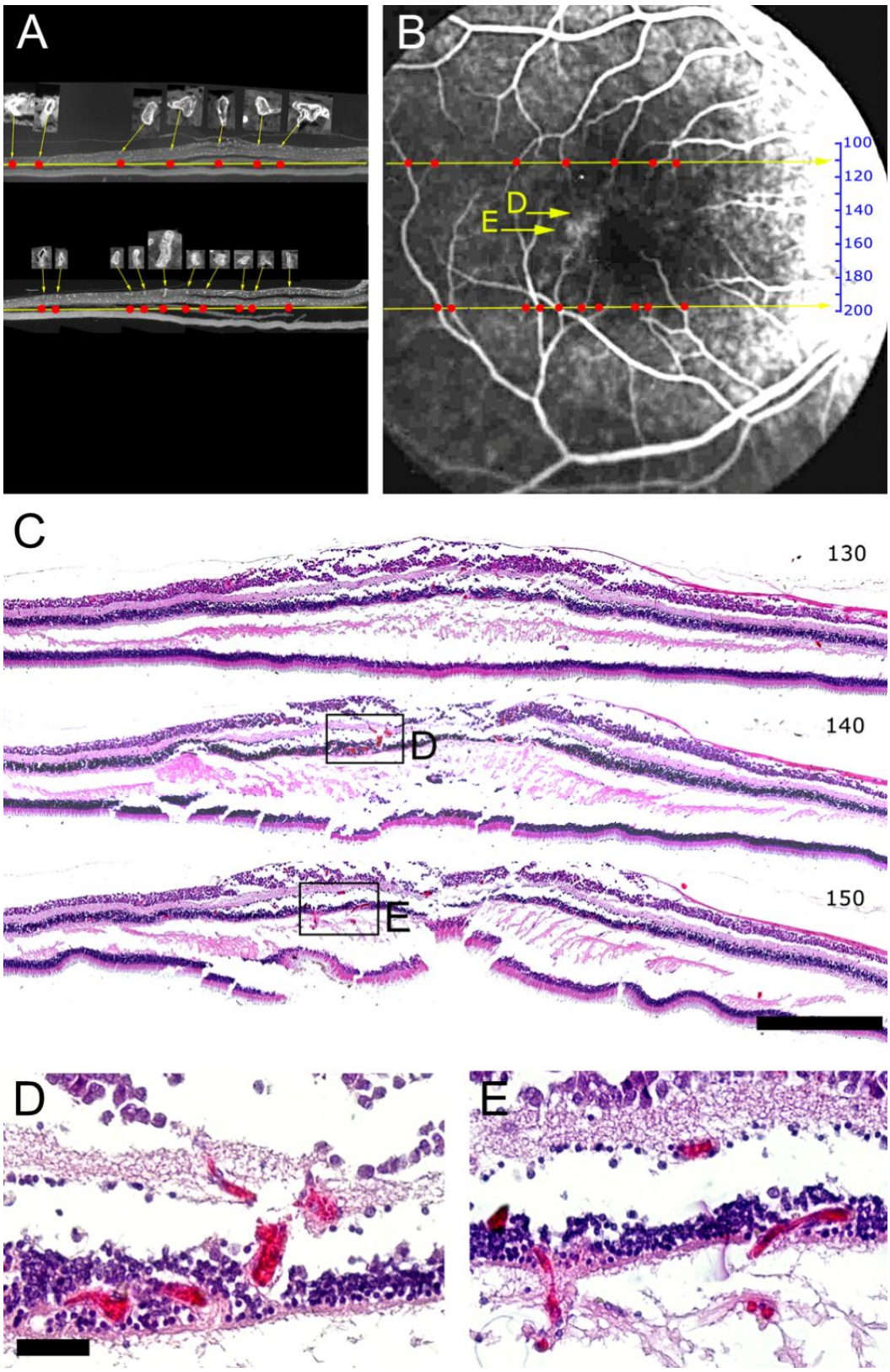

Figure 2.3. Mapping of wax sections onto the angiogram.
Two sections (110, superior, and 198, inferior to the macula) stained against collagen IV show the distribution of vessels (**A**). Larger vessels were identified (insets in **A**) and plotted as red dots in the naso-temporal axis. The distribution of red dots was used to define the superior-inferior position of the two sections and to position a scale that gives the approximate

position of every section in the angiogram (**B**). H&E stains of three sections (**C**, section 130, 140 and 150) shows that vascular abnormalities (visible at higher magnification in **D, E**) match well to fluorescein leakage visible in the angiogram (yellow arrows in **B**). Scale bar is 500μm in **C** and 50μm in **D**.

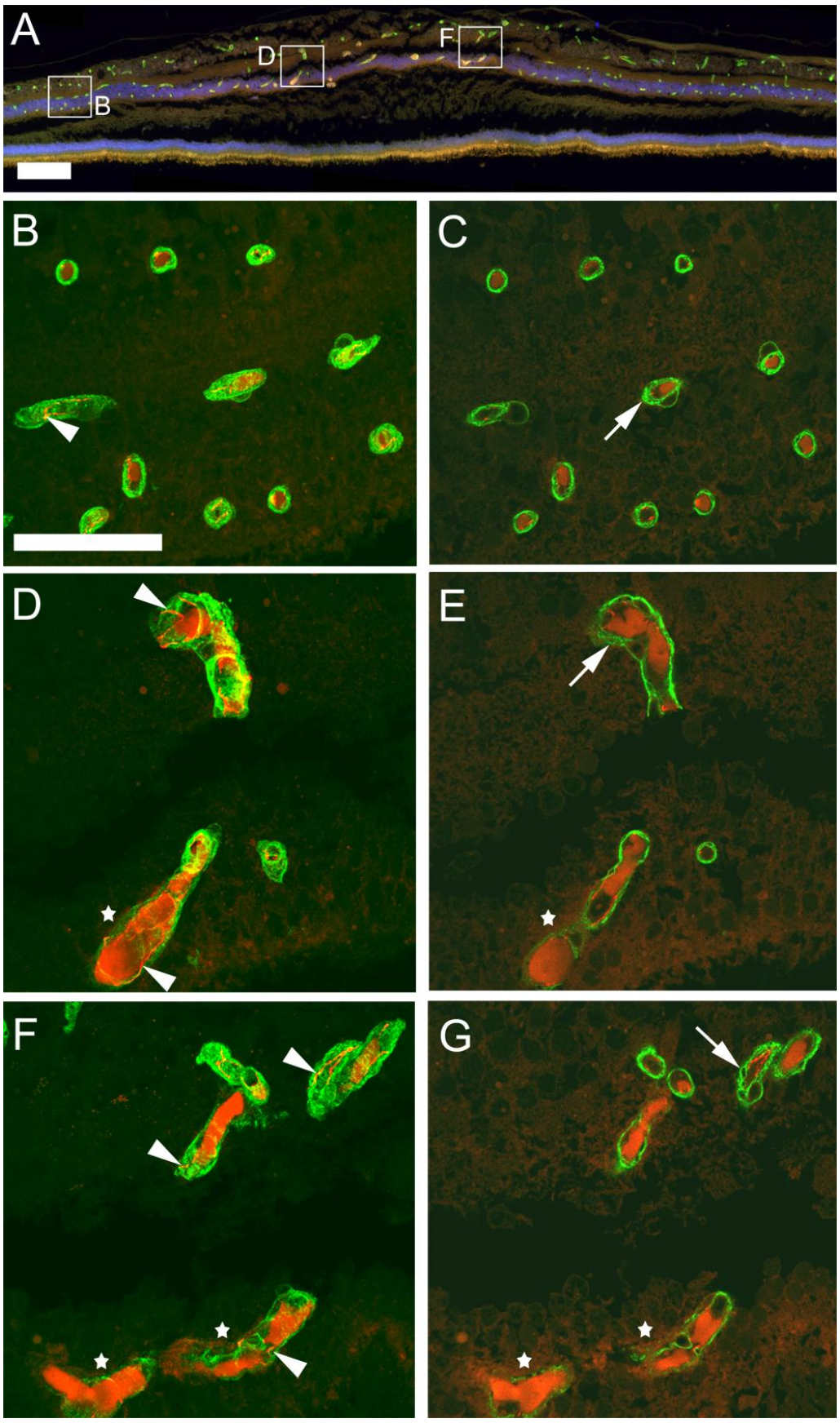
A
B
D
F
B
C
D
E
F
G

Figure 2.4. Vasculature

Immunohistochemistry with antibodies against collagen IV (green) and claudin-5 (red) labels retinal blood vessels (section 133) of MacTel type 2 retina. A non-specific luminal stain is also visible in the red channel and is prominent in telangiectatic, deeper plexus vessels. This is particularly obvious in the overview micrograph (**A**) as an orange stain. However, confocal microscopy through the entire thickness of the wax section (**B, D, F**) from selected regions shows that claudin-5 staining can be clearly distinguished as a junctional stain (arrowheads in **B, D, F**). Single confocal slices (**C, E, G**) reveal fine vacuoles (arrows **C, E, G**) in vascular basal lamina throughout the retina. In telangiectatic vessels collagen IV staining appears diffuse and interrupted (white stars in **D-G**). Temporal is to the left and nasal to the right. Scale bar is 200μm in **A** and 50μm in **B**.

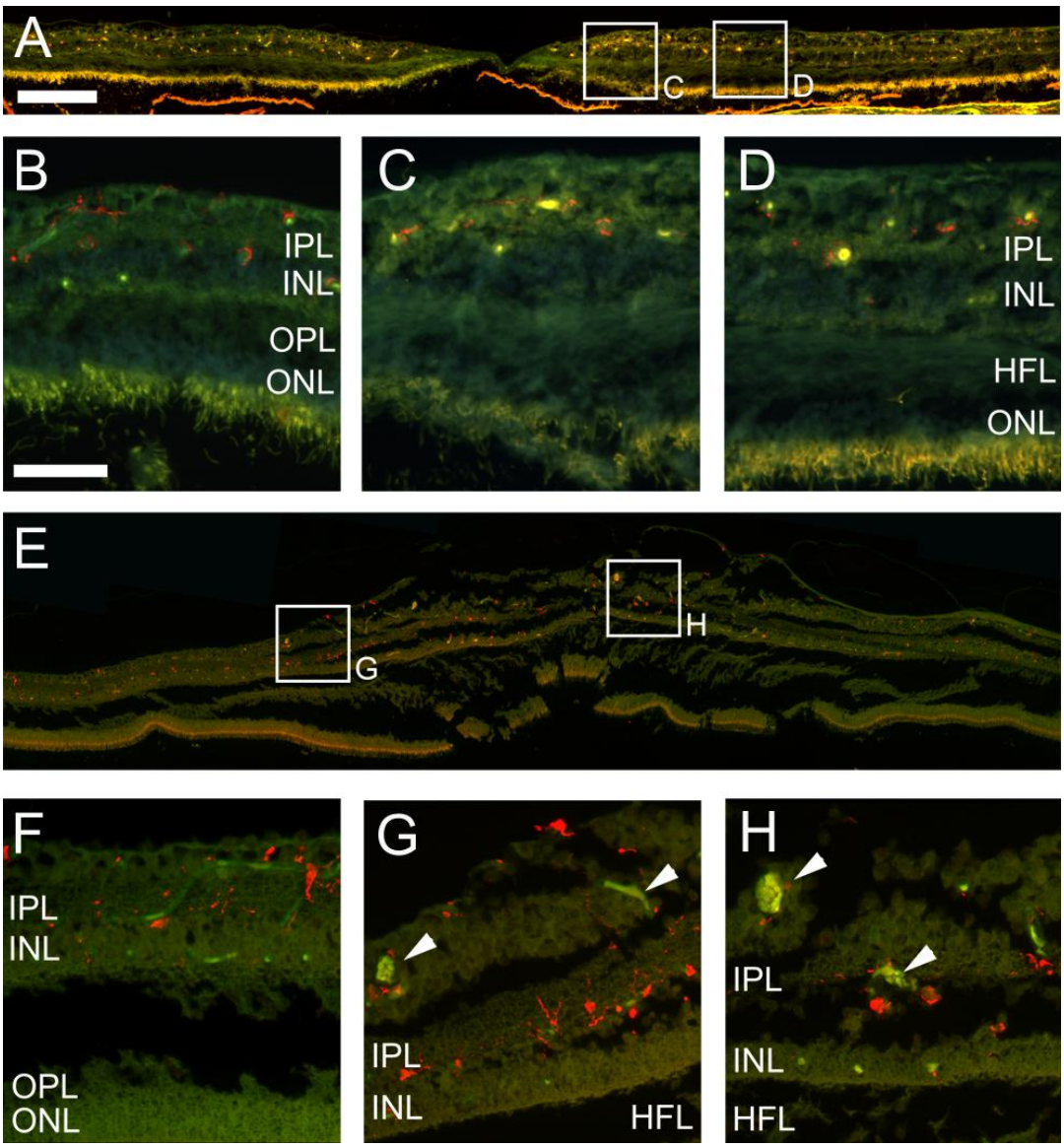

Figure 2.5. Microglia

Immunohistochemistry with the Iba1 antibody (red) labelling macrophages in the control (**A-D**) and the MacTel type 2 eye (**E-H**, section 153). Macrophages are distributed in both samples throughout the RGC layer, IPL and INL in the periphery (**B, F**) and the macula (**C, D, G, H**). They tend to be associated with blood vessels (visible as green/yellow autofluorescence), telangiectatic vessels indicated with arrowheads in **G, H**. RGC; retinal ganglion cell, IPL; inner plexiform layer, INL; inner nuclear layer, HFL; Henlé fibre layer, OPL; outer plexiform layer, ONL; outer nuclear layer. Temporal is to the left and nasal to the right. Scale bar is 200µm in **A** and 50µm in **B**.

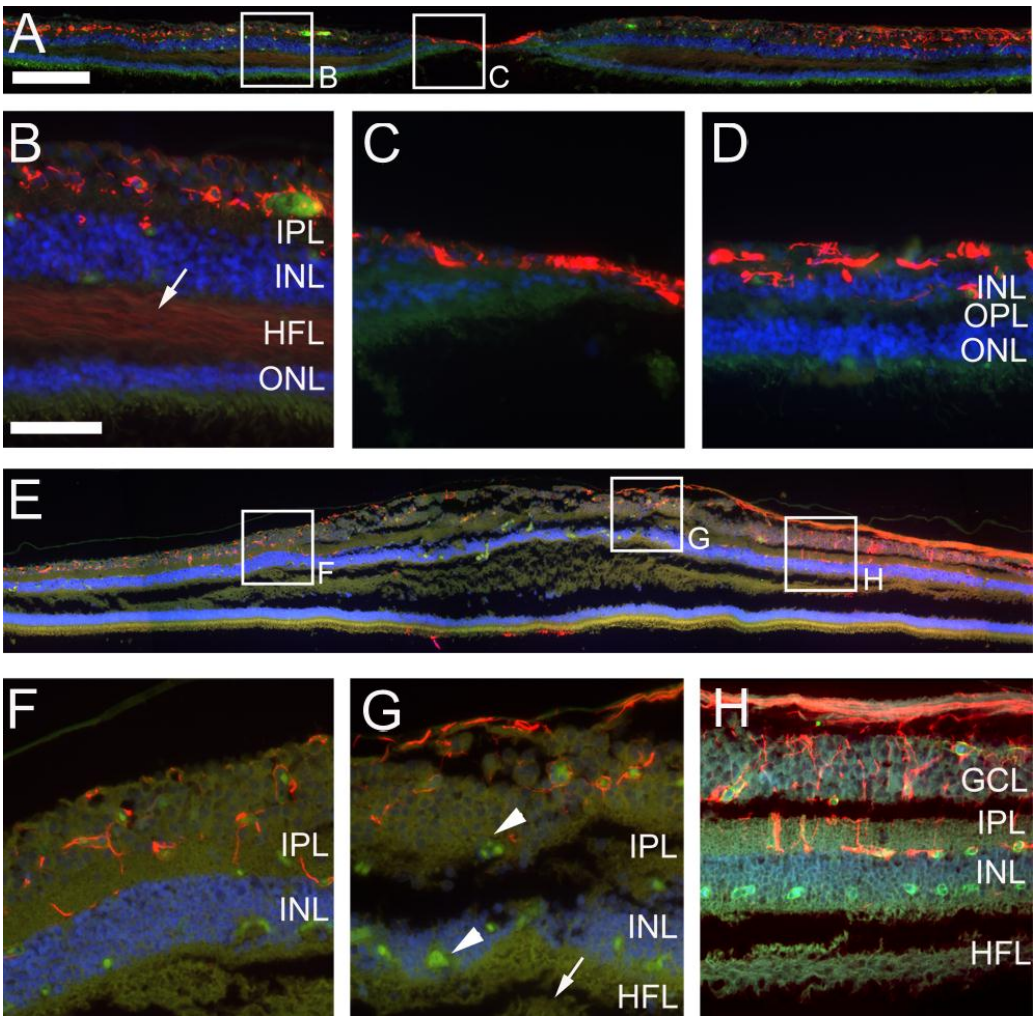

Figure 2.6. Retinal glia

Immunohistochemistry with an antibody directed against glial fibrillary acidic protein (GFAP) (red). GFAP immunostaining labels retinal astrocytes in a control retina (**A-D**) and the MacTel type 2 specimen (**E-H**, section 134). Strong GFAP labelling in the fovea of the control eye (**A, C**) might indicate the "Müller cell cone". There is also weak labelling in Henlé fibre layer (arrow **B**). Retinal astrocytes are associated with blood vessels and nerve fibres in both samples and appear in similar distribution and density. Blood vessels are visible as green/yellow autofluorescence (telangiectatic vessels; arrowheads **G**). No GFAP labelling is visible in Henlé fibre layer of the MacTel eye (arrow **G**). GCL; ganglion cell layer, IPL; inner plexiform layer, INL; inner nuclear layer, HFL; Henlé fibre layer, OPL; outer plexiform layer, ONL; outer nuclear layer. Temporal is to the left and nasal to the right. Scale bar is 200µm in **A** and 50µm in **B**.

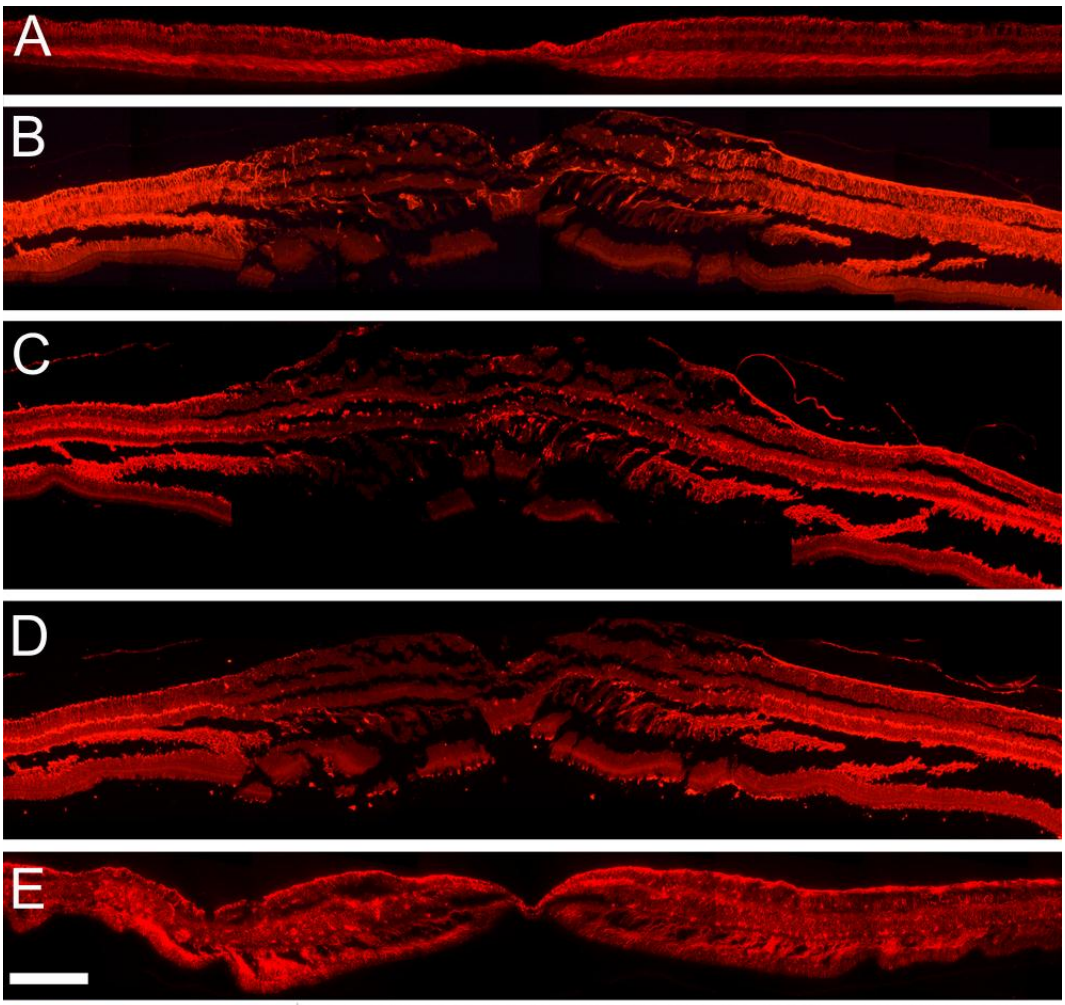
A
B
C
D
E

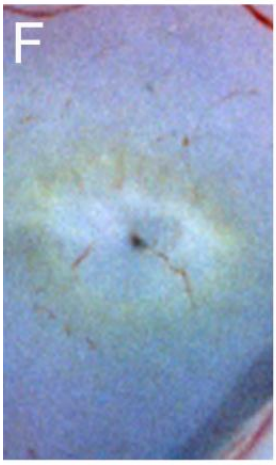
F

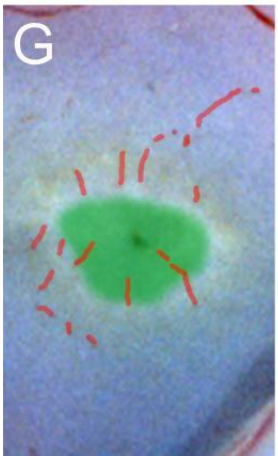
G

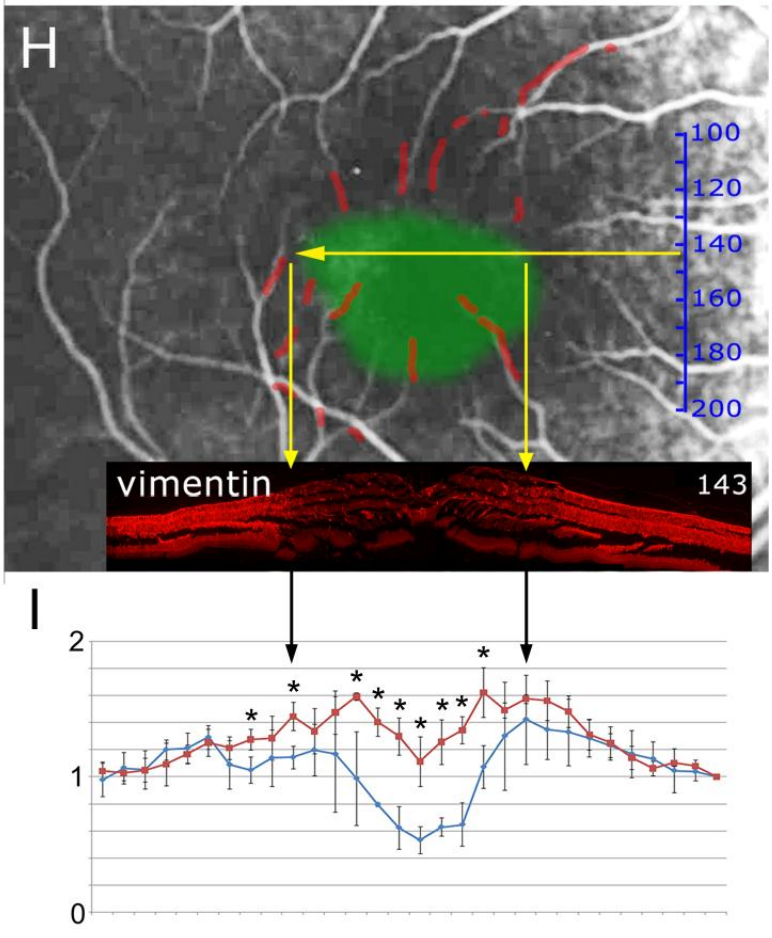
H
100
120
140
160
180
200
vimentin
143
I
2
1
0

Figure 2.7. Müller cells

Immunohistochemistry with antibodies directed against three different Müller cell markers (**A-E**). The distribution of vimentin (**A, B**) indicates the presence of Müller cells throughout the macula and periphery in the control eye (**A**) but a strong reduction in the macula of the MacTel eye (**B**). Similarly, glutamine synthetase, GS (**C**) and retinaldehyde binding protein 1, RLBP1 (**D**) are reduced in the MacTel macula. A 48 hour postmortem delay before fixation did not affect vimentin staining in the macula of a control eye (**E**). In order to compare the area of macular pigment depletion with the area of Müller cell depletion, blood residues were traced in the colour photograph (**F, G**). The image was scaled to match vessels in the angiogram, which locates the approximate position of the area of pigment depletion (green area) in the angiogram (**H**). The vimentin immunostaining (**B**) was scaled and centred on the angiogram (based on the size relationship established in Fig. 3), which demonstrates a rough correlation between macular pigment and Müller cell depletion (yellow arrows in **H**). The relative frequency of cell nuclei in the inner nuclear layer (based on H&E stained, perifoveal sections) is plotted in **I** and shows a reduction in the perifoveal region in the MacTel specimen (blue) versus control (red). Stars in I indicate statistical significance with a p-value below 0.05. Temporal is to the left and nasal to the right. Scale bar in **E** is 200µm

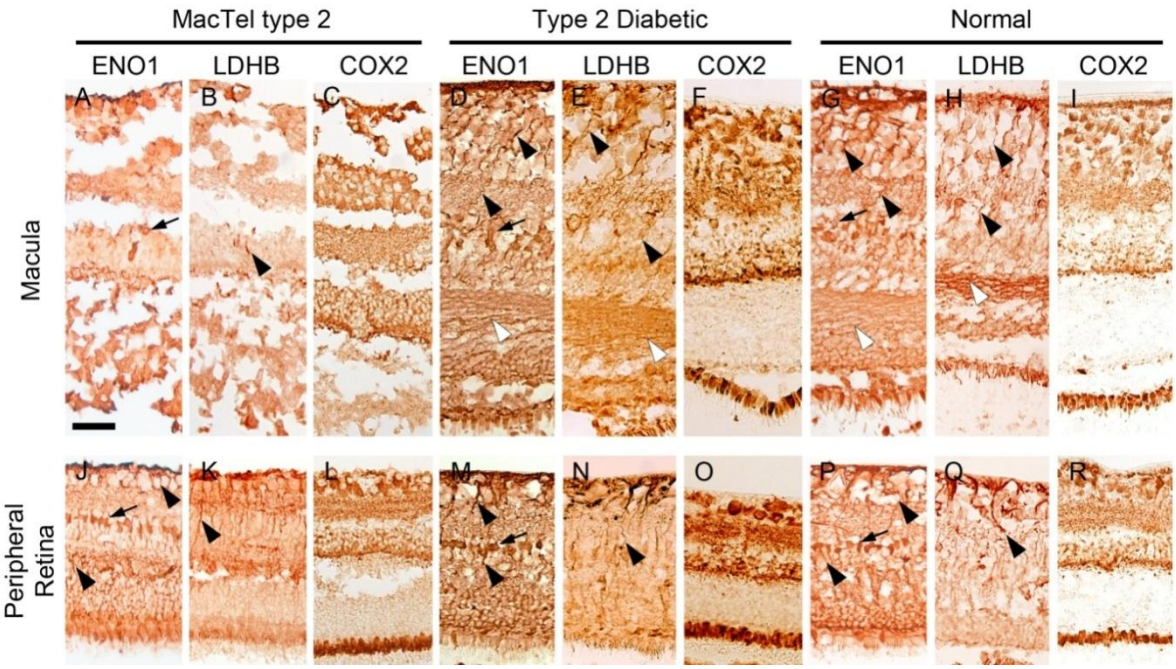

Figure 2.8. Glycolytic pathway proteins are down regulated in macular Müller cells in the MacTel type 2.

Immunohistochemistry on wax sections (**A-C, J-L**), a control eye from a patient with diabetes (**D-F, M-O**) and a normal control eye (**G-I, P-R**) using antibodies against ENO1 (**A, D, G, J, M, P**) and LDHB (**B, E, H, K, N, Q**) showed reduced staining of glycolysis markers ENO1 and LDHB in the diseased macula (**A, B**) in comparison to the retinal periphery (**J, K**) in the MacTel patient. In contrast, staining of the oxidative phosphorylation cytochrome unit COX2 and (**C, F, I, L, O, R**) was similar in diseased and control tissue. Müller cell processes are marked with black arrowheads in the inner retina and with white arrowheads in Henlé fibre layer. Black arrows indicate Müller cell bodies.

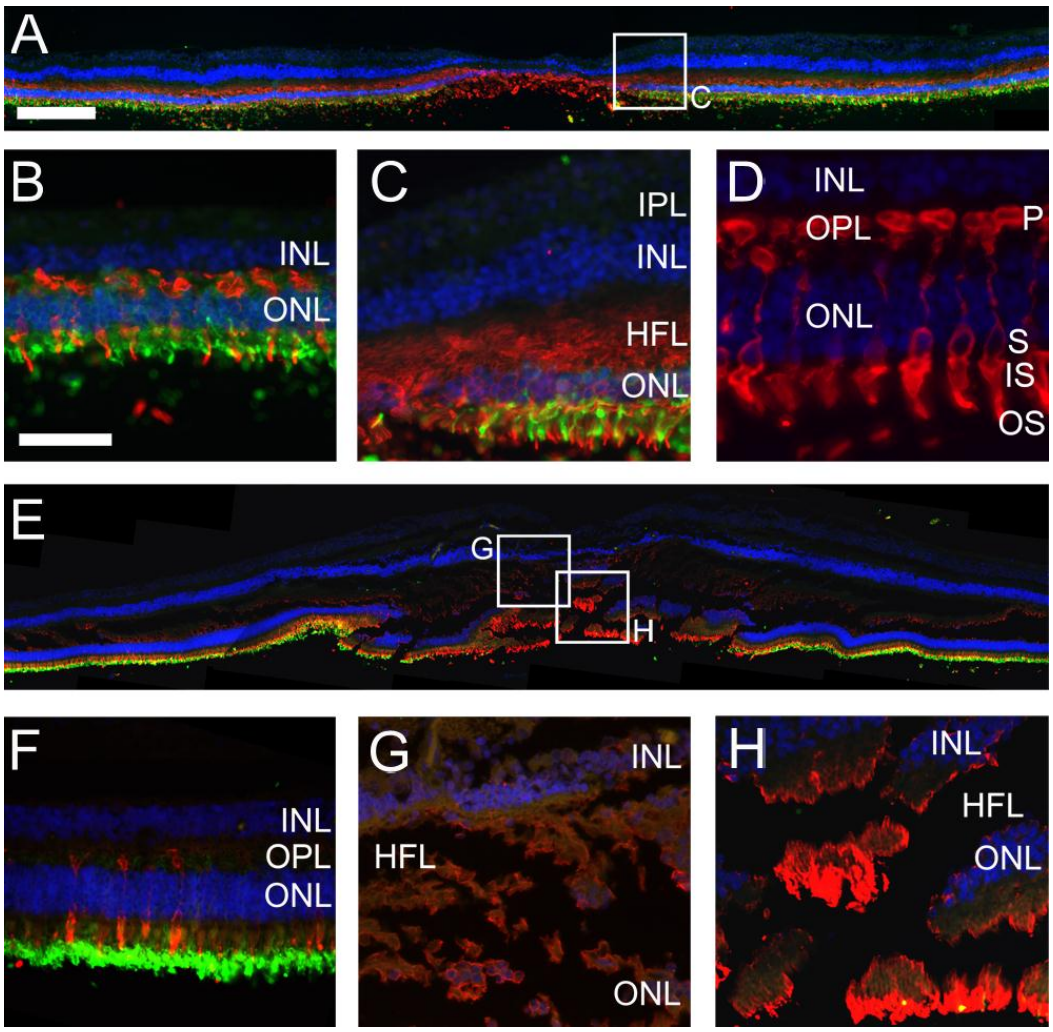

Figure 2.9. Photoreceptors
Immunohistochemistry showing the distribution of ML-opsin (red) and rhodopsin (green) in the control (**A-D**) and the MacTel eye (**E-H**, section 143).In both samples rods (green) are reduced and cones (red) are increased in the fovea. In the control Henlé fibre layer is stained by the ML-opsin antibody (**C**) and high magnification of the ML-opsin stain (**D**) confirms that this particular antibody stains the entire cone cell, including cone axons. ML-opsin stain in the MacTel Henlé fibre layer (**G, H**) suggests the presence of cone axons but is weaker in comparison to the control (**C**). Nevertheless, strong ML-opsin stain is visible in the MacTel fovea (**H**). IPL; inner plexiform layer, INL; inner nuclear layer, HFL; Henlé fibre layer, OPL; outer plexiform layer, ONL; outer nuclear layer. Photoreceptor structure: P; pedicle, S; soma, IS; inner segment, OS; outer segment. Temporal is to the left and nasal to the right. Scale bar is 200µm in A and 50µm in B.

3. Microvessels of the peripheral retina

The results reported in this chapter have been published in:

Powner MB, Scott A, Zhu M et al. Basement membrane changes in capillaries of the ageing human retina. Br J Ophthalmol 2011;95(9):1316-1322.[277]

3.1 Introduction:

The clinical phenotype of MacTel type 2 is restricted to the central macula and to date no disease phenotype has been reported in the periphery. However one of the two previous histopathologic case studies[249] has addressed the peripheral retina vascular phenotype using conventional light microscopy and transmission electron microscopy (TEM). They reported a thickening of retinal capillaries, most likely due to the excess production of basement membrane in a multi lamellae configuration, and also sporadic narrowing of the lumen calibre[249]. Degeneration of pericytes was noted using retinal trypsin digests, pericyte counts and TEM. Occasional areas showed loss of endothelial cells (only noticeable with TEM). Similar findings were found in perimacula capillaries as well as the peripheral retina; the degree of lamination was reported to be the same pan retina, whereas the number of lipid inclusions in the capillary basement membranes were decreased in number but still present, in peripheral tissue. Cellular debris from these degenerated endothelial cells and pericytes, and multimembranous lamellar lipid were separated by basement membrane layers, lipids present within the basement membrane, visualised both at a TEM level and using oil-red O and sudan black B staining and light microscopy. However fluorescein angiography of this patient revealed no peripheral vascular abnormalities prior to enucleation, be it leakage or significant dilation of the vessels.[249]

The phenotype described by Green *et al*[249], although thorough, was not compared in any form to control tissue. They do postulate the findings of vascular phenotype are similar to those found in diabetic and prediabetic patients[278, 279] yet the patient had no history of diabetes and glucose tolerance tests appeared normal. This is potentially misrepresentative of the disease as the phenotype cannot be ruled out as being 'normal' or a processing artefact.

Histopathological studies of the retinal vasculature in postmortem human tissue are crucial in understanding retinal disease mechanisms. In diabetic retinopathy, for example, degenerative changes in the microvasculature such as non-perfused capillaries and the formation of microaneurysms are hallmarks of disease that have been characterised extensively both in living patients and in postmortem material. Ultrastructural analysis of cross sections of retinal capillaries can provide critical insight into the health of the microvasculature that is not possible with normal light microscopy.

In diabetic retinopathy microvascular pathologies such as reduced pericyte - endothelial cell ratios and thickened capillary basement membranes have both been recognised for decades.[278, 280-283] There are numerous studies demonstrating in various diabetic animal models degenerating pericytes and capillary basement membranes of irregular and increased thickness, comprising debris-like inclusions and vacuoles, whereas the healthy control animals maintain intact pericytes and the vessels have basement membrane with homogenous density and uniform, 'normal' thickness.[284-287]

Studies attempting to quantify these pathological changes in human tissue specimens are less conclusive. Firstly, fixation procedures in humans are usually less than ideal because in most cases eye tissue can only be retrieved and fixed several hours after death. These postmortem delays might introduce artifacts. Secondly, in 'healthy' adult humans the basement membrane of retinal capillaries is irregular, containing numerous vacuoles and has a "Swiss-cheese" appearance.[283, 288] Furthermore, evidence of pericyte degeneration is also a common finding in non-diabetic retinas,[289] similar in many ways to the phenotypes observed in diabetes. Against this background of 'pseudo pathology' it is more difficult to measure changes in humans in comparison to animal models, which in general maintain pristine capillary ultrastructure throughout adult life and can be processed immediately after death. It can therefore be challenging to interpret findings in human samples on an ultrastructural level, in particular in case studies, in which controls and statistical comparisons are often unavailable.

We herefore used postmortem retina samples from anonymous human donors with no known ocular complaints and compared the ultrastructural integrity of capillaries in samples with different postmortem fixation delays, different fixation methods and different donor

ages, and thus created a baseline of capillary phenotype. Peripheral retina from our MacTel type 2 sample (along with the necessary diabetic, retinopathy and no retinopathy controls) have been studied in order to determine whether there is a peripheral retina microvascular phenotype like that described by Green *et al*.[249]

3.2 Aim:

To determine whether previously reported ultrastructural changes in MacTel type 2 are disease specific.

3.3 Materials and Methods:

Technical acknowledgements: I would like to thank Greg Hageman, University of Iowa, for the provision of the pre-embdded MacTel type 2 retina sample. I would also like to thank Mark Gillies and Meidong Zhu, University of Sydney, for the provision of the fixed control tissue used. Further thanks go to Peter Munro, University College London, for the embedding and ultra thin sectioning of the tissue reported in this chapter.

3.3.1 Donors and tissue processing

Postmortem retinae were obtained from; a rhesus macaque aged 17 years, 20 anonymous human donors with no known ocular disease, aged between 1 to 97 years, 4 type 2 diabetic donors without and one with diagnosed proliferative diabetic retinopathy and one donor with diagnosed MacTel type 2. All retina samples were taken from the mid- to far-periphery of nasal-inferior retina. Table 3.1 contains the donor and tissue fixation details; retina samples were fixed immediately in Karnovsky's fixative (3% (w/v) glutaraldehyde, 1% (w/v) paraformaldehyde in 0.08M sodium cacodylate buffered to pH 7.4 with 0.1M HCl) or tannic acid/glutaraldehyde mix. Alternatively they were fixed initially in 2% paraformaldehyde (PFA) and later transferred into Karnovsky's fixative.

3.3.2 Electron microscopy and image analysis

All tissue was osmium tetroxide treated, dehydrated through a series of alcohols and embedded in araldite resin. Ultrathin sections were cut and floated onto 150x hexagonal mesh grids. Microvessels with a diameter of less than 10µm were imaged using a Jeol 1010 transmission electron microscope (Jeol, UK) fitted with a Gatan Orius^{TM} SC1000B camera (Gatan, UK). Epoxy resin embedded tissue was also serially sectioned and imaged using the Gatan 3VIEW serial block face imaging system (Gatan, UK) fitted to a Zeiss Sigma variable

pressure field emission electron microscope (Zeiss, UK). 3D-reconstruction and Boissonnat surface modelling was performed using Digital Micrograph (Gatan UK, UK)and Reconstruct software[290] (Boston university, USA).

The degree of basement membrane vacuolisation was established by assigning a score to each capillary cross-section based on the percentage of the total basement membrane area that is covered by vacuoles (0=0%, 1=1-20%, 2=21-40%, 3=41-60%, 4=61-80% and 5=81-100%, Fig. 3.3 A,A'). Endothelial cell numbers were established by counting the number of zonula occludens between endothelial cells forming the lumen (Fig. 3.4 A, A'). Pericyte profile coverage was assessed by using the percentage of the circumference of the outer surface of the endothelial cell that was covered by a pericyte profiles (Fig. 3.4 B,B'). Basement membrane lamination was assessed by scoring the highest number radially of separate lamellae per capillary cross-section. (Fig. 3.4 C, C'). Averages were calculated for each donor. The images were scored independently by myself and verified by a colleague (Andrew Scott, University College London) and the quantification process was blinded. Spearman's rank correlation coefficient was used to determine significance levels. The r value and p values were calculated using the software Stata10 Intercooled (StataCorp, USA).

3.4 Results:

3.4.1 Fixation and postmortem delays

A problem with human postmortem material is that significant time periods can elapse between the death of the donor and the fixation of the tissue. Since the cellular and ultrastructural changes that may occur after death are not well characterised, it could be argued that ultrastructural abnormalities in human retinal capillaries may be based on postmortem or fixation artifacts. In order to establish how postmortem delays and fixation methods may influence the ultrastructural appearance of retinal capillaries we used a well preserved monkey retina as an example to demonstrate "normal looking" capillaries and compared this with three differently fixed human samples. The monkey eye was fixed within 15 minutes of death in Karnovsky's fixative (a fixative containing glutaraldehyde and paraformaldehyde). Retinal capillaries displayed normal looking basement membranes, endothelial and pericyte profiles (Fig. 3.1 A). In contrast, a human sample (donor age 80) contained large vacuoles in the basement membrane near the glia interface (arrowheads in Fig. 3.1 B). However, this sample was fixed 13 hours after death with paraformaldehyde, stored for 19 months and then post-fixed in Karnovsky's. It is therefore possible that the vacuoles may have been caused by the long postmortem delay or by suboptimal fixation;

paraformaldehyde penetrates tissue fast, but its ability to cross link proteins is relatively slow, (sufficient cross linking to survive dehydration may take over 24hours), whereas glutaraldehyde fixation rapidly cross links proteins, however the penetration rate is slower due to the larger polymers that form in solution. Therefore a mixture of the two fixatives is ideal in electron microscopy, the formaldehyde penetrates and stabilises the tissue, whist the glutaraldehyde follows on and cross links the tissue further.

We therefore analysed a sample (donor age 75) that has been fixed within 4 hours of death directly in Karnovsky's fixative. Remarkably, the same vacuoles could be found in the capillary basement membrane (arrowheads Fig. 3.1 C).

To further exclude postmortem delay as a factor causing the basement membrane vacuoles, we used a sample from an enucleated eye (donor age 55) that was fixed in tannic acid and glutaraldehyde within less than 30 minutes of enucleation. Extensive basement membrane vacuolisation was also found in all capillaries (Fig. 3.1 D). The vacuoles in this sample appear to consist of more 'rounded bubbles' when compared to previous examples, however this structure is visible in parts of the 4 hours after death fixation example (Fig. 3.1 C), in parts the bubbles however seem to have merged, and in the 16 hour postmortem example (Fig. 3.1 B) larger vacuoles are seen, perhaps due to smaller vacuoles merging postmortem. Nevertheless, these findings demonstrate that basement membrane vacuolisation is not an artefact of postmortem delay but a normal feature present in adult human peripheral retinal capillaries.

To obtain more insight into the morphology of the basement membrane vacuoles we serially sectioned a portion of a retinal capillary from our best preserved sample (enucleated eye, fixed in under 30 minutes) using the Gatan 3VIEW system (Fig. 3.1 E). The outer surface of endothelial cells, pericyte profiles and basement vacuoles were traced in each section and then reconstructed and displayed as smoothened Boissonnat surfaces (Fig. 3.1 F). This showed that the vacuoles were isolated or connected patches of varying size and shape, distributed in a seemingly random manner along the vessel.

3.4.2 Donor age

Since it has been previously reported that basement membrane vacuoles are virtually absent in children,[276, 291] we analysed retinas from donors with different ages. In the retina from a 14 month old donor (with a 37 hour postmortem delay) we found that the basement membranes from most capillaries did not contain any vacuoles (Fig. 3.2 A). Due to the very long postmortem delay in this case, the tissue surrounding the capillaries was not well preserved. But importantly, this had no effects on the integrity of the capillary basement membrane, which further demonstrates that basement membrane vacuoles are not a postmortem or fixation artefact. In samples from older donors (19, 47 and 80 years old) basement membrane vacuoles could be readily detected (Fig. 3.2 B-D). In some instances, in particular in older donors, the vacuolisation reached dramatic levels where capillaries were entirely surrounded by vacuoles (Fig. 3.2 D).

In order to quantify how basement vacuolisation correlates with donor age we analysed capillaries in the retinal periphery from 20 anonymous donors (with no known eye pathologies) aged between 1 and 97 years. 29±7 capillaries from each donor were imaged and assessed. Vacuolisation was quantified by creating a severity scale with 0 representing no vacuoles at all and 5 complete vacuolisation of the basement membrane in its entire circumference (Fig. 3.3 A). Interestingly, the severity of this ultrastructural abnormality correlated clearly and directly with age (Fig. 3.3 B, Spearman's rank correlation coefficient, $r= 0.7203$, $p= 0.0003$).

Most of our samples were fixed within 24 hours of death but we also included three samples that were fixed 50 hours after death (Table 3.1). Plotting the amount of basement membrane vacuolisation against postmortem fixation delays revealed no obvious correlation. To further exclude the possibility of postmortem artefacts we included some controlled fixation delays. To this end we used a pair of eyes from a young donor (34 years old) with relatively low vacuolisation. One eye was fixed immediately (postmortem delay of 8 hours) and the other eye was kept in phosphate buffered saline for an additional 48 hours at room temperature. This controlled delay did not introduce any major changes in vacuolisation score. The same was repeated with the eyes from an older donor (63 years old) and they too scored in the same range irrespective of fixation delays (Fig. 3.3 C).

3.4.3 Endothelial cell numbers in capillaries

Only vessels smaller than 10µm in diameter were included in our analysis. Green *et al.* (1980) proposed an endothelial drop out in MacTel type 2; as such the average number of

endothelial cells that contribute to the lumen of a capillary was established by counting the number of tight junctions between endothelial cells. The tight junctions (zonula occludens) are easily recognisable as electron dense areas at an EM level (Fig. 3.4 A). On average the number of tight junctions was between 1.5 and 2 (per capillary cross section) confirming the size uniformity of our capillary sample populations and there were no significant changes in relation to the age of the donors (Spearman's rank correlation, r = -0.2742, p= 0.2420, Fig. 3.4 D).

3.4.4 Other ultrastructural abnormalities

One possible explanation for the occurrence of basement membrane vacuoles could be that they are remnants of degenerated pericytes. In fact, we found in numerous samples (from donors of all ages) signs of degenerating pericytes and many examples of capillaries with complete absence of any recognisable pericytes. Pericyte drop out and reduced pericyte coverage are well known signs of diabetic retinopathy but were frequently found in our non-diabetic population. In order to obtain an indication of pericyte frequency in our samples we therefore measured the percentage of vessel surfaces covered by pericytes (Fig.3. 4 B). There was no evidence of decreasing pericyte frequency with increasing age in our non-diabetic donors (Spearman's rank correlation coefficient, r=-0.0602, p=0.8008, Fig. 3.4 E).

Furthermore, in many capillaries the basement membrane displayed extensive lamination (Fig. 3.4 C). This ultrastructural abnormality was sporadically found in most samples studied. It is conceivable that successive rounds of pericyte degeneration and regeneration could lead to the formation of multiple basement membranes, which might explain the basement membrane lamination we observed in many of our samples. We therefore quantified this feature by scoring the maximum number of basement membranes in a given capillary (Fig. 3.4 C). Although there was a slight increase in basement lamination with increasing age (Fig. 3.4 F), this was not statistically significant (Spearman's rank correlation coefficient, r= 0.1469, p= 0.5364). Furthermore, there was no significant correlation between the level of pericyte coverage and basement lamination in our samples (Spearman's rank correlation coefficient, r= 0.3004, p= 0.1982). There was also no significant correlation between these two features and postmortem delays (not shown).

3.4.5 Comparison of MacTel type 2 to the established baseline

Having established a baseline for the occurrence of ultrastructural abnormalities in the normal population, we can test how the ultrastructural features seen by Green *et al.* (1980)

in MacTel type 2 compare. Our MacTel type 2 sample, available for comparison, additionally had diabetes type 2 and had not been seen in clinics for 10 years prior to death so the development of retinopathy could not be ruled out. As such relevant diabetics were first investigated to rule out any diabetic effects. In a case with known diabetic retinopathy (71 year old) we found numerous capillaries that were completely depleted of pericytes and endothelial cells, with only the basement membrane remaining (Fig. 3.5 A). Such acellular capillaries are a well described characteristic of diabetic retinopathy. Other capillaries in the same sample had severely vacuolated basement membranes and many lacked pericytes (Fig. 3.5 B). Not surprisingly, this case with diagnosed diabetic retinopathy scored very low in the pericyte coverage measurements (black triangle in Fig. 3.5 G), serving as a positive control and confirming the validity of our method to assess pericyte coverage. However the other traits (basement membrane vacuolisation and lamination and endothelial cell numbers) were found at equal frequency as in our control population (black triangles in Fig. 3.5 E, F and H). Four cases with reported diabetes but no diabetic retinopathy (Fig. 3.5 C) scored very similar to our control population in all four measurements (open triangles in Fig. 3.5 E-H).

Peripheral retina from the MacTel type 2 demonstrated many capillaries that lacked pericytes and displayed basement membrane vacuolisation and lamination (Fig. 3.5 D). However, quantification of this sample revealed that the extent of ultrastructural abnormalities was very similar to our control population (circle in Fig. 3.5 E-H), suggesting that peripheral capillaries in our MacTel type 2 case are normal for a person that age.

3.5 Discussion:

This study has revealed that with increasing age retinal capillaries in adult humans accumulate vacuoles in the basement membrane at the glia interface. We have demonstrated that these vacuoles are not postmortem artefacts or caused by suboptimal fixation. Firstly, they were very rare in the retina from a 14 month old donor that was fixed 37 hours after death (one of the longest postmortem delays in our study). Secondly, the vacuoles were widespread in our two samples that were fixed within 30 minutes and 4 hours after enucleation. Thirdly, even the introduction of artificial postmortem delays had no noticeable influence on the morphological abnormalities measured in our study. And lastly, there was a statistically highly significant correlation between the amount of vacuolisation and donor age.

Interestingly, even grossly abnormal looking capillaries did not seem to be disease specific and were common in the elderly. Obviously, it is difficult to completely exclude any

underlying retinal or vascular disease in anonymous donors. However, the fact that the vacuolisation appeared in all of the samples we tested and that it increased with age strongly suggests that this is a 'normal' ageing process. Although it was demonstrated in the early 1960s that basement membranes in adult human retinal capillaries contain vacuoles,[291] this is not widely reported in the literature. Therefore it is not well known that retinal capillaries in normal adult humans appear to have a phenotype that normally would be considered as pathological. In fact, 'healthy' normal looking capillaries are only present in children;[291] and remarkably, even in mature animals of several species (monkeys, dogs, cats and rats) capillaries do not display the ultrastructural abnormalities seen typically in adult humans.[292-294] In keeping with that, the macaque eye used in this study came from an elderly female (past its reproductive age, 17 years old) but showed only very minor capillary abnormalities. It is therefore possible that basement membrane vacuolisation relates to absolute lifespan or alternatively, it might be a phenomenon specific to the human species.

So far the chemical nature of the basement membrane vacuoles is not clear. Their morphology is reminiscent of age-related lipid inclusions previously described in Bruch's membrane.[295] Furthermore, it has been shown that lipids can accumulate in larger retinal vessels in diabetic retinopathy.[296] Also Green *et al.*[249] stained paraffin embedded retinal sections and found a faint positive stain for lipids (using Oil-red O and sudan black B) in the walls of the capillaries, however they did not correlate this staining directly to the vacuoles observed in the basement membrane. So the molecular composition of vacuoles in capillary basement membrane has yet to be established. It is also not clear by what mechanism the basement membrane abnormalities are created. It is possible that the basement membrane vacuoles are remnants of pericytes that have degenerated. This would imply a significant turnover of degenerating and regenerating pericytes throughout the human lifespan. Similarly, multiple basement membrane sheaths could be generated by such a process. However, so far no studies have tested such a hypothesis specifically and our study did not find a correlation between basement membrane lamination and pericyte drop-out. Neither did these two aspects correlate with age. Long-term stress, such as hypoxia, might be a contributing factor to vacuole formation; in particular in the outer retina, which is more prone to experience hypoxic stress .[297] However, we did not notice any obvious differences between the inner and outer vascular plexus. Furthermore, our analysis was limited to the retinal periphery where hypoxic stress is likely to be less pronounced than in the macula. Green *et al*[249] did compare macular and mid-periphery, and observed that the microvessels of equatorial mid peripheral retina had 'less intense' lipid deposition (vacuoles) compared to the temporal parafoveal area. Whether this relates to hypoxic stress, or whether vacuoles

are a feature increased in number by telangiectasis of parafoveal MacTel type 2 vessels it cannot be determined without control data from macular vessels.

Despite the widespread abnormalities in our non-diabetic population we still managed to identify our case of diabetic retinopathy as clearly abnormal, based on reduced pericyte coverage. Traditionally, pericyte coverage has been assessed by counting cell nuclei in trypsin digests of entire retinas.[298] Nevertheless, the electron microscopy based method of quantifying pericyte coverage used in this study seems to be suitable to distinguish clearly the case of diabetic retinopathy against our non-diabetic population, confirming the validity of such an approach.

Our study suggests that caution should be exercised in the interpretation of ultrastructural capillary abnormalities in case studies of retinal vasculature diseases. For example, in our case of MacTel type 2 we found in the peripheral retina strong basement membrane vacuolisation and lamination confirming the findings of two previous MacTel type 2 case reports.[249, 250] However, our quantification showed that these two ultrastructural features were within a range of capillary phenotypes typical for a person of that age, suggesting that MacTel type 2 does not induce these disease specific changes in peripheral retinal capillaries.

The question remains how capillaries with such grossly distended basement membranes, as we observed in some elderly, normal donors, can remain functional at all. With the advent of novel high resolution in vivo image technology[299, 300] it may be possible in the future to address these questions of capillary function in the aging retina directly. But so far it is not even known whether these changes are beneficial or detrimental to vascular function. If the latter were the case, such a progressively worsening function of the glia-vascular unit might contribute to age related pathologies in the retina.

Table 3.1: Donor tissue and fixation information

Age (yrs)	Cause of death	Postmortem delay	Initial fixative	Time until Karnovsky's fixative	Ophthalmic history
Rhesus Macaque (*Macaca mulatta*)					
17	Euthanasia	15 minutes	Karnovsky's	-	-
Human Normal Controls					
1	Unknown	37 hours	2% PFA	22 months	None reported
10	Unknown	25 hours	2% PFA	18 months	None reported
18	Cardiac arrest	13 hours	2% PFA	2 months	None reported
19	Motorbike accident	18 hours	2% PFA	2 months	None reported
24	Intracranial haemorrhage	55 hours	Karnovsky's	-	None reported
34*	Lung cancer	8 hours*	2% PFA	3 weeks	None reported
42	Hanging suicide	20 hours	2% PFA	16 months	None reported
43	Prescription drug overdose	17 hours	2% PFA	19 months	None reported
47	Rectal carcinoma	8 hours	2% PFA	19 months	None reported
55	Surgical enucleation	<30 minutes	Tannic acid-Glutaraldehyde	-	Extra ocular tumour
63*	Prostate cancer	8 hours*	2% PFA	4 months	None reported
71	Throat cancer	11 hours	2% PFA	4 months	None reported
73	Cholangiocarcinoma	7 hours	2% PFA	19 months	None reported
74	Lung cancer	14 hours	2% PFA	3 months	None reported
75	Unknown	4 hours	Karnovsky's	-	Healthy eye from a unilateral Coats' disease case
79	Lung cancer	13 hours	2% PFA	19 months	None reported
80	Chronic obstructive pulmonary disease type II	13 hours	2% PFA	19 months	None reported
84	Lung cancer	9 hours	2% PFA	19 months	None reported
96	Unknown	47 hours	2% PFA	3 months	None reported
97	Unknown	48 hours	2% PFA	3 months	None reported
Type 2 Diabetics					
74	Intracranial haemorrhage	7 hours	2% PFA	13 months	None reported
77	Pancreatic cancer	8 hours	2% PFA	3 months	None reported
78	Stroke	9 hours	2% PFA	15 months	None reported
79	Cardiac arrest	9 hours	2% PFA	14 months	None reported
Diabetic Retinopathy					
71	Cerebrovascular accident	<12 hours	2% PFA	6 months	Diabetic retinopathy, laser surgery
Macular Telangiectasia Type 2 and Diabetes Type 2					
65	Unknown	4 hours	Karnovsky's	-	MacTel type 2, No retinopathy
Postmortem Degradation Controls					
34*	Lung cancer	56 hours*	2% PFA	3 weeks	None reported
63*	Prostate cancer	56 hours*	2% PFA	4 months	None reported

Table 3.1. Donor tissue and fixation information. 'Time until Karnovsky's fixative' refers to the time between initial fixation of the tissue and its transfer into Karnovsky's fixative (3% (w/v) glutaraldehyde, 1% (w/v) paraformaldehyde in 0.08M sodium cacodylate buffered to pH 7.4 with 0.1M HCl). 2% PFA, 2% (w/v) paraformaldehyde; * indicates the normal controls from which the other donor eye was used as a post-mortem degradation control.

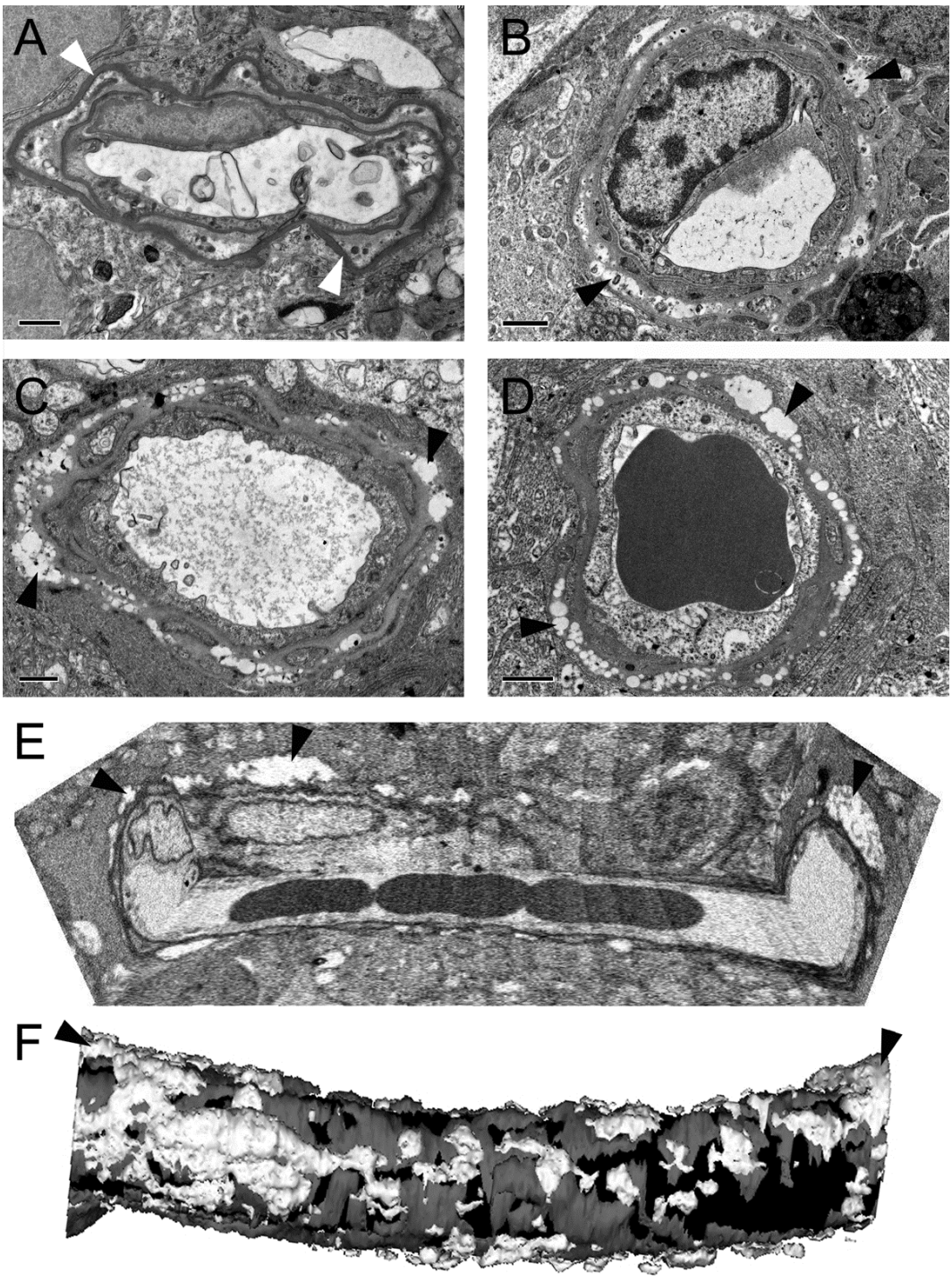

Figure 3.1. Vacuolisation of the basement membrane in human retinal microvessels.
A capillary from a rhesus macaque retina (**A**) showed intact basement membranes and good pericyte coverage. In contrast, in humans (**B**-**F)** numerous vacuoles were present within the vascular basement membrane (arrowheads in **B**-**F**) irrespective of fixation methods and postmortem delays. The tissue in **B** was fixed 13 hours after death and stored in 2% paraformaldehyde for 19 months before fixation in Karnovsky's fixative for electron microscopy processing, whereas tissue in **C** was fixed directly in Karnovsky's 4 hours after death, and tissue in **D-F** was fixed within 30 minutes after surgical enucleation in tannic acid-

glutaraldehyde solution. **E:** Reconstruction of a vessel (from the enucleated eye) using 300 consecutive sections. **F:** 3D-reconstruction of the vessel in (E); endothelial cells and lumen (black), pericytes (grey) and basement membrane vacuoles (white). Scale bars are 1µm in A-D.

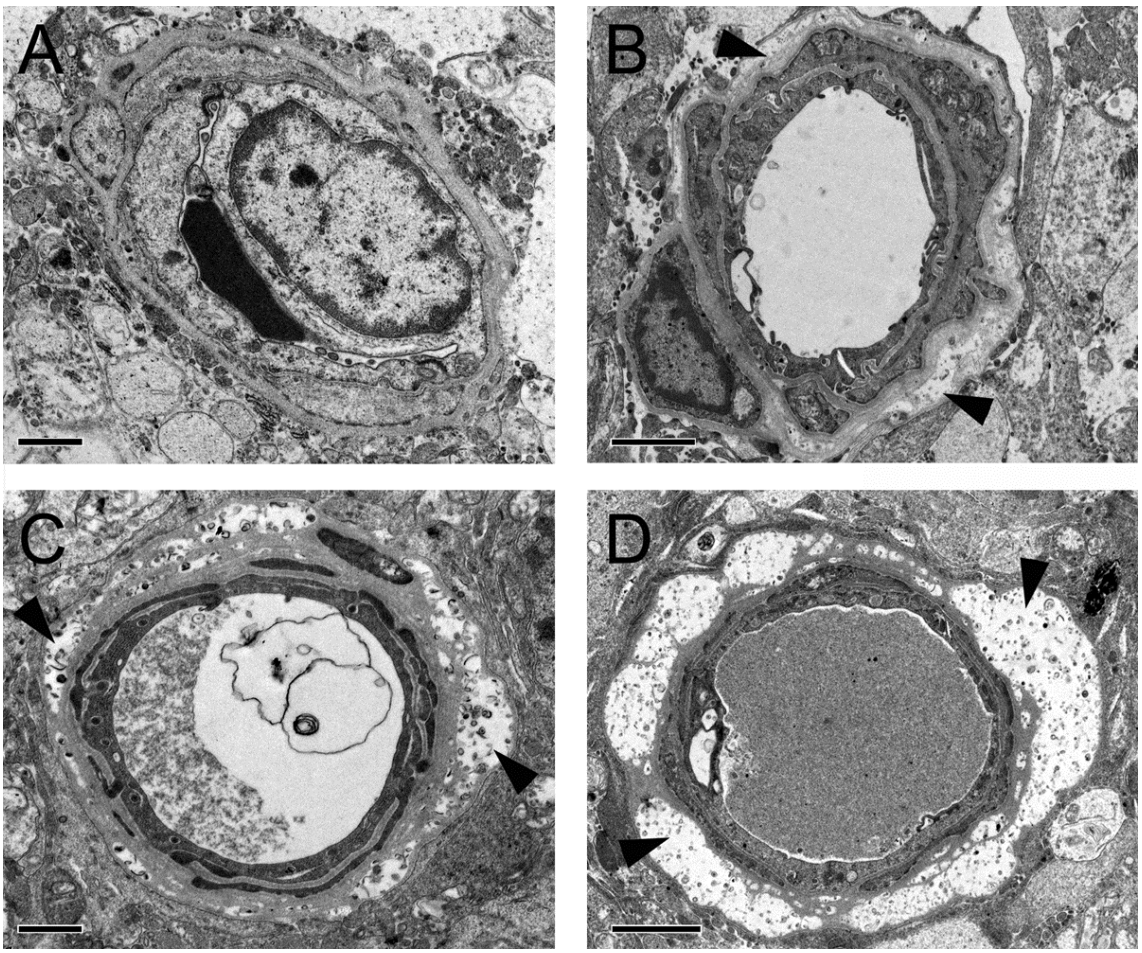

Figure 3.2. Vacuolisation of peripheral retinal capillary basement membrane is age dependant (**A**: 14 months, **B**: 19 years, **C**: 47 years and **D**: 80 years old).
The majority of retinal capillaries of a 14 month old have no vacuoles in the basement membrane (**A**). Vacuoles increase in number and density in older donors (arrow heads in **B-D**). Scale bars are 1µm in A-C and 2µm in D.

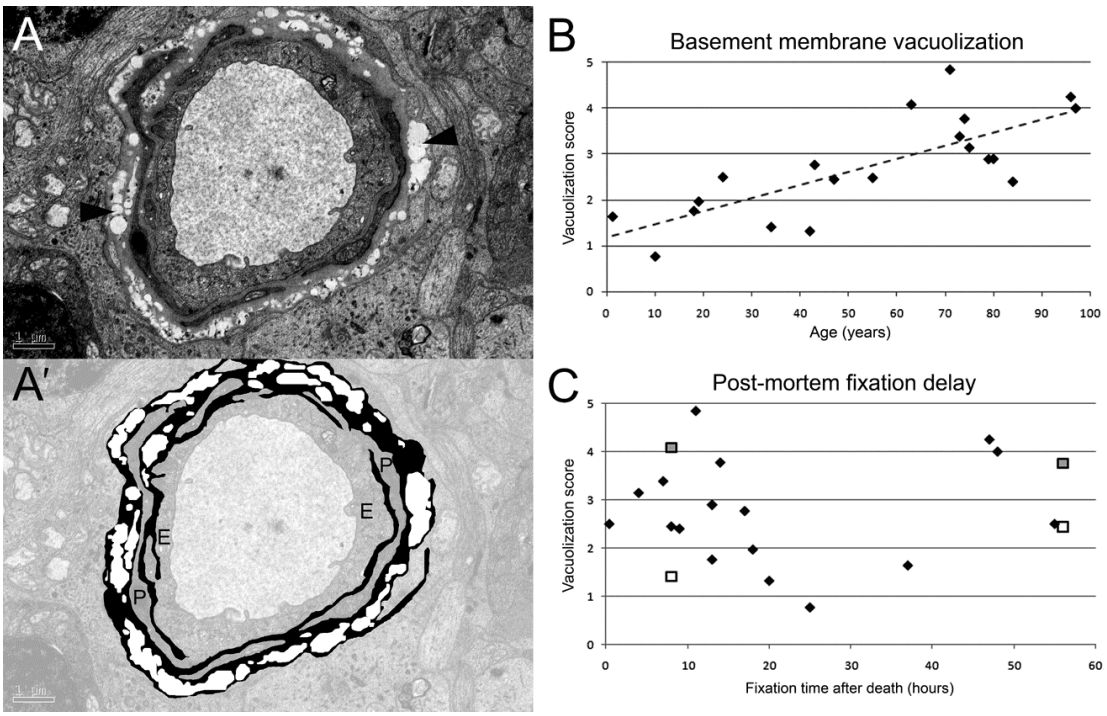

Figure 3.3. Quantification of basement membrane vacuolisation.
Vacuolisation was quantified by assessing the proportion between the area of the vacuoles (arrowheads in **A**, white areas in **A'**) and the total area of the basement membrane (black areas in **A'**). A score between 0 and 5 was then given to capillaries based on the percentage of vacuoles (0 = no vacuoles, 1 = 1-20%, 2 = 21-40%, 3 = 41-60%, 4= 61-80% and 5 = 81%-100%). The example in **A** had a score of 4. **B:** The scores for each donor were averaged and plotted against the donor's age. **C**: Plotting vacuolization scores (from all normal donors, ◆) against postmortem delays did not reveal any correlation. Furthermore, tests with pairs of eyes (squares), where one eye was fixed 8 hours after death and the other eye was kept in phosphate buffered saline for an additional 48 hours at room temperature, showed no major changes regarding vacuolization (☐ 34 year old donor; ■ 63 year old donor). E, endothelial cell; P, pericyte profile; line in **B** is line of best fit. Scale bar in **A** is 1µm.

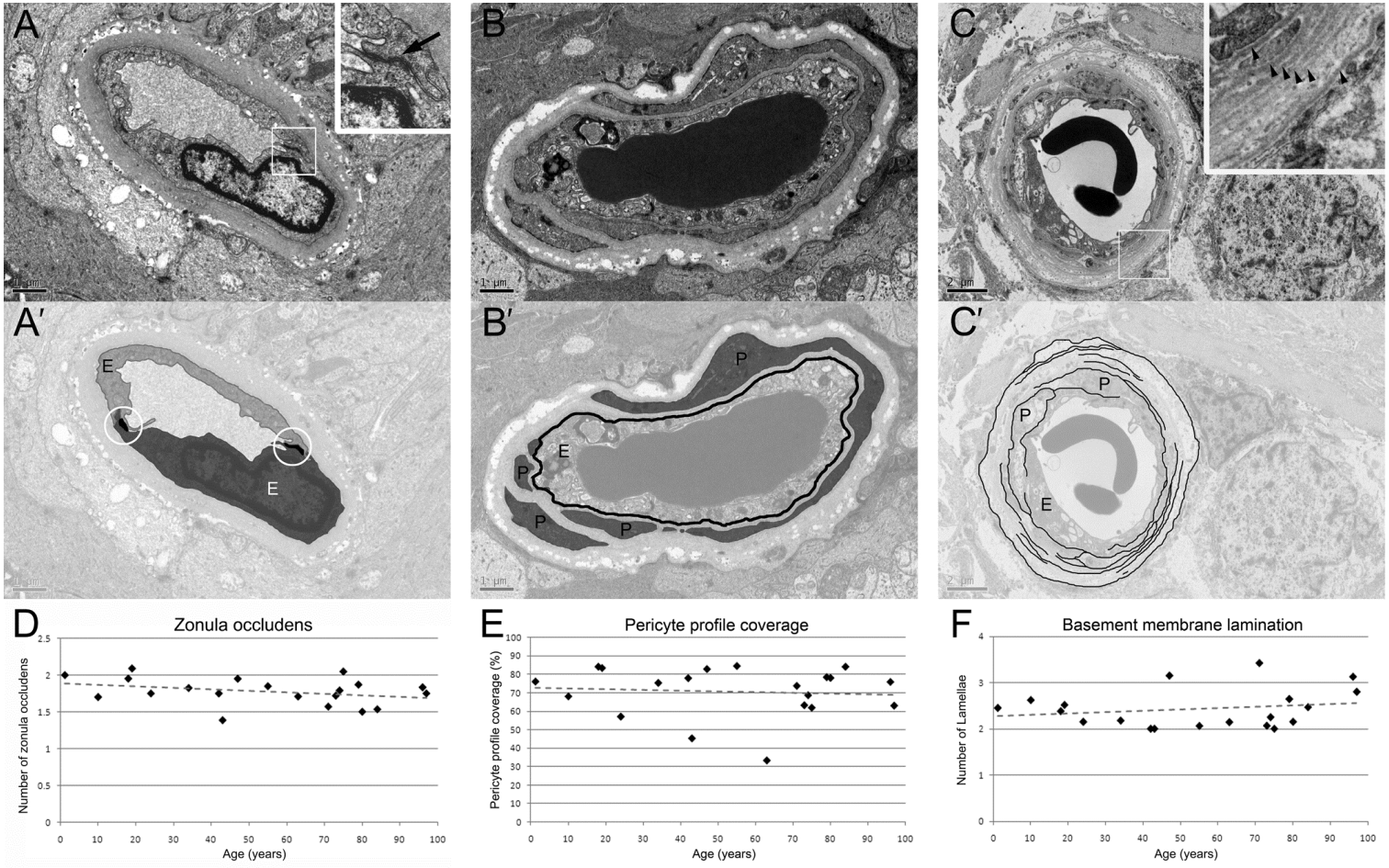
A
B
C
A′
B′
C′
E
P
D
Zonula occludens
Number of zonula occludens
Age (years)
E
Pericyte profile coverage
Pericyte profile coverage (%)
Age (years)
F
Basement membrane lamination
Number of Lamellae
Age (years)

Figure 3.4. Other structural features.
A: Endothelial cell numbers were quantified by counting zonula occludens (black arrow in inset in **A**) per capillary profile. Two zonula occludens are marked in black and circled in **A'**. The two endothelial cells are highlighted in different shades of grey. Plotting zonula occludens numbers against donor age showed no age-related changes (**D**). **B**: Pericyte profile coverage was calculated by determining the percentage of endothelial cell basement membrane (black line in **B'**) that was covered by pericyte profiles (marked in grey). The example in **B** shows coverage of 93%. Plotting pericyte profile coverage against donor age showed no age-related changes (**E**). **C**: Basement membrane lamination (arrowheads in inset in **C**) was quantified by scoring the maximum number of lamellae (black lines in **C'**) across a given capillary radius. In this example the score was 7. **E:** Plotting averaged lamination scores against donor age showed no age-related changes (**F**). E, endothelial cell; P, pericyte profile; Z, zonula occludens; stippled lines in D, E and F are lines of best fit. Scale bar is 1µm in **A**, **B** and 2µm in **C**.

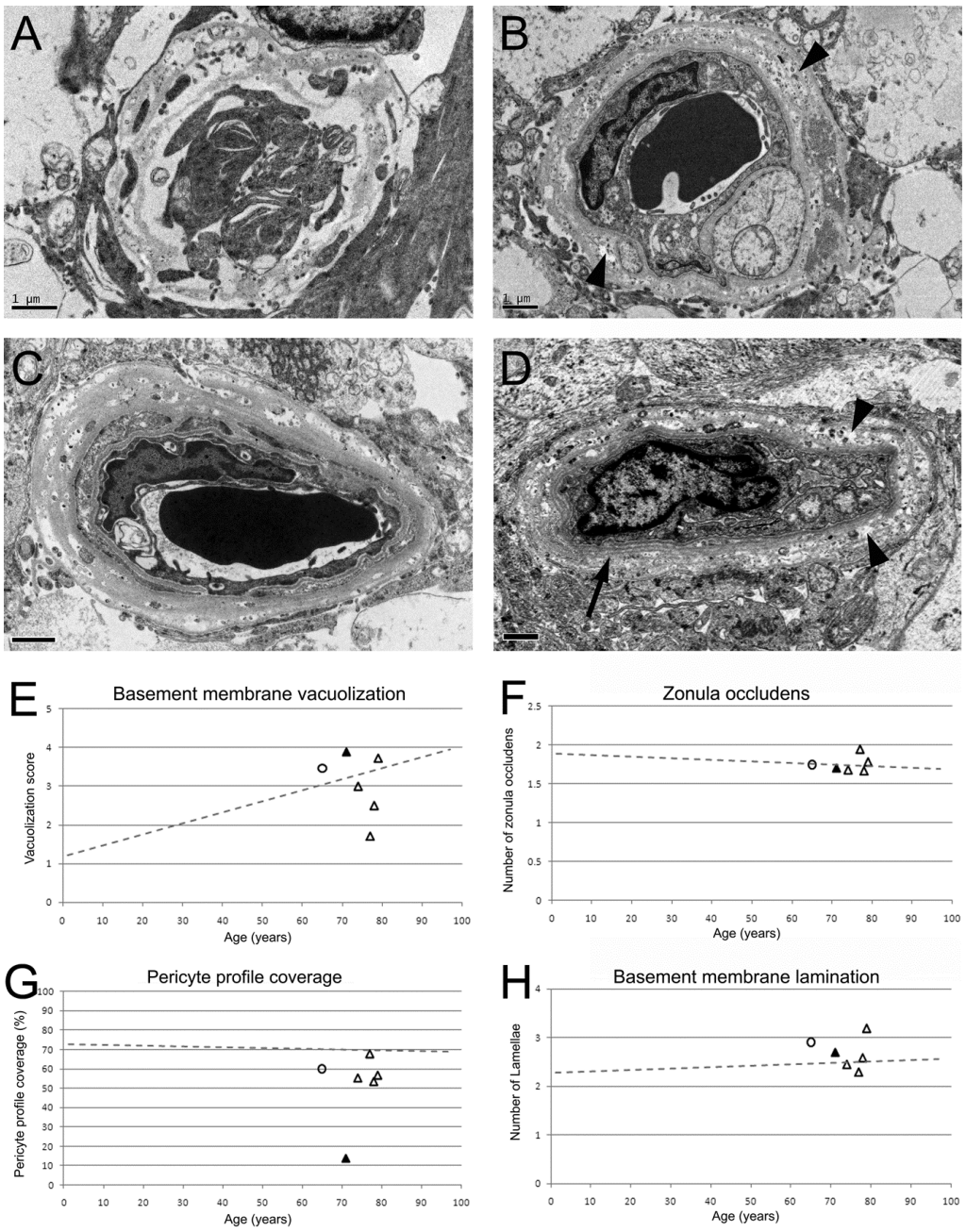

Figure 3.5. Retinal capillary phenotypes in cases with known retinal diseases.
A-B: The retina from a 71 year old donor with diabetic retinopathy showed acellular capillaries (**A**) and capillaries with no discernable pericyte profiles (**B**). Basement membrane vacuolization (arrow heads in **B**) was also observed. **C** shows a capillary from a 74 year old donor with type 2 diabetes but no diabetic retinopathy. **D**: Capillaries from a MacTel type 2 donor also show ultrastructural abnormalities such as extensive lamination (arrow in **D**) and vacuolization of the basement membrane (arrowheads in **D**) and lack of pericyte profiles. **E**-**H** shows quantification of individual disease cases compared to the line of best fit previously determined for normal healthy donors. △ type 2 diabetics; ▲ diabetic retinopathy; ○ MacTel type 2; stippled line is line of best fit through normal donors only. Scale bars are 1µm in **A-D**.

4. Characterising the macula

4.1 Introduction:

4.1.1 Reviewing the clinical phenotype of MacTel type 2

As I have previously reported, MacTel type 2 has a clinical phenotype that is restricted to the macula. Confocal blue reflectance and Red-Free imaging show an elliptical boundary; a restricted region of hyper reflectance around the fovea (Fig. 4.1 A), in a study of 62 MacTel type 2 eyes, by Charbel Issa and colleagues, the region of hyper reflectivity was seen in 94%.[137] It is unknown exactly what the blue light reflectance is an indication of, but it is suggested that the increased hyper reflectance is due to the loss of macular pigment in the central macula,[137] it has also been proposed that the hyper reflectivity could be a result of crystals or other neuroretinal deposits that are hyper reflective, such as that seen in canthaxanthin retinopathy (chapter **1.3.3**), however MacTel type 2 also exhibits crystalline deposits, which are clearly seen in confocal blue light reflectance as individual bright flecks (arrow heads Fig. 4.1 B). [137] This does not rule out hyper reflective deposits, but makes the scenario less likely as the concentration would have to be so high that they would be visible with OCT imaging,[301] which no one has reported. Macular pigments, zeaxanthin, meso-zeaxanthin and lutein are all yellow carotenoids, which absorb light preferentially in the blue spectrum, and therefore a reduction in the absorbance from the retina would lead to apparent hyper reflectance compared to a control (Fig. 4.1 B). Macular pigment depletion, shown by Charbel Issa and colleagues, is restricted to the parafoveal region, leaving what can be described as a halo of macular pigment, again elliptical in shape, with a clearly demarcated inner edge, and more diffuse peripherally,[139] correlating with this theory of blue light reflectance. All vascular telangiectasis is parafoveal (Fig. 4.1 C), dominantly starting in the temporal region and progressing to encircle the fovea with disease progression.[137-141] Leakage in late phase fluorescein angiogram also has a consistent pattern; the leakage diffuses radially through the retina, but stops abruptly leaving an ellipse of leakage parafovealy (Fig. 4.1 D).[148] Oedema can be present, found primarily at the fovea itself, resulting in a 'foveal drape'.[146]

When the clinical phenotypes are superimposed, macular pigment loss clearly correlates with the region of hyper reflectance in blue light and the region of macular pigment depletion forms an external 'boundary' point. No vascular telangiectasis or oedema has been reported outside of the region of macular pigment depletion and the leakage from late phase fluorescein angiogram diffuses up to a point just within this boundary, but is never seen to spread further (Fig. 4.1 E-H). Also retinal crystals have only been reported within this region

(arrow heads in Fig. 4.1 E). Importantly is has been shown that the size and shape of the area affected in the disease remains constant over time, unlike AMD and diabetic retinopathy the disease does not spread into peripheral retina. The region affected also appears to be consistent in size, shape and location between patients.

4.1.2 The macula boundaries

There is no anatomical or biochemical boundary that defines the edges of the macula as previously stated in chapter **1.1**. It is therefore interesting that the disease phenotype of MacTel type 2 has such a defined limit to its spread through the retina. The ganglion cell nuclei gradually decrease to a single layer with increased radial distance from the fovea, there is a high density of cone photoreceptors decreasing gradually to periphery and an increase in rod numbers, however there is no sudden change in pattern at this point.

4.1.3 Biochemical tools to investigate sample differences

There are two main ways to approach this question; either to study the genes that are differentially expressed between macula and peripheral retina (genomics) or to study the proteins that are differentially expressed (proteomics). DNA micro arrays can be used to study genomic comparisons, and they give you a full coverage of expression levels across the genome, however this would require extremely fresh tissue samples to work with.

RNA is unstable after death and because of the unavoidable delays inherent in human postmortem organ donation, difficult to analyse. Postmortem human eye tissue that we have available can be retrieved for processing within 6-12 hours and this material is therefore not suitable for genomic analysis. However, proteins in human samples are remarkably stable postmortem. Several studies have previously been able to acquire meaningful data from proteomic screens of human retina with postmortem delays between 4.5 and 17 hours.[302-306] Therefore with the tissue available to us, the most suitable approach was comparative proteomics. Proteomics, unlike genomics, does not give full coverage of all proteins expressed, but will be able to guide towards pathways and families of proteins that are differentially expressed.

A proteomic method that uses isobaric tags for relative and absolute quantitation (iTRAQ) has been used successfully for biomarker discovery in human specimens.[307-311] iTRAQ labels are isobaric labels that will react with the primary and secondary amines of peptides. iTRAQ labels can be purchased as sets of four labels (4-plex) and eight labels (8-plex). Each of the

labels has an identical mass, but upon collision induced fragmentation during MS/MS analysis, they fractionate differentially, releasing a reporter moiety and balance moiety (Fig. 4.2 A). This allows the samples to be distinguished. Fractionation of label 113, for example, will generate a 113m/z ion in an MS/MS spectrum (Fig. 4.2 A). The peak of this area is proportional to the relative abundance of the peptide derived protein from the analysed sample. The protein ratio between up to eight samples can be determined using iTRAQ, followed by separation and MS/MS analysis; the ratio between the different isobaric reporter moieties, which indicate the fragmented peptide's relative abundance, can be determined in a mixed pool of peptides from different samples (Fig. 4.2 B).

iTRAQ is performed by first trypsinising the individual samples for analysis. The peptides in each sample are then labelled with one of the different isobaric labels. For 4-plex the isobaric labels are 114, 115, 116 and 117, whereas 8-plex has the additional labels, 113, 118, 119 and 121. These samples (4 or 8) are then mixed together at equimolar concentrations, and next further separated by two-dimensional chromatography. The sample is then run through a mass spectrometer, the individual peptides are fragmented and each peptides amino acid sequence determined. Whilst at the same time the ratio of that peptide is determined between the different samples originally mixed, this is done using the ratio between the different iTRAQ reporter ions (Fig. 4.2 B).

The primary advantage of using iTRAQ over other methods of relative quantitation proteomics is that after trypsinisation, iTRAQ labelling and mixing, all the subsequent separation conditions are identical for all samples (as they occur at the same time), this results in low coefficients of variance and faster analysis. It is also possible to include a pooled standard control in multiple plates, this allows all samples to be compared against the pooled control, and quantitation can be made between plates allowing larger sample numbers to be compared.

4.2 Aim:

To identify proteins with regional differential expression in the macula versus peripheral retina.

4.3 Materials and Methods:

Technical acknowledgements: I would like to thank Alice Len, University of Sydney, for her extensive work towards the proteomics reported here, the methods carried out by her have been clearly labelled in chapter 4.3.3. I would also like to thank Catherine Egan, Moorfields Eye Hospital, for her provision of the anonymised clinical images which I have analysed in this chapter.

4.3.1 Image analysis from clinical blue light reflectance

Digital confocal blue reflectance or red-free photos of 35 eyes from 22 patients were aligned so that the fovea and centre of the optic disc were on a horizontal line. The distance, in pixels, from the edge of the optic disc to the foveal centre was measured for each sample and set as 100%, the height (A) and width (B) of the region of increased blue light reflectance were determined as a proportion of this distance. Ratios were compared between samples, averaged and standard deviations calculated because the centre of the fovea was not always obvious, we overlaid the confocal blue reflectance images with colour fundus images using the vascular arcades as landmarks.

The dimensions in µm of the ellipse were measured in 14 samples where a scale was available; these were averaged and standard deviations calculated.

4.3.2 Dissection tools

The dimensions obtained from the confocal blue reflectance/red free analysis were used to manufacture a series of four concentric elliptical trephines of dimensions; 1.42mm by 1.25mm, 2.48mm by 1.60mm, 3.34mm by 2.65mm and 3.93mm by 3.36mm (Fig. 4.3 A-C) . Therefore being able to dissect and collect tissue from within the 'MacTel area' and a tissue sample from outside (non-'MacTel area'), with a buffer region between to allow for sample variation (Fig. 4.3 D).

4.3.3 Proteomics

4.3.3.1 Tissue collection and processing - Proteomics

Control post mortem retinal samples were collected and dissected at the 'Save Sight Institute', University of Sydney, Sydney, Australia. Tissue was collected from five donors, of ages; 21, 63, 64, 72 and 79 years old (Table 4.1). All with no known ophthalmic complaints or

diabetes. Tissue used had a postmortem time of between 3-11 hours; sufficient to maintain protein quality for proteomic analysis, as determined from previous publications.[302-306]

Whole eye cups were stored in sterile PBS at +4°C until dissected.

Retinae were removed from the sclera/RPE-choroid complex. The vitreous was dissected away. Two regions of retina were isolated using the aforementioned trephines (chapter **4.3.2**). These retinae samples were briefly washed in 0.1X PBS and then fresh frozen in 10µl protease inhibitor cocktail (Roche Diagnostics, USA). (Salt can interfere with downstream processing in the proteomics protocol, therefore a brief wash in 0.1X PBS is required to remove some of the salts prior to snap freezing).

4.3.3.2 Retina: Protein partitioning based on solubility

Tissue samples were thawed and fractionated on the principle of protein solubility based on the methods used by Fujiki *et al*.[312] To each tissue sample 5ml of ice cold 0.1 M Na_2CO_3 (pH 11.0) was added, then the sample was sonicated (Branson, Danbury, USA, output control of 2, 2x 30 seconds, 20–22˚C with cooling on ice between each burst) before being stirred on ice for 1 hour. The carbonate-treated membranes were sedimented by ultracentrifugation at 120,000*g* for 1 hour at 4 °C. The supernatant was separated and retained (see below), and the membrane pellet was washed once with ice cold 0.1 M Na_2CO_3 (pH 11.0) and then resuspended in 100µL 1% SDS (w/v) in preparation for protein assay and trypsin digestion.

4.3.3.3 Protein quantification and protein reduction/alkylation (performed by Dr. Alice Len)

Retinal derived protein concentrations were determined through the analysis of the quantity of individual amino acids per sample using a precolumn derivatisation HPLC method. An aliquot of 5µL of each sample to be analysed was dried down in a SpeedVac® concentrator (Savant [GMI, MN, USA]). Each aliquot of sample was then supplemented with 10µL of 100pmol internal standard (α-amino butyric acid; AABA) prior to derivatising according to manufacturer's instructions using an AccQ Tag Ultra derivatisation kit (Waters Corporation). HPLC analysis was based on the method of Cohen (2001) but adapted for use with an ACQUITY UPLC system (Waters Corporation). The column employed was an ACQUITY UPLC BEH C18 1.7um column with detection at 260nm and a flow rate of 0.7 ml/min. This enabled a 10.2 minute analysis time per sample. Each sample was analysed in duplicate and the results averaged. Each sample of retinal derived protein sample, 20µg, was diluted to a final concentration of 0.1% SDS (w/v), 0.5M TEAB, pH 8.5 and 50% (v/v) methanol. Protein

samples were reduced with 5mM Tris(2-carboxyethyl)phosphine (TCEP) for 1 hour at 60°C, and alkylated with 10mM *s*-methylmethanethiosulfonate (MMTS) at room temperature for 10 minute in preparation for the digestion of proteins with trypsin.

4.3.3.4 Tryptic digestion and iTRAQ reagent labelling of peptides *(performed by Dr. Alice Len)*

Two 8-plex experiments were run. Run1 consisted of digested retinal derived protein samples obtained from 4 control individuals, pooled with corresponding regions from each individual, keeping soluble (S) and less soluble (LS) fractions separate (experiment plan, Run 1, Table 4.2); the 2 regions indicated in Fig. 4.3, plus two additional regions, one mid-peripheral nasal retina and one mid-peripheral temporal retina, were used for labelling with iTRAQ labels 113, 114, 115 and 116, S fractions and 117, 118, 119 and 121 LS fractions, obtained from iTRAQ 8-plex reagent kit. Tagging was carried out according to the manufacturer's instructions (Fig. 4.2 A [Applied Biosystems, CA, USA]). Less soluble (LS) and soluble (S) fractions obtained from partitioning as described in chapter **4.3.3.2**. All LS fractions were diluted with 50% (v/v) methanol to obtain a concentration of SDS < 0.1% in preparation for trypsin digestion. Run 2 was performed using only S fractions from two individual donors, one of which was also included in the pooled sample. From a 64 year old donor, regions were labelled with iTRAQ labels 113, 114, 115 and 116 respectively, whilst tissue from a 72 year old donor was labelled with 117, 118, 119 and 121 isobaric tags (as per experimental plan, Run 2, Table 4.2). MALDI TOF/TOF MS was used to verify iTRAQ reagent labelling of each sample's peptides using a 4700 Proteomics Analyser (Applied Biosystems/MDS Sciex, CA, USA). Samples were initially desalted and concentrated using PerfectPure C_{18} tips (Eppendorf, Hamburg, Germany) and eluted off the column using 0.8µL of 4mg mL^{-1} α-cyano-4-hydroxycinnamic acid in 70% v/v acetonitrile (ACN) and 0.1 % trifluroacetic acid (TFA), then subsequently spotted onto a 4700 MALDI target plate (Applied Biosystems) for MS/MS analysis. All spectra were acquired manually, with typically 200 shots accumulated at each spot. Peptide mass spectra was obtained in reflector positive mode, 4 peptides from each sample were then further analysed through MS/MS using a positive mode with a 1kV potential to confirm the presence of reporter iTRAQ tags.

4.3.3.5 Strong Cation Exchange *(performed by Dr. Alice Len)*

Once labelling was verified all 8 labelled samples were combined from each iTRAQ experiment and subjected to batch offline strong cation exchange chromatography. A 50µL

aliquot of Macro-Prep S Ion Exchange Support (BioRad, CA, USA) homogenous slurry was sedimented at 300x *g* for 30 seconds, washed with Buffer A (5mM K_3PO_4, 350mM KCl, CH_3CN 25% (v/v), pH 2.7) and equilibrated with Buffer B (5mM K_3PO_4, CH_3CN 25% (v/v), pH 2.7). Combined labelled samples were then added to the equilibrated support and incubated on a platform rocker for 1hour at RT. Support bound labelled peptides were then centrifuged (300x *g* for 30 seconds) and the supernatant removed. The support was then gently washed with 500µL Buffer B, sedimented (300x*g* for 30 seconds) and the supernatant removed, this step was repeated once more. Peptides were released by adding 50µL Buffer A, vortexing briefly, centrifuging (300x *g* for 30 seconds) and collecting the supernatant. This step was repeated three times to obtain a total volume of 200µl of eluted peptides. The sample was filtered using a Millipore Ultrafree-MC centrifugal device (Millipore, Billerica, MA, USA) to remove residual support.

4.3.3.6 RP nano-LC ESI MS/MS (performed by Dr. Alice Len)

MS/MS analysis of iTRAQ labelled peptides was carried out using an Agilent 1100 nanoLC system (Agilent, Santa Clara, CA, USA) and QStar XL MS/MS system (Applied Biosystems). After SCX clean up, the sample was dried with SpeedVac and resuspended with 50µl of 0.1% (v/v) TFA and 2% (v/v) ACN. A 3µl aliquot of the sample was taken and further diluted to 40µl and loaded onto a reverse phase peptide Captrap (Michrom Bioresources, Auburn, CA, USA) and desalted with buffer solution A (97.9% [v/v] 18 MΩH_20/0.1% [v/v] TFA/2% [v/v] ACN). After desalting, the trap was switched on line with a 150µm x 10cm C_{18} 3µm 300A ProteCol column (SGE, Ringwood, Victoria, Australia). The Buffer B (90% [v/v] ACN/9.9% [v/v] 18 MΩ H_20/0.1% [v/v] formic acid) gradient rose from 5% to 10% in two minutes and then to 50% in 80 minutes to elute peptides.

The LC eluent went through positive ion nanoflow electrospray analysis in an information dependant acquisition mode (IDA). A TOFMS survey scan was acquired whilst in IDA mode (m/z 350-1600, 0.5 second), with the 3 most intense multiply charged ions, those with counts greater than 70, in the survey scan sequentially subjected to MS/MS analysis. MS/MS spectra were accumulated for 2 seconds in the mass range m/z 100-1600 with a modified Q2 transition setting favouring low mass ions so that the reporting iTRAQ tag ion (113, 114, 115, 116, 117, 118, 119 and 121 Da) intensities were enhanced for quantification.

4.3.3.7 LC MALDI MS/MS (performed by Dr. Alice Len)

iTRAQ labelled peptides were also analysed via LC MALDI MS/MS. Sample was resuspended in 2% (v/v) ACN/0.1% (v/v) TFA to make a final concentration of 0.5mg ml^{-1}. The iTRAQ labelled peptides were separated by LC using a Tempo LC MALDI system (Applied Biosystems/MDS Sciex). Sample (10µl) was injected onto a reversed phase column (Chromolith® CapRod® Monolith Capillary column, 150 x 0.1mm [Merck, Darmstadt, Germany]). Peptides were eluted from the column using a linear solvent gradient from 2% (v/v) ACN (10 minutes) then switching to 50% (v/v) ACN for 60 min and then stepping to 90% (v/v) ACN for 5 minutes at a flow rate of 2µl $minute^{-1}$. Eluent was collected from T = 10 minutes until T = 77 minutes. The LC eluent was mixed with matrix (α-cyano-4-hydroxycinnamic acid, 4mg ml^{-1} in 90% (v/v) ACN, 10% (v/v) 10mM ammonium hydrogen citrate) at a flow rate of 1µl $minute^{-1}$ and spotted onto a MALDI target plate at a rate of 5025mS $spot^{-1}$ and allowed to air dry. MALDI MS was performed with an Applied Biosystems QSTAR Elite MS (Applied Biosystems/MDS Sciex) operating in an IDA mode.

In IDA mode a TOFMS survey scan was acquired (m/z 800-3500), with the five largest ions per spot (Exit factor 15) with a maximum of 2000 precursors per plate in the survey scan subjected to MS/MS analysis. MS/MS spectra were accumulated for 45 seconds (m/z 100-3500).

4.3.3.8 Bioinformatic analysis

Protein identification (using Swiss-Prot *Homo sapiens* database (version 54.8 containing 18,349 protein sequences) and iTRAQ quantification of peptides was performed with ProteinPilot 1.0 (Applied Biosystems/MDS Sciex) using the Paragon algorithm[313] where a 95% confidence (> 1.3 Protscore) setting was used for protein identification. Loading error was taken into consideration and data were normalised using the bias correction function in protein pilot. It has been previously demonstrated from analysing repeat run data generated from QStar XL MS/MS system and analysed using ProteinPilot (Applied Biosystems), that it provides excellent reproducibility with a coefficient of variance of 11.7%.[314] This exact same analysis system was employed for our iTRAQ analysis and therefore we have used a fold changed of at least 1.3.

4.3.4 Histology

4.3.4.1 Tissue donor information and embedding - Histology

Retinal tissue was used from 17 anonymous healthy donors with no reported ophthalmic complaints (Table 4.1)

Retinal tissue was wax embedded as per chapter **2.3.1.**

Further retinal samples were embedded for cryosectioning. A region of the posterior globe that included the optic disc, fovea and a section of nasal periphery was dissected and the vitreous carefully removed from the retinal surface. Tissue was equilibrated in 30% sucrose overnight and transferred to optimal cutting temperature compound (Agar, UK), orientated and frozen over dry ice. Sections were then cut at 10µm and collected onto Superfrost® plus slides (VWR, UK). For tissue orientation please refer to chapter **4.3.4.4**. Slides were stored at -20°C and dried for at least 2 hours under a fan prior to further processing.

4.3.4.2 Antigen retrieval and Immunohistochemistry

Antigen retrieval and immunohistochemistry were performed as previously described in chapter **2.3**. For GFAP, LDHB and CRYAB stains, slides were heated to 135°C in citrate buffer for 10 minutes (wax sections), 125°C in citrate buffer for 10 minutes (cryo sections). For the sections that were both stained with fluorescence immunohistochemistry and DAB; sections were hydrogen peroxide treated to block endogenous peroxidases prior to antigen retrieval. Sections were then stained using the standard fluorescence immunohistochemistry protocol in chapter **2.3.4**. Images were taken, after which the coverslips were carefully removed and the sections washed in PBS for 2 hours. The standard DAB immunohistochemistry was then carried out as per chapter **2.3.5**. Slides were coverslipped and corresponding images taken using an Olympus BHX series epifluorescent microscope.

4.3.4.3 Primary antibodies

GFAP-Cy3 (C9205, Sigma, UK), LDHB (H00003945-M01, Abnova, UK), αB crystallin (Chemicon AB1546), all used at 1:200 dilution.

4.3.4.4 Tissue orientation and image analysis

Tissue shrinkage is a known fixation and processing artefact.[315] Absolute measurements from retinal sections can therefore not be used for comparison against clinical images. To

accommodate for this proportional measurements against landmarks of the tissue assumed to remain constant during fixation and processing. The distance between the edge of the optic disc and fovea is known to remain relatively constant between people, at 11.8° or 3.4mm temporal.[316] Assuming tissue shrinkage is constant pan retina, it is possible to correlate sections with clinical images using the fovea and optic nerve edge as landmarks.

GFAP stained sections, directly through the centre of the fovea and optic nerve were used for analysis. In the naso-temporal axis, 7 donors were analysed. Pixel distances were taken between the start of the neural retina at the optic nerve edge, and the point where GFAP staining ceases to be positive in all Müller cell processes at the outer limiting membrane. From this point to the centre of the fovea, and the distance from the fovea to the extent of the GFAP staining at the nasal edge.

A further 7 donor eyes were sectioned to retrieve the dimension of GFAP staining in the inferior-superior axis through the fovea. These sections lack the optic nerve as a landmark to establish the degree of shrinkage during processing, therefore sections were taken in the inferior-superior axis, staring at the temporal side of the fovea. Once the foveal pit was passed, the cryo block was re-orientated 90° so that sections were taken through the optic nerve and the nasal edge of the 'MacTel area'. The distance between the inferior and superior extents of the GFAP staining were then measured, whilst still allowing the distance between the edge of the optic nerve and nasal extent of the GFAP staining to be measured. This third distance then allows the degree of tissue shrinkage to be determined.

4.4 Results:

4.4.1. The 'MacTel area' is consistent between patients

Measurements from 35 eyes of 22 MacTel type 2 patients revealed that the dimensions of hyper reflectivity in confocal blue reflectance images were very consistent between patients. This region of hyper reflectivity will be referred to as the 'MacTel area' (Fig. 4.4 A). The height (A) was 65.3% and the width (B) was 83.8% (Fig. 4.4 A and B) of distance C, the distance between fovea and optic disc edge (set at the internal constant standard). This equates to 2.34mm (height, A) by 3.00mm (width, B) (Fig. 4.4 C), and the distance from fovea to the optic disc edge 3.45mm; as determined with 14 images where a scale was available. As the images taken clinically reflect a curved surface in 2D, this has to be taken into consideration with this type of analysis. It has been previously calculated that the distance between the optic disc and the fovea is 3.4mm, using the formula by Drasdo and Fowler[316] which corrects

for the curvature of the back of the eye using standard imaging distances. The difference between the measured result and that given by the formula with curvature correction is 0.05mm, or 1.47%. This result shows that the difference between 2D image measurements and corrected *in vivo* measurements is smaller than the standard deviation of measurements (7%), making measurements from 2D images applicable in this format.

The area and location affected by MacTel type 2, 'MacTel area', is consistent between patients.

4.4.2 Protein identification in retinal tissue

We collected retinal samples from the two macula regions (Fig. 4.3) and from two mid-peripheral regions in temporal and nasal retina. The two mid-peripheral retina sample results are not reported in this thesis as analysis has yet to be completed, and is not directly relevant for the question posed; only data from the comparison of the two macula regions is reported.

Tissue was dissected from 5 donor retinae. To increase the breadth of the proteome map, each tissue region was partitioned into soluble (S) and less soluble (LS) fractions, using sodium carbonate treatment[312] followed by trypsin digestion. To compare the different samples, two iTRAQ runs were performed (Table 4.2). The first iTRAQ run comprised of pooled protein from four of the donors; a smaller amount of protein was extracted in LS fraction, as such multiple donors LS fraction were pooled to have a sufficient amount (>6 µg) to run. After labelling, all samples were further fractionated at a peptide level using SCX chromatography, then separated and analysed using 2D LC MS/MS.

Comparative proteomics identified 419 non redundant proteins in Run 1 and 492 proteins in Run 2. The data from the 64yr old single sample shows 66 up and 99 down regulated proteins within the 'MacTel area', the 72yr old data shows 107 up and 128 down regulated proteins, Pooled sample (LS) has 32 up and 41 down regulated proteins and Pooled sample (S) has 28 up and 26 down regulated proteins. When cross compared, the two runs (4 sample region pairs) show 44 proteins identified as up regulated within the 'MacTel area' in two or more comparisons, and 61 proteins down regulated in two or more comparisons (list of protein hits, downregulated inside the 'MacTel area', Table 4.3 and upregulated within the 'MacTel area', Table 4.4).

4.4.3 Sample comparisons

All proteins that were differentially regulated between samples (i.e. up in the macula of one sample, but down in another sample) have been excluded. Only proteins identified in more than two comparisons have been investigated further. Proteins that had a restricted expression pattern to the macula, when confirmed with immunohistochemistry, were mapped against the 'MacTel area' to assess if there was any correlation.

4.4.3.1 Innate immune system proteins

One protein was identified as differentially expressed in all four samples; Long palate lung and epithelial carcinoma protein 1 (LPLUNC1). This protein is known to be a member of the innate immune response, normally associated with the respiratory system.[317] Other members of the innate immune system were also up regulated within the 'MacTel area' in two or more samples; Leukocyte elastase precursor (ELANE), Bacteriacidal/permeability increasing protein-like 1 (LPLUNC2), Lysozyme C precursor (LYZ), Lactotransferrin (LT), Neutrophil defensin 3 precursor (DEF3A) and Neutraphil gelatinase-associated lipocalin (LCN2). Preliminary investigation showed LPLUNC1 expression in the nuclei of ganglion cells (data not shown), and DEF3A expression in ganglion cell nuclei and cone inner segments (data not shown). The other proteins of interest have yet to be investigated further. The expression of these two proteins in ganglion cell and cone photoreceptors explains the regional differences in the proteomic results. Even though effort was taken to reduce cell type concentration differences between the two regions compared, there is a significant increase in cone photoreceptor and ganglion cell concentration in the 'MacTel area' sample. There is no distinct boundary seen in the expression of these proteins, the expression followed the distribution of cell types and decreased gradually towards peripheral retina as cell numbers decreased, thus making them unlikely candidates of interest in determining the susceptibility of the macula with respect to MacTel type 2.

4.4.3.2 Aerobic and anaerobic energy

The glycolytic pathway is known to be predominantly active in retinal glia, [265, 266] while retinal neurons generate ATP through oxidative phosphorylation,[264] as referred to in chapter **2**. The proteomic results have shown glycolytic proteins and oxidative phosphorylation proteins both up and down regulated in the 'MacTel area' with no discernable pattern.

Cytochrome *c* oxidase subunit 4 isoform 1, Cytochrome *c* oxidase subunit VIb isoform 1, ATP synthase subunit alpha and beta mitochondrial precursors and ATP synthase-coupling factor 6, mitochondrial precursor were downregulated whilst cytochrome *c and* ATP synthase delta

chain are up regulated in the 'MacTel area' (Table 4.3 and Table 4,4). The glycolytic enzymes; fructose-bisphosphate aldolase C, fumarate hydratase, pyruvate kinase isozymes M1/M2 and transaldolase (pentose phosphate pathway but interconverts D-Glucose-6P and Glyceraldyde-3P used in glycolysis) were down regulated in the 'MacTel area' and yet conversely glucose-6-phosphate was up regulated.

The unclear nature of the results prompted a closer look at the two pathways. An antibody directed against cytochrome *c* oxidase (COX2) showed strong staining within the cone photoreceptor inner segments [highest concentration of mitochondria,[318] (Fig. 2.8 R) and punctate staining within the IPL and OPL (Fig. 2.8 R). Two distinct bands are visible within the IPL, this correlates to the ON/OFF layering of bipolar and ganglion cell synapses. COX2 staining of the plexiform layer thickens with increasing packing density of the ganglion cells and interneuron's towards the fovea (Fig. 2.8 I), but absent at the fovea. Cone numbers increase in number and packing density towards the fovea, the highest density under the fovea, this was reflected by the increased COX2 positive photoreceptor inner segments at the fovea. Immunohistochemistry showed an increase in COX2 towards the central macula, however this was only a reflection of one protein from the oxidative phosphorylation pathway.

LDHB, down regulated in the 'MacTel area' from the proteomic screen, was expressed within the ganglion cell layer and throughout the nerve fibre layer, with the dendritic morphology consistent with astrocyte processes. There was also a strong expression within the Henlé fibre layer (arrowhead in Fig. 4.5 A and B). It is known that the glycolytic pathway is dominant in glia of the retina,[319] so it stands to reason that LDHB is expressed by astrocytes and Müller cells, but Müller cells in Henlé fibre layer have a higher expression than those in the periphery (Fig. 4.5. B and C).

The expression pattern of COX2 and mixed data from proteomics led us to the conclusion that oxidative phosphorylation in the retina bared no relation to the 'MacTel area'. The immunohistochemistry with LDHB did however show restricted expression to the Müller cell processes within the Henlé fibre layer, implying that differences in glycolytic metabolism might be present across the human retina.

4.4.3.3 Carotenoid binding protein

Glutathione S Transferase (GSTP1), the Pi isoform has been shown to bind the carotenoid zeaxanthin[320] and to be located within the IPL and OPL of the retina with the strongest staining with immunohistochemistry at the macula.[320] It was therefore not surprising that

GSTP1 was found to be up regulated within the 'MacTel area' in our proteomic screen. It has been shown previously that there is no distinct boundary in the expression of this protein.

4.4.3.4 Lens proteins

The well-established lens proteins, αA crystallin and αB crystallin, are both up regulated within the 'MacTel area'. αB crystallin is known to be widely spread throughout the body in different organs, however αA crystallin expression was more restricted. Immunohistochemical confirmation of αB crystallin expression in the retina revealed staining of the astrocytes and Müller cell processes. There was increased staining within the Henlé fibre layer (Fig. 4.6). αA crystallin expression will be discussed in more detail in chapter **5**.

4.4.3.5 Reactive Müller cell and classic astrocyte protein

The proteomic data showed GFAP was downregulated within the 'MacTel area'. GFAP is primarily expressed by astrocytes in the human retina, however gliotic Müller cells upregulate GFAP. The foveal avascular zone (FAZ) at the fovea is devoid of astrocytes, which could explain the decrease in GFAP expression, however the FAZ is only 0.7mm in diameter,[321] significantly smaller than the inner edge of the 'MacTel area' ring sample (1.42mm x 1.25mm, Fig. 4.3), so this will not have had an impact on the astrocyte content of the sample. It is also unexpected as the anti-GFAP antibodies used in chapter 1 show a faint GFAP positive stain in the Henlé fibre layer but no expression in the outer plexiform of the peripheral retina.

Fluorescent immunohistochemistry with an antibody directed against GFAP showed strong staining of astrocytes within the ganglion cell and upper half of the inner nuclear layer (Fig. 2.6 A-D). There was a significant number of GFAP positive astrocytes surrounding the ganglion cell projections in the nerve fibre layer. The nerve fibre layer was relatively thin on the temporal side of the fovea and in the immediate parafoveal region. The GFAP positive astrocytes revealed that the nerve fibre layer rapidly increased in thickness from the apex of the foveal pit towards the optic nerve. A faint GFAP positive stain was found in the Henlé fibre layer (arrow in Fig. 2.6 B).

A more sensitive immunohistochemical approach (that utilises amplification to generate a greater intensity stain per bound primary antibody) was used to investigate the faint GFAP expression within the Henlé fibre layer. This revealed that GFAP expression was not restricted to astrocytes, processes were revealed that span the entire depth of the retina and formed part of the Henlé fibre layer, consistent with Müller cell morphology. However the stain was restricted to parafoveal retina (Fig. 4.7 A-D).

The finding of increased LDHB staining within the Henlé fibre layer was opposite to the proteomic data for LDHB. This was most likely due to expression of LDHB within retinal astrocytes, seen with immunohistochemistry. The number of retinal astrocytes increased within the nerve fibre layer towards the optic disc form the fovea. This was due to the increase in the number of ganglion cell axons merging and projecting back to the brain, and subsequent increase in the number of associated astrocytes which are essential in maintaining neuronal homeostasis. Therefore the increased number of astrocytes, that express LDHB, outside of the 'MacTel area' had masked the increase in LDHB expression within the Henlé fibre layer.

4.4.4 A sub population of macula Müller cells

αB crystallin positive staining co-labelled with the Müller cell specific marker vimentin within the Henlé fibre layer (Fig. 4.8). While the expression of vimentin persisted into peripheral retina, the expression of αB crystallin was restricted to Müller cells within the Henlé fibre layer. The expression patterns of GFAP, LDHB and αB crystallin correlate with each other, and all have morphology expectant of Müller cells. Expression of all three markers stopped prior to the edge of the Henlé fibre layer, there we found a small population of laterally displaced Müller cells that do not express GFAP at the outer edges of the Henlé fibre layer.

In summary, we found a sub population of Müller cells in the central macula that has a different molecular expression pattern to adjacent Müller cells in the peripheral retina.

4.4.5 'MacTel area' correlates to the sub population of Müller cells

Clinical observations indicate that the elliptically shaped 'MacTel area' extends about half way from the fovea to the edge of the optic disc. Our GFAP immunohistochemistry staining was strikingly similar (Fig. 4.9 A).

Taking measurements at the outer limiting membrane (Fig. 4.9 B and B'), GFAP stained sections through the fovea from 7 donors (naso-temporal axis) and 7 donors (inferior to superior axis) revealed that the dimensions of GFAP stained Müller cells, as a ratio of the distance between the optic disc edge and fovea centre, directly correlated with the confocal blue reflectance dimensions from MacTel type 2 patients (Fig. 4.9 A). The correlation showed no statistically significant differences (A/C $p = 0.9$, B/C $p = 0.9$). Although this was not a formal proof that the Müller cell sub population and 'MacTel area' were statistically similar, the high p value and spread of results shown by the graphs (Fig. 4.9 C and D) strongly suggested that the regions correlated.

4.5 Discussion:

We chose quantitative peptide labelling with iTRAQ because it does not discriminate against peptides with certain physiochemical properties as much as other quantitative protein based techniques do. Increasing the number of proteins that can potentially be identified, and this approach is compatible with proteins derived from human tissue. In retrospect 4-plex rather than 8-plex would have been more appropriate for this study. Although it allows fewer samples to be compared at once, 4-plex has since been shown to obtain more protein and peptide identifications than 8-plex; by our collaborators in Sydney, Dr. Alice Len and Prof. Mark Gillies (data not shown) and by others.[264] The S and LS fractions should also have been run on different plates; when the fractions are split, different protein populations are likely to be collected in the different fractions (due to the properties of membrane bound verses cytosolic proteins) therefore the probability that the same protein was identified in all 8 samples on one plate was decreased.

Although GFAP and LDHB were downregulated in the proteomic data, immunohistochemistry revealed that they were expressed in a population of cells only present at the macula. We know that the expression within these cells is comparatively low as it can only be visualised using amplification immunohistochemistry, therefore the difference seen with proteomics is likely a consequence of other cell types in the retina masking the expression of GFAP and LDHB in the macula Müller cell. GFAP is highly expressed, and LDHB to lesser extent in the retinal astrocytes. Astrocytes increase in number significantly on the nasal side of the fovea towards the optic nerve within the nerve fibre layer, where they ensheathed ganglion cell axons, aiding in signal conduction and cellular homeostasis. The ganglion cell axons project back to the optic nerve from all aspects of the retina, as such the density increased dramatically towards the optic nerve head. Although regions were dissected very close together to minimise the masking effects of changes in photoreceptor and ganglion cell distribution; the nerve fibre layer is a feature that also changes significantly over a short distance parafoveally. It is therefore likely that in our experiment macular expression changes were masked by other cell types.

The three markers that distinguish a new sub population of macula Müller cells have all been shown to be up regulated in retina as a stress response.[257, 322] Provis and colleagues have also previously shown that GFAP is specifically expressed within parafoveal Müller cells in late gestation/ new born healthy human retinae,[110] however they also report a loss of expression soon after birth. They have speculated that this represents localised stress within the developing macula that might cause an inherent weakness that persists into adulthood and

could be the reason for the susceptibility of the macula to disease.[104, 245] It cannot be ruled out that the expression of GFAP, LDHB and αB crystallin in the Henlé fibre layer does represent a localised stress response, be it postmortem or persistent in living tissue due to the higher metabolic demands of central retina. What can be stated is that the specificity of the region of GFAP, LDHB and αB crystallin expression does still imply that this is a sub population of Müller cells that differ from those that are adjacent. Müller cells have been shown to up regulate GFAP after laser photocoagulation, in Müller cells distant from the site of injury,[70, 71] in this respect such a consistent site of stressed Müller cells is unlikely. Our findings suggest that Müller cells in the macula are a differentially differentiated population of Muller cells that either; express GFAP, LDHB and αB crystallin constitutively, or that are more prone to stress and up regulation of these proteins in response.

The results of this chapter are a first on two accounts; it is the first time that biochemical markers for a specific region of the macula has been identified that are not based upon photoreceptor distribution. Further still it is the first time that a grouping of specialised Müller cells has been identified within the retina. Based on marker expression, Müller cells have previously been thought to be a homogenous population throughout the retina.

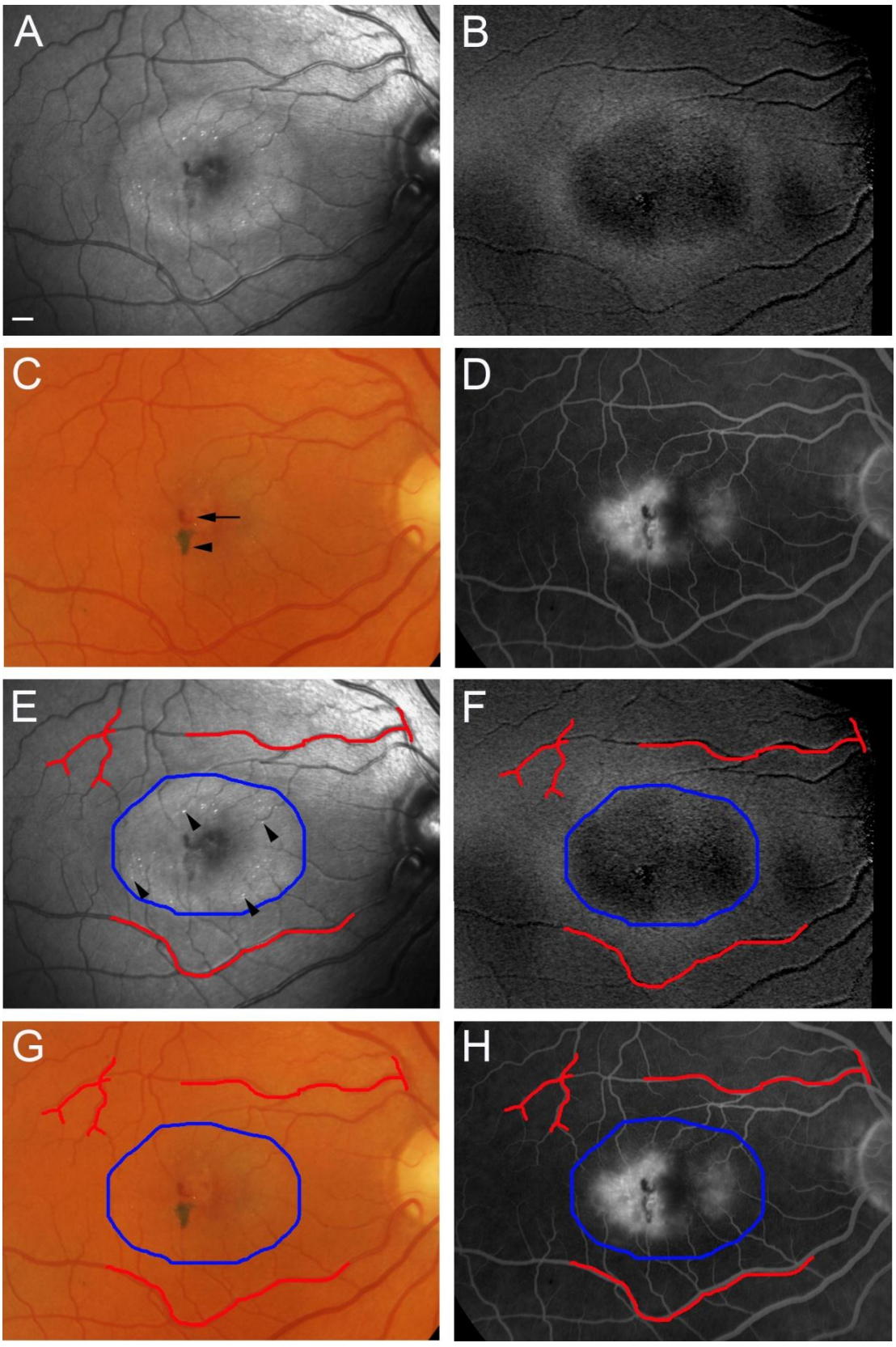

Figure 4.1. MacTel type 2 disease phenotype.
A parafoveal region of hyper reflectance is apparent on confocal blue light reflectance (**A**), a ring of macular pigment (imaged with DWAF) is left through central macular pigment loss (**B**). Telangiectatic vessels are visible with fundus photography (arrow in **C**, and pigment epithelium infiltration denotes a right angled venule temporal to the fovea (arrow head in **C**.

Late phase fluorescence angiography reveals parafoveal vascular leakage (**D**), primarily at the point of telangiectatic vessels (**C, D**). Vessel patterns (red lines **E-H**) allow the region of hyper reflectivity (blue line **E-H**) to be superimposed onto other imaging modalities. All clinical phenotypes of MacTel type 2 lie within the region of hyper reflectivity (**E-H**), including retinal crystals (arrow heads in **E**). Scale bar is 400μm. Clinical images from an anonymous MacTel type 2 patient, courtesy of Dr. Catherine Egan, Moorfields Eye Hospital, London, UK.

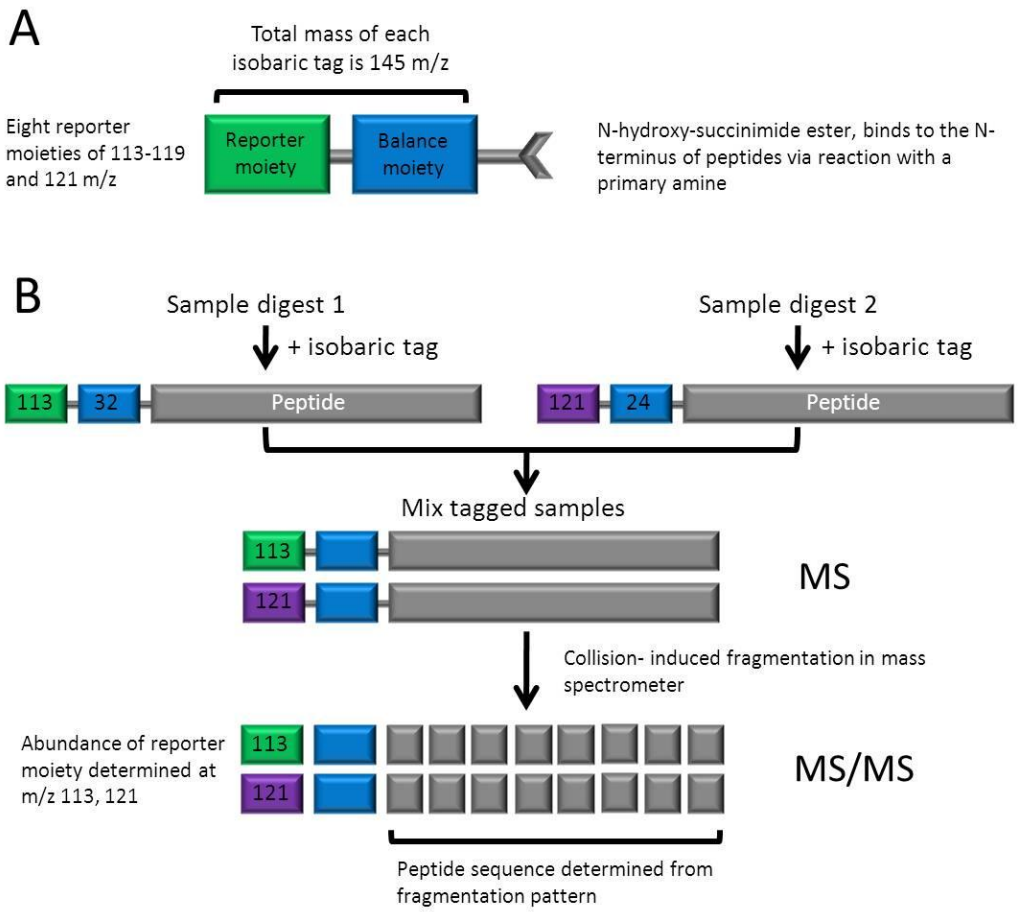

Figure 4.2. Overview of iTRAQ labelling and workflow.

iTRAQ isobaric tags consist of a reporter moiety of m/z 113-119 or 121, and a balance moiety which balances the total m/z of each tag to 145 m/z (**A**), linked to an *N*-hydroxy-succinimide ester allowing binding to a peptide. Labelled samples are mixed, fractionated by nanoLC and analysed by tandem mass spectrometry (MS/MS) (duplex experiment as example, **B**). Fragmentation data is then interpreted using established databases, and protein identifications made. The fragmentation of each moiety tag is measured and enables relative quantification of the peptides and hence proteins between samples run. m/z; mass to charge ratio.

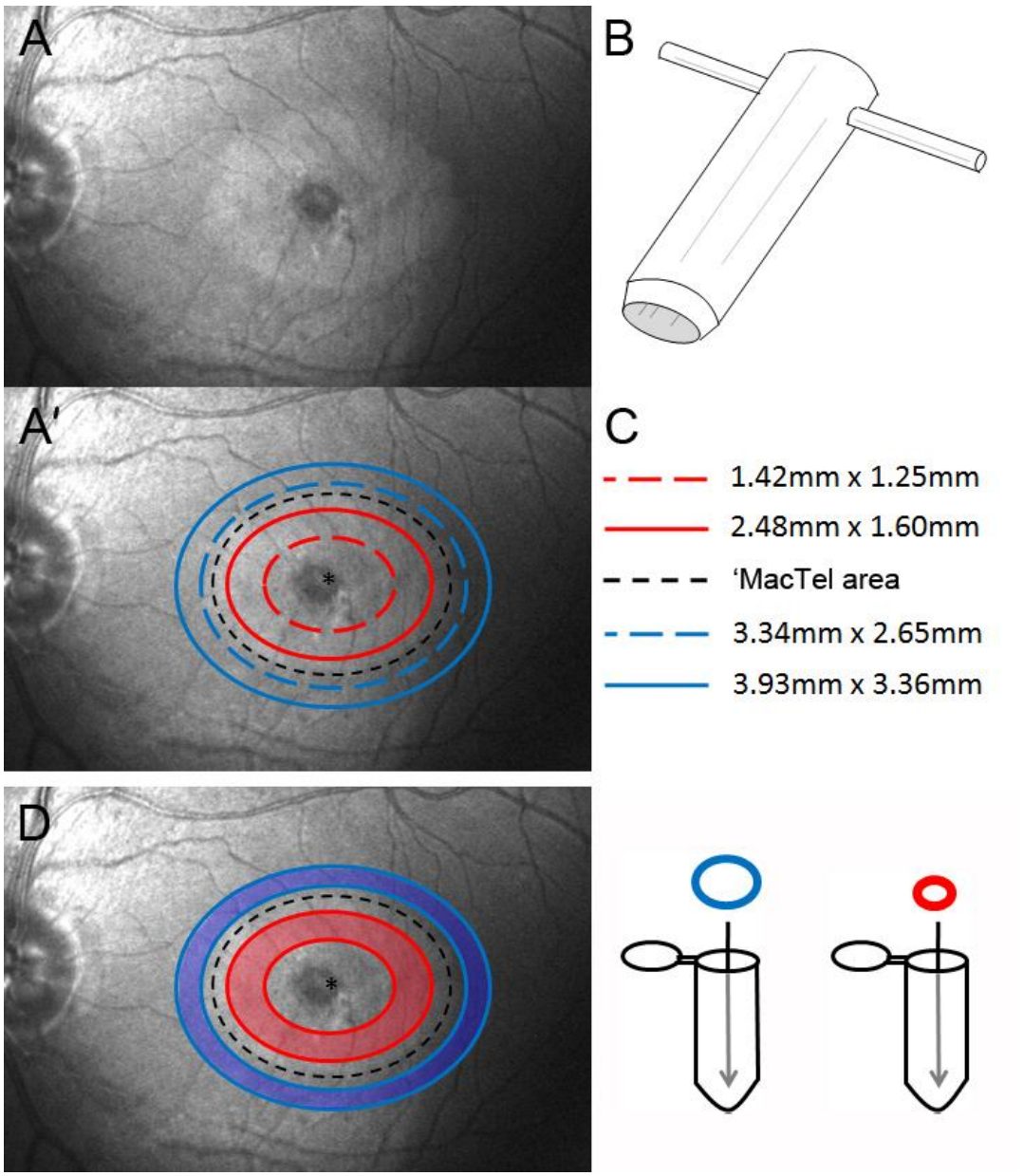

Figure 4.3. Retinal dissection trephines.

(**A,B**) Four trephines (dimensions **C**) designed to dissect retina. (**D**) Two regions are isolated from the macula; one inside the 'MacTel area' (red), one outside, non-'MacTel area' sample (blue).

Table 4.1: Donor tissue information

Age (yrs)	Cause of death	Postmortem delay	Processing	Ophthalmic history
Fresh frozen for Proteomic analysis				
21	Subdural haemorrhage	11 hours	Protein extraction	None reported
63	Heart attack	7 hours	Protein extraction	None reported
64	Heart attack	3 hours	Protein extraction	None reported
72	Colon cancer	8 hours	Protein extraction	None reported
79	Ovarian cancer	6 hours	Protein extraction	None reported
Fixed tissue for immunohistochemistry (2% PFA)				
54	Breast cancer	7 hours	Wax sectioned	None reported
56	Colon cancer	6 hours	Wax sectioned	None reported
61	Heart attack	18 hours	Cryo sectioned	None reported
62	Unknown	14 hours	Cryo sectioned	None reported
66	Stroke	13 hours	Cryo sectioned	None reported
66	Heart attack	8 hours	Cryo sectioned	None reported
67	Subdural haemorrhage	8 hours	Cryo sectioned	None reported
68	Heart attack	11 hours	Cryo sectioned	None reported
68	Heart attack	7 hours	Cryo sectioned	None reported
70	Subdural haemorrhage	20 hours	Cryo sectioned	None reported
75	Unknown	24 hours	Cryo sectioned	None reported
76	Heart attack	16 hours	Cryo sectioned	None reported
79	Colon cancer	12 hours	Cryo sectioned	None reported
86	Heart attack	12 hours	Cryo sectioned	None reported
92	Unknown	8 hours	Cryo sectioned	None reported
93	Stroke	9 hours	Cryo sectioned	None reported

Table 4.1. Donor tissue information. PFA; paraformaldehyde.

Table 4.2: Experimental plan for two 8-plex iTRAQ runs.
Run 1: (Pooled samples)

Isobaric tag		**113**	**114**	**115**	**116**	**117**	**118**	**119**	**121**
Fraction		**Less Soluble (LS)**				**Soluble (S)**			
Sample region		***Non-'MacTel area'***	***'MacTel area'***	***Temporal***	***Nasal***	***Non-'MacTel area'***	***'MacTel area'***	***Temporal***	***Nasal***
Biological replicate	**21 yr old**	2.60µg	2.60µg	2.60µg	2.60µg	2.60µg	2.60µg	2.60µg	2.60µg
	63 yr old	2.60µg	2.60µg	2.60µg	2.60µg	2.60µg	2.60µg	2.60µg	2.60µg
	64 yr old	2.60µg	2.60µg	2.60µg	2.60µg	2.60µg	2.60µg	2.60µg	2.60µg
	79 yr old	2.60µg	2.60µg	2.60µg	2.60µg	2.60µg	2.60µg	2.60µg	2.60µg
Total amount of protein run per isobaric tag		10.4µg Pooled	10.4µg Pooled	10.4µg Pooled	10.4µg Pooled	10.4µg Pooled	10.4µg Pooled	10.4µg Pooled	10.4µg Pooled

Run 2:

Isobaric tag		**113**	**114**	**115**	**116**	**117**	**118**	**119**	**121**
Fraction		**Soluble (S)**				**Soluble (S)**			
Sample region		***Non-'MacTel area'***	***'MacTel area'***	***Temporal***	***Nasal***	***Non-'MacTel area'***	***'MacTel area'***	***Temporal***	***Nasal***
Biological replicate	**64 yr old**	8.71µg	8.71µg	8.71µg	8.71µg				
	72 yr old					8.71µg	8.71µg	8.71µg	8.71µg

Table 4.2. Experimental plan for two 8-plex iTRAQ runs, including the amount of each sample run. In Run 1, four donor samples were pooled for each sample region, in Run 2, two individual donors (Soluble fraction only) were run.

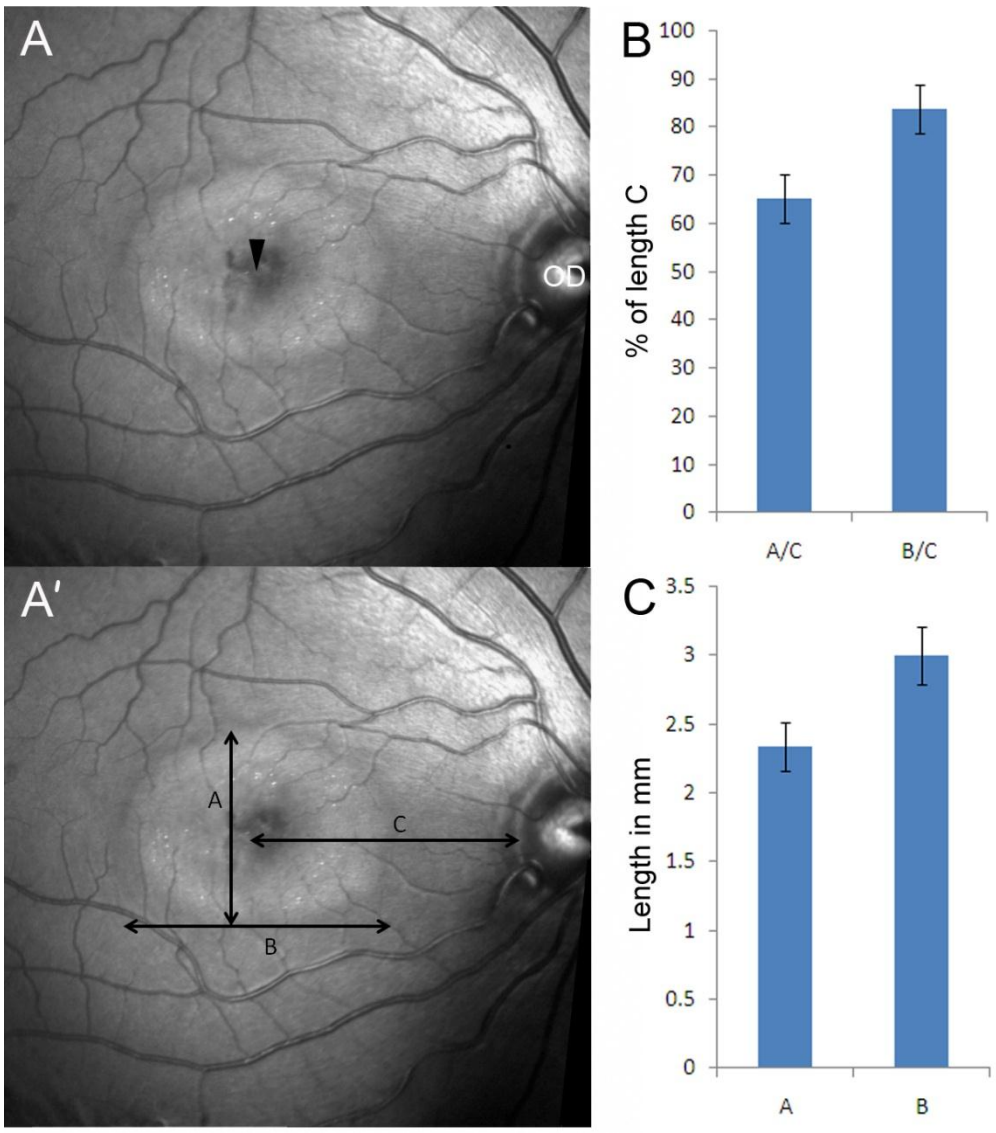

Figure 4.4. The 'MacTel area' is consistent between MacTel type 2 patients.
Area of hyper reflectivity in central retina (**A**) surrounds the fovea (arrow head), temporal to the optic disc (OD). Dimensions, A (inferior-superior axis), B (naso-temporal axis) and C (OD edge to fovea)(**A'**) were measured and found to be consistent between MacTel type 2 patients (**B**), n= 35 images. Dimensions were scaled as a proportion to distance C. These dimensions equate to actual distance of 2.34mm, A and 3.00mm, B (**C**), n= 14 images where a scale was available. Error bars; standard deviations from the mean. Clinical blue reflectance image courtesy of Catherine Egan, Moorfields Eye Hospital, London, UK.

Table 4.3: Proteomic results, down regulated proteins

Protein	Fold change			
	Run 2		Run 1	
	64 yr old (S)	72 yr old (S)	Pooled samples (LS)	Pooled samples (S)
Down regulated in 3 of the 4 comparisons				
Band 4.1-like protein 3		1.41	1.59	1.68
Guanine nucleotide-binding protein G(T) subunit gamma-T1 precursor	1.96	1.91		1.55
High mobility group protein B2	1.42	2.23		1.30
Non-histone chromosomal protein HMG-14	1.69	4.66		1.31
Splicing factor, arginine/serine-rich 3	1.56	2.73	1.45	
Heterogeneous nuclear ribonucleoprotein		3.05	1.34	1.43
Down regulated in 2 of the 4 comparisons				
10 kDa heat shock protein, mitochondrial	1.50	2.01		
14-3-3 protein eta	2.09	5.60		
14-3-3 protein gamma	1.47	1.54		
14-3-3 protein zeta/delta	1.49	1.57		
40S ribosomal protein SA	1.75	1.54		
Actin, cytoplasmic 2	1.64	9.12		
Aryl-hydrocarbon-interacting protein-like 1	2.33	1.33		
Aspartate aminotransferase, mitochondrial precursor	1.53	2.75		
ATP synthase subunit alpha, mitochondrial precursor	2.61	2.96		
ATP synthase subunit beta, mitochondrial precursor	2.63	6.85		
ATP synthase-coupling factor 6, mitochondrial precursor	1.39	1.64		
ATP-dependent DNA helicase 2 subunit 1	1.61	2.27		
Carbonic anhydrase 2	1.34	2.94		
Core histone macro-H2A.1	3.22	8.47		
Cytochrome c oxidase subunit 4 isoform 1	1.31	1.57		
Cytochrome c oxidase subunit VIb isoform 1	1.45	2.36		
Cytosolic non-specific dipeptidase	1.69	4.41		
Elongation factor 1-delta	2.68	1.91		
Fatty acid-binding protein, brain	1.45	4.70		
Fructose-bisphosphate aldolase C	1.85	3.37		
Fumarate hydratase, mitochondrial precursor	1.66	3.02		
Glial fibrillary acidic protein	1.89	3.08		
Guanine nucleotide-binding protein G(t) subunit alpha-1	4.13	1.91		
Heat shock cognate 71 kDa protein	1.46	2.31		
Heterogeneous nuclear ribonucleoproteins C1/C2	1.49	1.75		
High mobility group protein HMG-I/HMG-Y	2.09	6.31		

Histone H4	2.75	1.87		
Keratin, type I cytoskeletal 10	2.25	1.84		
Keratin, type II cytoskeletal 2 epidermal	1.38	1.33		
Lamin-B2	1.61	11.59		
L-lactate dehydrogenase A chain	1.66	4.53		
L-lactate dehydrogenase B chain	1.58	1.39		
Neurofilament light polypeptide	1.47	3.53		
Non-POU domain-containing octamer-binding protein	1.41	3.53		
Nucleoside diphosphate kinase B	1.66	10.57		
Poly(rC)-binding protein 2	1.39	2.99		
Protein DJ-1	1.37	2.13		
Pyruvate kinase isozymes M1/M2	2.11	3.80		
RNA-binding protein Raly	1.75	1.58		
Stathmin	2.07	1.46		
Stress-induced-phosphoprotein 1	1.51	2.75		
T-complex protein 1 subunit zeta	2.70	3.40		
Transketolase	1.33	1.85		
Tubulin alpha-1A chain	2.61	4.41		
Tubulin beta-2C chain	4.29	2.09		
Ubiquitin	1.58	4.02		
Vesicle-fusing ATPase	1.31	1.87		
Stress-70 protein, mitochondrial precursor	1.45		1.35	
Cell adhesion molecule 2 precursor		2.56	1.55	
Heterogeneous nuclear ribonucleoprotein A3		1.53	1.53	
Peptidyl-prolyl cis-trans isomerase A		1.85	1.36	
Synaptophysin		1.31	1.58	
T-complex protein 1 subunit theta		3.16	1.34	
Spectrin alpha chain, brain		1.61		1.37
Spectrin beta chain, brain 1		2.63		1.33
Transaldolase	1.53			1.32

Table 4.3. Proteomic results. List of proteins down regulated within the 'MacTel area'. Values indicate fold change compared to non-'MacTel area' sample. Greyed out cells are proteins that were not identified as down regulated. S; soluble fraction, LS; less soluble fraction.

Table 4.4: Proteomic results, up regulated proteins

Protein	Fold change			
	Run 2		Run 1	
	64 yr old (S)	72 yr old (S)	Pooled samples (LS)	Pooled samples (S)
Up regulated in all 4 comparisons				
Long palate, lung and nasal epithelium carcinoma-associated protein 1 precursor	1.89	3.25	1.41	1.35
Up regulated in 3 of the 4 comparisons				
60S ribosomal protein L7a	1.34	1.31		1.89
αA crystallin	2.19	3.73		1.51
Leukocyte elastase precursor	3.37	8.39	1.80	
Polymeric immunoglobulin receptor precursor	2.29	3.19	1.56	
Tubulin-specific chaperone A	2.23	1.67	2.43	
Up regulated in 2 of the 4 comparisons				
Glutathione S-transferase P		1.79	1.32	
Superoxide dismutase [Cu-Zn]	1.63			1.31
Centromere protein F			1.59	1.59
Endoplasmic reticulum protein ERp29 precursor			2.77	1.39
Glucose-6-phosphate isomerase			1.34	1.31
Keratin, type I cytoskeletal 19			1.42	1.57
Tubulin beta-2B chain			1.30	1.45
αB crystallin B chain	2.44	4.25		
Antileukoproteinase precursor	2.36	8.09		
ATP synthase delta chain, mitochondrial precursor	1.92	5.06		
Bactericidal/permeability-increasing protein-like 1 precursor	1.82	2.09		
Calretinin	1.56	4.06		
Cytochrome *c*	1.47	11.91		
DNA-(apurinic or apyrimidinic site) lyase	1.61	2.11		
Elongation factor 1-alpha 1	1.82	1.46		
Glutathione S-transferase Mu 5	1.33	1.92		
Heterogeneous nuclear ribonucleoprotein D0	1.31	1.74		
Heterogeneous nuclear ribonucleoprotein K	1.53	2.83		
Ig alpha-1 chain C region	3.08	5.65		
Ig lambda chain C regions	1.41	1.46		
Lactotransferrin precursor	1.87	3.05		
Lysozyme C precursor	3.22	5.40		
Mitogen-activated protein kinase 1	1.75	1.33		
N(G),N(G)-dimethylarginine dimethylaminohydrolase 1	1.57	2.05		
Neuroepithelial cell-transforming gene 1 protein	1.46	1.41		
Neutrophil defensin 3 precursor	11.59	12.13		

Neutrophil gelatinase-associated lipocalin precursor	1.74	2.25		
Phenylalanyl-tRNA synthetase beta chain	1.39	1.75		
Proline-rich protein 4 precursor	3.28	4.37		
Proteasome subunit alpha type-6	1.50	1.66		
Protein S100-A8	3.91	23.12		
Protein S100-A9	2.01	4.83		
Protein UNQ773/PRO1567 precursor	1.57	14.45		
Purine nucleoside phosphorylase	3.31	1.42		
Ras-related protein Rap-1A precursor	5.01	9.82		
Small ubiquitin-related modifier 3 precursor	1.32	1.91		
Uteroglobin precursor	1.37	2.49		
WD repeat-containing protein 1	1.82	1.94		

Table 4.4. Proteomic results. List of proteins up regulated within the 'MacTel area'. Values indicate fold change compared to non-'MacTel area' sample. Greyed out cells are proteins that were not identified as up regulated. S; soluble fraction, LS; less soluble fraction.

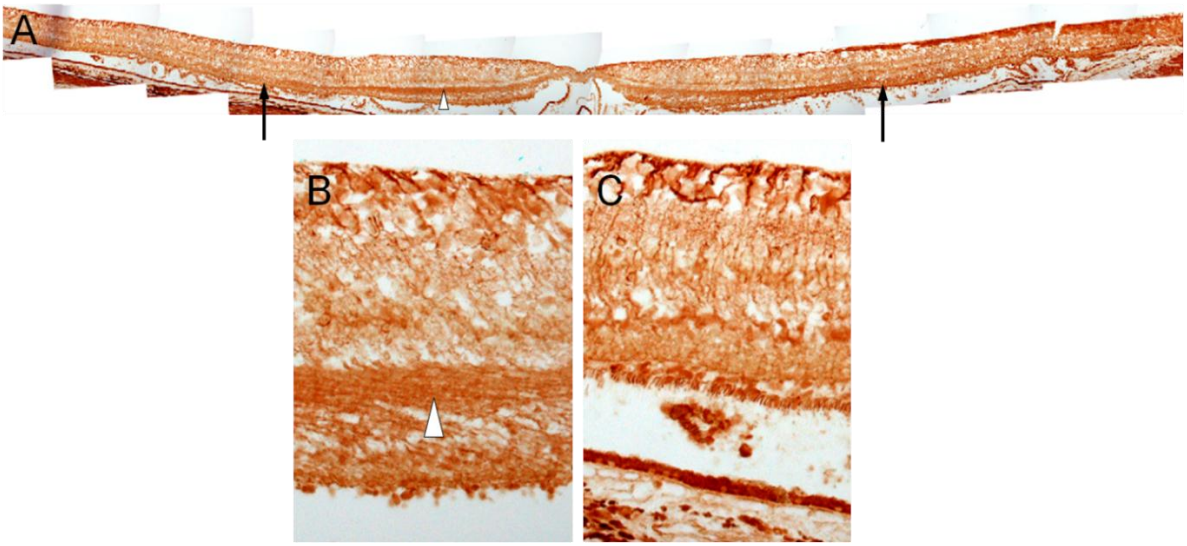

Figure 4.5. Lactate dehydrogenase expression in human retina.
Immunohistochemistry revealed lactate dehydrogenase (LDHB) expression in retinal glial cells (A). Ganglion cells appeared to uniformly express LDHB throughout the retina. Expression in Müller cells however was increased in processes of the Henlé fibre layer (region inside of arrows in **A**, arrowhead in **A** and **B**), compared to the OPL in the periphery (**C**).

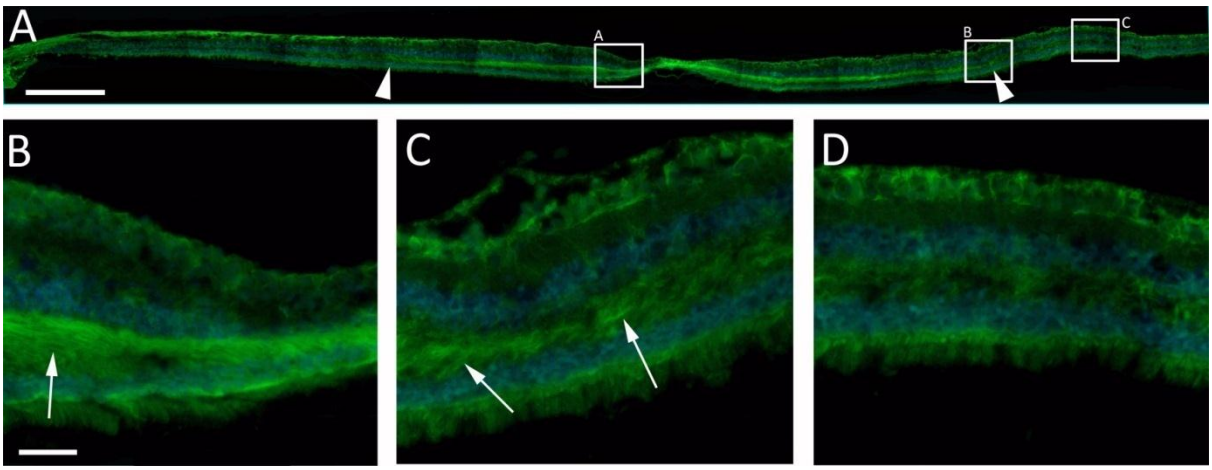

Figure 4.6. αB crystallin expression in the adult human macula.

Anti-αB crystallin immunohistochemistry revealed αB crystallin expression in retinal astrocytes pan retina, and an increase in expression in Henlé fibre layer, arrowheads in **A** mark the boundary of increased expression. Specific cell processes can be seen in the Henlé fibre layer at the fovea, arrow in **B**. The expression within the Henlé fibre layer stopped in mid-macula (right arrow in **C**). No processes were evident in the outer plexiform layer of the periphery (**D**). Expression in astrocytes is present in all aspects of the retina. Scale bars are 500µm in **A** and 50µm in **B**.

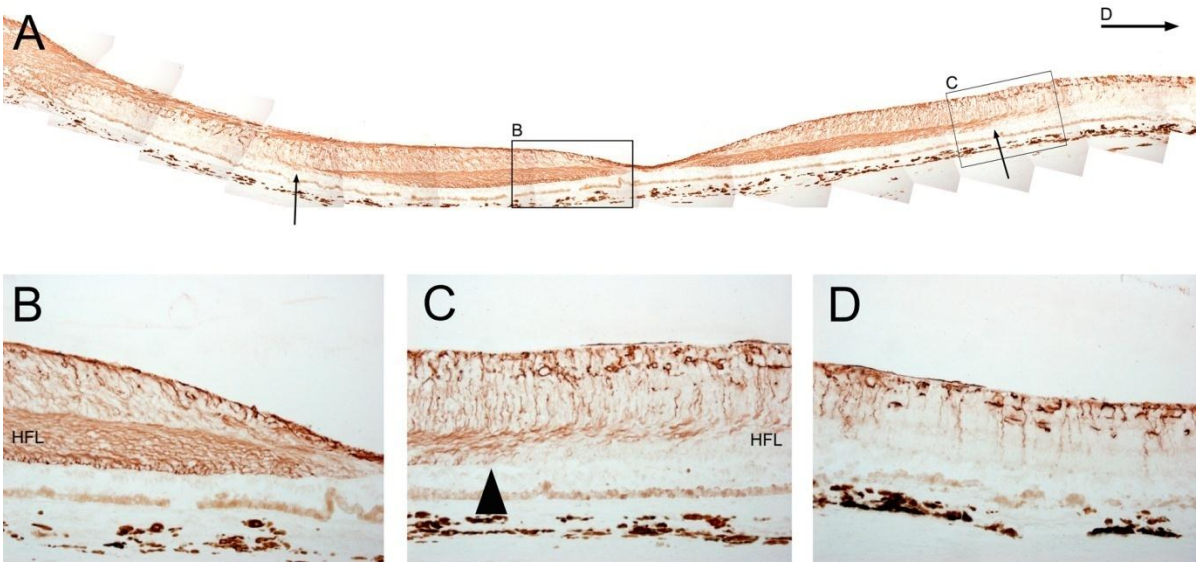

Figure 4.7. Glial fibrilliary acidic protein in macula Müller cells.

Anti-glial fibrilliary acidic protein (GFAP) immunohistochemistry with product amplification revealed a subpopulation of Müller cells in the Henlé fibre layer, HFL, of the human retina (arrows in **A**). All Muller cell processes at the fovea expressed GFAP (**B**). Muller cell GFAP expression stopped abruptly in the Henlé fibre layer (arrowhead in **C**) and was only expressed by a small population in peripheral retina (**D**).

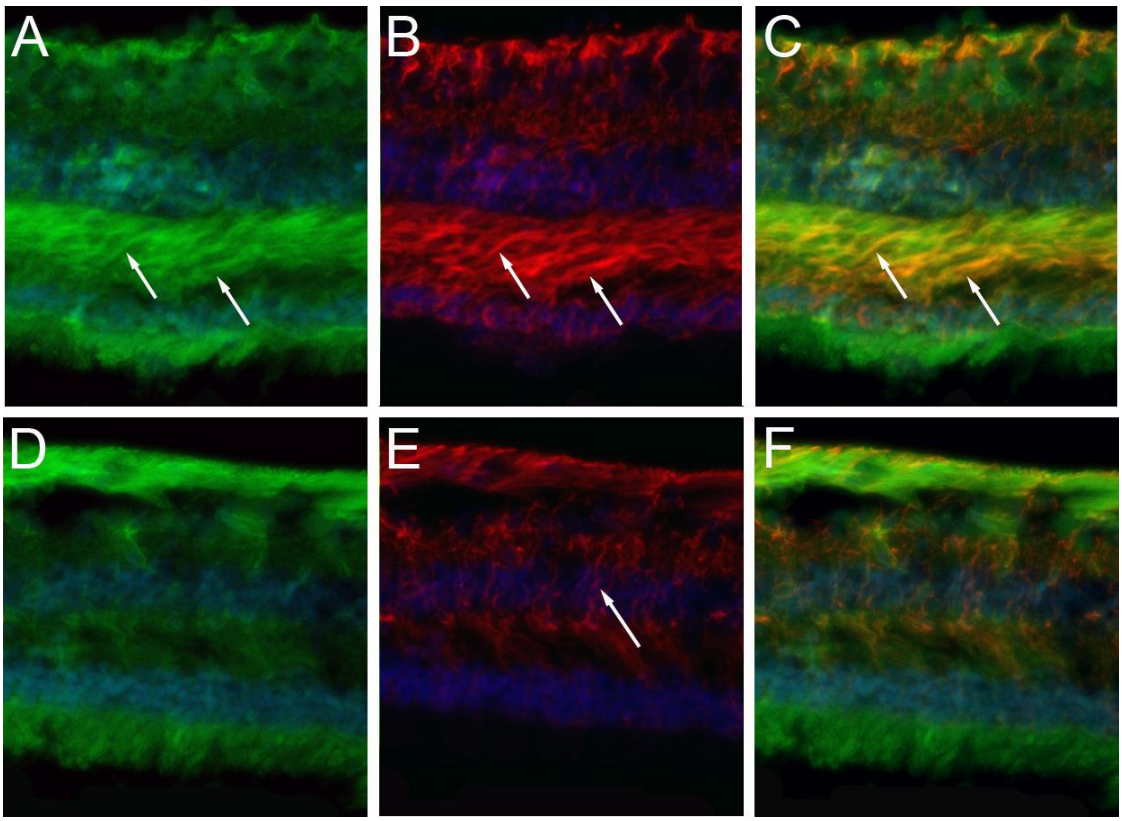

Figure 4.8. αB crystallin was expressed in Müller cell processes in the Henlé fibre layer. Within the Henlé fibre layer, αB crystallin (green, **A**) and the Müller cell marker vimentin (red, **B**) co-localised (arrows in **A-C**). Müller cells of the peripheral retina did not express αB crystallin (**D-F**).

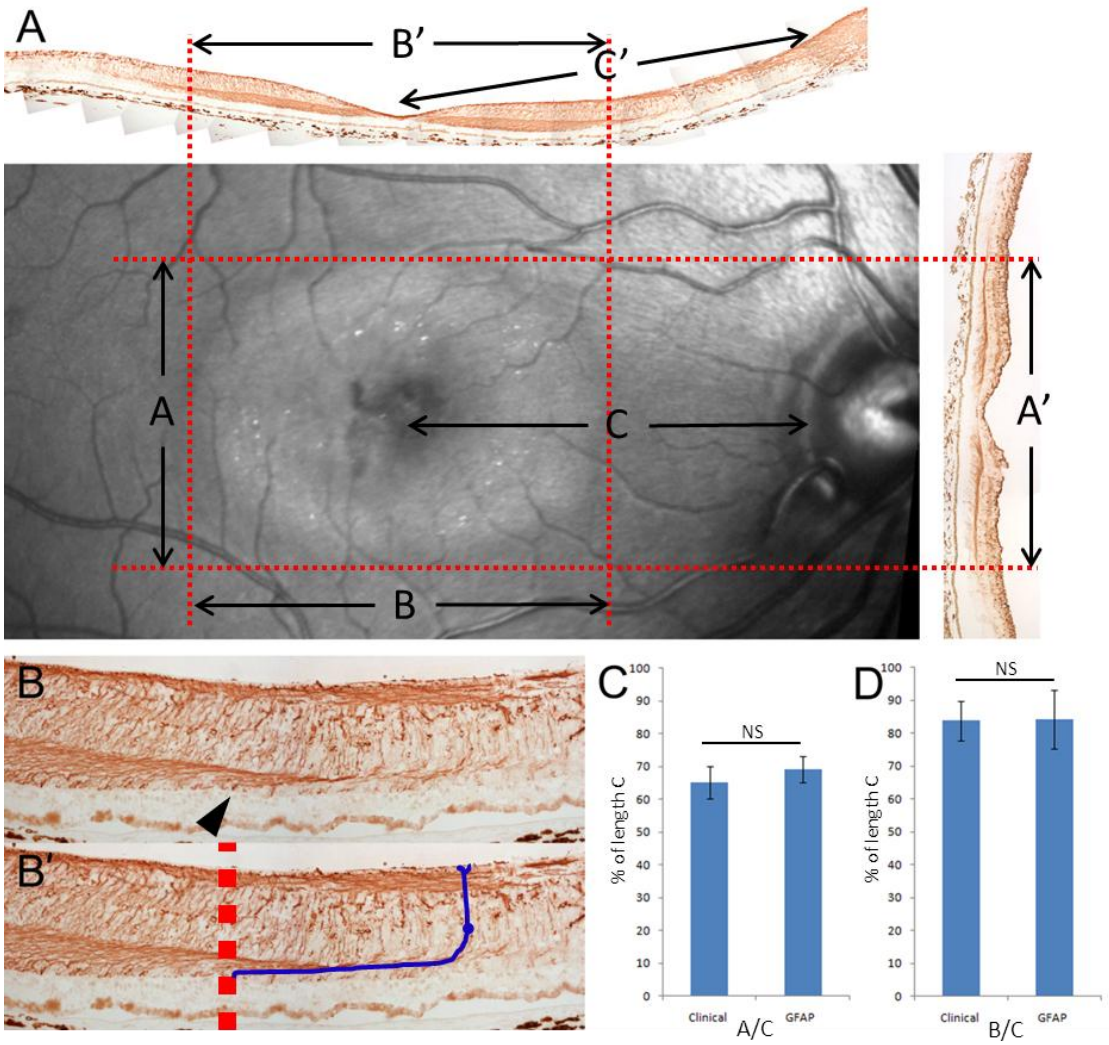

Figure 4.9. A sub population of Müller cells at the macula correlate in size and shape to the 'MacTel area'.

Measurements for the height (A) and width (B) from blue reflectance images can be scaled to measurements from immunohistochemistry A' and B', using the difference in distances C and C' as scaling factors (**A**). Measurements from GFAP immunohistochemistry stains are taken at the outer limiting membrane (arrow head in **B**); the Müller cell morphology shown in **B'**, blue line. Comparison of clinical data and histological data shows that there is no significant difference in the dimensions of the 'MacTel area' and GFAP stained Müller cells, height, A/C, p=0.9 (**C**) and width, B/C, p= 0.9 (**D**). Error bars; standard deviations from the mean. Clinical; confocal blue light reflectance, GFAP; immunohistochemical stain against GFAP on human retinal sections.

5. αA crystallin in central macula

5.1 Introduction:

The proteomic screen previously described in chapter 4 revealed a concentration of αA crystallin in central macula. In this chapter we will verify this finding with immunohistochemitry. Since macular pigment is also concentrated at the centre of the macula we also investigated a possible connection between αA and αB crystallins and macular pigment.

5.1.1 Crystallins

Crystallin can form very stable, strong complexes and yet are also water soluble proteins. There are two families of crystallins; α crystallins and βγ crystallins. Crystallins form a significant proportion of the lens of the eye where they help to maintain lens transparency by aggregating degenerating proteins and keeping them soluble, thus preventing cataract formation and loss of vision.

Ancestral stress proteins have been shown to regulate the gene expression of crystallins in the lens. Crystallins also have enzymatic activities in other species, and this concept of the use of an enzyme as a crystallin has been termed gene sharing.[323-325] Crystallins were evolutionarily recruited from enzymes and stress proteins. Some examples of these include argininesuccinate lysase (δ-crystallin in birds), glutathione-S-transferase (S-crystallins in cephalopods), duck lactate dehydrogenase (ε-crystallin), and *α*-enolase (τ-crystallin).

α crystallin

There are two α crystallins, αA crystallin (acidic) and αB crystallin (basic). In humans the αA crystallin gene (CRYAA) is located on chromosome 21 and encodes a polypeptide of 173 amino acids, while the αB crystallin gene (CRYAB) is located on chromosome 11 and encodes a 175 amino acid chain. There is ~58% sequence homolgy between the two α crystallin genes.[327] Both genes have similar 5' flanking sequences of -111/-18 core promoter region.[328] The α crystallins share an homologous domain, known as the conserved heat shock domain or α crystallin domain, with the other small heat shock proteins. This conserved domain is a large proportion of the gene, at ~80 amino acids, spanning amino acids 63 – 144 in αA crystallin and amino acids 68 – 148 in αB crystallin.[326] Studies from the 1980's have shown that the gene structure of CRYAA is highly conserved between various species, including

chicken and rodents.[329-332] This would imply that the rate of substitutions during evolution have been relatively low, at approximately 3 amino acids per 100, over 100 million years. [330]

Crystallins in the lens are regulated at a transcriptional level. Common transcription factors associated with crystallins are PAX6, retinoic acid receptors, MAF, SOX, CREB and AP1.[333-335] Five DNA binding transcription factors have been implicated as regulators specifically of CRYAA, these being Pax6, c-Maf, CREB, CREM and USF.[335-339]

αA crystallin has taken on many functional roles throughout the body. A primary function seen is that of a chaperone. In vitro they have been shown to interact with non-native proteins or degenerating proteins and in doing so, maintain that protein as soluble.[332, 340] This is a function that it shares with αB crystallin, other small heat shock proteins and the ATP-dependant chaperones GroE and Hsp70.[341-344] The conserved C-terminal sequence that it shares with small heat shock proteins is believed not to be directly involved in substrate binding, but is thought to be essential for increasing the solubility of the protein, and thus contributing directly to its chaperone function.[345] α crystallin has an extremely high binding capacity for substrates; it has been shown that substrates will preferentially bind to α crystallins, even if other chaperones are available.[346] These crystallin-substrate complexes can form higher order aggregates, and it has been suggested that hereditary cataract formation might be caused by a mutation in α crystallin which makes the oligomer have a higher binding capacity, leading to the loss of solubility and lens fibre opacification.[347] The exact binding substrates of the two α crystallins have yet to be determined.

An anti-apoptotic function of α crystallins has been proposed.[348-350] Over expression of αB crystallin in muscle cells subjected to stress, showed that this protein can stall the maturation of the protease involved in apoptosis, caspase 3.[348] These studies have now been confirmed in lens epithelial cells. Cells induced to over express *α*A or *α*B crystallin have been shown to have enhanced resistance to stress conditions, including thermal and photochemical.[351, 352] *α*A crystallin was better at protecting against apoptosis compared to *α*B crystallin in cultured cells.[352] *α*A crystallin knockout lens epithelial cells were also found to have a higher level of cell death compared to wild type cells, even under normal (non-stressed) conditions.[353] A possible mechanism of action may be through binding to proapoptotic proteins such as p53.[354] Researchers have found that the mechanisms by which *α*A and *α*B crystallins suppress stress induced apoptotic pathways are distinctly different.[349] While these effects are essential in the lens, it can be suggested that the ability of *α*A and *α*B crystallin to interfere

with apoptosis in the retina would offer a novel way to suppress age related cell death of retinal photoreceptor cells in patients with AMD and in models of retinal dystrophy.

αB crystallin has also been shown to play a role in protein degeneration. It acts by binding to the C8/alpha7 subunit of the 20S proteasome (shown *in vitro* and *in vivo*)[355] and by doing so either affects the proteasome complex, or facilitates the degeneration of the αB crystallin bound unfolded substrate.

5.1.2 Macular pigment

Macular pigment consists of two xanthophylls carotenoids, lutein and zeaxanthin. There are over 600 carotenoids known to exist, of which 30-50 are in the human diet, yet only 15 of these have been found in human serum[356] showing the selectivity of the body to carotenoids. Further still only the two macular pigments and their metabolites are present within the retina.[357-360] The carotenoid concentration is maximal at the fovea, where it reaches ~1mM and the ratio of lutein:zeaxanthin:*meso*-zeathanthin is 1:1:1.[361] Macula pigment concentration rapidly decreases with eccentricity from the fovea and within a few millimetres the concentration drops 100 fold.[357] Lutein persists into the peripheral retina while zeaxanthin and lutein's metabolite *meso*-zeaxanthin concentration decreases more rapidly, at a 3:1:0 ratio.[357] The main location of macular pigment is the Henlé fibre layer and the parafoveal inner nuclear layer,[256, 362] when seen in cross section, and can span anything from 200-900μm diameter from the fovea.[362-364] The macular pigment concentration of the retina is dependent upon dietary supplement[365-367] and the amount seen in the retina varies significantly between people. At the centre of the fovea there is a Müller cell cone, it has been proposed that this structural feature maintains the pit formation and also a primary reservoir for macular pigment. [256, 368]

Mechanisms of macular pigment deposition parafoveally are unclear. The function of macular pigment is also a matter of debate, its absorption at ~460nm means that it acts as a blue light filter reducing photopic damage and glare, it might also minimise the effects of chromatic aberration and thus improve visual acuity (fine detail and contrast sensitivity).[359, 362, 363] Another proposed theory is that it acts as an anti-oxidant, neutralising free radicals produced in the human retina thus protecting the outer retina, RPE and choroidal vasculature from oxidative damage.[358, 362]

Bernstein and colleagues have identified two carotenoid binding proteins within the human macula; glutathione s transferase (GSTP1) which binds zeaxanthin and StARD3 which binds

lutein. GSTP1 has been shown to be located within the Henlé fibre layer and the IPL,[320] a pattern that correlates with the cross sectional distribution of macular pigment by Snodderly,[369, 370] whilst Bernstein has recently located StARD3 primarily within the inner segments of the photoreceptors and neurons.[371] This recent binding protein distribution does not correlate with the distribution of maximal macular pigment seen in cross section. This does not mean that the data is wrong, but could imply that lutein and zeaxanthin have distinctly different patterns of distribution in the retina; GSTP1 localisation does correlate with macular pigment cross sectional distribution, implying perhaps that zeaxanthin is the main component of the intensely visible carotenoid.

DL-α-aminoadipic acid (DL-α-AAA) has been reported as a glial specific toxin and acts by suppressing GS function.[67, 372-374] Retinal cultures with DL-α-AAA show that Müller cells are the primary site of DL-α-AAA accumulation,[375] not surprising as DL-α-AAA is a homologue of the excitatory amino acid L-glutamate and Müller cells sequester excess L-glutamate. [37, 38] To investigate the relationship between Müller cell loss and a proposed Müller cell dysfunction in MacTel type 2, Gillies and colleagues attempted to selectively target Müller cells in primate central retina.[376] They injected DL-α-AAA into the sub retinal space below the macula. However, unlike in rat models, DL-α-AAA did not result in Müller cell dysfunction in primates; it instead disrupted the cone photoreceptors.[376] It is interesting that in this study, although selectively killing the cone photoreceptors (the main axonal component of the Henlé fibre layer), there was no effect on macular pigment distribution. The Henlé fibre layer appears thinned whereas the sites of inner and outer photoreceptor segment loss in their study[376] implying axonal degeneration as well, seeing as GS staining was unaffected. This could have implications regarding the debate over macular pigment deposition sites, implying a Muller cell storage site. However, no marker was used to target the neuronal axons, such as ml-opsin, so they might still persist after cell death and have macular pigment bound. It could be that macular pigment is found in both Müller cells and photoreceptor axons, and when photoreceptors are affected then there is no visible loss, whereas if there is Müller cell dysfunction then the route for macular pigment transport from the blood system to the retina is affected and as such no macular pigment can be transported into the retina for it to become bound to Müller cells or photoreceptor cells. Although it has also been proposed by Bernstein and colleagues that macular pigments enter the retina not through the retinal vasculature, but via the choroidal vasculature through the RPE. They speculate that the carotenoids, having similar chemical structures to retinoic acid, are transported to the photoreceptor cells by inter photoreceptor retinoid binding protein.[377]

5.2 Aim:

Establish the distribution of αA and αB crystallins in the human retina and test a potential link to retinal pigment distribution

5.3 Materials and Methods:

Technical acknowledgements: I would like to thank Glen Jeffery, University College London, for the provision of the marmoset tissue used in this chapter. Also thanks to Preejith Vachali and Paul Bernstein, University of Utah, for undertaking the Surface Plasmon Resonance (SPR) binding studies for us.

5.3.1 Tissue and processing

5.3.1.1 Tissue information

Fixed adult human tissue was used (Table 4.1).

Retinal tissue was obtained from Rhesus Macaque (17 year old), Marmoset, Pig and a 12 month old C57B6 mouse, and also from embryonic day 21 chick and embryonic day 26 duck.

5.3.1.2 Embedding and sectioning

Human tissue and marmoset tissue was embedded in wax, as described in chapter **2.3.1**, all animal tissue was fixed for 2 hours in 4% PFA, equilibrated in 30% sucrose, orientated and embedded in optimal cutting temperature compound (Agar, UK) and frozen on dry ice. Tissue was then sectioned through the area centralis/visual streak/fovea as appropriate. Sections were cut at 10µm and collected onto Superfrost® plus slides (VWR, UK).

5.3.2 Antigen retrieval and Immunohistochemistry

Antigen retrieval and immunohistochemistry were performed as previously described in chapter **2.3**. For human, marmoset and rhesus macaque tissue, slides stained for anti-CRYAA were heated to 130°C in citrate buffer for at least 10 minutes. Antigen retrieval was not required for other species.

5.3.3 Primary antibodies

αA crystallin (Santa Cruz, Sc-22743), αA crystallin (Abcam, ab14821), αB crystallin (Chemicon, AB1546), all diluted 1:200. Vimentin, LDHB and COX2, as per Table 1.2.

5.3.4 Surface Plasmon Resonance (SPR) binding studies (performed by Dr. Preejith Vachali and Prof. Paul Bernstein)

The amine coupling reagents; N-hydroxysuccinimide and 1-ethyl-3-(3-dimethylaminopropyl) carbodiimide hydrochloride, the GST coupling kit and 1M sodium ethanolamine hydrochloride pH8.5, were used as per manufacturers recommendations (Biacore AB, Sweden). αA and αB crystallin proteins (Abcam, Cambridge, MA, USA) were used. Gifts of carotenoids (3R,30R)-zeaxanthin (ZeaVision, USA), (3R,30S)-mesozeaxanthin (DSM, Basel, Switzerland), (3R,30R,60R)-lutein (Kemin Health, USA), and (3S,30S)-astaxanthin (Cardax Pharmaceuticals, USA). All carotenoids were crystalline, with >98% isomeric and chemical purity confirmed by HPLC.[371]

αA and αB crystallin were immobilised on a COOH-5 SPR chip using a standard amine coupling protocol.[371] The crystalline carotenoids were dissolved in running buffer (10mM PBS (pH 7.4), 0.01% TritonX-100, 1.26mM EDTA and 0.4mM sucrose monolaurate) and were tested in a 2-fold dilution series (0.1μM-10μM concentration range). Blanks were included in each analysis. The analyte concentration series was injected as two-fold dilutions in running buffer using the FastStep™ gradient injection mode with a flow rate of 200μl/minute. A FastStep™ concentration series of sucrose [20% (w/v) sucrose in running buffer] was injected to create the concentration gradient for analysis.[371]

SPR measurements were recorded on a SensiQ (ICx Nomadics, Oklahoma City, OK, USA) instrument at 25°C. SensiQ employs a miniature SPR-based sensor, designed in a Kretschmann's configuration, where monochromatic light is reflected from the sensing surface over a range of incident angles, and the reflectance minimum will occur with respect to the incident angle and is detected by a photodiode array. A planar glass chip with a ~50nm gold film coating is the sensing surface.[371]

Affinity determination SPR response data (sensorgrams) were zeroed on both the response and time axes at the beginning of each injection and double referenced. First, bulk refractive index changes were corrected by subtraction of the responses generated over an unmodified reference surface from the binding responses generated over the protein surfaces. Any

systematic artifacts between the proteins and reference flow cells were corrected by subtraction of the response generated by an average of the buffer injections from the binding responses generated by carotenoid injections. Simple interactions were adequately fit to a steady-state, single-site, bimolecular interaction model (A + B = AB),[371] yielding a single dissociation constant (K_D) for αA crystallin, αB crystallin.

5.4 Results:

5.4.1 Foveal αA crystallin

The proteomic screen highlighted αA crystallin as up regulated in central macula, as such we wanted to investigate the distribution further in adult human retina, using immunohistochemistry.

αA crystallin is highly expressed within the ocular lens, it constitutes up to 40% of all protein.[378] Therefore in all eyes studied lens tissue was used as a positive control for antibodies directed against αA crystallin.

In adult human retina, anti-αA crystallin antibodies revealed a high concentration of αA crystallin at optic nerve edge and fovea (Fig. 5.1 A). The foveal expression was concentrated in the pit, and spread into the parafoveal plexiform layers (Fig. 5.1 B). Co-labelling with anti-vimentin showed that αA crystallin was expressed within a subpopulation of the macular Müller cells described in the previous chapter. The expression pattern from both αA crystallin antibodies listed previously was identical (data from only one antibody shown).

5.4.2 αA crystallin expression in other animals.

In order to establish whether αA crystallin is also marker for central vision in other animals, a variety were investigated using immunohistochemistry; including old and new world monkeys, mouse, pig and squirrel, and also retina from chicken and duck.

In a Rhesus Macaque (17 yr old, old world monkey) which has a fovea and macula similar to humans, αA crystallin is expressed by Müller cells at the fovea. A marmoset monkey (new world monkey) showed the same foveal expression pattern for αA crystallin. Primates are the only mammals with a foveal specialisation. Other mammals do have visual streaks/area centralis', which are regions of the retina with an increase in cone number and/or ganglion cell density and are believed to be responsible for higher acuity vision in those animals. αA crystallin was only expressed in foveal Müller cells of the primate retina, so are their equivalent Müller cells in lower mammals. A C57B6 mouse (12 month old) showed αA crystallin expression diffusely within the ganglion cell and inner nuclear layers throughout the retina, this corresponds to previously published data.[353] The expression level between litter mates was variable, and as reported in the literature,[353] this was possibly a result of a light induced stress response. Pigs have a more pronounced visual streak, and being diurnal have a higher concentration of cone photoreceptors in central retina. Control lens tissue

confirmed αA crystallin antibody specificity, however no crystallin was seen within peripheral retina or visual streak (data not shown).

Birds have a highly developed visual system, the majority have a cone rich area centralis and some, including raptors also have a central foveal pit (or more). E21 chicken, and E26 duck retina have a fully formed retina and defined area centralis. Cross sections through the area centralis and optic nerve showed no expression of αA crystallin within the retina (data not shown), whilst lens tissue showed Immunoreactivity (Supplementary Fig.1).

We found that αA crystallin expression is limited to Müller cells of the primate fovea; there is no expression in other animals, even though lens expression was confirmed.

5.4.3 α crystallin interactions with carotenoids

There is no known cellular specialisation in the αA crystallin expressing location around the fovea. The only other restricted specialisation of the fovea is the high concentration of zeaxanthin, *meso*-zeaxanthin and lutein, the macular carotenoid pigments. The distribution of αA crystallin at the fovea resembles the expression pattern of macula pigment seen in cross section (Fig. 5.2 A-D), with a wedge of pigment and αA crystallin at the foveal slope at the level of the Henlé fibre layer and IPL (Fig. 5.2 C and D).

Because of the similar distribution it is possible that the crystallins interact with the macular pigment carotenoids. Therefore we have studied the *in vitro* binding potential between crystallins and carotenoids. The binding between crystallin proteins and macular pigment carotenoids (lutein, zeaxanthin and meso-zeaxanthin) has been determined, along with two control carotenoids not found in the retina; β-carotene and astaxanthin.

αA crystallin and αB crystallin bound the carotenoids tested, with differing levels of affinity (Fig. 5.3). The macular pigment carotenoids, lutein and zeaxanthin, showed a slightly stronger affinity (~ 1μM) compared to non-macular pigment carotenoids, beta carotene and astaxanthin (Fig. 5.4 A-D). The K_D values (Table 5.1) were close to that of human serum albumin previously reported by Bernstein and colleagues, (lutein, 1.69±0.05 and zeaxanthin, 1.11±0.03 and *meso*-zeaxanthin, 1.12±0.05)[371] and lacto-globulin (personal correspondence, unknown specific K_D values); they classified both human serum albumin and lacto-globulin as Class 2 carotenoid binding proteins. Class 1 carotenoid binding proteins such as GSTP1 (strong affinity for zeaxanthin and *meso*-zeaxanthin) and StARD3 (strong affinity for lutein) generally have higher affinities (0.1-0.5μM) for just one carotenoid.[371]

5.5 Discussion:

The specificity of the αA crystallin was established by using lens tissue from each species as a control (Supplementary Figure 1), as αA crystallin has been reported to make up, up to 40% of total lens protein, it is a valid control to use. The expression pattern in human and both monkey tissues was verified by two antibodies directed against αA crystallin from different suppliers. Both αA crystallin antibodies used are raised against the full length recombinant protein (amino acids 1-173) of human origin, and therefore both recognise the conserved heat shock domain of αA crystallin. The CRYAA gene, as previously stated, is known to be highly conserved between species[329, 331] and as such the antibody recognising multiple species is not unexpected. Further discussion about the specificty of the αA crystallin antibodies against human tissue will be covered in chapter **6.5**.

Immunohistochemistry verified the proteomic results from chapter **4**. In the adult human retina, αA crystallin had a peak of expression in the fovea. This expression pattern was further determined in both old world, (Rhesus macaque) and new world monkeys (marmoset). At the visual centre of other animals (area centralis or visual streak) no peak in αA crystallin expression was found, although we were able to confirm αA crystallin expression in the lens. The finding that crystallin was restricted to the fovea of primate retina and was not found within the central retina of other animals implies expression was possibly induced during the evolution of foveal pit in primates. The primate foveal pit contains an inverted Müller cell cone.[368] The precise function of this cone is unknown, it might serve a structural role but it has also been proposed as a reservoir for macular pigment.[256, 368]

A unique primate foveal specialisation (compared to other animals) is a high concentration of macular pigments. We tested to see whether αA crystallin might be involved in the transport of macular pigments in the retina. The affinity between both crystallin proteins to the two dietary retinal carotenoids (lutein and zeaxanthin) was higher than the affinity for β-carotene and astaxanthin (non retinal carotenoids) and *meso*-zeaxanthin (Table 5.1), this implies some degree of specificity towards the retinal macular carotenoids. Furthermore the K_D values at ~1μM were lower than that shown by Bernstein and colleagues between human serum albumin and lutein and zeaxanthin (lutein, 1.69±0.05 and zeaxanthin, 1.11±0.03). Carotenoids are transported around the body within blood serum.[356, 379] This leaves a potential role for αA and/or αB crystallin in the transport of lutein and/or zeaxanthin from the blood serum into the Müller cell, and potentially shuttling the carotenoid to GSTP1[380] or StARD3[371] which have been shown by Bernstein ad colleagues to be Class 1 carotenoid binding proteins. This possible mechanism for carotenoid transport into the retina does not

negate the model proposed by Bernstein and colleagues[377] whereby carotenoids enter through the RPE and are transported by interphotoreceptor retinoid binding protein to the photoreceptor cells, it is possible that two different supplies are at work.

To summarise, α crystallins are located only in Müller cells at the fovea of primate retina. α crystallins are not a class 1 carotenoid binding proteins, however the binding affinities could suggest that they are involved in the transport of macular pigments in the retina.

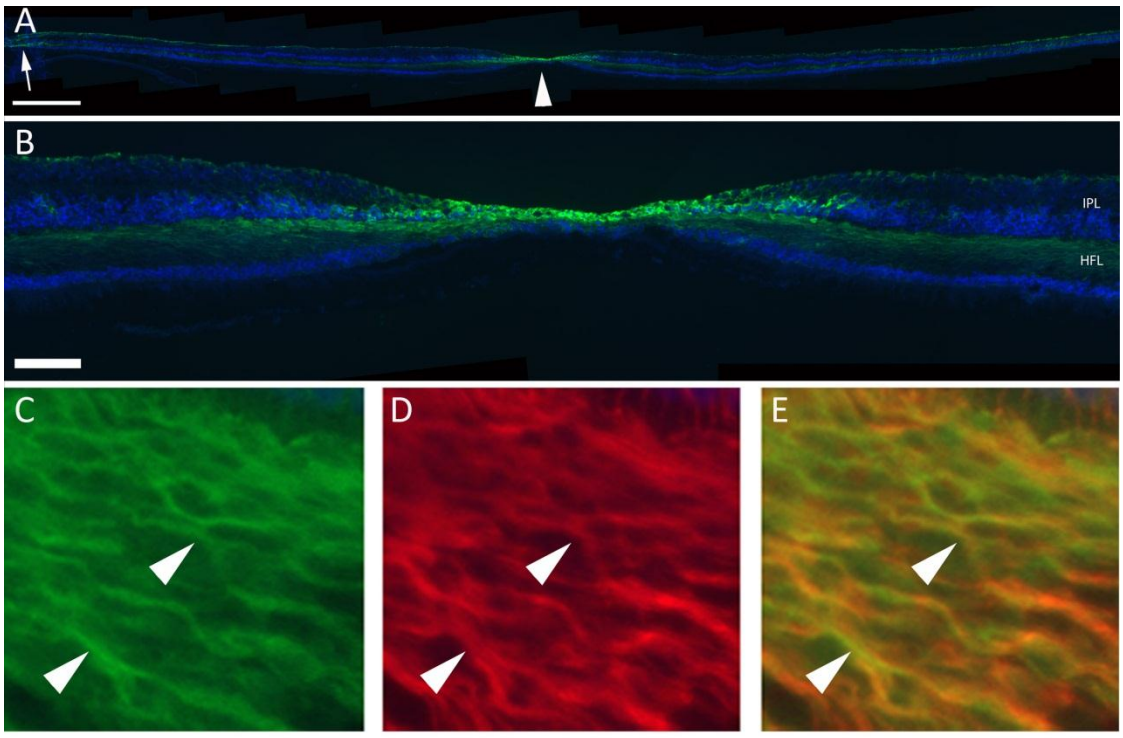

Figure 5.1. Foveal αA crystallin expression in adult human retina. Immunohistochemistry with an anti-αA crystallin antibody revealed expression at the optic nerve (arrow in **A**) and at the fovea (arrowhead in **A**), localised to the foveal pit and parafoveal plexiform layers (**B**). αA crystallin (arrowheads in **C**) and vimentin (arrowheads in **D**) co-localised (arrowheads in **E**), which showed that αA crystallin is expressed in foveal Müller cells. Scale bars are 500µm in **A** and 100µm in **B**. IPL; inner plexiform layer, HFL; Henlé fibre layer. Nasal to the left, temporal to the right.

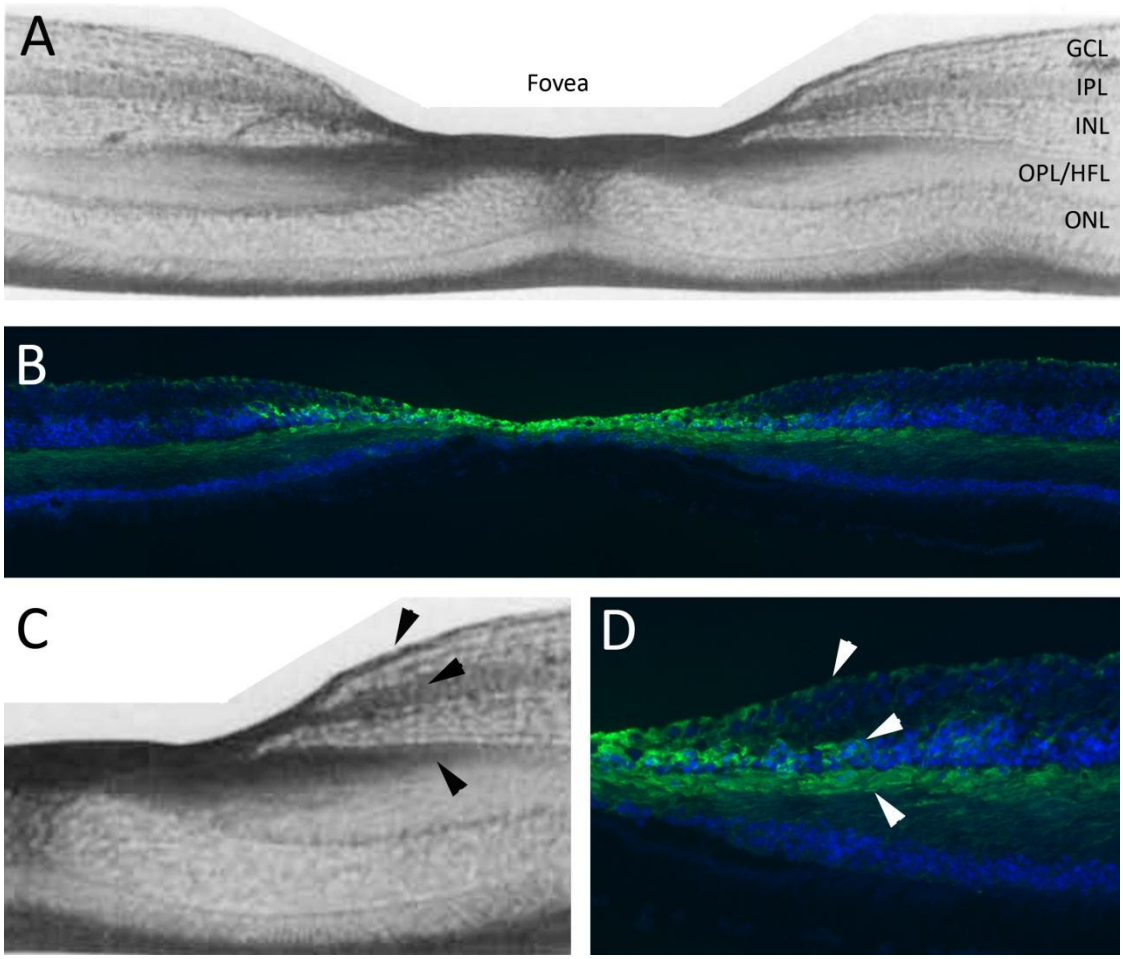

Figure 5.2. Macular pigment and αA crystallin distributions in primate retina are similar. Macular pigment distribution (**A**) adapted from Snodderly[370] shows localisation to the primate fovea with wedges extending into the Henlé fibre layer and inner plexiform layers. This pattern is mirrored in αA crystallin expression, localisation at the fovea (**B**) and expression into the parafoveal plexiform layers (arrow heads in **C** and **D**). GCL; ganglion cell layer, IPL; inner plexiform layer, INL; inner nuclear layer, OPL; outer plexiform layer, HFL; Henlé fibre layer, ONL; outer nuclear layer.

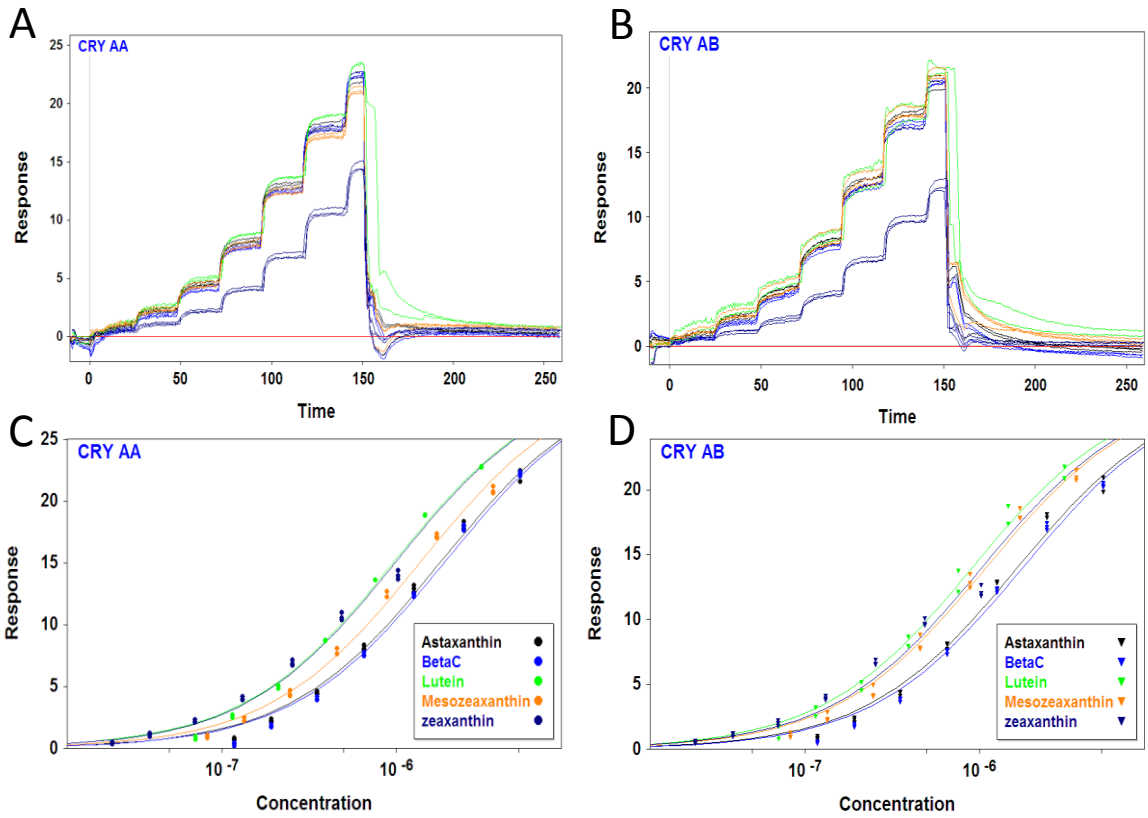

Figure 5.3. α Crystallin-Carotenoid interactions.

Surface Plasmon resonance (SPR) sensorgrams of astaxanthin, β-carotene (BetaC), lutein, *meso*-zeaxanthin and zeaxanthin binding to immobilised αA crystallin (CRYAA, **A**) and αB crystallin (CRYAB, **B**) proteins. **C** and **D**; Binding isotherm fit of the responses shown in panels **A** and **B**. Plotted versus injected carotenoid concentration and fit to a 1:1 binding isotherm.

(results provided by Dr. Preejith Vachali and Prof. Paul Bernstein, University of Utah, USA)

Carotenoid	Equilibrium dissociation constant (K_D)	
	αA Crystallin	***αB Crystallin***
Zeaxanthin	1.00 ±0.10μM	1.04 ±0.10μM
meso-Zeaxanthin	1.38 ±0.01μM	1.10 ±0.01μM
Lutein	0.97 ±0.10μM	0.92 ±0.10μM
Astaxanthin	1.80 ±0.02μM	1.66 ±0.02μM
β-Carotene	1.90 ±0.02μM	1.78 ±0.02μM

Table 5.1. Equilibrium dissociation constants (K_D).

Equilibrium dissociation constants (K_D) for αA crystallin and αB crystallin were determined in relation to 5 carotenoids. K_D values were determined using the SensiQ Pioneer Surface Plasmon resonance biosensor platform, at 25^0C.

(results provided by Dr. Preejith Vachali and Prof. Paul Bernstein, University of Utah, USA)

6. Macula development

6.1 Introduction:

To better understand the macula in adults we have also to investigate how it develops. In this chapter I will therefore focus on the embryonic eye development. Because our investigation directed us towards retinoic acid signalling in the retina, details about retinoic acid in development and how it acts as a morphogen will also be discussed.

6.1.1 Eye development

The optic cup forms from the developing diencephalon (forebrain); the optic placode begins to develop during neural tube formation, a stage called neurulation, at post conception day 22 (CS10)[381] and then starts to evaginate at day 24 (CS11) to form the optic vesicles. At the point when the optic vesicle comes in contact with the overlying surface ectoderm and the lens placode forms, the optic vesicle is triggered to invaginate to form a bilayered optic cup. The lens placode itself is also triggered to invaginate, pinch off and form the lens.[382]

The neural retina and RPE originate from the same sheet of ectoderm. The neural retina develops from the ventral side of the optic vesicle and the RPE from the dorsal.[383, 384] The homeobox gene VSX2 (formerly CHX10) and bHLH transcription factor MITF are the first genes to show domain specific expression. VSX2 localised to the developing neural retina, whilst MITF specifies developing RPE.[385-387] VSX2 and MITF are both essential in patterning and cell fate in the developing optic vesicle, VSX2 has also been shown to play a role in regulating proliferation.[387, 388]

LIM homeobox transcription factor LHX2 is the earliest patterning gene involved in eye development, it is expressed during eye field determination.[389, 390] In LHX2 knockout mice, optic vesicle patterning has been shown to be greatly disturbed; expression of MITF, VSX2 and TBX5 are not initiated, whilst expression of RAX, PAX2 and VAX2 (eye field determinants) are initiated but not maintained.[390]

RPE differentiation is essential for the proper formation of the neural retina; it controls lamination of the retina and regulates differentiation of the photoreceptors.[391-393] MITF and OTX2 are the key regulators of RPE specification. They are turned on throughout the optic vesicle prior to pigmentation of the cells; however they are down regulated in presumptive neural retina in the same pattern that MITF is down regulated.[392, 394, 395] Patterning of the

neural retina from the anterior optic vesicle requires the MAP kinase FGF signalling pathway. FGF signalling from the lens is crucial in determining retinal neurogenesis, the lens (surface ectoderm) is a source of FGF1 and FGF2.[396, 397] It has been demonstrated that the removal of lens surface ectoderm in chick embryos interferes with neuronal marker expression in the neural retina[397, 398] But at the same time some studies in zebrafish and chick have shown that the ocular neuroepithelium acts itself as an FGF signalling centre.[399-402] Mouse retinogenesis has however been shown to not be patterned by FGF/tyrosine receptor signalling, so there might be species specific adaptations.[403]

MAPK FGF signalling is known to be essential for retina/ RPE specification FGF9 knockouts show RPE domain expansion into presumptive retina in the optic vesicle, therefore FGF9 has a role in retina/RPE boundary establishment.[404] Cai *et al*. (2010)[403] further defined the role of FGF in retina specification by manipulating tyrosine phosphatase SRC homology 2 (SHP2), a protein that is required for activation of FGF signalling through association with FGF tyrosine kinases.[403] Conditional inactivation of SHP2 prior to retinal specification in early optic vesicle development in mouse results in a lack of VSX2 expression in presumptive retina and persistence of MITF expression in the anterior optic vesicle. The entire optic vesicle remains RPE like and all cells develop pigment.[403] Likewise in reverse the presumptive RPE can be induced to transdifferentiate into retina with fully developed retinal layering, by gain of function mutants and over expression of the MAPK FGF pathway.[386, 397, 398, 404-416] VSX2 mediates FGF activity, shown by the fact that VSX2 null mutant mice cannot induce retina from RPE in the optic vesicle,[417] and supported by VSX2 knockout mice which maintain pure RPE phenotype to the optic vesicle and do not induce retina specification.[417, 418] It has been suggested that MITF gene activation can suppress VSX2 action in anterior optic vesicle,[419] indicating that FGF is upstream of VSX2. FGF is not the only growth factor to have been shown to be essential in neural retina development. BMP signalling has been implicated to play a role; BMP7 null mice display microphthalmia and anophthalmia. In the anophthalmic mice the lack of BMP7 results in a downregulation of retina specifying genes and maintenance of the MITF and subsequent RPE phenotype in the whole optic vesicle.[420] However, due to the lack of lens formation within these mice it is possible that induction of the retina might be hindered due to the loss of FGF signalling (directly or indirectly) from the lens.

6.1.2 Retinal cell differentiation

Experiments to trace cell fate determination of retinal cells during development using [3H]-Thymidine labelling and autoradiography, has revealed an evolutionary conserved mechanism of cell fate determination.[421] Retinal cells differentiate in sequence, with initiation of their first mitotic events in the optic vesicle. In mammals, RGCs differentiate first followed by cone photoreceptors and amacrine cells, with horizontal and rod photoreceptor cells next. Bipolar cells and Müller cells are reportedly the last cells in retinal histogenesis.[422-427] The differentiation time points of different cells types overlap during development. It is possible that the timing of cell type differentiation is triggered or hindered by the other differentiating cell populations. However, this would also lead to the assumption that if postnatal neural epithelial progenitor cells were cultured with early embryonic retinal progenitors, the cell fates at the earlier stage of development would be adopted. Experimental data has however revealed that intrinsic "barriers" in neural epithelial progenitor cells halt their re-specification capability, if they had any to begin with that is.[427] This co-culture does however block the differentiation of later time point cell types. Similarly, embryonic retinal neural epithelial progenitor cells fail to adopt later cell fates when cultured in excess with postnatal progenitor cells from mice. Therefore, intracellular signalling pathways are essential retinal neural progenitor cell differentiation and preservation of stem cell properties.

Ablation and transplantation studies have shown that the retinotectal projection pattern along the anterior-posterior axis is established during the optic vesicle stage in chick,[428, 429] however the dorsal-ventral axis not established until optic cup formation.[430, 431] Both events occur before the first mitotic events in retinal cell fate determination, and therefore the positional identity of the progenitor cell already directs the final cell fate, and is instrumental in retinal patterning.[432]

6.1.3 Retinoic acid in development

Vitamin A (retinol) is the precursor to retinoic acid; retinol is oxidised to retinaldehyde by retinol dehydrogenases, following this conversion retinaldehyde dehydrogenses subsequently covert retinaldehyde into all-trans retinoic acid. Retinoic acid can then bind to the cellular retinoic acid binding proteins, CRABP1/2. Ligand binding induces a conformational change which exposes a nuclear localisation motif on CRABP2 and the complex is then shuttled transported into the nucleus. Retinoic acid then interacts with its receptors to activate the transcription of target proteins.

There are two protein families involved in retinoic acid signalling; the retinoic acid receptors, RARα, β and γ, and the retinoid X receptors, RXRα, β and γ. RAR and RXR form heterodimers (RAR/RXR) when bound to a retinoic acid response element of a target gene.[433, 434] RARα, β and γ, in the developing eye are expressed in overlapping domains resulting in functional redundancy;[435] mice lacking individual RAR receptors show minor phenotypes[436, 437] whilst a double knockout or RAR receptors leads to significant phenotypes and lethality.[438, 439]

Retinoic acids ability to act as a morphogen in development has been controversial. It has been reported to be essential in anterior-posterior patterning; however whether it determines cell fate or is merely permissive for specifying cell fate has been up for debate. Classical morphogens specify a cells fate in a concentration dependant manner, and receptors on the cells stop migration or interpret cell fate dependent upon the environmental concentration. Observations in retinoic acid deficient mice, quail, rat and zebrafish have implied that retinoic acid only acts permissively in the patterning of hindbrain; as it has been shown that the normal patterning can be rescued when exposed to a uniform concentration of retinoic acid across the hindbrain.[440-447] Other experiments have determined the opposite, showing retinoic acid does function like a classic morphogen. For example, retinol deficient embryos, or loss-of-function mutants in the retinoic acid synthetic enzyme aldehyde dehydrogenase 1A2 (ALDH1A2 or RALDH2), show loss of posterior hindbrain rhombomeres 5-7, and expansion of anterior rhombomeres 2-4.[441-443, 447, 448] RAR antagonists in chick embryos also cause a progressive anteriorisation in a concentration dependent fashion.[449] Conversely, embryo exposure exogenous retinoic acid causes a concentration dependent loss of forebrain and subsequent eyes, and ultimately a progressive posteriorisation of rhombomere identities.[444, 450-453] Loss of cytochrome P450 A1 (CYP26A1), a retinoic acid degrading enzyme also causes rhombomere 5-7 to develop anteriorly in mice and zebrafish,[454-456] and the combined depletion of CYP26A1 and related enzymes CYP26B1 and CYP26C1, and subsequent loss of available retinoic acid, results in severe posteriorisation of the zebrafish hindbrain.[440] This evidence suggests that retinoic acid can act like a classic morphogen, and that gradients can be established across a tissue by the action of localised retinoic acid degrading enzymes.

CRABP1 is likely involved in the regulation of retinoid homeostasis in cells that are the targets for retinoid. In the anteroposterior axis formation in chicken limb development, two opposing gradients have been observed, one of retinoic acid and another reciprocal gradient of CRABP1. It was proposed that these opposing gradients would result in an even distribution of retinoic acid-CRABP1 complex, but in a steeper gradient of free retinoic acid available for binding to retinoic acid receptors (RARs).[457] Boylan and Gudas[458] also showed

that an increase in expression of CRABP1 reduces the expression of retinoic acid induced genes, thus further showing that CRABP1 influences the availability of free retinoic acid within cells. CRABP1 has also been shown to act as a conduit in the pathway of retinoic acid catabolism.[459]

6.1.4 Retinoic acid in retinal morphogenesis and patterning

Expression patterns of components of retinoic acid signalling are temporally and spatially restricted. Transgenic mouse and fish reporter strains have been used to study retinoic acid signalling in development based on the ability of multiple retinoic acid response elements (RAREs) to direct expression of a linked *lacZ* reporter gene (in transgenic mice)[460-463] or a green fluorescent protein (GFP).[464] These transgenic strains, coupled with knockouts for retinoic acid signalling components, such as RALDH1$^{-/-}$,[465] RDH10$^{-/-}$,[466] or knockouts for genes that control eye development, such as PAX6,[461] have shown active retinoic acid signalling in the optic vesicle, in patterning presumptive retina/RPE and continued expression in developing retina.

Raldh3 is present in the RPE[467] and can therefore signal via retinoic acid to the retina and dictate morphogenesis in the retina that subsequently leads to invagination of the anterior optic vesicle.[467] Retinoic acid is also required to induce apoptosis in the extraocular mesenchyme, one gene that is targeted is PITX2, a transcription factor required in RPE differentiation[468-470]

Raldh3 is expressed in mouse and chick ventral retina during development. Shortly after the expression of Raldh3 in ventral retina, the retinoic acid degradation enzyme CYP26A1 is upregulated in dorsal retina, just hours after this Raldh1 expression is induced in the far dorsal retina.[471-473] Initially RALDH1 and CYP26A1 expression overlaps, but before retinal neurogenesis begins the two expression patterns become clearly defined, with CYP26A1 expression becoming limited to the central, horizontal meridian, CYP26C1 expression has been identified in a further band across the retina of both mice and chickens, restricted to an even thinner region across the retina (Fig. 6.1 A-C). This generates a gradient of retinoic acid across the retina. Raldh3 produces retinoic acid in ventral retina, but the levels would decrease towards the central meridian, where CYP26A1 degrades any free retinoic acid in the environment, and CYP26C1 completely degrades any free retinoic acid in a strip across the very central retina.[474] Towards dorsal retina, retinoic acid levels increase due to production by RALDH1 and reduction by CYP26 enzymes.[463, 475] The regions occupied by both RALDH's

have many morphologic markers in common, to date though no morphogenetic marker has been correlated with the expression pattern of CYP26A1 and C1.

6.1.5 Macula development

Macula specification and development is not well understood and largely characterised on the basis of the structural morphology and differentiation of specific cell types.

The optic vesicle is formed at 4 weeks post conception (Carnegie Stage 13, CS13) but the fovea is not fully formed until 4 years of age;[476] a large time frame in which the macula/fovea can develop. During development, the prospective macula first goes through a phase of ganglion cell proliferation, the ganglion cells in central retina start to double at 4.5 months,[477] by 6 months gestation they have reached 8-9 cells deep[477] at the centre of the 'mound'. By the seventh month the cells within the inner nuclear layer and the ganglion cell layer at the centre of the prospective macula start to migrate radially, beginning the formation of the foveal depression. This process is known as lateral displacement.[477] Lateral displacement leaves only 2 ganglion cells at the fovea by the eighth month of gestation and a single cell deep by the ninth;[477] the fovea continues to develop through to 4 years after birth though. A closer study of retinal morphology however shows that the earliest time point where the presumptive macula can be identified is at 9-10 weeks (F2). Lineage tracing identified the incipient macula as the region of the retina that matures first, cells start to differentiate and then there is a wave of differentiation radially through the retina. As cells differentiate from the progenitor epithelia they start to form the different retinal layers. This will occur first at the presumptive macula following the line that cells here differentiate first. Hendrickson and colleagues[478] identified this at 9-10 weeks gestation (WG); the stage where the outer nuclear layer is visible in central retina, and peripheral retina still contains two neuroblastic layers.[478] (summarised in Fig. 6.2 A)

Immunostaining for synaptic proteins[479, 480] highlighted that the first synapses are formed in the IPL of the primate retina at the incipient fovea, but data as to whether these synapses are amacrine and/or bipolar is conflicting.[481-484] Followed by synaptogenesis in the OPL, which in humans occurs at 11WG in foveal cones.[482] Rods generate synapses later in development than cones.[480] It is known that the incipient fovea differentiates first in human development,[482, 485] as such photoreceptor differentiation occurs here first. This can be used to pinpoint the incipient fovea. ML opsin (red/green photoreceptors) and rhodopsin are first detected with immunohistochemistry at 16WG[478] at the incipient fovea/prospective macula. S opsin is expressed earlier in development at 14WG.[478] So photoreceptor opsin expression can track the developing fovea/macula back to 14WG, opsins however are not the first

markers of photoreceptors to be expressed. Interphotoreceptor retinoid binding protein (IRBP), tubby-like protein (TULP) and neural retina-specific leucine zipper protein (NRL) can all be detected during the 9th week of gestation by immunohistochemistry.[478] These are the earliest known photoreceptor proteins to be expressed in the human retina, as such we can trace the location of the macula back to 9WG, the same time point at which morphologically the outer nuclear layer forms (summarised in Fig. 6.2 B). Lineage tracing shows that ganglion cells are the first cells to become postmitotic, and primates studies have shown this to be at foetal day 33,[424, 486] which corresponds to >7-8WG. Ganglion cell differentiation therefore is the earliest indicator for the incipient fovea known to date.

Current knowledge of the position of the developing macula all stems from differentiation initiating at that point. There has to date been no data answering the question as to why this is the region that differentiates first, and more so there is no data published that shows any macula specialisation compared to peripheral retina during development.

6.2 Aim:

To characterise embryonic development of the macula and find potential signalling pathways that regulate this.

6.3 Materials and Methods:

Technical acknowledgements: I would like to thank Dianne Girrelli and her team at the London HDBR for the provision of and staging of the embryonic/foetal tissue used.

6.3.1 Tissue and processing

6.3.1.1 Samples

Embryonic/foetal eye tissue was obtained from London HDBR facility at the UCL Institute of Child Health, UK. Tissue was staged at the HDBR prior to organ distribution; staging was done according to the Carnegie Stages (CS) and Foetal developmental protocol (F) (Supplementary Table 1).

6.3.1.2 Fixed samples

Immunohistochemistry- sections

Whole eye globes were fixed in 4% (w/v) PFA overnight and transferred into 30% (w/v) sucrose/ PBS-DEPC to equilibrate. Globes were orientated and embedded in OCT compound (Agar, UK) on dry ice. Sections through the optic nerve and prospective fovea were cut and

mounted onto Superfrost® plus slides (VWR). 3 eyes from each developmental stage, CS19-F2, were investigated for immunohistochemistry in sections.

Immunohistochemistry- flatmount

Whole eye globes were fixed in 4% (w/v) PFA overnight, the cornea/lens removed and the retina was dissected out. Vitreous and hyloid vasculature were also removed. 3 eyes from each developmental stage, CS19-F2, were investigated for flatmount immunohistochemistry.

In situ hybridisation

The retina was dissected from the whole globe, four radial incisions made and flattened. Vitreous and hyloid vasculature removed. It was then fixed in 4% (w/v) PFA for 20 minutes, transferred through graded methanol concentrations/DEPC treated dH_2O, into 100% glacial methanol, and stored at -20°C. 3 eyes (CS23/F1) were studied using in situ hybridisation.

6.3.1.3 RNA extraction (Trizol extraction)

For RNA purification from retinal tissue, TRI Reagent™ (Sigma-Aldrich, UK) was used. Table 6.1 lists the reagents used for RNA extraction.

Tissue was removed from -80°C and 1ml TRI Reagent™ was added immediately to the still frozen sample. Samples were allowed to stand for 5 minutes at room temperature to allow lysis to start. The solution was repeatedly passed through a needle to completely disaggregate the tissue. 0.2ml of chloroform was added and shaken for 15 seconds. Lysates were left at room temperature for 10 minutes and centrifuged at 12,000g for 15 minutes at 4°C. Centrifugation separated the solution into 3 layers; a pink phase containing protein, an interphase containing DNA and an upper phase (aqueous) containing the RNA. The upper phase was collected into a new eppendorf (the remaining two layers are discarded). To precipitate the RNA, 0.5ml isopropanol and 1µl glycogen was added, mixed and left at room temperature for 15 minutes. The sample was centrifuged at 12,000g for 10 minutes at 4°C so that a pellet forms. Supernatant was discarded and pellet washed with 1ml 75% Ethanol before vortexing and centrifuging again at 7,500g for 5 minutes at 4°C. Supernatant was poured off and the pellet was air dried to remove all ethanol. The pellet was then resuspended in RNAsecure and placed on a heat block at 50°C for 10 minutes to ensure complete resuspension. The RNA was kept on ice and the concentration measured with a NanoDrop® Spectrophotometer ND-1000 and NanoDrop® 1000 v3.7.1 software (LabTech International, UK).

6.3.1.4 Reverse transcription

cDNA was transcribed using Quantitect® reverse transcription kits (Qiagen, UK), as per manufacturer's instructions.

Samples were kept on ice at all times. 1µg RNA (in 12µl) was first incubated with 2µl gDNA wipeout for 5 minutes at 42°C, to remove any contaminating genomic DNA. Next the reverse transcription master mix was added, consisting of 4µl Quantiscript RT buffer (5X), RT 1µl Primer mix (primers and dNTPs) and 1µl of the enzyme, Quantiscript Reverse transcriptase. This mix was then incubated at 42°C for 15 minutes, and then ramped up to 95°C for 3 minutes to inactivate the enzyme. cDNA was now prepared ready for use in quantitative real time polymerase chain reaction (qPCR).

6.3.2 Immunohistochemistry

6.3.2.1 Primary antibodies

αA crystallin (Santa Cruz, Sc-22743), αA crystallin (abcam, ab14821), Ki67 (Vector labs, vpk451), CD44 (AbD Serotec MCA89T), Nestin C-20 (Santa Cruz, Sc-21247). All used at a 1:200 dilutions. CRALBP, GS, vimentin and GFAP as per Table 2.1. SOX9 was a gift from Dagmar Wilhelm, University of Queensland, Australia.

6.3.2.2 Antigen retrieval

Mild antigen retrieval was required for anti-CD44 labelling of foetal sections. Sections were dried overnight under a fan and washed in PBS to remove OCT. They were then placed in a solution of 90% glycerol (molecular grade, Sigma, UK), 10% 0.01M citrate buffer pH6.0, and heated to 95°C in a microwave for 5 minutes. Allowed to cool for 30 minutes and washed in PBS prior to immunohistochemistry.

6.3.2.3 Flatmount

Whole retinas were incubated in flatmount block (1% (w/v) BSA, 0.5% (v/v) TritonX-100 /PBS) for 2 hours at room temperature. They were then transferred into flatmount block plus primary antibody and left over night at room temperature on a mild shaker. Tissue was washed 3 times, 40 minutes each wash in flatmount block at room temperature, and it was next incubated in secondary antibody, (diluted in flatmount block), for 3 hours at room

temperature. Finally tissue was washed overnight at room temperature in excess whole mount block. 4 radial incisions were made in the retina to allow the tissue to flatten on a slide. They were then mounted in mowiol and coverslipped. Imaged using an Olympus dissection stereo microscope (SZX16) with an Olympus fluorescent lamp (U-RFL-T), fitted with a Hamamatsu camera (C4742-95) and Simple PCI software v6.6.

6.3.2.4 Sections

Both fluorescent and HRP-DAB immunohistochemistry was carried out as previously described in chapters **2.3.3** and **2.3.4**. Sections were dried for 2 hours under a fan before blocking was started/or antigen retrieval if necessary.

6.3.3 Quantitative Real Time Polymerase Chain reaction (qPCR)

cDNA from foetal retina samples were used. SYBR™ Green (Qiagen, UK) was used for qPCR analysis.

SYBR™ Green I is a cyanine dye that when bound to DNA will absorb light at ~497nm and emit green light at 520nm. It is used as a measure of double stranded DNA production. SYBR™ Green preferentially binds to double stranded DNA, therefore as the PCR progresses the light emitted is proportional to the amount of double stranded DNA amplified.

1µl cDNA was mixed with 43.75µl Power SYBR™ (Qiagen, UK) and 0.6µM of both forward and reverse primers in dH_2O to a total volume of 87µl. 20µl of this master mix was loaded into each of three wells in a 96 well PCR plate, so that each gene was checked in triplicate per sample. The primers used are listed in Table 6.2. Beta Actin (ACTB) was used as an endogenous baseline control for each sample run. The PCR reaction was loaded into a BioRad DNAEngine® Peltier Thermal Cycler (BioRad, UK) and run with the cyclic conditions listed in Table 6.3.

Primer pairs were checked for efficiency using the stage 3 of the PCR sequence (Table 6.3) and run with a whole foetal (CS23) retina cDNA sample. Primers were checked that they had a strong peak at a single dissociation temperature; multiple peaks showed multiple PCR product formation and non-specificity of primers. Primer dimer formation can also be assessed. Primers were redesigned if multiple products or primer dimers were found.

Collected data was analysed using DART-PCR software,[487] data sets for genes of interest were standardised using ACTB.

6.3.4 Differential gene display

Genefishing™ DEG premix kit (Seegene Inc, Korea) was used to carry out differential gene display.

Genefishing™ DEG premix kits are designed to identify differentially expressed genes between two or more nucleic acid samples. The process consists of three steps (ACP; annealing control primer).

Step 1: Reverse transcription creates first strand cDNA, the 3' end core portion of the dt-ACP1 primer used contain a poly-T tail which will bind to the poly-A tail of the mRNA transcripts. The first strand cDNA therefore bears the universal sequence of dT-ACP1 at its 5' end.

Step 2: The first strand cDNA is mixed with arbitrary ACP (5' primer) and dt-ACP2 (3' primer). The 3' end core portion, 10-mer, of the arbitrary ACP consists of a hybridising sequence that is sufficiently complimentary to a region on the first strand cDNAs. The first stage of the PCR sequence is conducted under conditions that allow only the arbitrary ACP to anneal with its 3' end core to the first strand PCR. The conditions used do not allow the binding of the 3' end core portion of dT-ACP2 to anneal to first strand cDNA. The result is that second strand cDNA is synthesised that bears the complementary sequence of the universal sequence of dT-ACP1 on its 3' end and the universal sequence of the ACP on it 5' end.

Step 3: The PCR then enters a third stage, which has higher stringency conditions that allows both dT-ACP2 and the arbitrary ACP to bind to the 3' and 5' ends (generated in steps 1 and 2) respectively. These annealing events exclusively involve the universal sequences of the two primers. This results in amplification of the targeted PCR products only.

6.3.4.1 Primers

Refer to Table 6.4 for a full list of primers.

6.3.4.2 Reverse transcription

Reverse transcription was carried out using Quantitect® Reverse transcription kit (Qiagen, UK) with the following adaptations; the RT primer mix was replaced with the RT primer (10µM dt-ACP1) supplied with Genefishing™ DEG premix kit (Seegene Inc, Korea), 2mM dNTP's (Biolabs, UK) and 0.5µl RNase inhibitor (40U/µl RNAaseOUT, Invitrogen, UK).

The same method was used for RNA extracts from presumptive macula and peripheral retina.

Total RNA from Trizol® extraction was first treated to eradicate contaminating DNA; 911.25ng RNA was incubated with 7X gDNA Wipeout Buffer, in a total of 7.5µl, for 5 minutes at 42°C. 2ul of 10µM dt-ACP1 was added on ice and incubated for 3 minutes at 80°C. On ice 4µl 5xQuantiscript RT buffer, 0.5µl RNaseOUT, 5µl 2mM dNTP and 1µl Quantiscript Reverse transcriptase is added and the mix incubated at 42°C for 90 minutes. It was heated to 94°C for 2 minutes to inactivate the enzyme. cDNA is now prepared.

6.3.4.3 Genefishing™ PCR

The cDNA preparation was diluted to a concentration of 45.5ng/7µl for the two regions separately. 7µl of this cDNA was mixed 2µl of one of the 20 annealing control primer (5µM ACP [3' primer]), 1µl 10µM dT-ACP2 (3' primer) and 10µl 2X SeeAmp™ ACP™ MasterMix (Seegene Inc, Korea). The PCR was then run following the cyclic conditions in Table 6.5. 10µl of the resultant 20 PCR products from presumptive macula and 20 PCR products from peripheral retina was run on a 2% agarose gel containing ethidium bromide. PCR products from presumptive macula and peripheral for each individual ACP were run in adjoining wells to ease comparisons.

6.3.4.4 Gel extraction

Gel extraction was carried out using a GENECLEAN® *Turbo* kit (1102-200, MP Biomedicals, UK). Agarose gel pieces were weighed and 100µl of GENECLEAN® *Turbo* salt solution was added per o.1g of gel. The gel was then dissolved at 55°C for 5 minutes. The solution was then transferred to a GENECLEAN® *Turbo* cartridge (column) and spun for 5 seconds at 12,000rpm. Eluate was discarded and 500µl GENECLEAN® *Turbo* wash solution was spun through the column at 12,000rpm for 5 seconds. Eluate was discarded and the column spun for a further 4 minutes to remove all residual wash solution. The column was transferred to a collection tube and 30µl GENECLEAN® *Turbo* elution solution was added directly to the GLASSMILK®-embedded membrane, incubated at room temperature for 5 minutes and then the DNA was eluted by spinning for 1 minute at 12,00rpm. DNA was stored at 4°C until needed.

6.3.4.5 Ligation/Cloning/Transformation

TOPO TA cloning kit (Invitrogen, UK) was used to clone the Genefishing™ PCR products. 2µl of gel extract was mixed with 1µl dilute salt solution, 2µl RNAase free water and 1µl TOPO®

vector. This was then left at room temperature for 15 minutes. One shot® Electroporation was then used to transform the bacteria. One shot® Electrocomp® cells were defrosted on ice, diluted 1:3 with dH_2O. 40µl was transferred to a cuvette with 1µl TOPO® Cloning reaction. They were then electroporated at Eco1 setting on a BioRad MicroPulser™ (BioRad, UK). Cells were then recovered with 200µl LB and incubated in a water bath at 37°C for 1 hour. Cells were then plated onto pre warmed LB agar plates with 100µg/µl ampicilin, inverted and incubated at 37°C overnight. Colonies were picked and grown up in 4ml LB plus ampicillin, overnight shaking vigorously at 37°C.

6.3.4.6 Extraction of plasmid DNA

1ml of culture medium was spun at 14,000rpm. LB was aspirated off completely. 100µl solution 1 (50mM Glucose, 25mM Tris HCL pH8.0, 10mM EDTA) was added and vortexed to resuspend the pellet. 200µl of solution 2 (0.2M NaOH, 1% SDS) was added and incubated on ice for 5minutes to lyse the bacteria. Removed from ice, solution 3 (60ml KoAC, 11.5ml glacial acetic acid, 28.5ml H_2O) was added to stop lysis. The tubes were then inverted numerous times and centrifuged for 2minutes at 14,000rpm. The aqueous phase was transferred to a new eppendorf and the rest discarded. 1ml of glacial ethanol was added to precipitate the DNA. This was centrifuged for 7 minutes at 14,000rpm, the ethanol was poured off from the resulting pellet. The pellet was washed with 70% ethanol and further spun for 15seconds at 14,00rpm. The ethanol is aspirated off completely and the DNA pellet resuspended in 100ul dH_2O at 55°C for 10 minutes. DNA was then stored at 4°C.

6.3.4.7 Sequencing protocol

Sequencing was carried out using a Big Dye 3.1 cycle sequencing kit (#4336917, Applied Biosystems, UK), 1µl of DNA was added to 0.5µl Big Dye reaction mix (Applied Biosystems, UK), 2µl Big Dye buffer (Applied Biosystems, UK) and 6.5µl of primer (at 0.25µM concentration). The primer sequences used are; M13 Forward (-20) 5'GTAAAACGACGGCCAG-3', and M13 Reverse 5'-CAGGAAACAGCTATGAC-3'. The mix was run (cyclic conditions, Table 6.6) on a BioRad DNAEngine® Peltier Thermal Cycler (BioRad, UK).

The plasmid DNA was cleaned using Genetix genCLEAN 96 well Dye terminator removal plate plates (Genetix) prior to sequencing. genCLEAN plates were brought to room temperature. They were spun at 910g for 5 minutes to remove water from wells. 100µl dH_2O is spun through the plates at 910g for 5 minutes to wash the gel. 20µl of Plasmid DNA was added to

the well and centrifuged at 910g for 5 minutes and collected in a sequencing plate. The cleaned DNA is then run through an Applied Biosystems HITACHI 3730 DNA analyser (Applied Biosystems, UK) and sequences determined.

6.3.4.8 Gene identification

Sequences were viewed using DNASTAR® Lasergene 8 (DNASTAR®, UK). The primer sets used and vector sequence were located. Sequence data only from the insert was run through NCBI BLAST® to determine gene origin.

6.3.5 *In situ* hybridisation

6.3.5.1 Probe manufacture

6.3.5.1.1 Primers /PCR

Optimal annealing temperature for the primers was established using a gradient block in the thermal cycler.

Cyp26a1 primers used were; forward, 5' TGTGTGTGTCTAGAACAAGCAGCGCAAGAAGGTGA 3' and reverse, 5' TGTGTGTGCTCGAGATTGTAGGAGGTCCATTTAGAAGC 3'. The product length was 1052bp.

The gene product was amplified using the cyclic conditions listed in Table 6.7 with a BioRad DNAEngine® Peltier Thermal Cycler (BioRad, UK).

cDNA was run on a 0.9% agarose gel, the PCR product band was isolated from the gel and purified using GENECLEAN® *Turbo* kit (#1102-200, MP Biomedicals, UK), as per chapter **6.3.4.4**.

6.3.5.1.2 Ligation/Cloning/Transformation

TOPO vector kit was used as previously described in chapter **6.3.4.5.** Bacteria were grown on agar/amp plates and colonies picked and grown up as previously described.

6.3.5.1.3 Sequencing

Sequencing was carried out as per section **6.3.4.7**.

The sequence results were viewed using DNASTAR® Lasergene 8 (DNASTAR®, UK) and the orientation of the insert established.

6.3.5.1.4 Extraction of plasmid DNA

Qiagen Plasmid Midi Kit (#12143, Qiagen, UK) was used. Two columns were run to extract more plasmid DNA. Samples were run as per manufacturer's instructions.

0.2ml of culture medium was incubated overnight in 250ml LB plus 100µg/µl ampicillin, at 37°C with vigorous shaking. Cells were harvested by centrifuging at 6000g for 15 minutes at 4°C. The pellet was resuspended in 4ml Buffer P1 (50mM Tris-Cl pH8.0, 10mM EDTA, 100µg/ml RNase A), then lysed at room temperature with 4ml Buffer P2 [200mM NaOH, 1% SDS (w/v)] for 5 minutes. Next 4ml of chilled Buffer 3 (3.0M potassium acetate pH5.0) was added to the lysate and mixed thoroughly. The lysate was then immediately poured into a QIAfilter cartridge and incubated for 10 minutes at room temperature. During this incubation a QIAGEN-tip 100 was equilibrated with 4ml of Buffer QBT [750mM NaCl, 50mM MOPS pH7.0, 15% isopropanol (v/v), 0.15% Triton X-100 (v/v)]. The lysate was then passes through the QIAfilter into the equilibrated QIAGEN-tip 100. Once the lysate has entered the resin through gravity, wash the QIAGEN-tip twice with 10ml Buffer QC (1mM NaCl, 50mM MOPS pH7.0, 15% isopropanol (v/v). The DNA was eluted from the column using 5ml Buffer QF (1.25M NaCl, 50mM Tris-Cl pH8.5, 15% isopropanol (v/v)). The DNA was then precipitated out of solution with 3.5ml of room temperature isopropanol and centrifuged at 15,000g for 30 minutes at 4°C, and the supernatant poured off. The pellet was washed with 2ml of 70% ethanol and centrifuged for a further 10 minutes at 15,000g. The supernatant is poured off and the pellet air dried at room temperature. The pellet was then resuspended in 100µl of TE (10mM Tris-Cl pH8.0, 1mM EDTA).

6.3.5.1.5 RNA probe protocol

The plasmid was first linearised. Digested using Xho1 (New England Biolabs, UK) for 2 hours in Buffer 2 plus BSA (x100) (New England Biolabs, UK).

The plasmid DNA underwent a cleanup step. To the 100µl of plasmid DNA in TE; 1µl proteinaseK, 3µl 6% (w/v) SDS, was incubated for 30 minutes at 55°C. 100µl of TE pH8 was added and 200µl phenol are added and the tube shaken. Next 200µl chloroform was added and the tube centrifuged for 5 minutes at 13,200rpm. The top phase was removed and kept. A further 200µl chloroform was added to the removed top phase and spun for a further 5

minutes at 13,200rpm. The top phase was again removed and kept. To this 30µl 3M sodium acetate and 500µl of 100% ethanol are added. Kept at -80°C for at least 1 hour. Spun for 5 minutes at 13,200rpm and discarded the supernatant. Washed with 70% ethanol. Spun for a further 5 minutes. The pellet was air dried and the DNA dissolved in 50µl dH_2O.

Next 5µl of the template DNA was added to 2µl 10X DIG mix, 2µl DTT and 2µl of Sp6 (Roche, UK) and 6µl dH2O. This was incubated at 37°C for 2 hours. 3µl of EDTA was added to stop the reaction and the probe was diluted in 80µl dH_2O and stored at -80°C.

6.3.5.2 In situ hybridisation protocol

Retinas stored in glacial methanol were put through graded methanol concentrations to DEPC treated dH_2O. Washed with PBT (DEPC treated) for 10 minutes. They were then partially digested using 1/100 ProteinaseK (Roche, UK) in 6.6% (w/v) SDS. Digestion was then stopped by fixation for 4 minutes with a 4% (w/v) paraformaldehyde and 1% (v/v) glutaraldehyde solution in PBS. Retinas were the washed in PBT-DEPC for 10 minutes. Retinae were then covered in Hybridisation buffer (5ml Hybridisation buffer salts [2M NaCl, 100mM Tris HCl, 50mM NaH_2PO_4, 50mM Na_2HPO_4], 25ml formamide, 5g dextran sulphate, 0.2mg/ml tRNA, 1ml denhardts solution, 16ml dH_2O) and placed at 65°C for 10 minutes. Hybridisation buffer plus 1/1000 probe was pre-warmed to 65°C for 5 minutes and the retina added, this was then incubated at 65°C overnight.

Wash buffer (50% (v/v) formamide, 1xSSC, 0.1% (v/v) Tween20) is preheated to 65°C, the probe was removed and washed 3 times for 20 minutes at 65°C. Then at room temperature the retina was washed 2 times, 20 minutes each, in 1xMABT (58g Maleic acid, 44g NaCl, 38.5g NaOH, 5ml Tween20 in 5L dH_2O). The retina were then incubated in block (8g blocking reagent [Roche, UK], 20% sheep serum, 1.25X MABT/dH_2O) for 20 minutes. Next into secondary antibody, anti Digoxigenin-AP (11093274910, Fab fragment, Roche), 1/1500 in block overnight at room temperature. Retinas were washed in 1xMABT repeatedly throughout the day (overnight for better background results). They were then washed in staining buffer (5.84g NaCl, 12.11g Tris Base in 1l dH_2O, pH9.0) for 10 minutes, prior to being incubated in staining solution to develop the stain. Staining solution (6.5ml staining buffer, 24.5µl BCIP, 37.8µl NBT, 700µl 1M MgCl, 14µl Tween20 and toped up to 14ml total volume with 10% (w/v) PVA) was added and left on overnight at room temperature and removed once the stain has developed. Staining is stopped by washing with staining buffer repeatedly and leaving overnight at room temperature to reduce background. Retina could then be mounted on slides in 100% glycerol and coverslipped. Imaged using an Olympus dissection

stereo microscope (SZX16) with an Olympus fluorescent lamp (U-RFL-T), fitted with a Hamamatsu camera (C4742-95) and Simple PCI software v6.6.

6.3.6 Protein lysate analysis

6.3.6.1 Sodium dodecyl sulphate-polyacrylamide gel electrophoresis (SDS-PAGE)

The mini-gel system Protean II (BioRad) was utilised for SDS-PAGE and set up as per manufacturer's instructions. A 10% separating gel was used which consisted of; 3.34ml Acrylamide: bis-acrylamide (37.5:1) , 2.5ml 1.5M Tris pH8.8, 4ml dH_2O, 100µl 10% SDS, 80µl 10% APS and 4µl TEMED. The stacking gel used (5%) consisted of; 0.75ml acrylamide: bis-acrylamide, 0.63ml 1M Tris pH6.8, 3.4ml dH_2O, 50µl 10% SDS, 75µl 10% APS and 10µl TEMED. The gels were left to polymerise before use. 20µl of boiled lysate (lysed in 2X sample buffer with DTT) were loaded per well, with a low (97, 66, 45, 30, 20.1 and14.4 kDa, GE Healthcare) molecular weight marker loaded into an adjacent well. The gel tank chamber was topped up with running buffer (25µM Tris, 0.1% SDS, 192mM glycine) and the gel was run at constant amperage of 15mA for the stacking gel and 30mA for the separating gel.

6.3.6.2 Western Blotting

Following SDS-PAGE the proteins were transferred onto Whatman protran nitrocellulose membrane using a BioRad semi dry transfer cell. Gels were then equilibriated in transfer buffer (25mM Tris, 192mM glycine, 20% methanol) for 10 min. The gel was loaded into the semi dry transfer cell with 5 sheets of filter paper and the nitrocellulose membrane (all soaked in transfer buffer) below, and a further 5 sheets of soaked filter paper above. Protein transfer took 30 min at a constant 12V. Next the membrane was stained with 0.1% (w/v) ponceau red (in 5% acetic acid) to verify successful protein transfer and identify the position of the molecular markers.

6.3.6.3 Immunodecoration

The nitrocellulose membrane was incubated in block (1% (w/v) Bovine Serum Albumin (BSA)/0.2% TritonX-100/0.1% Tween-20 in TBS) for 2 hours at room temperature. The primary antibody was diluted 1:5000 in block and the membrane incubated for 2 hours at room temperature. The membrane was then washed twice, each 10 min, in block. They were then incubated in secondary (HRP conjugated) antibody (diluted in 1% (w/v) BSA/ 0.2%

TritonX-100/0.1% Tween-20 in PBS). The membranes were then washed in 0.2% TritonX-100/0.1% Tween-20 in TBS twice, each 10 min and a final wash in TBS.

Enhanced chemiliminescence (ECL) was then used to detect the HRP conjugated secondary antibody. The membrane was placed in 10ml ECL mix/membrane (5ml of each lumi-light western blot substrate solution, Roche) for 5 min. Excess solution was removed and the membrane placed in clingfilm and exposed to film.

6.4 Results:

6.4.1 Markers of the mature macula can be found in foetal retina

The proteomic data lead to the identification of new markers of the adult macula. We investigated whether the expression of any of these proteins could be used to identify the presumptive macula in development.

GFAP, LDHB, αB crystallin and αA crystallin, shown in chapters **4** and **5**, mark two sub-populations of Müller cells at the adult macula. GFAP, LDHB and αB crystallin showed no expression in foetal retina, at any time point between CS19 and F2. However, αA crystallin which specifically marked foveal Müller cells, was expressed. Flat mount retina preparations showed that αA crystallin was expressed in a single circular 'spot' temporal to the optic nerve (arrow head in Fig. 6.3). There was also a ring of αA crystallin expression circling the optic nerve head. The inferior nasal edge of the optic nerve head always had a triangular pattern of expression of αA crystallin (arrow in Fig. 6.3). CS19 showed expression at the optic disc but no expression in temporal retina. Some dispersed single spherical cells expressed αA crystallin at CS19 (Fig. 6.4 A), however upon further investigation with retinal cross sections, these cells were within the vitreous and co-label with Iba1 (data not shown), showing that they were contaminating microglial cells from the vitreous. The αA crystallin 'spot' in temporal retina was first expressed at CS20 (50 days) (Fig. 6.4 B).

The 'spot' of αA crystallin expression was present through development to F2 (later stage points not currently accessible for analysis). The 'spot' remained consistent in size in relation to the optic disc, showing that expression does not spread throughout the retina and remained localised (Fig. 6.4 B-F). Expression of αA crystallin was restricted to the fovea/central macula of the adult retina, suggesting that there is direct correlation between the cell population at the developing macula and the Müller cell of the adult macula. This means, we have discovered a marker for an area in the embryonic retina that clearly relates

(spatially and biochemically) to the centre of the adult macula. For the sake of simplicity and the purpose of this thesis we will refer to the αA crystallin positive area as “presumptive macula”.

In summary we have found a novel marker of the presumptive macula in development. The expression of this marker, at the start of the 7th week of gestation, is prior to any other known marker to date. It is expressed prior to the differentiation of ganglion cells, the first cell type to differentiate in the human retina.

6.4.2 A subset of progenitor cells express αA crystallin at the presumptive macula

Specific localisation of αA crystallin to a single spot in temporal retina was confirmed in cross sections (Fig. 6.5 A-F), no αA crystallin was found in peripheral retina (Fig. 6.5 C), and a small population of cells was found adjacent to the optic nerve (Fig. 6.5 F). Expression of αA crystallin was also confirmed in lens tissue (Fig. 6.5 D), αA crystallin is known to be highly expressed in the lens as previously stated, and therefore antibody reactivity in the lens acts as a positive control for the antibodies used. SDS-PAGE followed by western blotting was also carried out to confirm the specificity of the antibodies used; a band corresponding to the molecular weight of αA crystallin, ~19.9kDa, was present (Supplementary Fig. 2).

Cross sections of retina revealed that the αA crystallin positive cells span the entire depth of the retina (Fig. 6.6 A-L). This morphology was similar to that of neural epithelial progenitor cells. αA crystallin co-stained with neural progenitor markers vimentin (Fig. 6.7 A-H) and nestin (not shown) in developing retinas from CS20 to F2. Vimentin and nestin positive neural epithelial progenitor cells of the peripheral retina did not express αA crystallin. This means that there was a subpopulation of the neural epithelial progenitor cells at the presumptive macula that express αA crystallin.

To test whether the αA crystallin expression might have been a response to higher levels of proliferation in the presumptive macula compared to the peripheral retina, an anti-Ki67 antibody was used to determine the numbers of proliferating cells. However, it would appear that there was no difference in the number of Ki67 nuclei found between central (Fig. 6.8 A) and peripheral retina (Fig. 6.8 B), or at the optic nerve (Fig. 6.8 C), but further quantitative analysis is required to confirm this.

6.4.3 Müller cell differentiation at the presumptive macula

We found αA crystallin in the adult retina is expressed in Müller cells (chapter **5**). However, CS20 in the human retina is prior to cell specific differentiation, and through lineage tracing it has been shown that Müller cells are among the last cells in the retina to differentiate,[421] so the question arises, what cell type expressed αA crystallin in the presumptive macula?

We have used immunohistochemistry with antibodies against known Müller cell markers to establish what cell type expressed αA crystallin.

In foetal retina, parallel sections showed that αA crystallin was expressed in the same region as a localised expression of CRALBP, an established mature Müller cell marker (Fig. 6.9 A and B). Other parallel sections were however negative GS and GFAP (known Müller cell markers, data not shown). CRALBP was expressed in the same restricted retinal area as αA crystallin, through until foetal stage F2. It has previously been reported by Walcott and Provis[423] that CRALBP expression in neural epithelial progenitor cells are present in central retina at 16WG and then spreads radially with development, however we have now shown that this expression actually starts much earlier. CD44, shown to be a marker of progenitor cells destined to become Müller cells[77] and a marker of mature Müller cells,[77] was also expressed in the presumptive macula (arrow head in Fig. 6.9 C). Both CRALBP and CD44 were expressed in cells with morphology similar to that of αA crystallin, the neural epithelial progenitor cells (Fig. 6.9 D and E).

Vimentin expression was significantly higher at the presumptive macula compared to peripheral progenitor cells (Fig. 6.8). Vimentin labels both neural epithelial progenitor cells and adult mature Müller cells, whether vimentin is upregulated during Müller cell maturation is unknown, but this could be an explanation for the regional differences seen.

All neural epithelial progenitor cells in the outer neuroblastic layer of the developing retina express SOX9. Upon differentiation expression is suppressed,[488] except in Müller cells where SOX9 expression has been found in adult mice.[488] The cells at the presumptive macula in an F2 retina expressed SOX9 in a single layer of nuclei in the outer neuroblastic layer (arrowhead in Fig. 6.9 F), surrounded by cells negative for SOX9. All cells of the outer neuroblastic layer in the periphery were positive for SOX9 (arrowhead in Fig. 6.9 G).

Our data supports the theory that Müller cells start to mature first at the developing macula, prior to ganglion cell and photoreceptors as previously thought. The progenitor cells with a determined Müller cell fate persisted in expressing nestin, indicating that they are not fully matured Müller cells and maintain their ‘stemness’.

6.4.4 Retinoic acid signalling plays a role in macula position determination

αA crystallin is not a known morphogen or transcription factor. It is unlikely to play a direct role in the determination of the presumptive macula. However using the expression of αA crystallin as a marker of presumptive macula made it possible to compare sample regions, and determine more fundamental factors involved in the specification of this region.

Fresh tissue was dissected from temporal retina where we have previously identified the presumptive macula, and peripheral retina from between the presumptive macula and optic nerve was isolated from embryos. qPCR using primers specific for αA crystallin, CRYAA (using ACTB as a housekeeping gene to baseline against) was used to confirm accurate dissection of the two regions, from a CS20 embryo (the time point at which αA crystallin protein was first expressed). mRNA from the two regions of the same retina was used for a differential gene display comparison using the Genefishing^{TM} PCR (chapter **6.3.4**). The differential gene display PCR revealed 32 PCR products that differed in expression (arrow heads in 6.10 A-D). Sequencing of these PCR products identified 23 sequences, of which 14 genes were identified; 12 upregulated within the presumptive macula and 2 downregulated (Table 6.8). One of the genes identified stood out from the rest; cellular retinoic acid binding protein 1, CRABP1, known to mediate transport of retinoic acid derivatives during retinoic acid signalling. The differential expression of this protein between presumptive macula and peripheral retina was confirmed using qPCR on tissue from 5 embryonic/foetal retinae of stages; CS20, CS21, CS22, CS23 and F1 (including the CS20 retina used for differential gene display). For each sample, qPCR for CRYAA was used to confirm correct dissection (Fig. 6.11 A and B).

Retinoic acid gradients are known to be formed through degradation sinks where degradation enzymes limit the amount of retinoic acid. The expression levels of degradation enzymes can be spatially regulated at a transcriptional level. CYP26A1, CYP26B1 and CYP26C1 are known retinoic acid degradation enzymes and have been shown to play a key role in retinoic acid gradient formation. CYP26B1 was not found in the developing human retina with qPCR (data not shown); however CYP26A1 and CYP26C1 were both found to be significantly differentially expressed between the presumptive macula and the peripheral retina (Fig. 6.11 C and D). Expression of both CYP26 enzymes was significantly increased in the presumptive macula (Fig. 6.11 C and D), with an average fold change of 8.7↑ for CYP26A1 (P = 0.002) and 20.3↑ (P = 0.00004) for CYP26C1. Whole mount *In situ* hybridisation revealed that CYP26A1 expression at a single 'spot' in temporal retina at F1

(Fig. 6.11 E), this ‘spot’ correlated with the CRYAA expression pattern (Fig. 6.11 F). A parralel negative control (Fig. 6.11 G) was carried out for the in situ hybridisation, where the mRNA probe was not included. This demonstrated that the 'spot' seen was not background staining. A sink of retinoic acid must therefore exist at the presumptive macula, suggesting that a lack of retinoic acid might play a role in the determination of macula retina in the human retina.

6.5 Discussion:

The αA crystallin expression at the presumptive macula was confirmed using two antibodies from different suppliers, and both antibodies identified exactly the same expression pattern. This antibody specificity, along with the lens tissue acting as an internal positive control for each eye studied confirmed that the antibody staining represents protein distribution. Further to that western blots show the same banding pattern with both αA crystallin antibodies in adult human retina and foetal retina; a band was present at ~19.9kDa, the expected molecular weight of αA crystallin. An additional band was also present in the adult tissue western blot, at ~21kDa, which could correspond to αB crystallin (Supplementary Fig. 2). The manufacturers of the two antibodies state that there is a possibility of binding with αB crystallin. As a separate antibody directed against αB crystallin was also tested in both adult and foetal tissue, we know αB crystallin is expressed in adult retina and not in foetal, this could explain the presence of the 21kDa band only in the adult tissue western blot. The αA crystallin antibodies did not however colocalise with the αB crystallin expression in the adult macula, this might be due to the antibody being more specific for immunohistochemistry; during SDS-PAGE protein conformations are changed, this could allow the binding sites of αB crystallin to which the αA crystallin antibodies recognise, to become exposed. The higher molecular weight bands in all blots might be due to binding of other small heat shock proteins through the conserved heat shock domain. Further evidence of antibody specificity is that αA crystallin was seen increased in the macula of the adult eye with comparative proteomics (Table 4.4), and qPCR confirmed increased levels of CRYAA mRNA in foetal presumptive macula (Fig. 6.11 A), both correlating with the immunohistochemistry data.

The tissue used was from aborted embryos, collected by the commonly used vacuum-aspiration abortion method. This method could induce a stress response in the harvested tissue, and as αA crystallin has been shown to be upregulated under stress it is possible that the crystallin expression represents focused stress on the retina due to the method. However, the consistent expression pattern seen between, and within gestational ages (αA

crystallin expression was confirmed with at least three embryos per gestational age), indicates clearly that this is not a random stress response. Other markers also correlated with the αA crystallin expression in the foetal tissue and these markers which are not known stress response proteins, making it unlikely again that expression patterns here are purely a postmortem stress response.

We therefore believe that we have discovered a new marker for the developing macula, one which for the first time does not rely upon general cell differentiation initiating in central retina, and one that is specific for a population of cells found purely in central retina and which can be traced to expression patterns in adult tissue. Furthermore this marker labels the presumptive macula prior to ganglion cell differentiation. Considering optic fissure closure only occurs at CS18 (in GW6), our definition of a specific macula protein at the presumptive macula at CS20 is remarkably early (Fig. 6.12).

It was surprising that we found Müller cell markers in epithelial progenitor cells starting at 7WG. Previous lineage tracing identifies Müller cells as the last cell type to differentiate within the developing retina.[421] We found neural epithelial progenitor cells express mature Müller cell markers whilst still maintaining their pluripotant state in the human retina. It has been argued by other authors that Müller cells and neural epithelial progenitor cells are overlapping cell populations,[423] and that the progenitor cells do not necessarily differentiate into Müller cells, but merely mature into them. There is evidence for that scenario at the macula of the human eye; the neural epithelial progenitor cell morphology is similar to that of Müller cells, spanning the retinal depth with end feet forming the retina limits. It has also been shown that mature adult Müller cells have the capability of giving rise to neuronal progenitors. The macula progenitor cells express vimentin at higher levels than the peripheral progenitor cells which could be an implication of a switch to Müller cell fate, accompanied by the expression of αA crystallin, CD44 and CRALBP and the persistence of SOX9. This suggests that a Müller cell fate switch occurs in the macula early in development.

Co-localisation of the retinoic acid degradation enzymes CYP26A1 and C1 and αA crystallin in the retina has been identified. This presumed retinoic acid free region correlates with the area centralis and visual streak in other mammals and birds. However, the functional role for this lack of retinoic acid, or for retinoic acid signalling in peripheral retina is poorly understood. Two distinct phases of retinoic acid signalling have been identified in murine and chick model systems; an early phase necessary for optic cup formation (mouse E9.5-10.5), and a later phase essential in development of the anterior structures (mouse E10.5-13.5). A lack of the retinaldehyde dehydrogenase enzymes that generate retinoic acid, RALDH3 and

RALDH1, leads to complete overgrowth of the mesenchyme during cornea and eye lid formation due to subsequent loss of retinoic acid in the optic cup.[467, 470, 489] However a disruption in retinoic acid gradients across the retina during development has topologic effects on cell types. VAX2, along with TBX5, is essential in patterning the retinoic acid metabolising enzymes of the retina.[490] An overexpression of VAX2 influences the topographic expression of rod photoreceptors in chick,[491] and has been found to be required for asymmetric expression of cone marker genes in the vertebrate retina (mouse and medaka fish studied).[492] The precise molecular mechanisms of cone-specific gene expression still remains elusive but is heavily studied.[493-500] Retinoic acid has been shown to play an important role in cone photoreceptor determination. It has been shown that the retinoid X receptor, RXRγ, and the thyroid hormone receptor, THRB, can act together and repress expression of the S-opsin gene in dorsal retina of the mouse.[496, 498] Retinoic acid receptor-related orphan receptorβ (RORβ) has also been shown to act as a transcriptional activator of S-opsin, along with the cone-rod homeobox transcription factor, CRX.[499] RORα also acts as a transcriptional activator of the S-opsin, M-opsin and cone arrestin in mouse retina, with reductions in expression levels in knock-out mice.

Retinoic acid has also been shown to promote the formation and survival of rods from cultured retinal progenitor cells of developing rate retina[501-503] and embryonic stem cells.[504] Studies in zebrafish have shown an increase in rod density and correlating decrease in cone density after endogenous retinoic acid exposure,[505] Stevens and colleagues have also shown that this change in photoreceptor mosaic is not due to selective cone death; they did however notice increased cell death within the inner nuclear layer, a possible downstream response from cone loss and inter neuron number/ratios with rods versus cones.[505] This data supports the theory that retinoic acid is crucial in rod/cone cell fate decisions during development. This animal model data shows a direct link between retinoic acid signalling in the retina and photoreceptor fate decisions and thus rod/cone patterning.

How this relates to human and primate retina patterning is not known, but correlation between photoreceptor patterning and retinoic acid distribution in mouse retina and chick retina (i.e. a decrease in rod density correlating with the retinoic acid free central zone, and cone concentrations) mimics that seen in humans.

Müller cell fate determination in neural epithelial progenitor cells prior to photoreceptor gene expression, in a region that correlates to a retinoic acid free zone in the retina, could also imply that a macular Müller cell population within the human retina influences cone development; further investigation into this scenario is warranted.

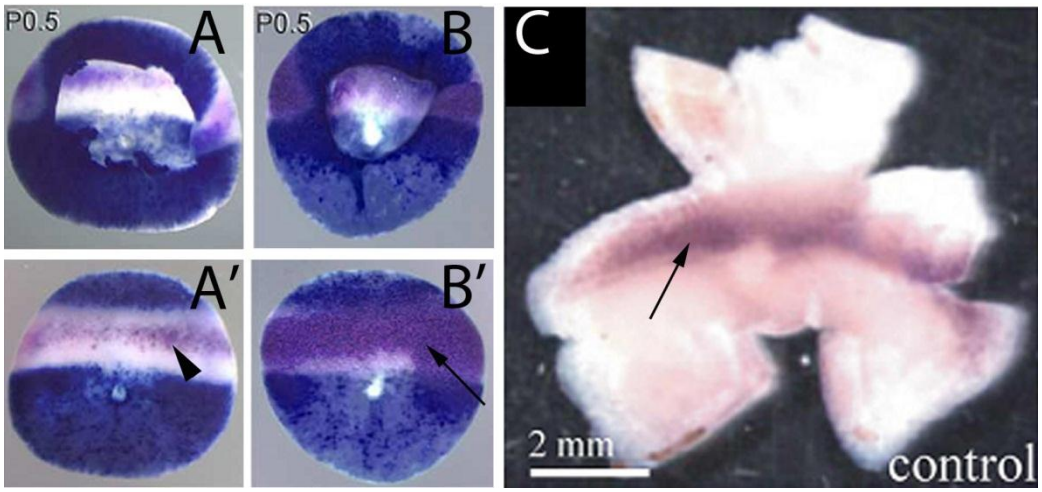

Figure 6.1. CYP26 enzyme expression in mouse and chick retina.

A and **B**: Postnatal day 0.5 retina from transgenic mice. X-gal reaction for retinoic acid reporter transgene indicates regions of retinoic acid (blue), while the purple bands indicate regions of CYP26C1 (**A**) and CYP26A1 (**B**) visualised with in situ hybridisation. A corresponding region of CYP26A1 is expressed in chick retina (purple strip in **C**), again using in situ hybridisation. Images adapted from Sakai *et al.*[474] (**A** and **B**) and from Golz *et al.*[490] (**C**).

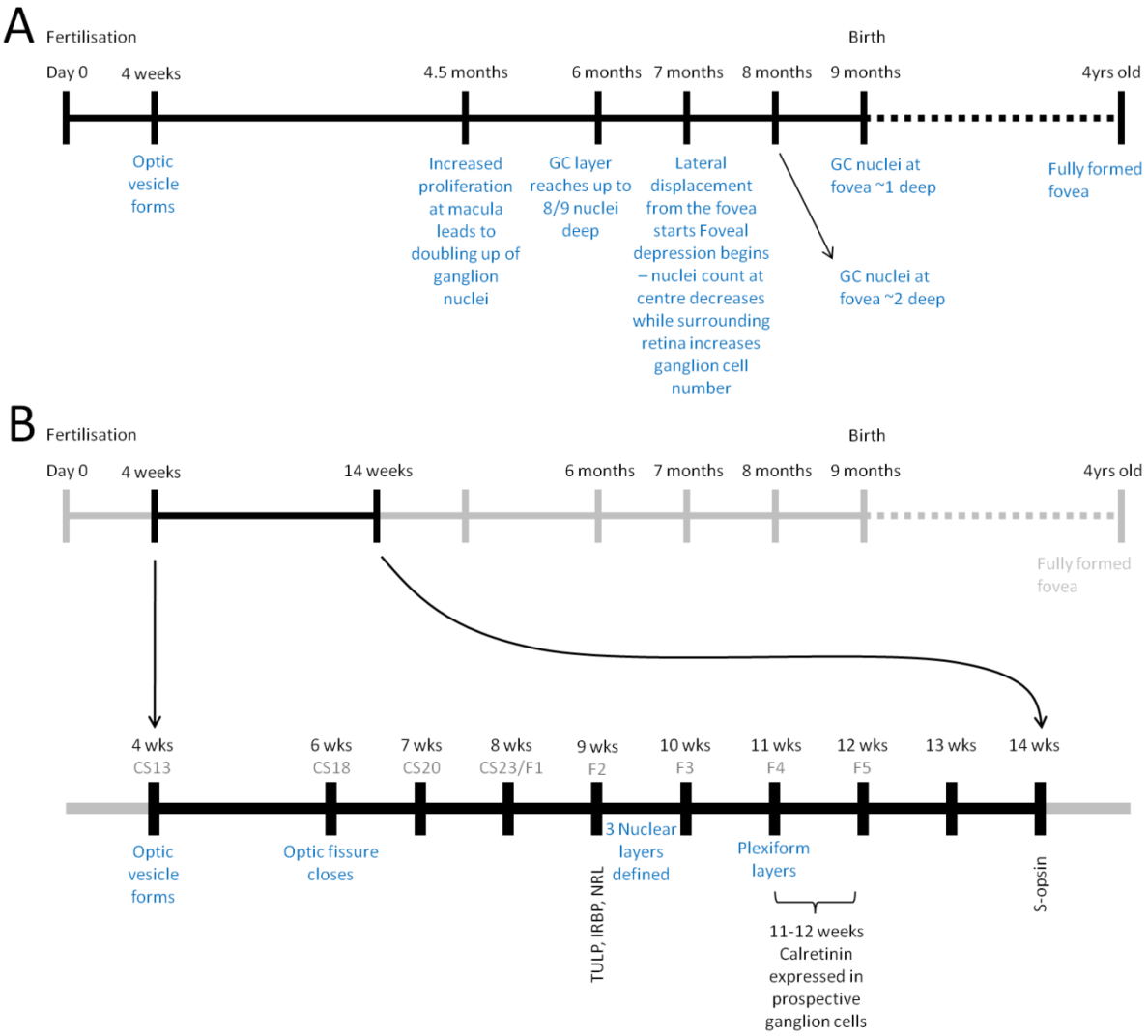

Figure 6.2. Timeline of human macula development.

Main morphological landmarks in macula development (**A**), and marker expression time points for photoreceptors and ganglion cells (**B**). Blue text indicates morphological landmarks, Black text, marker expression and cell differentiation. wks; weeks.

Table 6.1: TRI REAGENT™ RNA extraction reagents

Reagent	Supplier	[Stock]
TRI Reagent™	Sigma, UK	N/A
Chloroform	Sigma, UK	100%
2-Isopropanol	Sigma, UK	100%
Glycogen	Ambion, UK	100%
Ethanol	Hayman, UK	75% (v/v) / DEPC dH_2O
RNAsecure	Ambion, UK	N/A

Table 6.1. TRI REAGENT™ RNA extraction reagents

Table 6.2: qPCR primers

Gene	Primer sequence	
ACTB	***Forward***	CCTGGACTTCGAGCAAGAGATG
	Reverse	AGGAAGGAAGGCTGGAAGAGTG
CRYAA	***Forward***	GTACCAAAGCTGAACATGGA
	Reverse	GAGAAGTGCTTCACATCGAG
*CYP26A*1	***Forward***	CACTAAAGCAATCTTCAACGCA
	Reverse	GCAAAGTAAACCCTTACTCTTCAG
*CYP26C*1	***Forward***	TGGAGAACCTCTTCTCACTG
	Reverse	CTTGCACTGTGAATGATTAGG
*CRABP*1	***Forward***	AACTTATCCTGACGTTTGGC
	Reverse	CAGCTCAGAACTATGACATATTCC

Table 6.2. qPCR primer sequences.

Table 6.3: Quantitative Real-Time PCR cycling conditions

Temperature	Time	Purpose
Stage 1: single cycle		
95°C	10 minutes	Activates enzyme
Stage 2: repeated 40 cycles		
95°C	15 seconds	Denatures double stands
60°C	1 minute	Annealing and Elongation
Data collection		
Stage 3: (dissociation curve) single cycle		
95°C	15 seconds	Denature
60°C	15 seconds	Annealing
Slow ramp to 95°C		Records temperature(s) at which denaturing occurs
95°C	15 seconds	Full denaturing of double stands
Data collection		

Table 6.3. Quantitative Real-Time PCR cycling conditions

Table 6.4: Differential gene display (Genefishing^{TM}) primers.

Primer	Sequence
5' primer	
ACP1	5'-GTCTACCAGGCATTCGCTTCATGGGGGGCCATCGACC-3'
ACP2	5'-GTCTACCAGGCATTCGCTTCATGGGGGAGGCGATGCC-3'
ACP3	5'-GTCTACCAGGCATTCGCTTCATGGGGGCCGGAGGATG-3'
ACP4	5'-GTCTACCAGGCATTCGCTTCATGGGGGGCTGCTCGCG-3'
ACP5	5'-GTCTACCAGGCATTCGCTTCATGGGGGAGTGCGCTCG-3'
ACP6	5'-GTCTACCAGGCATTCGCTTCATGGGGGGGCCACATCG-3'
ACP7	5'-GTCTACCAGGCATTCGCTTCATGGGGGCTGCGGATCG-3'
ACP8	5'-GTCTACCAGGCATTCGCTTCATGGGGGGGTCACGGAG-3'
ACP9	5'-GTCTACCAGGCATTCGCTTCATGGGGGGATGCCGCTG-3'
ACP10	5'-GTCTACCAGGCATTCGCTTCATGGGGGTGGTCGTGCC-3'
ACP11	5'-GTCTACCAGGCATTCGCTTCATGGGGGCTGCAGGACC-3'
ACP12	5'-GTCTACCAGGCATTCGCTTCATGGGGGACCGTGGACG-3'
ACP13	5'-GTCTACCAGGCATTCGCTTCATGGGGGGCTTCACCGC-3'
ACP14	5'-GTCTACCAGGCATTCGCTTCATGGGGGGCAAGTCGGC-3'
ACP15	5'-GTCTACCAGGCATTCGCTTCATGGGGGCCACCGTGTG-3'
ACP16	5'-GTCTACCAGGCATTCGCTTCATGGGGGGTCGACGGTG-3'
ACP17	5'-GTCTACCAGGCATTCGCTTCATGGGGGCAAGCCCACG-3'
ACP18	5'-GTCTACCAGGCATTCGCTTCATGGGGGCGGAGCATCC-3'
ACP19	5'-GTCTACCAGGCATTCGCTTCATGGGGGCTCTGCGAGC-3'
ACP20	5'-GTCTACCAGGCATTCGCTTCATGGGGGGACGTTGGCG-3'
3' primer	
dt-ACP2 (10µM)	5'-CTGTGAATGCTGCGACTACGATGGGGGTTTTTTTTTTTTTT-3'

Table 6.4. Differential gene display (Genefishing^{TM}) primers. ACP, annealing control primer

Table 6.5: Genefishing™ PCR cycling conditions

Temperature	Time	Purpose
Stage 1: single cycle, *PCR for second strand cDNA synthesis*		
Pre-heat thermal cycler to 94°C		
94°C	5 minutes	Denature
50°C	3 minutes	Initial annealing temperature, only 10mer core sequence of arbitrary ACP will bind to first cDNA strand with 8-10 pair matches
72°C	1 minute	Elongation, second strand cDNA synthesised in one cycle
Stage 2: repeated 40 cycle, *PCR for amplifying the second-strand cDNA*		
94°C	40 seconds	Denatures double stands
65°C	40 seconds	Allows annealing of universal sequences of ACP while being stringent enough to prevent core sequence binding. Allows dT-ACP2 binding. ACP and dT-ACP2 cannot anneal to first strand at 65°C
72°C	40 seconds	Elongation, only targeted PCR products amplified
Stage 3: single cycle		
72°C	5 minutes	Final elongation

Table 6.5. Genefishing™ PCR cycling conditions

Table 6.6: Sequencing reaction cyclic conditions

Temperature	Time	Purpose
Stage1: single cycle		
96°C	1 minute	Denature any double strands
Stage 2: repeated 25 cycles		
96°C	10 seconds	Denature
50°C	5 seconds	Annealing
60°C	4 minutes	Elongation
Finished, store at 4°C		

Table 6.6. Sequencing reaction cyclic conditions

Table 6.7: Cyclic conditions for CYP26A1 In situ hybridisation probe

Temperature	Time	Purpose
Stage 1: single cycle		
94°C	5 minutes	Denature double strands/primer dimers
Stage 2: repeated 40 cycles		
95°C	30 seconds	Denature double strands
59.9°C	30 seconds	Annealing
72°C	60 seconds	Elongation
Stage 3: single cycle		
72°C	10 minutes	Final elongation step
4°C	as necessary	Storage

Table 6.7. Cyclic conditions for CYP26A1 *In situ* hybridisation probe

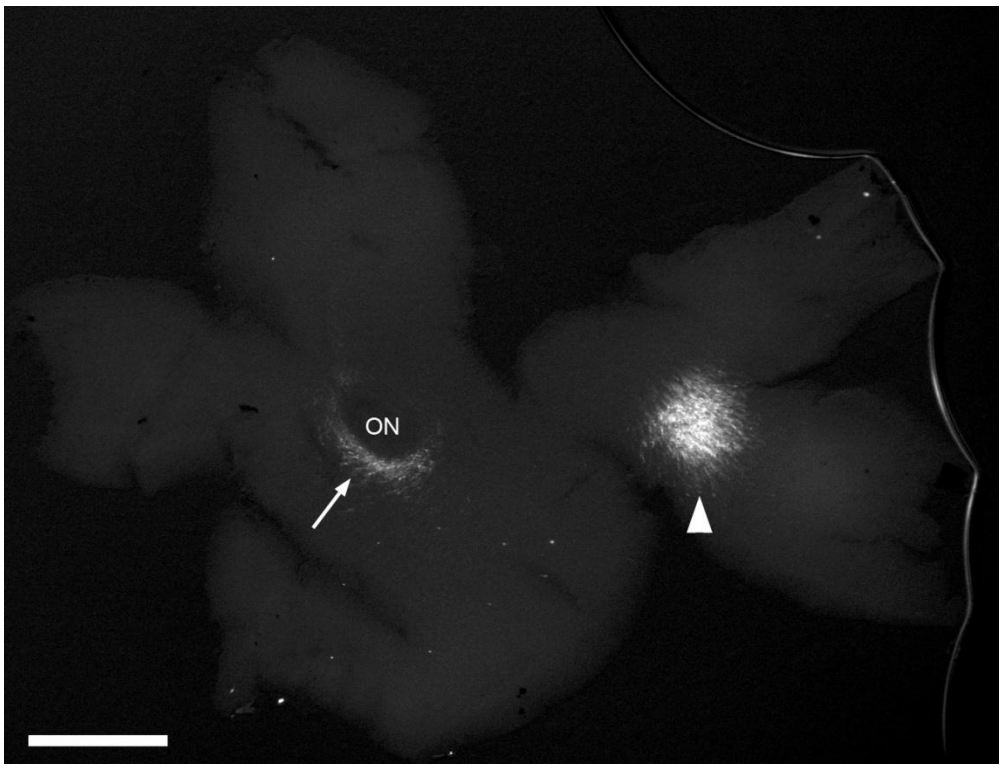

Figure 6.3. αA crystallin expression in temporal retina during development
αA crystallin expression in human embryonic retina at CS22. Anti-αA crystallin antibodies reveal a 'spot' of expression in temporal retina (arrowhead). Expression is also located at the optic nerve rim, more pronounced to the inferionasal side (arrow). No expression is visible in peripheral retina. ON; optic nerve. Scale bar is 500µm.

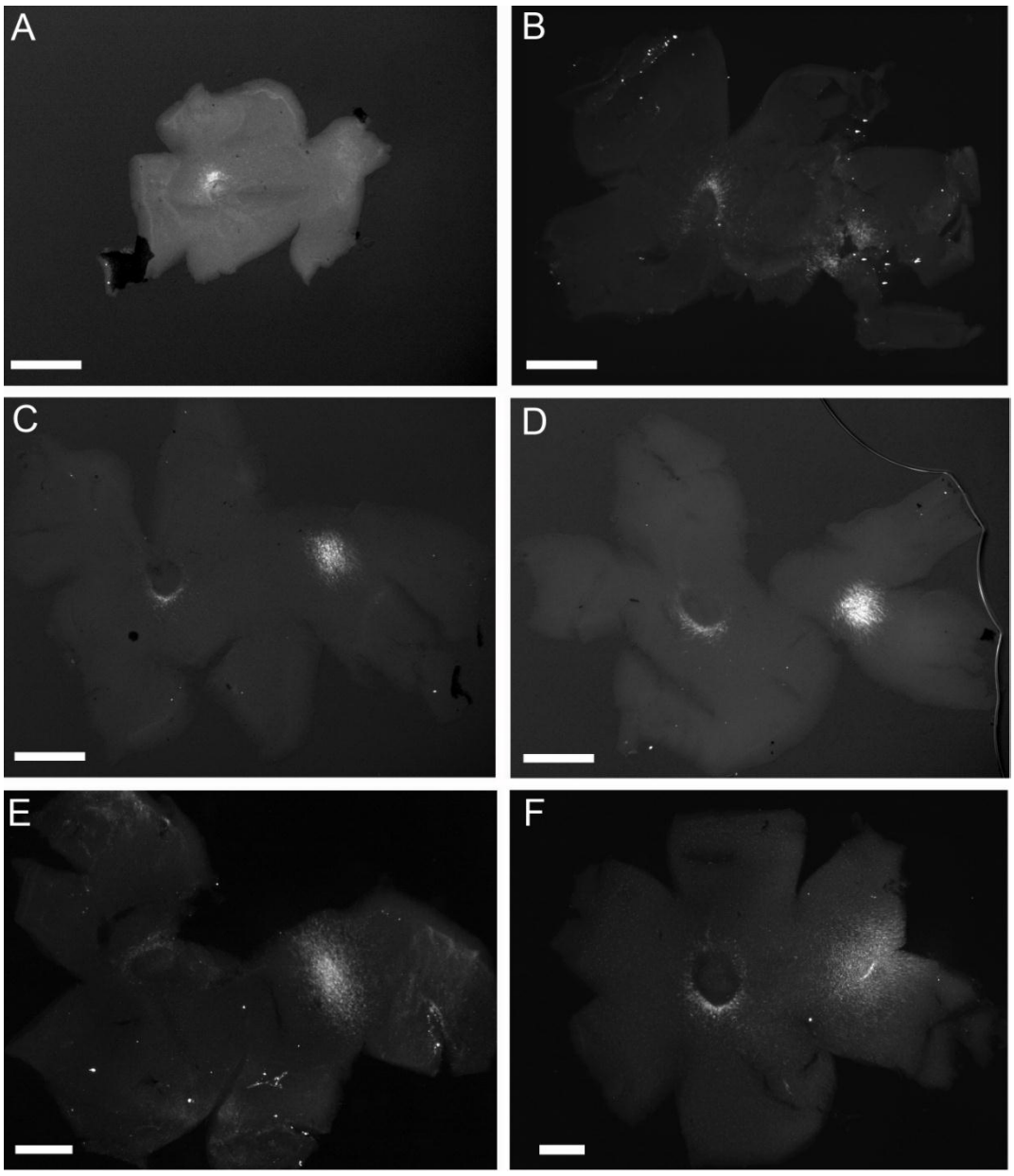

Figure 6.4. Time course of αA crystallin expression in human embryonic retina.
Anti-αA crystallin antibody stained embryonic and foetal retinas (**A-F**). Expression is found at the optic nerve rim in a CS19 retina but a spot is absent in temporal retina. Expression in temporal retina starts as CS20 (7WG) (**B**) and is expressed through development, CS21 (**C**), CS22 (**D**), CS23 (**E**) and F1 (**F**). No expression is found in peripheral retina at any time point. Expression was confirmed in 3 eyes from each developmental stage. Scale bars are 500µm.

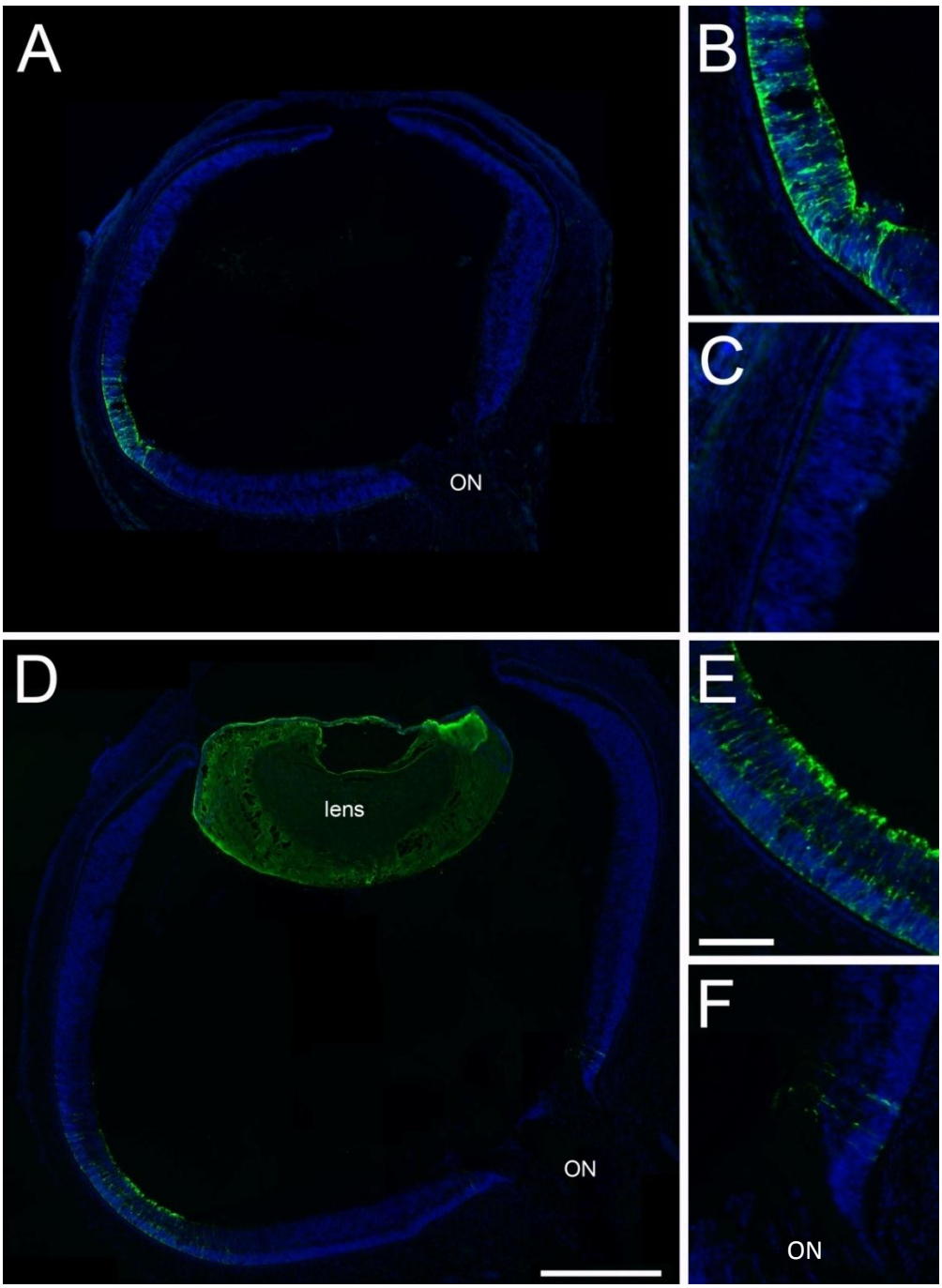

Figure 6.5. αA crystallin expression in foetal retina cross sections.
αA crystallin expression is limited to the presumptive macula and a small region at the optic nerve. Cross sections through the optic nerve (ON) and presumptive macula of CS23 eye globe (**A**). Restricted spatial expression of αA crystallin (green) in central retina (**A**), expression through all layers of the retina (B), peripheral retina shows no expression (**C**). The eye globe of an F2 foetus shows the same restricted pattern (**D**), expression through all layers of the retina (**E**) and no expression in the periphery. Expression at the optic nerve edge spans the depth of the retina also (**F**). αA crystallin positive lens tissue confirms antibody specificity (**D**), lens was lost during processing in **A**. Scale bars are 500µm in **D** and 100µm in **E**.

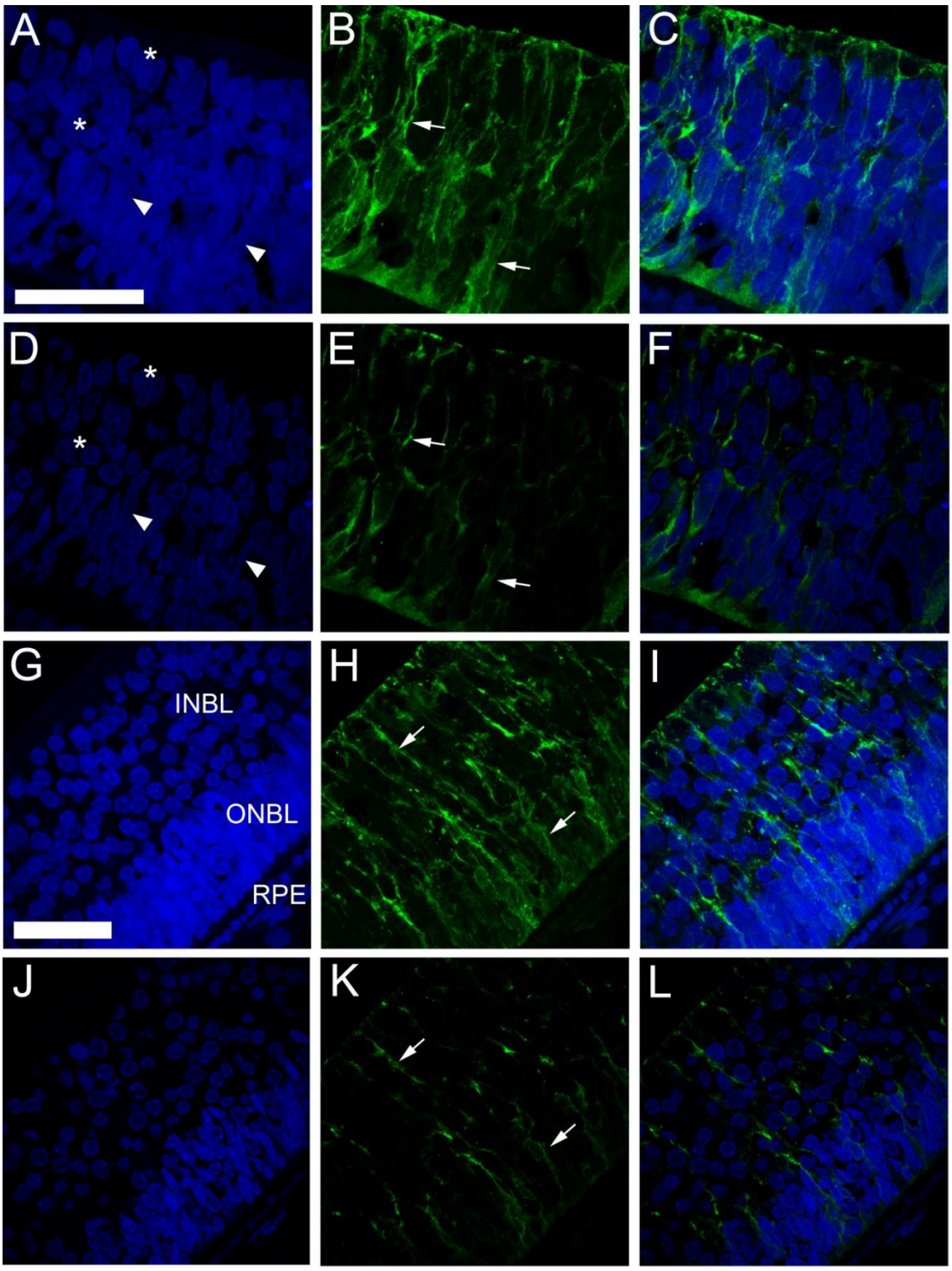

Figure 6.6. αA crystallin positive cells at the presumptive macula have epithelial progenitor cell morphology.

Confocal microscopy images of αA crystallin positive cells at the presumptive macula of an embryo CS22 (**A-F**) and foetus F2 (**G-L**); **A-C**, **G-I** are merged stacks, **D-F**, **J-L** are single slice images. The transient layer of chievitz is just forming at CS22 (**A** and **D**), cells of the inner neuroblastic layer are beginning to become disorganised and spherical (asterisks in **A** and **D**), whilst the outer neuroblastic layer is organising into columnar lines of nuclei with an elongated morphology (arrow heads in **A** and **D**). αA crystallin positive (green) cells can be

seen to span the entire retinal depth (arrows in **B** and **E**). Cell processes broaden and meet at the prospective inner and outer limiting membranes. By F2 the inner and outer neuroblastic layers (INBL and ONBL respectively) are fully differentiated, separated by the layer of chievitz (**G**). αA crystallin positive cell morphology remains constant through gestation, the radial cells persist in spanning the entire depth of the retina (arrows in **H** and **K**). Scale bars are equal to 50μm.

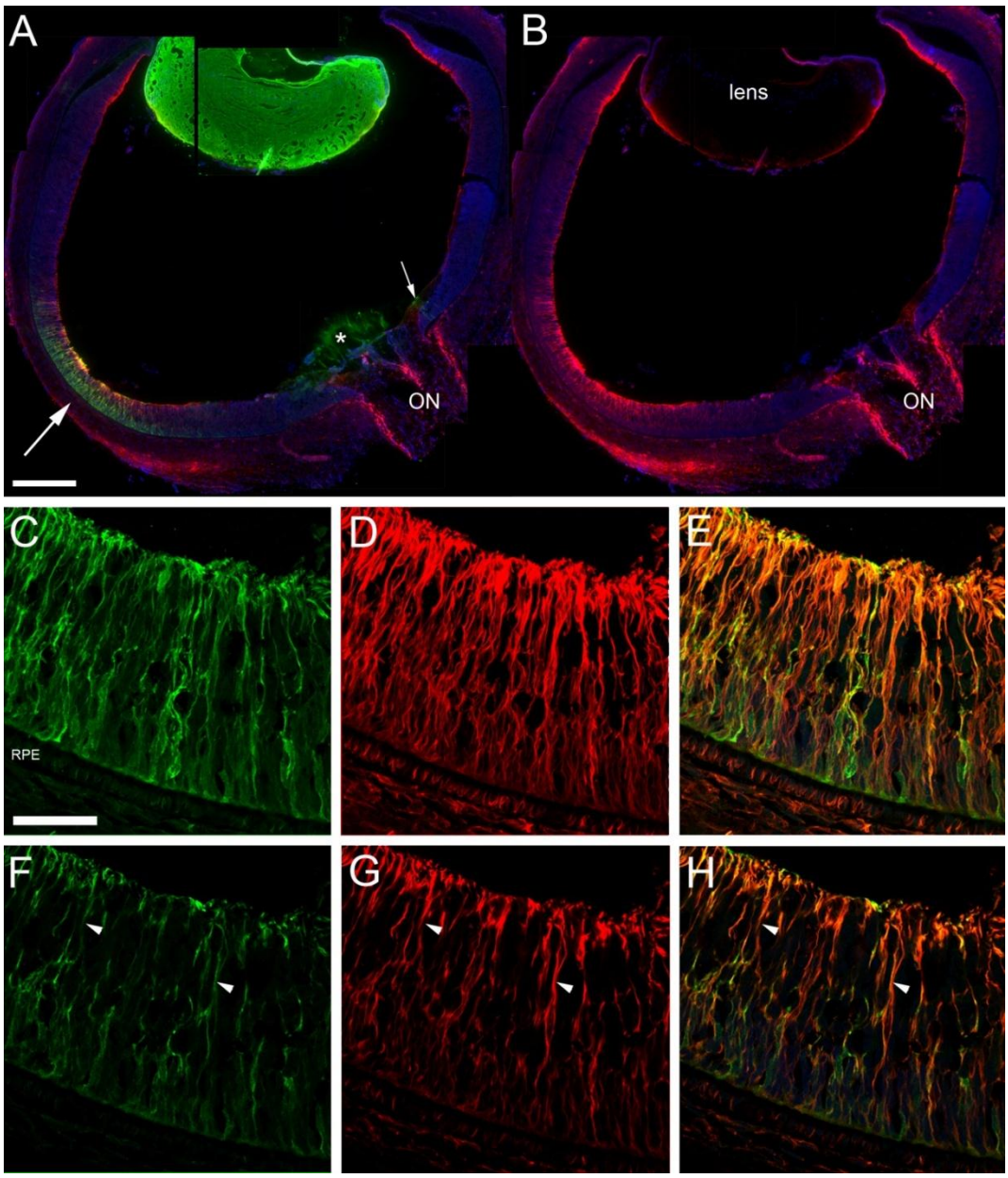

Figure 6.7. Neural epithelial progenitor cells at the presumptive macula are αA crystallin positive in an F2 retina.

Lens tissue acts as a control for αA crystallin antibody specificity (**A**). The αA crystallin positive presumptive macula (large arrow **A**) and αA crystallin positive cells at the edge of the optic nerve (small arrow **A**) are present within the section. An antibody directed against vimentin (red) highlights neural epithelial progenitor cells throughout the retina (**A** and **B**), vimentin staining is stronger around the presumptive macula (**B**) compared to peripheral retina. Confocal microscopy imaging (**C-H**) reveals that αA crystallin (**C** and **F**) co-localises with vimentin (**D** and **G**), all αA crystallin positive cells stain for vimentin at the presumptive macula (**E** and **H**). Arrow heads highlight specific cells in a single confocal slice confirming co-localisation (**F-H**). ON; optic nerve, RPE; retinal pigment epithelium, asterisk in **A** indicates αA crystallin positive hyloid vasculature. Scale bars are 500µm in **A** and 50µm in **C**.

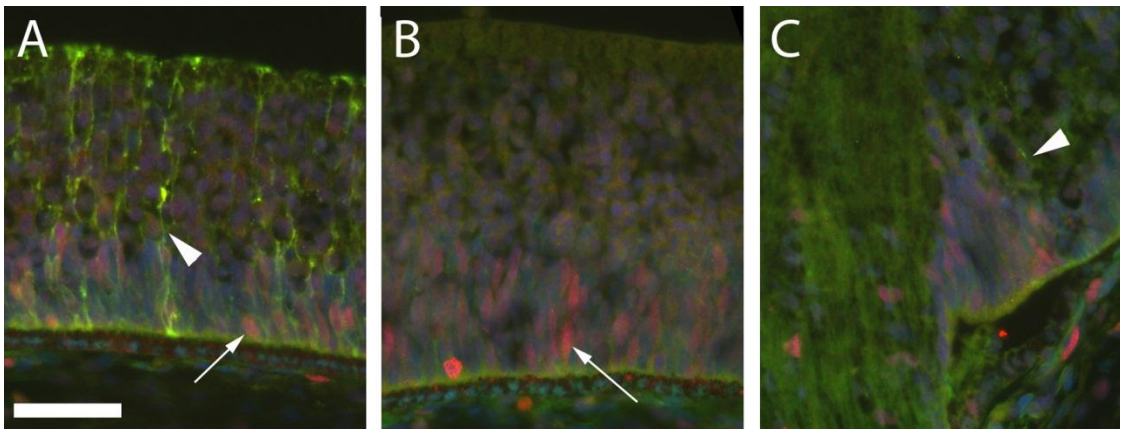

Figure 6.8. Proliferation in the retina.
αA crystallin expression (arrow heads, green) at the macula (**A**) but missing from peripheral (**B**) and is expressed in a small region at the edge of the optic nerve (**C**). Anti-Ki67 staining highlights proliferating cells (red). There was no difference in the numbers of Ki67 positive cells (arrows) in presumptive macula compared to the periphery or optic nerve. Scale bar is 50µm.

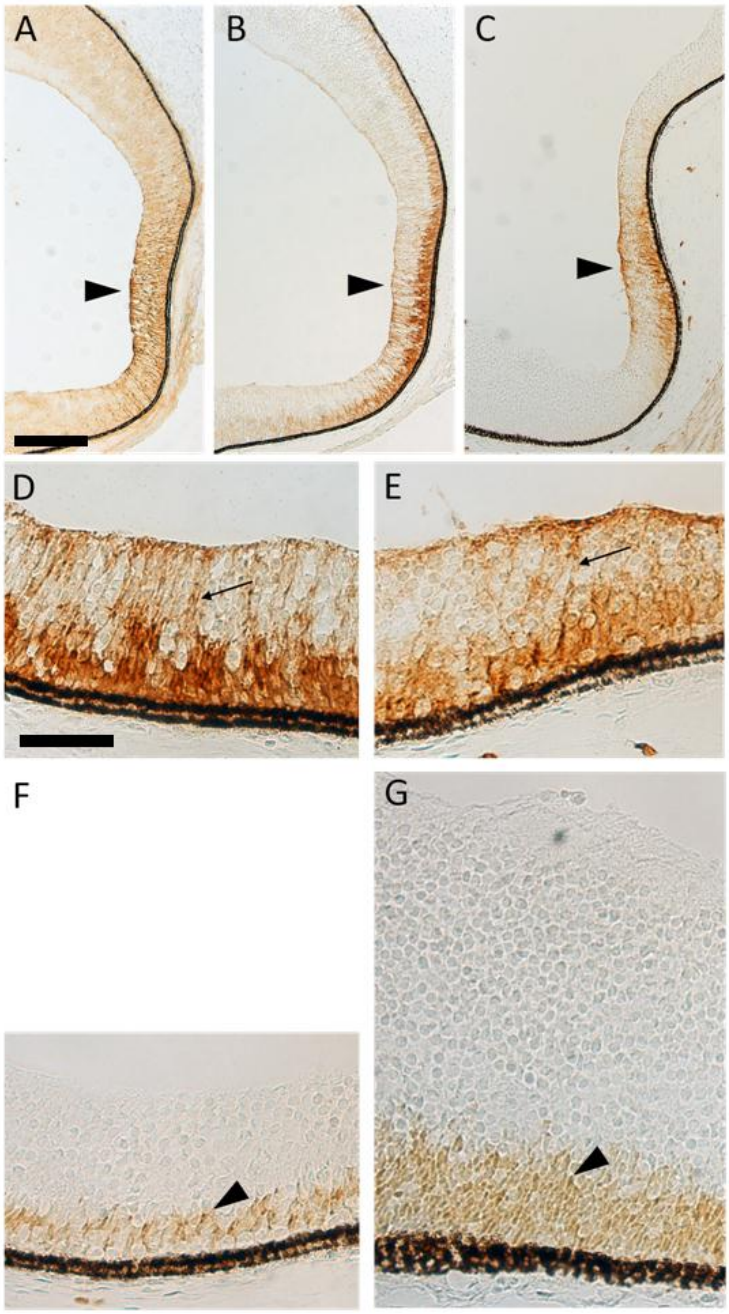

Figure 6.9. Muller cell marker expression at the presumptive macula. Immunohistochemistry revealed that αA crystallin (arrowhead in **A**) co-localised with expression of CRALBP (arrow head in **B**) and CD44 (arrowhead in **C**) at the presumptive macula of an F1 retina. Both CRALBP (**D**) and CD44 (**E**) positive cells had neural epithelial progenitor cell morphology, spanning the retinal depth (arrows in **D** and **E**). A limited population of the nuclei in the outer neuroblastic layer expressed SOX9 at the presumptive macula (arrowhead in **F**), while all nuclei of the outer neuroblastic layer in the periphery expressed SOX9 (arrowhead in **G**). Scale bars are equal to 200µm in **A** and 50µm in **D**.

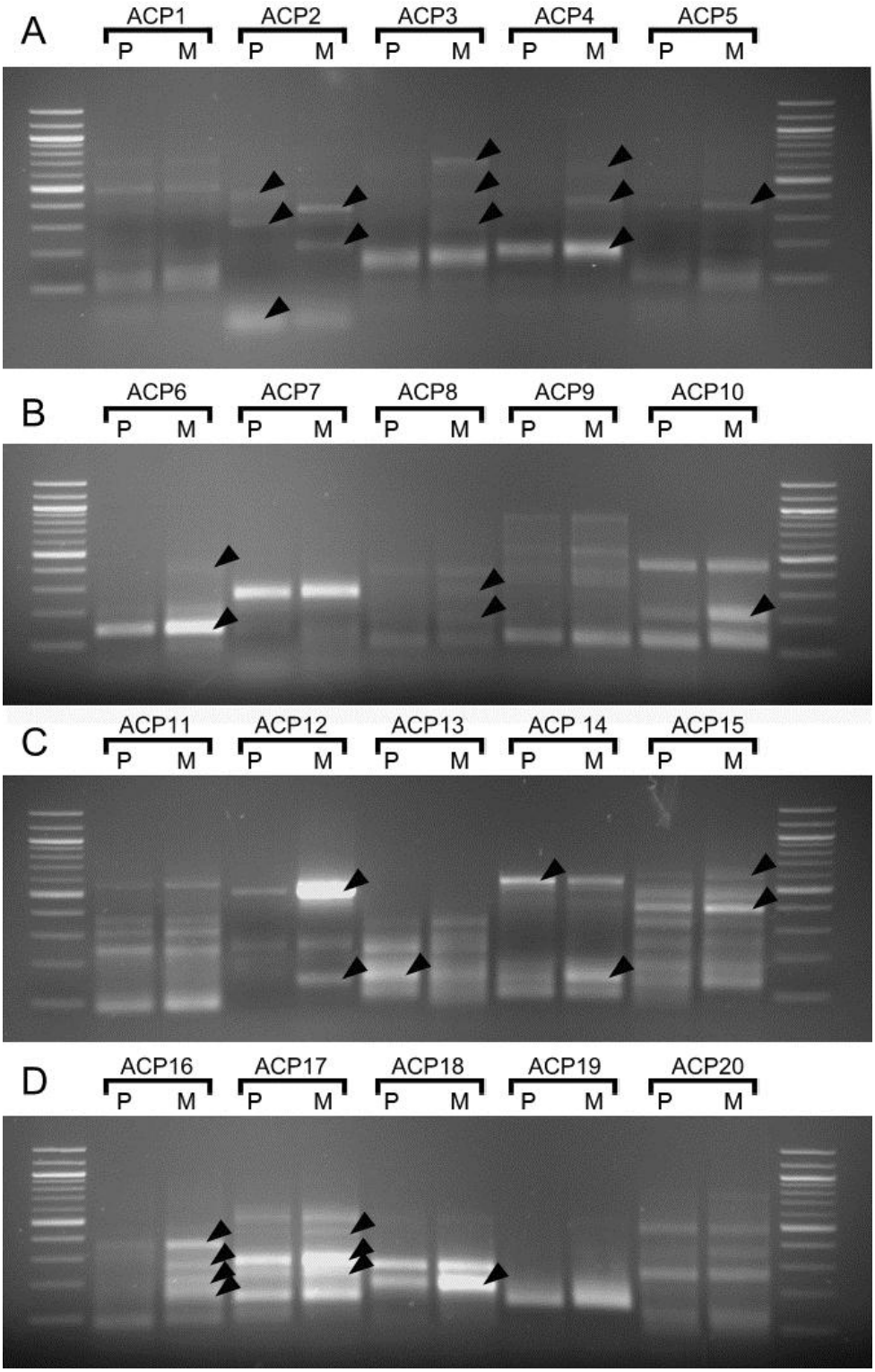

Figure 6.10 Differential gene display
Differential gene display PCR bands (**A-D**). Arrow heads indicate bands selected for sequencing. ACP; Annealing control primer, P; peripheral, M; presumptive macula.

Table 6.8: Sequenced genes from differential gene expression profiling.

Up regulated in the presumptive macula

1. CCCTC-binding factor (zinc finger protein) (CTCF), transcript variant 2
2. cDNA: FLJ22826 fis, clone KAIA4022
3. **Cellular retinoic acid binding protein 1 (CRABP1)**
4. Chromosome 10 clone RP11-183E9
5. Chromosome 17, clone RP11-87N3
6. DNA sequence from clone RP11-15N12 on chromosome 6
7. DNA sequence from clone RP11-429A24 on chromosome 10
8. DNA sequence from clone RP1-3J17 on chromosome 6q14.3-16.2
9. Genomic DNA, chromosome 11 clone:CMB9-65A1
10. Isolate I9 mitochondrion
11. Multiple endocrine neoplasia 1, (MEN1)
12. Peroxidasin homolog (Drosophila) (PXDN)
13. Polymerase (RNA) III (DNA directed) polypeptide H (22.9kD) (POLR3H)
14. RAN, member RAS oncogene family (RAN)
15. Ribosomal protein S8 (RPS8)
16. Serine/arginine repetitive matrix 2 (SRRM2)
17. Transmembrane protein 185A (TMEM185A), transcript variant 2
18. Ubiquitin domain containing 2 (UBTD2)
19. Ubiquitin specific peptidase 11 (USP11)
20. Weakly Serine/threonine protein kinase Kp78

Down regulated in the presumptive macula

1. Chromosome 5 clone CTD-2073O6
2. Diazepam binding inhibitor (GABA receptor modulator, acyl-CoA binding protein) (DBI), transcript variant 1
3. Nuclear transport factor 2 pseudogene 2 (NUTF2P2)

Table 6.8. Sequenced genes from differential gene expression profiling.

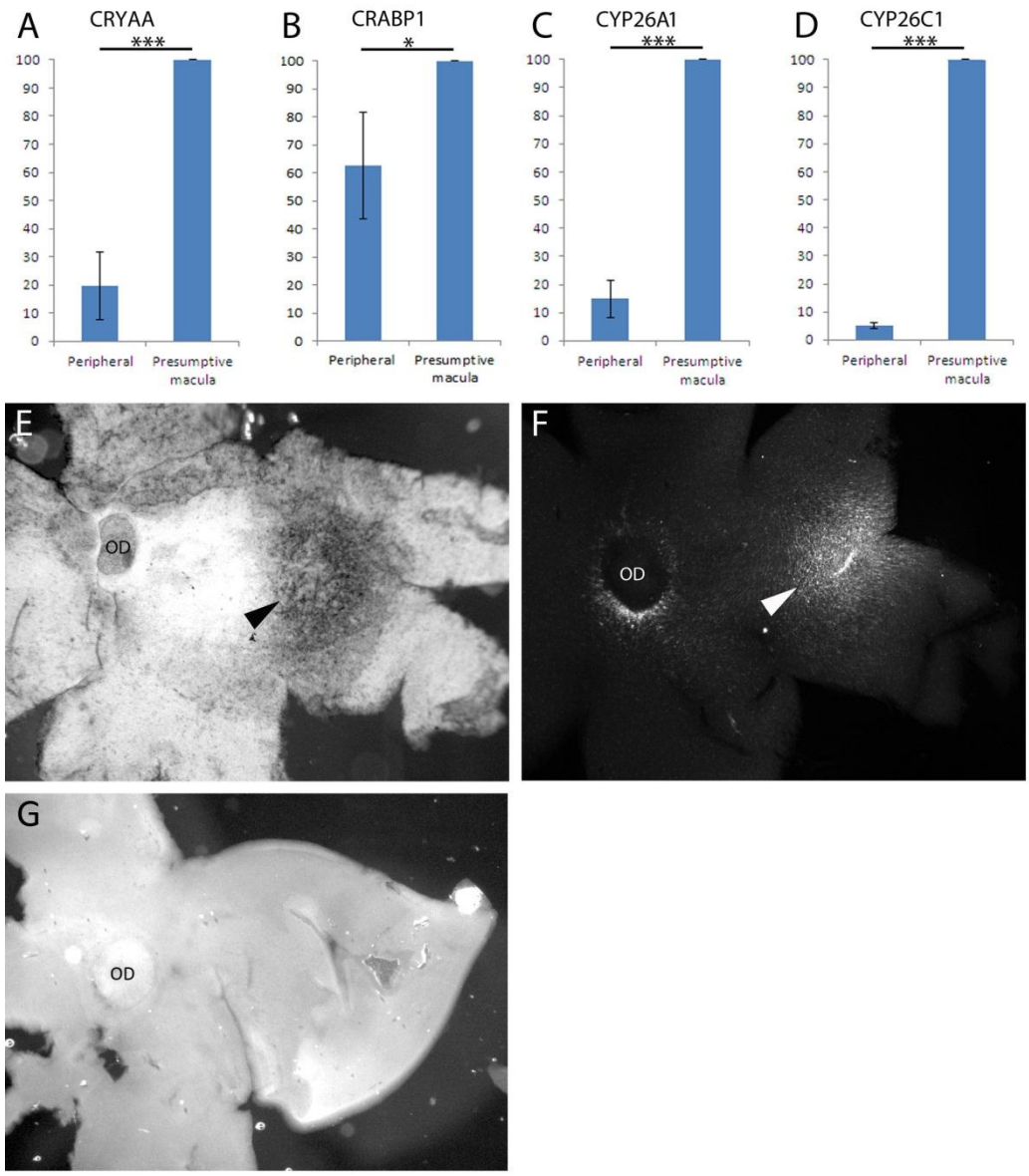

Figure 6.11. CYP26 enzymes are concentrated at the presumptive macula.
qPCR confirmed αA crystallin (CRYAA) expression in dissected retinal samples (**A**). Confirmation of differential gene display, using qPCR and tissue from 5 foetal eyes, CS20, CS21, CS22, CS23 and F1, showed CRABP1 was significantly increased in the presumptive macula (**B**). Other enzymes involved in retinoic acid signalling, CYP26A1 and CYP26C1, were also significantly increased in the presumptive macula (**C** and **D**). *In situ* hybridisation against CYP26A1 revealed a spot in temporal retina of an F1 foetus (arrowhead in **E**), similar in size and location to that of αA crystallin immunohistochemistry in another F1 foetus (arrowhead in **F**), which is not present in a negative control (**G**). * $p<0.05$, ** $p< 0.01$, *** $p< 0.001$, OD; optic disc.

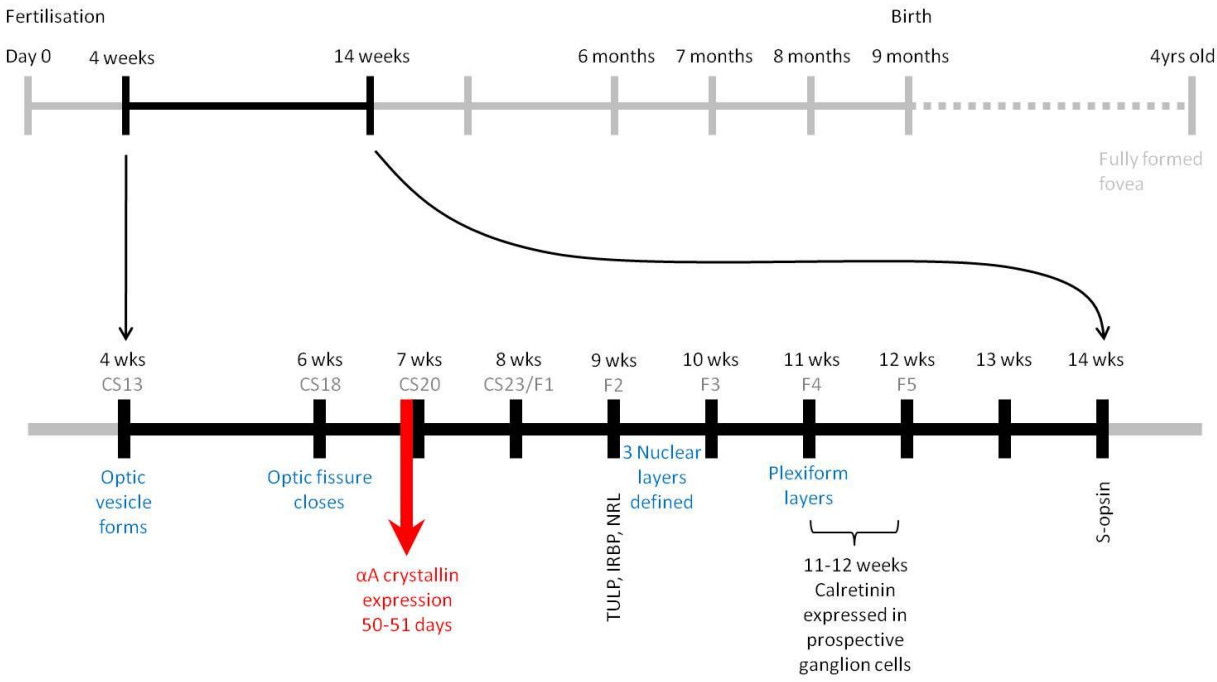

Figure 6.12. Timeline of human macula development, updated.

αA crystallin expression plotted on the timeline of development at 7 weeks gestation (CS20). Blue text indicates morphological landmarks, Black text refers to marker expression and cell differentiation. wks; weeks.

7. Final discussion and Outlook

Discussion

This thesis has shown for the first time that there is a subpopulation of Müller cells at the macula of the human retina (based on biochemical expression patterns). This sub population of Müller cells (GFAP+, LDHB+, αB crystallin+) correlates in size and location with the retinal region affected clinically in MacTel type 2 (the 'MacTel area'). Furthermore, we found in a MacTel type 2 postmortem sample, a loss of Müller cells specifically at the macula. This Müller cell loss in MacTel type 2 correlated with macular pigment loss seen in gross dissection, and this again correlated with the clinically affected 'MacTel area', which is demarcated by the macular pigment loss (chapters 2 and 4). Together, these findings give rise to a conceptionally novel role of Müller glia in retinal disease. In the case of MacTel type 2, we propose the existence of a specific sub population of Müller cells in the macula that is specifically affected by the disease, possibly due to specific metabolic properties or specific susceptibilities to certain insults.

This thesis has also demonstrated that the previously reported micro vascular phenotype in the peripheral retina in MacTel type 2 is not disease specific (chapter 3). Instead we have found that with increasing age human retinae accumulate vacuoles within the basement membrane of the capillaries; vacuoles normally associated with disease in animal models. This poses the question as to whether this feature has any detrimental effect on vision or retinal function. It is possible that these vacuoles might be a contributing factor in retinal pathology with increasing age. More importantly, this work has further confirmed that the vascular pathology MacTel type 2 is limited to the macula, further strengthening the theory of a macula specific Müller cell disease concept.

A macula specific sub population of Müller cells not only has implications with regards to MacTel type 2, but could also have implications for the specificity or susceptibility of other macular diseases. Although a detailed study into the dimensions of the region spared from crystal deposit in canthaxanthin retinopathy has not been undertaken, from observations of published images the region spared is very similar in size and shape to the 'MacTel area'. This sub population of Müller cells might also play a role in the role in other retinal diseases that affect the macula. As mentioned above, it is possible that the metabolism of Müller cells in the macula is different from the peripheral retina. Our proteomic analysis has identified components from several metabolic pathways (chapter 4) and would support such a view.

Furthermore, in this thesis we have identified novel biochemical markers of the macula and fovea (chapters 4 and 5). This will be very useful in further research aimed at uncovering specific disease susceptibilities of the macula.

Lastly, in this thesis we have also advanced our understating about the early embryonic development of the macula in humans and we have taken a first step at elucidating the molecular signalling mechanisms that control macula development, a process which until now has posed elusive.

Outlook

There are three primary questions posed from this thesis that need to be addressed; further characterisation of the MacTel type 2 histology, characterisation of the sub population of Muller cells in the 'MacTel area' and characterisation and mechanisms involved behind retinoic acid and macula development.

1) Further characterization and confirmation of the disease phenotype of MacTel type 2. The donation of another sample with MacTel type 2 is needed for confirmation of the results in chapter 2. A donor program was established 5 years ago by Marcus Fruttiger, recruiting patients from the clinical groups involved in the MacTel project from all over the world. This program has been successful and recently a pair of eyes from a second clinically confirmed MacTel type 2 patient have been donated. Preliminary unpublished results from one of these eyes confirmed the loss of parafoveal Müller cells. Preliminary data also showed a degeneration of the photoreceptors in temporal parafovea, which we aim to correlate with clinical data that was recorded prior to death. Further analysis of this tissue will allow an even greater depth of understanding about the disease and potentially direct us towards the cause.

2) Further characterisation of the sub population of Muller cells within the 'MacTel area' needs to be undertaken and more markers other than GFAP, LDHB and alpha B crystallin need to be established. This can be done by two approaches; firstly, the proteomic data reported in this thesis could still hold more information to address this. Alternatively our collaborators Prof. Mark Gillies and Dr. Alice Len (Save Sight Institute, University of Sydney, Australia), undertook a proteomic screen comparing MacTel type 2 macula versus periphery and control data, including analysis of the vitreous (Len *et al*. manuscript under review). They have found that the Muller cell markers were also downregulated in the MacTel type 2 retina, confirming our findings; furthermore an increase in these proteins

was found in the vitreous, implying protein release from Muller cells in the vitreous upon cell death. A number of other unexpected proteins were identified as up regulated in the vitreous of the MacTel type 2 patient, these have an expression pattern similar to those of Vimentin and CRALBP. As such they can be regarded as potential Muller cell proteins and further investigation into their distribution in the retina needs to be taken. The second approach could be to carry out a comparative genomic screen of the two regions investigated here with proteomics. This can either be conducted using qPCR or full genomic profiling of the regions using array techniques.

3) Now that an early marker of the presumptive macula (CRYAA) has been established, further differentially expressed genes can be identified. Manual dissection of presumptive macula, which relies on a certain amount of guess work, can now be confirmed as accurate using a qPCR against CRYAA. So far this has given a very strong lead into understanding macula development (retinoic acid signalling), however a complete mechanism has yet to be established. The Genefishing^{TM} kit used was based on a 20 primer set, another 5 sets are available commercially. Obviously this method does not provide a complete picture of gene expression such as gene array technology, but as clearly demonstrated in this thesis, the method is a powerful and efficient way to identify differentially expressed genes from extremely small amounts of tissue, which is essential as only small amounts of RNA can be retrieved from the foetal eyes. Comparative gene profiling could also be undertaken, but to have enough material prior mRNA amplification steps would have to be undertaken, which can introduce bias. Again probing of the sample sets could be undertaken against components of the classic morphogenic pathways, such as WNT, NOTCH and SHH. In situ hybridization and immunohistochemistry could then be used to confirm distribution patterns. Temporal relationships between differentially expressed genes would also need to be established to be able to deduce possible functional relationships.
   Characterisation of the CRYAA+ cells also needs to be undertaken, the data presented in this thesis shows that adult Müller cells express CRYAA in the central macula, and that embryonic/foetal CRYAA+ cells express three mature Müller cell markers. CD44 has been proposed to distinguish neuronal progenitor cells from immature Muller cells.[77] Therefore other Müller cell and progenitor cell markers (such as GLAST, NDP, GLUL) could help to further characterise the CRYAA+ cells.
   Working on a primate specific feature, with focus on human tissue, there are limited experimental options available to address function directly. Gene knock-out and transgenic technology, which have been instrumental in mouse developmental biology,

cannot be applied easily. One potential way to determine transcriptional relationships is to expose retinal explants to potential morphogens and use qPCR as a read out of gene expression changes.

In further understanding the pathobiology of MacTel type 2, and the specialisation of the Müller cells in the 'MacTel area' it will hopefully be possible to inform in the future a therapeutic approach to treat MacTel type 2, and other macular diseases. In better understanding the development of the macula and the cells involved in its specialisation, it might also be possible to direct a regenerative stem cell approach, whereby specialised photoreceptors or Müller cells can be generated and transplanted into the macula, hopefully regenerating central, high acuity vision.

8. Supplementary data

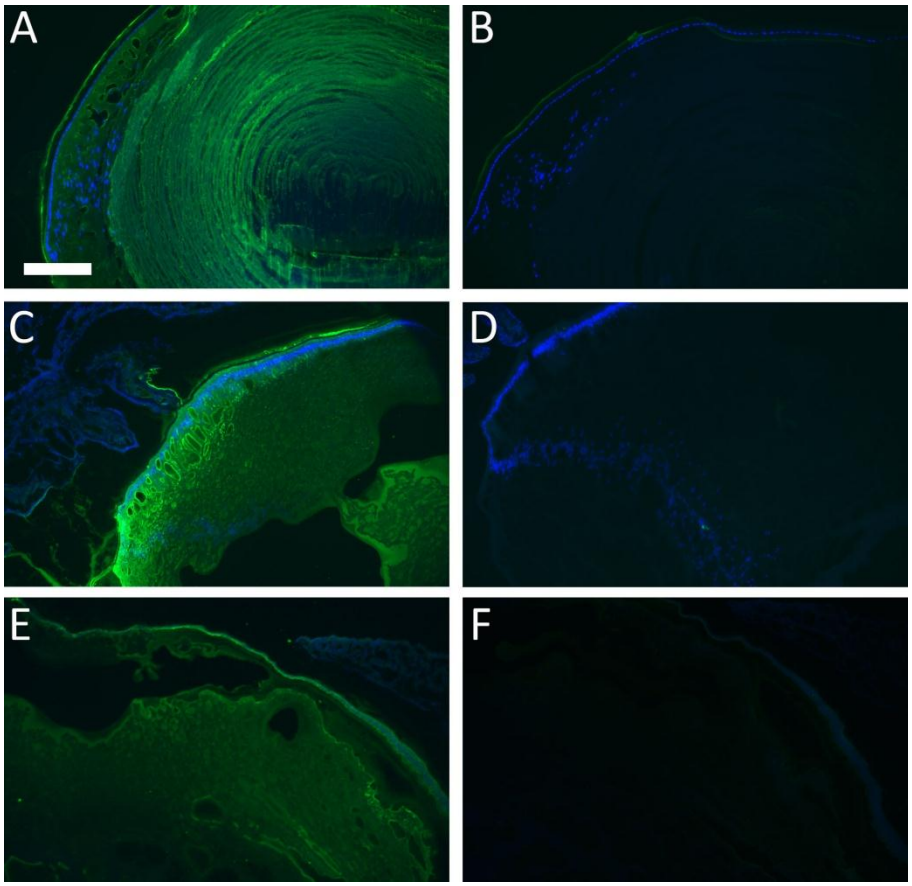

Supplementary Figure 1. αA crystallin expression in lens tissue.

αA crystallin immunoreactivity (green) of the lens of a C57BL6 mouse acts as a positive control for the antibody (**A**), compared to the autoflourescence of the negative control (no primary antibody) for mouse lens tissue (**B**). αA crystallin expression in the lens from a duck (**C**) and negative control (**D**), and also from the lens tissue from a chick (**E**) compared to the negative control (**F**) confirm specificty in avian tissue. Data from the Santa Cruz antibody is displayed above, however both αA crystallin antibodies colocalised with each other. Scale bar is equal to 100µm.

Supplementary Table 1: Embryonic and foetal staging criteria.

Embryo staging				
Carnegie stage (CS)	***Somite stage***	***Crown rump length (mm)***	***Embryonic age***	***Morphological land marks***
CS 1		0.1-0.15 (diameter)	**1 day**	Fertilisation, Unicellular
CS 2		0.1-0.2 (diameter)	**1.5-3 days**	More than 1 cell but no blastocystic cavity.
CS 3		0.1-0.2 (diameter)	**4 days**	Free blastocyst
CS 4		0.1-0.2 (diameter)	**5-6 days**	Attaching blastocyst
CS 5		0.1-0.2 (diameter)	**7-12 days**	Implanted but previllious
CS 6		0.2 mm (diameter)	**13 days**	Chorionic villi: primitive streak may appear
CS 7		0.4 mm (length)	**16 days**	Notochordal process
CS 8		1.0-1.5 (length)	**18 days**	Presomitic, primitive pit; notochordal canal; neural folds may appear.
CS 9	1-3 somites	1.5-2.5 (length)	**20 days**	Somites appear. Head fold present
CS 10	4-12 somites	1.5-3.0 (length)	**22 days**	Fusion of neural folds is imminent or in progress. Otic sulcus may have appeared. Pharyngeal arch 1 begins to be visible.
CS 11	13-21 somites	2.5-4.5 (length)	**24 days**	Rostral neuropore is in the process of closing. Otic invagination is shallow or still widely open. Pharyngeal arches 1 and 2 are evident.
CS 12	21-29 somites	3-5 (length)	**26 days**	Three pharyngeal arches are visible; the dorsal curvature of the body is becoming filled out into a smooth convexity; Caudal neuropore is closing or closed: the otic vesicles are almost closed but not detached; the upper limb buds are appearing, centred around a condensation opposite somites 8-18. After stage 12 the number of pairs of somites becomes increasingly difficult to determine and so is no longer used in staging.
CS 13	30+ somites	4-6 (length)	**28 days (4 weeks)**	All four limb buds are usually visible; otic vesicle is closed; the lens disc is generally not yet indented
CS 14		5-7 (length)	**32 days (4 weeks plus)**	Invagination of the lens disc but with an open lens pit; a well defined endolymphatic appendage; elongated and tapering upper limb buds. In some specimens the marginal vessel can be recognised in the upper limb bud.

CS 15		7-9 (length)	**33 days (4 weeks plus)**	Lens vesicles are closed; nasal pits are appearing; hand plates are forming. Embryos appear wider than the previous stage due to growth of spinal ganglia, muscular plates and mesenchyme tissue in the trunk.
CS 16		11-14 (length)	**37 days (5 weeks plus)**	The nasal pits are coming to face ventrally and to disappear from the profile view; retinal pigment is becoming visible externally; pharyngeal arch 2 is more massive and more conspicuous whereas arch 3 is receding from the surface; auricular hillocks are beginning to appear. Somites can be seen distinctly in the caudal part of the trunk. The marginal vein is distinct in the lower limb bud.
CS 17		11-14 (length)	**41days (5 weeks plus)**	The head is relatively larger than previously; the main axis of the trunk has become straighter and a slight indication of a lumbar curvature may be found; the nasal pit is further medial and is directed ventrally so that the nostril is not visible in profile views and nasofrontal grooves are distinct; the full complement of auricular hillocks is present on the mandibular and hyoid arches; the hand plate exhibits definite digital rays and the foot has acquired a rounded digital plate; surface elevations of individual somites are becoming limited mostly to the lumbosacral region.
CS 18		13-17 (length)	**44 days (6 weeks plus)**	The body is more of a unified cuboidal mass and both cervical and lumbar flexures are indicated; the limbs are longer, the digital plate of the hand is definitely notched, the elbow region is usually discernible. The hand plate develops crenations at the rim caused by the projecting tips of the individual digits. Toe rays can be identified in some specimens; eyelid folds are present in the more advanced embryos; a distinct tip of the nose can be seen in profile; auricular hillocks are being transformed into specific parts of the external ear.
CS 19		17-20 (length)	**47-48 days (6 weeks plus)**	The trunk has begun to elongate and straighten slightly; with the result that the head no longer forms a right angle with the line of the back of the embryo. The limbs extend nearly directly forward. The toe rays are more prominent but interdigital notches have not yet appeared in the rim of the foot plate.

CS 20		21-23	**50-51 days (7 weeks plus)**	Details of internal structures may now be obscured from surface view because of the thickening mesoderm. Thus the cerebellum is no longer distinct as seen from the surface. The upper limbs have increased in length and become slightly bent at the elbow. The hands with their short stubby fingers are still far apart but they are curving slightly over the cardiac region and approach the lateral margins of the nose. A delicate fringe-like vascular plexus now appears in the superficial tissues of the head. In the temporofrontal region a growth centre arches over the eye and in the occipital region a second growth centre occurs above the ear. The edge of the plexus is approximately halfway between the eye-ear level and the vertex of the head
CS 21		22-24	**52 days (7 weeks plus)**	The superficial vascular plexus of the head has spread upward to form a line at somewhat more than half the distance from the eye-ear level to the vertex. The fingers are longer and extend further beyond the ventral body wall than they did in the previous stage. The distal phalangeal portions appear slightly swollen and show the beginning of tactile pads. The hands are slightly flexed at the wrists and nearly come together over the cardiac eminence. The feet are also approaching each other and the toes of the two sides sometimes touch.
CS 22		25-27	**54 days (7 weeks plus)**	The eyelids which have been thickening gradually are now rapidly encroaching upon the eyes. The formation of the auricle has progressed noticeably the tragus and antitragus especially are assuming a more definite form. The superficial vascular plexus of the head extends upwards and three-quarters of the way above the eye-ear level. The hands extend further out in front of the body of the embryo and the fingers of one hand may overlap those of the other.

CS 23		Full range 23-30 but most measure 28-30	**56-57 days (8 weeks plus)**	The head has made rapid progress in its bending towards the erect position. The head is distinctly rounded out, and the cervical region and trunk are of a more mature shape. The eyelids may show some fusion laterally and medially but the eyes may be largely open. The limbs have increased markedly in length and show more-advanced differentiation of their subdivisions. The forearm ascends to or above the level of the shoulder. The superficial vascular plexus is rapidly approaching the vertex of the head leaving only a small non vascular area that will soon become bridged by anastomosing branches. The external genitalia are well developed but do not suffice for the detection of sex. Only in foetuses of about 50mm is it safe to make an assessment of sex. Head more rounded and shows human characteristics. External genitalia still have sexless appearance. Distinct bulge still present in umbilical cord caused by herniation of intestines. Tail has disappeared. "Praying feet" may be visible. Foot length less than 5mm, Crown rump length less than 40mm

Foetal staging

Foetal Stage (F)	***Foot length (mm)***	***Knee-heel length (mm)***	***Crown rump length (mm)***	***Foetal age***	***Morphological land marks***
F1	Above 5 to 6	8	41-50	**>56.5 weeks**	
F2	Above 6 to 8	11	51-60	**9 weeks**	Head is almost half of the foetus. As the head extends and the chin is raised from the thorax the neck develops. The eyelids have fused. The fingernails appear.
F3	Above 8 to 9	13	61-70	**10 weeks**	Midgut herniation returns to the enlarged abdomen.
F4	Above 9 to 12	17	70-85	**11weeks**	
F5	Above 12 to 16	24	86-98	**12 weeks**	Sex distinguishable externally. Well defined neck. The ear has moved from the neck on to the head. The eyes have moved to the front of the face. Toe nails develop

Supplementary table 1. Embryonic and foetal staging criteria. Staging carried out at the London HDBR facility at the UCL Institute of Child Health, UK.

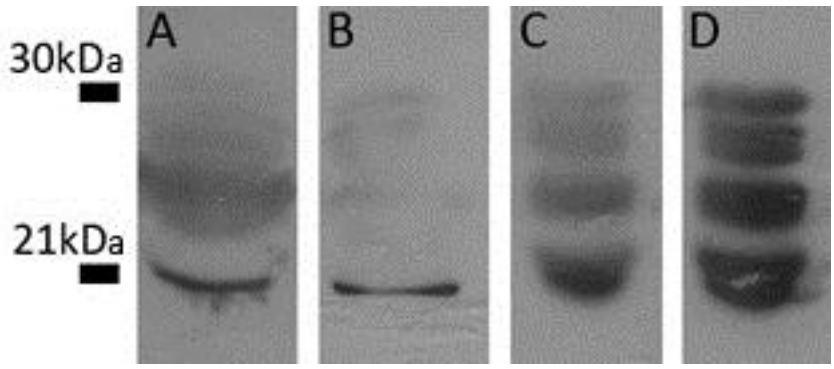

Supplementary Figure 2. αA crystallin western blots.

Western blots can be used to check antibody specificity, by confirming that the product has the expected molecular weight. αA crystallin has a molecular weight of ~19.9KDa. Foetal human whole retina tissue was probed using both αA crystallin antibodies, Santa Cruz (**A**) and Abcam (**B**). Both antibodies gave the same pattern on the gel and a band was present at the expected weight for αA crystallin. Adult human macula tissue was also probed using both αA crystallin antibodies (Santa Cruz, **C** and Abcam, **D**). The same banding pattern as with foetal tissue was seen, with the addition of a band at around 21kDa.

9. References

1. Provis JM, Diaz CM, Dreher B. Ontogeny of the primate fovea: a central issue in retinal development. Prog Neurobiol 1998;54(5):549-580.

2. Curcio CA, Sloan KR, Kalina RE, Hendrickson AE. Human photoreceptor topography. J Comp Neurol 1990;292(4):497-523.

3. Curcio CA, Allen KA, Sloan KR et al. Distribution and morphology of human cone photoreceptors stained with anti-blue opsin. J Comp Neurol 1991;312(4):610-624.

4. Bumsted K, Hendrickson A. Distribution and development of short-wavelength cones differ between Macaca monkey and human fovea. J Comp Neurol 1999;403(4):502-516.

5. Bone RA, Sparrock JM. Comparison of macular pigment densities in human eyes. Vision Res 1971;11(10):1057-1064.

6. Bone RA, Landrum JT, Tarsis SL. Preliminary identification of the human macular pigment. Vision Res 1985;25(11):1531-1535.

7. Johnson EJ, Hammond BR, Yeum KJ et al. Relation among serum and tissue concentrations of lutein and zeaxanthin and macular pigment density. Am J Clin Nutr 2000;71(6):1555-1562.

8. Malinow MR, Feeney-Burns L, Peterson LH, Klein ML, Neuringer M. Diet-related macular anomalies in monkeys. Invest Ophthalmol Vis Sci 1980;19(8):857-863.

9. Polyak SL. The Retina. Chicago: University Chicago Press; 1941.

10. Curcio CA, Allen KA. Topography of ganglion cells in human retina. J Comp Neurol 1990;300(1):5-25.

11. Provis JM, Hendrickson AE. The foveal avascular region of developing human retina. Arch Ophthalmol 2008;126(4):507-511.

12. Hageman GS, Gehrs K, Johnson LV, Anderson D. Age-Related Macular Degeneration (AMD). 1995.

13. Kolb H, Nelson R, Ahnelt P, Cuenca N. Cellular organization of the vertebrate retina. Prog Brain Res 2001;131:3-26.

14. Lamb TD, Pugh EN, Jr. Dark adaptation and the retinoid cycle of vision. Prog Retin Eye Res 2004;23(3):307-380.

15. Yau KW, Hardie RC. Phototransduction motifs and variations. Cell 2009;139(2):246-264.

16. Reichenbach A, Stolzenburg JU, Eberhardt W, Chao TI, Dettmer D, Hertz L. What do retinal muller (glial) cells do for their neuronal 'small siblings'? J Chem Neuroanat 1993;6(4):201-213.

17. Newman E, Reichenbach A. The Muller cell: a functional element of the retina. Trends Neurosci 1996;19(8):307-312.

18. Willbold E, Berger J, Reinicke M, Wolburg H. On the role of Muller glia cells in histogenesis: only retinal spheroids, but not tectal, telencephalic and cerebellar spheroids develop histotypical patterns. J Hirnforsch 1997;38(3):383-396.

19. Brew H, Gray PT, Mobbs P, Attwell D. Endfeet of retinal glial cells have higher densities of ion channels that mediate K+ buffering. Nature 1986;324(6096):466-468.

20. Nilius B, Reichenbach A. Efficient K+ buffering by mammalian retinal glial cells is due to cooperation of specialized ion channels. Pflugers Arch 1988;411(6):654-660.

21. Newman EA. Inward-rectifying potassium channels in retinal glial (Muller) cells. J Neurosci 1993;13(8):3333-3345.

22. Ishii M, Horio Y, Tada Y et al. Expression and clustered distribution of an inwardly rectifying potassium channel, KAB-2/Kir4.1, on mammalian retinal Muller cell membrane: their regulation by insulin and laminin signals. J Neurosci 1997;17(20):7725-7735.

23. Skatchkov SN, Eaton MJ, Shuba YM et al. Tandem-pore domain potassium channels are functionally expressed in retinal (Muller) glial cells. Glia 2006;53(3):266-276.

24. Kofuji P, Ceelen P, Zahs KR, Surbeck LW, Lester HA, Newman EA. Genetic inactivation of an inwardly rectifying potassium channel (Kir4.1 subunit) in mice: phenotypic impact in retina. J Neurosci 2000;20(15):5733-5740.

25. Newman EA, Frambach DA, Odette LL. Control of extracellular potassium levels by retinal glial cell K+ siphoning. Science 1984;225(4667):1174-1175.

26. Karwoski CJ, Lu HK, Newman EA. Spatial buffering of light-evoked potassium increases by retinal Muller (glial) cells. Science 1989;244(4904):578-580.

27. Reichenbach A, Henke A, Eberhardt W, Reichelt W, Dettmer D. K+ ion regulation in retina. Can J Physiol Pharmacol 1992;70 Suppl:S239-S247.

28. Newman EA. Voltage-dependent calcium and potassium channels in retinal glial cells. Nature 1985;317(6040):809-811.

29. Chao TI, Skachkov SN, Eberhardt W, Reichenbach A. Na+ channels of Muller (glial) cells isolated from retinae of various mammalian species including man. Glia 1994;10(3):173-185.

30. Bringmann A, Schopf S, Faude F, Skatchkov SN, Enzmann V, Reichenbach A. The activity of a transient potassium current in retinal glial (Muller) cells depends on extracellular calcium. J Hirnforsch 1999;39(4):539-550.

31. Francke M, Pannicke T, Biedermann B et al. Loss of inwardly rectifying potassium currents by human retinal glial cells in diseases of the eye. Glia 1997;20(3):210-218.

32. Bringmann A, Reichenbach A, Wiedemann P. Pathomechanisms of cystoid macular edema. Ophthalmic Res 2004;36(5):241-249.

33. Frigeri A, Gropper MA, Turck CW, Verkman AS. Immunolocalization of the mercurial-insensitive water channel and glycerol intrinsic protein in epithelial cell plasma membranes. Proc Natl Acad Sci U S A 1995;92(10):4328-4331.

34. Patil RV, Saito I, Yang X, Wax MB. Expression of aquaporins in the rat ocular tissue. Exp Eye Res 1997;64(2):203-209.

35. Nagelhus EA, Veruki ML, Torp R et al. Aquaporin-4 water channel protein in the rat retina and optic nerve: polarized expression in Muller cells and fibrous astrocytes. J Neurosci 1998;18(7):2506-2519.

36. Poitry S, Poitry-Yamate C, Ueberfeld J, MacLeish PR, Tsacopoulos M. Mechanisms of glutamate metabolic signaling in retinal glial (Muller) cells. J Neurosci 2000;20(5):1809-1821.

37. Otori Y, Shimada S, Tanaka K, Ishimoto I, Tano Y, Tohyama M. Marked increase in glutamate-aspartate transporter (GLAST/GluT-1) mRNA following transient retinal ischemia. Brain Res Mol Brain Res 1994;27(2):310-314.

38. Derouiche A, Rauen T. Coincidence of L-glutamate/L-aspartate transporter (GLAST) and glutamine synthetase (GS) immunoreactions in retinal glia: evidence for coupling of GLAST and GS in transmitter clearance. J Neurosci Res 1995;42(1):131-143.

39. Barnett NL, Pow DV. Antisense knockdown of GLAST, a glial glutamate transporter, compromises retinal function. Invest Ophthalmol Vis Sci 2000;41(2):585-591.

40. Matsui K, Hosoi N, Tachibana M. Active role of glutamate uptake in the synaptic transmission from retinal nonspiking neurons. J Neurosci 1999;19(16):6755-6766.

41. Linser P, Moscona AA. Induction of glutamine synthetase in embryonic neural retina: localization in Muller fibers and dependence on cell interactions. Proc Natl Acad Sci U S A 1979;76(12):6476-6480.

42. Li Q, Puro DG. Diabetes-induced dysfunction of the glutamate transporter in retinal Muller cells. Invest Ophthalmol Vis Sci 2002;43(9):3109-3116.

43. Lieth E, LaNoue KF, Antonetti DA, Ratz M. Diabetes reduces glutamate oxidation and glutamine synthesis in the retina. The Penn State Retina Research Group. Exp Eye Res 2000;70(6):723-730.

44. Garcia M, Vecino E. Role of Muller glia in neuroprotection and regeneration in the retina. Histol Histopathol 2003;18(4):1205-1218.

45. Egensperger R, Maslim J, Bisti S, Hollander H, Stone J. Fate of DNA from retinal cells dying during development: uptake by microglia and macroglia (Muller cells). Brain Res Dev Brain Res 1996;97(1):1-8.

46. Burke JM, Foster SJ. Culture of adult rabbit retinal glial cells: methods and cellular origin of explant outgrowth. Curr Eye Res 1984;3(10):1169-1178.

47. Crafoord S, Dafgard KE, Seregard S, Algvere PV. Cellular migration into neural retina following implantation of melanin granules in the subretinal space. Graefes Arch Clin Exp Ophthalmol 2000;238(8):682-689.

48. Risau W. Induction of blood-brain barrier endothelial cell differentiation. Ann N Y Acad Sci 1991;633:405-419.

49. Janzer RC, Raff MC. Astrocytes induce blood-brain barrier properties in endothelial cells. Nature 1987;325(6101):253-257.

50. Laterra J, Guerin C, Goldstein GW. Astrocytes induce neural microvascular endothelial cells to form capillary-like structures in vitro. J Cell Physiol 1990;144(2):204-215.

51. Tout S, Chan-Ling T, Hollander H, Stone J. The role of Muller cells in the formation of the blood-retinal barrier. Neuroscience 1993;55(1):291-301.

52. Sahel JA, Albert DM, Lessell S. [Proliferation of retinal glia and excitatory amino acids]. Ophtalmologie 1990;4(1):13-16.

53. Rutka JT, Smith SL. Transfection of human astrocytoma cells with glial fibrillary acidic protein complementary DNA: analysis of expression, proliferation, and tumorigenicity. Cancer Res 1993;53(15):3624-3631.

54. Bringmann A, Reichenbach A. Role of Muller cells in retinal degenerations. Front Biosci 2001;6:E72-E92.

55. Bringmann A, Pannicke T, Grosche J et al. Muller cells in the healthy and diseased retina. Prog Retin Eye Res 2006;25(4):397-424.

56. Reichenbach A, Wurm A, Pannicke T, Iandiev I, Wiedemann P, Bringmann A. Muller cells as players in retinal degeneration and edema. Graefes Arch Clin Exp Ophthalmol 2007;245(5):627-636.

57. Guidry C, Bradley KM, King JL. Tractional force generation by human muller cells: growth factor responsiveness and integrin receptor involvement. Invest Ophthalmol Vis Sci 2003;44(3):1355-1363.

58. Fischer AJ, Reh TA. Muller glia are a potential source of neural regeneration in the postnatal chicken retina. Nat Neurosci 2001;4(3):247-252.

59. Bringmann A, Wiedemann P. Involvement of Muller glial cells in epiretinal membrane formation. Graefes Arch Clin Exp Ophthalmol 2009;247(7):865-883.

60. Sueishi K, Hata Y, Murata T, Nakagawa K, Ishibashi T, Inomata H. Endothelial and glial cell interaction in diabetic retinopathy via the function of vascular endothelial growth factor (VEGF). Pol J Pharmacol 1996;48(3):307-316.

61. Amin RH, Frank RN, Kennedy A, Eliott D, Puklin JE, Abrams GW. Vascular endothelial growth factor is present in glial cells of the retina and optic nerve of human subjects with nonproliferative diabetic retinopathy. Invest Ophthalmol Vis Sci 1997;38(1):36-47.

62. Reichenbach A, Faude F, Enzmann V et al. The Muller (glial) cell in normal and diseased retina: a case for single-cell electrophysiology. Ophthalmic Res 1997;29(5):326-340.

63. Korte GE, Hageman GS, Pratt DV, Glusman S, Marko M, Ophir A. Changes in Muller cell plasma membrane specializations during subretinal scar formation in the rabbit. Exp Eye Res 1992;55(1):155-162.

64. Crabb JW, Johnson CM, Carr SA, Armes LG, Saari JC. The complete primary structure of the cellular retinaldehyde-binding protein from bovine retina. J Biol Chem 1988;263(35):18678-18687.

65. Bridges CD. Vitamin A and the role of the pigment epithelium during bleaching and regeneration of rhodopsin in the frog eye. Exp Eye Res 1976;22(5):435-455.

66. Bunt-Milam AH, Saari JC. Immunocytochemical localization of two retinoid-binding proteins in vertebrate retina. J Cell Biol 1983;97(3):703-712.

67. Linser PJ, Moscona AA. Induction of glutamine synthetase in embryonic neural retina: its suppression by the gliatoxic agent alpha-aminoadipic acid. Brain Res 1981;227(1):103-119.

68. Sakamoto T, Ueno H, Goto Y, Oshima Y, Ishibashi T, Inomata H. A vitrectomy improves the transfection efficiency of adenoviral vector-mediated gene transfer to Muller cells. Gene Ther 1998;5(8):1088-1097.

69. Lewis GP, Fisher SK. Up-regulation of glial fibrillary acidic protein in response to retinal injury: its potential role in glial remodeling and a comparison to vimentin expression. Int Rev Cytol 2003;230:263-290.

70. Humphrey MF, Chu Y, Mann K, Rakoczy P. Retinal GFAP and bFGF expression after multiple argon laser photocoagulation injuries assessed by both immunoreactivity and mRNA levels. Exp Eye Res 1997;64(3):361-369.

71. Humphrey MF, Constable IJ, Chu Y, Wiffen S. A quantitative study of the lateral spread of Muller cell responses to retinal lesions in the rabbit. J Comp Neurol 1993;334(4):545-558.

72. Wu KH, Madigan MC, Billson FA, Penfold PL. Differential expression of GFAP in early v late AMD: a quantitative analysis. Br J Ophthalmol 2003;87(9):1159-1166.

73. Madigan MC, Penfold PL, Provis JM, Balind TK, Billson FA. Intermediate filament expression in human retinal macroglia. Histopathologic changes associated with age-related macular degeneration. Retina 1994;14(1):65-74.

74. Ponta H, Sherman L, Herrlich PA. CD44: from adhesion molecules to signalling regulators. Nat Rev Mol Cell Biol 2003;4(1):33-45.

75. Chaitin MH, Wortham HS, Brun-Zinkernagel AM. Immunocytochemical localization of CD44 in the mouse retina. Exp Eye Res 1994;58(3):359-365.

76. Chaitin MH, Brun-Zinkernagel AM. Immunolocalization of CD44 in the dystrophic rat retina. Exp Eye Res 1998;67(3):283-292.

77. Shinoe T, Kuribayashi H, Saya H, Seiki M, Aburatani H, Watanabe S. Identification of CD44 as a cell surface marker for Muller glia precursor cells. J Neurochem 2010;115(6):1633-1642.

78. Chu Y, Hughes S, Chan-Ling T. Differentiation and migration of astrocyte precursor cells and astrocytes in human fetal retina: relevance to optic nerve coloboma. FASEB J 2001;15(11):2013-2015.

79. Mi H, Barres BA. Purification and characterization of astrocyte precursor cells in the developing rat optic nerve. J Neurosci 1999;19(3):1049-1061.

80. Mudhar HS, Pollock RA, Wang C, Stiles CD, Richardson WD. PDGF and its receptors in the developing rodent retina and optic nerve. Development 1993;118(2):539-552.

81. Fruttiger M, Calver AR, Richardson WD. Platelet-derived growth factor is constitutively secreted from neuronal cell bodies but not from axons. Curr Biol 2000;10(20):1283-1286.

82. Fruttiger M. Development of the mouse retinal vasculature: angiogenesis versus vasculogenesis. Invest Ophthalmol Vis Sci 2002;43(2):522-527.

83. Fruttiger M, Calver AR, Kruger WH et al. PDGF mediates a neuron-astrocyte interaction in the developing retina. Neuron 1996;17(6):1117-1131.

84. Ling TL, Stone J. The development of astrocytes in the cat retina: evidence of migration from the optic nerve. Brain Res Dev Brain Res 1988;44(1):73-85.

85. Stone J, Dreher Z. Relationship between astrocytes, ganglion cells and vasculature of the retina. J Comp Neurol 1987;255(1):35-49.

86. Schnitzer J. Retinal astrocytes: their restriction to vascularized parts of the mammalian retina. Neurosci Lett 1987;78(1):29-34.

87. Huxlin KR, Sefton AJ, Furby JH. The origin and development of retinal astrocytes in the mouse. J Neurocytol 1992;21(7):530-544.

88. Fruttiger M. Development of the retinal vasculature. Angiogenesis 2007;10(2):77-88.

89. Pierce EA, Foley ED, Smith LE. Regulation of vascular endothelial growth factor by oxygen in a model of retinopathy of prematurity. Arch Ophthalmol 1996;114(10):1219-1228.

90. West H, Richardson WD, Fruttiger M. Stabilization of the retinal vascular network by reciprocal feedback between blood vessels and astrocytes. Development 2005;132(8):1855-1862.

91. Provis JM, Leech J, Diaz CM, Penfold PL, Stone J, Keshet E. Development of the human retinal vasculature: cellular relations and VEGF expression. Exp Eye Res 1997;65(4):555-568.

92. Stone J, Itin A, Alon T et al. Development of retinal vasculature is mediated by hypoxia-induced vascular endothelial growth factor (VEGF) expression by neuroglia. J Neurosci 1995;15(7 Pt 1):4738-4747.

93. Hollander H, Makarov F, Dreher Z, van DD, Chan-Ling TL, Stone J. Structure of the macroglia of the retina: sharing and division of labour between astrocytes and Muller cells. J Comp Neurol 1991;313(4):587-603.

94. Dreher Z, Wegner M, Stone J. Muller cell endfeet at the inner surface of the retina: light microscopy. Vis Neurosci 1988;1(2):169-180.

95. Ogden TE. Nerve fiber layer astrocytes of the primate retina: morphology, distribution, and density. Invest Ophthalmol Vis Sci 1978;17(6):499-510.

96. Olsen ML, Sontheimer H. Functional implications for Kir4.1 channels in glial biology: from K+ buffering to cell differentiation. J Neurochem 2008;107(3):589-601.

97. Penfold PL, Madigan MC, Provis JM. Antibodies to human leucocyte antigens indicate subpopulations of microglia in human retina. Vis Neurosci 1991;7(4):383-388.

98. Provis JM, Penfold PL, Edwards AJ, van DD. Human retinal microglia: expression of immune markers and relationship to the glia limitans. Glia 1995;14(4):243-256.

99. Schmidt SY, Peisch RD. Melanin concentration in normal human retinal pigment epithelium. Regional variation and age-related reduction. Invest Ophthalmol Vis Sci 1986;27(7):1063-1067.

100. Weiter JJ, Delori FC, Wing GL, Fitch KA. Retinal pigment epithelial lipofuscin and melanin and choroidal melanin in human eyes. Invest Ophthalmol Vis Sci 1986;27(2):145-152.

101. Nguyen-Legros J, Hicks D. Renewal of photoreceptor outer segments and their phagocytosis by the retinal pigment epithelium. Int Rev Cytol 2000;196:245-313.

102. Young RW. Shedding of discs from rod outer segments in the rhesus monkey. J Ultrastruct Res 1971;34(1):190-203.

103. Thompson DA, Gal A. Vitamin A metabolism in the retinal pigment epithelium: genes, mutations, and diseases. Prog Retin Eye Res 2003;22(5):683-703.

104. Sandercoe TM, Madigan MC, Billson FA, Penfold PL, Provis JM. Astrocyte proliferation during development of the human retinal vasculature. Exp Eye Res 1999;69(5):511-523.

105. Hughes S, Yang H, Chan-Ling T. Vascularization of the human fetal retina: roles of vasculogenesis and angiogenesis. Invest Ophthalmol Vis Sci 2000;41(5):1217-1228.

106. Gariano RF, Iruela-Arispe ML, Hendrickson AE. Vascular development in primate retina: comparison of laminar plexus formation in monkey and human. Invest Ophthalmol Vis Sci 1994;35(9):3442-3455.

107. Ashton N. Oxygen and the growth and development of retinal vessels. In vivo and in vitro studies. The XX Francis 1. Proctor Lecture. Am J Ophthalmol 1966;62:412-435.

108. Ashton N. Retinal angiogenesis in the human embryo. Br Med Bull 1970;26(2):103-106.

109. Hughes S, Chang-Ling T. Roles of endothelial cell migration and apoptosis in vascular remodeling during development of the central nervous system. Microcirculation 2000;7(5):317-333.

110. Provis JM, Sandercoe T, Hendrickson AE. Astrocytes and blood vessels define the foveal rim during primate retinal development. Invest Ophthalmol Vis Sci 2000;41(10):2827-2836.

111. Risau W. Mechanisms of angiogenesis. Nature 1997;386(6626):671-674.

112. Chan-Ling T, McLeod DS, Hughes S et al. Astrocyte-endothelial cell relationships during human retinal vascular development. Invest Ophthalmol Vis Sci 2004;45(6):2020-2032.

113. Chan-Ling TL, Halasz P, Stone J. Development of retinal vasculature in the cat: processes and mechanisms. Curr Eye Res 1990;9(5):459-478.

114. Flower RW, McLeod DS, Lutty GA, Goldberg B, Wajer SD. Postnatal retinal vascular development of the puppy. Invest Ophthalmol Vis Sci 1985;26(7):957-968.

115. Gariano RF. Cellular mechanisms in retinal vascular development. Prog Retin Eye Res 2003;22(3):295-306.

116. Urbich C, Dimmeler S. Endothelial progenitor cells: characterization and role in vascular biology. Circ Res 2004;95(4):343-353.

117. Rehman J, Li J, Orschell CM, March KL. Peripheral blood "endothelial progenitor cells" are derived from monocyte/macrophages and secrete angiogenic growth factors. Circulation 2003;107(8):1164-1169.

118. Yamashita J, Itoh H, Hirashima M et al. Flk1-positive cells derived from embryonic stem cells serve as vascular progenitors. Nature 2000;408(6808):92-96.

119. Shalaby F, Rossant J, Yamaguchi TP et al. Failure of blood-island formation and vasculogenesis in Flk-1-deficient mice. Nature 1995;376(6535):62-66.

120. Dumont DJ, Fong GH, Puri MC, Gradwohl G, Alitalo K, Breitman ML. Vascularization of the mouse embryo: a study of flk-1, tek, tie, and vascular endothelial growth factor expression during development. Dev Dyn 1995;203(1):80-92.

121. Ruhrberg C, Gerhardt H, Golding M et al. Spatially restricted patterning cues provided by heparin-binding VEGF-A control blood vessel branching morphogenesis. Genes Dev 2002;16(20):2684-2698.

122. Marin-Padilla M. Early vascularization of the embryonic cerebral cortex: Golgi and electron microscopic studies. J Comp Neurol 1985;241(2):237-249.

123. Kurz H, Gartner T, Eggli PS, Christ B. First blood vessels in the avian neural tube are formed by a combination of dorsal angioblast immigration and ventral sprouting of endothelial cells. Dev Biol 1996;173(1):133-147.

124. Eichmann A, le Noble F, Autiero M, Carmeliet P. Guidance of vascular and neural network formation. Curr Opin Neurobiol 2005;15(1):108-115.

125. Gerhardt H, Golding M, Fruttiger M et al. VEGF guides angiogenic sprouting utilizing endothelial tip cell filopodia. J Cell Biol 2003;161(6):1163-1177.

126. Claxton S, Fruttiger M. Periodic Delta-like 4 expression in developing retinal arteries. Gene Expr Patterns 2004;5(1):123-127.

127. Saint-Geniez M, Masri B, Malecaze F, Knibiehler B, Audigier Y. Expression of the murine msr/apj receptor and its ligand apelin is upregulated during formation of the retinal vessels. Mech Dev 2002;110(1-2):183-186.

128. Lu X, le Noble F, Yuan L et al. The netrin receptor UNC5B mediates guidance events controlling morphogenesis of the vascular system. Nature 2004;432(7014):179-186.

129. Yu DY, Cringle SJ. Oxygen distribution and consumption within the retina in vascularised and avascular retinas and in animal models of retinal disease. Prog Retin Eye Res 2001;20(2):175-208.

130. Linsenmeier RA. Effects of light and darkness on oxygen distribution and consumption in the cat retina. J Gen Physiol 1986;88(4):521-542.

131. Abbott NJ, Ronnback L, Hansson E. Astrocyte-endothelial interactions at the blood-brain barrier. Nat Rev Neurosci 2006;7(1):41-53.

132. Marshall GE, Konstas AG, Lee WR. Ultrastructural distribution of collagen types I-VI in aging human retinal vessels. Br J Ophthalmol 1990;74(4):228-232.

133. Hawkins RA, O'Kane RL, Simpson IA, Vina JR. Structure of the blood-brain barrier and its role in the transport of amino acids. J Nutr 2006;136(1 Suppl):218S-226S.

134. Tornquist P, Alm A, Bill A. Permeability of ocular vessels and transport across the blood-retinal-barrier. Eye (Lond) 1990;4 (Pt 2):303-309.

135. Klein R, Blodi BA, Meuer SM, Myers CE, Chew EY, Klein BE. The prevalence of macular telangiectasia type 2 in the Beaver Dam eye study. Am J Ophthalmol 2010;150(1):55-62.

136. Lamoureux EL, Maxwell RM, Marella M, Dirani M, Fenwick E, Guymer RH. The longitudinal impact of macular telangiectasia (MacTel) type 2 on vision-related quality of life. Invest Ophthalmol Vis Sci 2011;52(5):2520-2524.

137. Charbel Issa P, Berendschot TT, Staurenghi G, Holz FG, Scholl HP. Confocal blue reflectance imaging in type 2 idiopathic macular telangiectasia. Invest Ophthalmol Vis Sci 2008;49(3):1172-1177.

138. Helb HM, Charbel Issa P, van der Veen RL, Berendschot TT, Scholl HP, Holz FG. Abnormal macular pigment distribution in type 2 idiopathic macular telangiectasia. Retina 2008;28(6):808-816.

139. Charbel Issa P, van der Veen RL, Stijfs A, Holz FG, Scholl HP, Berendschot TT. Quantification of reduced macular pigment optical density in the central retina in macular telangiectasia type 2. Exp Eye Res 2009;89(1):25-31.

140. Wong WT, Forooghian F, Majumdar Z, Bonner RF, Cunningham D, Chew EY. Fundus autofluorescence in type 2 idiopathic macular telangiectasia: correlation with optical coherence tomography and microperimetry. Am J Ophthalmol 2009;148(4):573-583.

141. Tikellis G, Gillies MC, Guymer RH, McAllister IL, Shaw JE, Wong TY. Retinal vascular caliber and macular telangiectasia type 2. Ophthalmology 2009;116(2):319-323.

142. Yannuzzi LA, Bardal AM, Freund KB, Chen KJ, Eandi CM, Blodi B. Idiopathic macular telangiectasia. Arch Ophthalmol 2006;124(4):450-460.

143. Gass JD, Blodi BA. Idiopathic juxtafoveolar retinal telangiectasis. Update of classification and follow-up study. Ophthalmology 1993;100(10):1536-1546.

144. Abujamra S, Bonanomi MT, Cresta FB, Machado CG, Pimentel SL, Caramelli CB. Idiopathic juxtafoveolar retinal telangiectasis: clinical pattern in 19 cases. Ophthalmologica 2000;214(6):406-411.

145. Paunescu LA, Ko TH, Duker JS et al. Idiopathic juxtafoveal retinal telangiectasis: new findings by ultrahigh-resolution optical coherence tomography. Ophthalmology 2006;113(1):48-57.

146. Charbel Issa P, Helb HM, Holz FG, Scholl HP. Correlation of macular function with retinal thickness in nonproliferative type 2 idiopathic macular telangiectasia. Am J Ophthalmol 2008;145(1):169-175.

147. Charbel Issa P, Helb HM, Rohrschneider K, Holz FG, Scholl HP. Microperimetric assessment of patients with type 2 idiopathic macular telangiectasia. Invest Ophthalmol Vis Sci 2007;48(8):3788-3795.

148. Charbel IP, Holz FG, Scholl HP. Findings in fluorescein angiography and optical coherence tomography after intravitreal bevacizumab in type 2 idiopathic macular telangiectasia. Ophthalmology 2007;114(9):1736-1742.

149. Barthelmes D, Sutter FK, Gillies MC. Differential optical densities of intraretinal spaces. Invest Ophthalmol Vis Sci 2008;49(8):3529-3534.

150. Hannan SR, Madhusudhana KC, Rennie C, Lotery AJ. Idiopathic juxtafoveolar retinal telangiectasis in monozygotic twins. Br J Ophthalmol 2007;91(12):1729-1730.

151. Menchini U, Virgili G, Bandello F, Malara C, Rapizzi E, Lanzetta P. Bilateral juxtafoveolar telangiectasis in monozygotic twins. Am J Ophthalmol 2000;129(3):401-403.

152. Gillies MC, Zhu M, Chew E et al. Familial asymptomatic macular telangiectasia type 2. Ophthalmology 2009;116(12):2422-2429.

153. Parmalee NL, Schubert C, Merriam JE et al. Analysis of candidate genes for macular telangiectasia type 2. Mol Vis 2010;16:2718-2726.

154. Xu Q, Wang Y, Dabdoub A et al. Vascular development in the retina and inner ear: control by Norrin and Frizzled-4, a high-affinity ligand-receptor pair. Cell 2004;116(6):883-895.

155. Kondo H, Hayashi H, Oshima K, Tahira T, Hayashi K. Frizzled 4 gene (FZD4) mutations in patients with familial exudative vitreoretinopathy with variable expressivity. Br J Ophthalmol 2003;87(10):1291-1295.

156. Warden SM, Andreoli CM, Mukai S. The Wnt signaling pathway in familial exudative vitreoretinopathy and Norrie disease. Semin Ophthalmol 2007;22(4):211-217.

157. Tasman W, Augsburger JJ, Shields JA, Caputo A, Annesley WH, Jr. Familial exudative vitreoretinopathy. Trans Am Ophthalmol Soc 1981;79:211-226.

158. Chen ZY, Battinelli EM, Fielder A et al. A mutation in the Norrie disease gene (NDP) associated with X-linked familial exudative vitreoretinopathy. Nat Genet 1993;5(2):180-183.

159. George ND, Yates JR, Moore AT. X linked retinoschisis. Br J Ophthalmol 1995;79(7):697-702.

160. Kellner U, Brummer S, Foerster MH, Wessing A. [X-chromosomal congenital retinoschisis. Clinical aspects and electrophysiology]. Fortschr Ophthalmol 1990;87(3):264-268.

161. George ND, Yates JR, Moore AT. Clinical features in affected males with X-linked retinoschisis. Arch Ophthalmol 1996;114(3):274-280.

162. Yu J, Ni Y, Keane PA, Jiang C, Wang W, Xu G. Foveomacular schisis in juvenile X-linked retinoschisis: an optical coherence tomography study. Am J Ophthalmol 2010;149(6):973-978.

163. Renner AB, Fiebig BS, Weber BH et al. Phenotypic variability and long-term follow-up of patients with known and novel PRPH2/RDS gene mutations. Am J Ophthalmol 2009;147(3):518-530.

164. Sauer CG, Gehrig A, Warneke-Wittstock R et al. Positional cloning of the gene associated with X-linked juvenile retinoschisis. Nat Genet 1997;17(2):164-170.

165. Wu WW, Wong JP, Kast J, Molday RS. RS1, a discoidin domain-containing retinal cell adhesion protein associated with X-linked retinoschisis, exists as a novel disulfide-linked octamer. J Biol Chem 2005;280(11):10721-10730.

166. Grayson C, Reid SN, Ellis JA et al. Retinoschisin, the X-linked retinoschisis protein, is a secreted photoreceptor protein, and is expressed and released by Weri-Rb1 cells. Hum Mol Genet 2000;9(12):1873-1879.

167. Molday LL, Hicks D, Sauer CG, Weber BH, Molday RS. Expression of X-linked retinoschisis protein RS1 in photoreceptor and bipolar cells. Invest Ophthalmol Vis Sci 2001;42(3):816-825.

168. Molday LL, Wu WW, Molday RS. Retinoschisin (RS1), the protein encoded by the X-linked retinoschisis gene, is anchored to the surface of retinal photoreceptor and bipolar cells through its interactions with a Na/K ATPase-SARM1 complex. J Biol Chem 2007;282(45):32792-32801.

169. Wetzel RK, Arystarkhova E, Sweadner KJ. Cellular and subcellular specification of Na,K-ATPase alpha and beta isoforms in the postnatal development of mouse retina. J Neurosci 1999;19(22):9878-9889.

170. Antonicek H, Persohn E, Schachner M. Biochemical and functional characterization of a novel neuron-glia adhesion molecule that is involved in neuronal migration. J Cell Biol 1987;104(6):1587-1595.

171. Gloor S, Antonicek H, Sweadner KJ et al. The adhesion molecule on glia (AMOG) is a homologue of the beta subunit of the Na,K-ATPase. J Cell Biol 1990;110(1):165-174.

172. Wolfensberger TJ, Mahieu I, Carter ND, Hollande E, Bohnke M. [Membrane-bound carbonic anhydrase (CA IV) in human corneal epithelium and endothelium]. Klin Monbl Augenheilkd 1999;214(5):263-265.

173. Walia S, Fishman GA, Molday RS et al. Relation of response to treatment with dorzolamide in X-linked retinoschisis to the mechanism of functional loss in retinoschisin. Am J Ophthalmol 2009;147(1):111-115.

174. Fishman GA, Gilbert LD, Fiscella RG, Kimura AE, Jampol LM. Acetazolamide for treatment of chronic macular edema in retinitis pigmentosa. Arch Ophthalmol 1989;107(10):1445-1452.

175. Grover S, Fishman GA, Fiscella RG, Adelman AE. Efficacy of dorzolamide hydrochloride in the management of chronic cystoid macular edema in patients with retinitis pigmentosa. Retina 1997;17(3):222-231.

176. Thobani A, Fishman GA, Genead M, Anastasakis A. Visual acuity loss in recessive retinitis pigmentosa and its correlation with macular lesions. Retina 2011;31(5):967-972.

177. Willemsen MA, Cruysberg JR, Rotteveel JJ, Aandekerk AL, Van Domburg PH, Deutman AF. Juvenile macular dystrophy associated with deficient activity of fatty aldehyde dehydrogenase in Sjogren-Larsson syndrome. Am J Ophthalmol 2000;130(6):782-789.

178. Fuijkschot J, Cruysberg JR, Willemsen MA, Keunen JE, Theelen T. Subclinical changes in the juvenile crystalline macular dystrophy in Sjogren-Larsson syndrome detected by optical coherence tomography. Ophthalmology 2008;115(5):870-875.

179. van der Veen RL, Fuijkschot J, Willemsen MA, Cruysberg JR, Berendschot TT, Theelen T. Patients with Sjogren-Larsson syndrome lack macular pigment. Ophthalmology 2010;117(5):966-971.

180. De L, V, Rogers GR, Hamrock DJ et al. Sjogren-Larsson syndrome is caused by mutations in the fatty aldehyde dehydrogenase gene. Nat Genet 1996;12(1):52-57.

181. Carney G, Wei S, Rizzo WB. Sjogren-Larsson syndrome: seven novel mutations in the fatty aldehyde dehydrogenase gene ALDH3A2. Hum Mutat 2004;24(2):186.

182. Rizzo WB, Craft DA. Sjogren-Larsson syndrome. Deficient activity of the fatty aldehyde dehydrogenase component of fatty alcohol:NAD+ oxidoreductase in cultured fibroblasts. J Clin Invest 1991;88(5):1643-1648.

183. Rizzo WB. Sjogren-Larsson syndrome. Semin Dermatol 1993;12(3):210-218.

184. Rizzo WB, Dammann AL, Craft DA. Sjogren-Larsson syndrome. Impaired fatty alcohol oxidation in cultured fibroblasts due to deficient fatty alcohol:nicotinamide adenine dinucleotide oxidoreductase activity. J Clin Invest 1988;81(3):738-744.

185. Chew BP, Park JS, Wong MW, Wong TS. A comparison of the anticancer activities of dietary beta-carotene, canthaxanthin and astaxanthin in mice in vivo. Anticancer Res 1999;19(3A):1849-1853.

186. Mayne ST, Parker RS. Antioxidant activity of dietary canthaxanthin. Nutr Cancer 1989;12(3):225-236.

187. Palozza P, Maggiano N, Calviello G et al. Canthaxanthin induces apoptosis in human cancer cell lines. Carcinogenesis 1998;19(2):373-376.

188. Lober CW. Canthaxanthin--the "tanning" pill. J Am Acad Dermatol 1985;13(4):660.

189. Boudreault G, Cortin P, Corriveau LA, Rousseau AP, Tardif Y, Malenfant M. [Canthaxanthine retinopathy: 1. Clinical study in 51 consumers]. Can J Ophthalmol 1983;18(7):325-328.

190. Cortin P, Corriveau LA, Rousseau AP, Tardif Y, Malenfant M, Boudreault G. [Maculopathy with golden particles]. Can J Ophthalmol 1982;17(3):103-106.

191. Ros AM, Leyon H, Wennersten G. Crystalline retinopathy in patients taking an oral drug containing canthaxanthine. Photodermatol 1985;2(3):183-185.

192. Daicker B, Schiedt K, Adnet JJ, Bermond P. Canthaxanthin retinopathy. An investigation by light and electron microscopy and physicochemical analysis. Graefes Arch Clin Exp Ophthalmol 1987;225(3):189-197.

193. McGuinness R, Beaumont P. Gold dust retinopathy after the ingestion of canthaxanthine to produce skin-bronzing. Med J Aust 1985;143(12-13):622-623.

194. White GL, Jr., Beesley R, Thiese SM, Murdock RT. Retinal crystals and oral tanning agents. Am Fam Physician 1988;37(3):125-126.

195. Arden GB, Oluwole JO, Polkinghorne P et al. Monitoring of patients taking canthaxanthin and carotene: an electroretinographic and ophthalmological survey. Hum Toxicol 1989;8(6):439-450.

196. Bopp S, el-Hifnawi E, Laqua H. [Canthaxanthin retinopathy and macular pucker--clinical picture and ultrastructural findings of macular pucker]. Fortschr Ophthalmol 1989;86(5):456-460.

197. Weber U, Michaelis L, Kern W, Goerz G. Experimental carotenoid retinopathy. II. Functional and morphological alterations of the rabbit retina after acute canthaxanthin application with small unilamellar phospholipid liposomes. Graefes Arch Clin Exp Ophthalmol 1987;225(5):346-350.

198. Weber U, Kern W, Novotny GE, Goerz G, Hanappel S. Experimental carotenoid retinopathy. I. Functional and morphological alterations of the rabbit retina after 11 months dietary carotenoid application. Graefes Arch Clin Exp Ophthalmol 1987;225(3):198-205.

199. Goralczyk R, Barker FM, Buser S, Liechti H, Bausch J. Dose dependency of canthaxanthin crystals in monkey retina and spatial distribution of its metabolites. Invest Ophthalmol Vis Sci 2000;41(6):1513-1522.

200. Macdonald K, Holti G, Marks J. Is there a place for beta-carotene/canthaxanthin in photochemotherapy for psoriasis? Dermatologica 1984;169(1):41-46.

201. Harnois C, Samson J, Malenfant M, Rousseau A. Canthaxanthin retinopathy. Anatomic and functional reversibility. Arch Ophthalmol 1989;107(4):538-540.

202. Hueber A, Rosentreter A, Severin M. Canthaxanthin retinopathy: long-term observations. Ophthalmic Res 2011;46(2):103-106.

203. Klein R, Peto T, Bird A, Vannewkirk MR. The epidemiology of age-related macular degeneration. Am J Ophthalmol 2004;137(3):486-495.

204. Bird AC, Bressler NM, Bressler SB et al. An international classification and grading system for age-related maculopathy and age-related macular degeneration. The International ARM Epidemiological Study Group. Surv Ophthalmol 1995;39(5):367-374.

205. Munoz B, West SK, Rubin GS et al. Causes of blindness and visual impairment in a population of older Americans: The Salisbury Eye Evaluation Study. Arch Ophthalmol 2000;118(6):819-825.

206. Vingerling JR, Dielemans I, Hofman A et al. The prevalence of age-related maculopathy in the Rotterdam Study. Ophthalmology 1995;102(2):205-210.

207. Weih L, McCarty CA, Taylor HR. Functional implications of vision impairment. Clin Experiment Ophthalmol 2000;28(3):153-155.

208. Crabb JW, Miyagi M, Gu X et al. Drusen proteome analysis: an approach to the etiology of age-related macular degeneration. Proc Natl Acad Sci U S A 2002;99(23):14682-14687.

209. Malek G, Li CM, Guidry C, Medeiros NE, Curcio CA. Apolipoprotein B in cholesterol-containing drusen and basal deposits of human eyes with age-related maculopathy. Am J Pathol 2003;162(2):413-425.

210. Mullins RF, Russell SR, Anderson DH, Hageman GS. Drusen associated with aging and age-related macular degeneration contain proteins common to extracellular deposits associated with atherosclerosis, elastosis, amyloidosis, and dense deposit disease. FASEB J 2000;14(7):835-846.

211. Bressler NM, Silva JC, Bressler SB, Fine SL, Green WR. Clinicopathologic correlation of drusen and retinal pigment epithelial abnormalities in age-related macular degeneration. Retina 1994;14(2):130-142.

212. Sarks S, Cherepanoff S, Killingsworth M, Sarks J. Relationship of Basal laminar deposit and membranous debris to the clinical presentation of early age-related macular degeneration. Invest Ophthalmol Vis Sci 2007;48(3):968-977.

213. Ferris FL, Davis MD, Clemons TE et al. A simplified severity scale for age-related macular degeneration: AREDS Report No. 18. Arch Ophthalmol 2005;123(11):1570-1574.

214. Green WR. Histopathology of age-related macular degeneration. Mol Vis 1999;5:27.

215. Kim SY, Sadda S, Pearlman J et al. Morphometric analysis of the macula in eyes with disciform age-related macular degeneration. Retina 2002;22(4):471-477.

216. Sarks JP, Sarks SH, Killingsworth MC. Morphology of early choroidal neovascularisation in age-related macular degeneration: correlation with activity. Eye (Lond) 1997;11 (Pt 4):515-522.

217. Grossniklaus HE, Green WR. Choroidal neovascularization. Am J Ophthalmol 2004;137(3):496-503.

218. Jackson GR, Owsley C, Curcio CA. Photoreceptor degeneration and dysfunction in aging and age-related maculopathy. Ageing Res Rev 2002;1(3):381-396.

219. Edwards AO, Ritter R, III, Abel KJ, Manning A, Panhuysen C, Farrer LA. Complement factor H polymorphism and age-related macular degeneration. Science 2005;308(5720):421-424.

220. Hageman GS, Anderson DH, Johnson LV et al. A common haplotype in the complement regulatory gene factor H (HF1/CFH) predisposes individuals to age-related macular degeneration. Proc Natl Acad Sci U S A 2005;102(20):7227-7232.

221. Haines JL, Hauser MA, Schmidt S et al. Complement factor H variant increases the risk of age-related macular degeneration. Science 2005;308(5720):419-421.

222. Zareparsi S, Branham KE, Li M et al. Strong association of the Y402H variant in complement factor H at 1q32 with susceptibility to age-related macular degeneration. Am J Hum Genet 2005;77(1):149-153.

223. Gold B, Merriam JE, Zernant J et al. Variation in factor B (BF) and complement component 2 (C2) genes is associated with age-related macular degeneration. Nat Genet 2006;38(4):458-462.

224. Yates JR, Sepp T, Matharu BK et al. Complement C3 variant and the risk of age-related macular degeneration. N Engl J Med 2007;357(6):553-561.

225. Dewan A, Liu M, Hartman S et al. HTRA1 promoter polymorphism in wet age-related macular degeneration. Science 2006;314(5801):989-992.

226. Winkler BS, Boulton ME, Gottsch JD, Sternberg P. Oxidative damage and age-related macular degeneration. Mol Vis 1999;5:32.

227. Fritsche LG, Loenhardt T, Janssen A et al. Age-related macular degeneration is associated with an unstable ARMS2 (LOC387715) mRNA. Nat Genet 2008;40(7):892-896.

228. Kanda A, Chen W, Othman M et al. A variant of mitochondrial protein LOC387715/ARMS2, not HTRA1, is strongly associated with age-related macular degeneration. Proc Natl Acad Sci U S A 2007;104(41):16227-16232.

229. Chong NH, Keonin J, Luthert PJ et al. Decreased thickness and integrity of the macular elastic layer of Bruch's membrane correspond to the distribution of lesions associated with age-related macular degeneration. Am J Pathol 2005;166(1):241-251.

230. Nackman GB, Karkowski FJ, Halpern VJ, Gaetz HP, Tilson MD. Elastin degradation products induce adventitial angiogenesis in the Anidjar/Dobrin rat aneurysm model. Surgery 1997;122(1):39-44.

231. Ramrattan RS, van der Schaft TL, Mooy CM, de Bruijn WC, Mulder PG, de Jong PT. Morphometric analysis of Bruch's membrane, the choriocapillaris, and the choroid in aging. Invest Ophthalmol Vis Sci 1994;35(6):2857-2864.

232. Brownlee M. Biochemistry and molecular cell biology of diabetic complications. Nature 2001;414(6865):813-820.

233. Sinclair SH. Macular retinal capillary hemodynamics in diabetic patients. Ophthalmology 1991;98(10):1580-1586.

234. Kristinsson JK, Gottfredsdottir MS, Stefansson E. Retinal vessel dilatation and elongation precedes diabetic macular oedema. Br J Ophthalmol 1997;81(4):274-278.

235. Fine BS, Brucker AJ. Macular edema and cystoid macular edema. Am J Ophthalmol 1981;92(4):466-481.

236. Gass JD, Anderson DR, Davis EB. A clinical, fluorescein angiographic, and electron microscopic correlation of cystoid macular edema. Am J Ophthalmol 1985;100(1):82-86.

237. Tso MO. Pathological study of cystoid macular oedema. Trans Ophthalmol Soc U K 1980;100(3):408-413.

238. Smith RT, Lee CM, Charles HC, Farber M, Cunha-Vaz JG. Quantification of diabetic macular edema. Arch Ophthalmol 1987;105(2):218-222.

239. Langham ME, Grebe R, Hopkins S, Marcus S, Sebag M. Choroidal blood flow in diabetic retinopathy. Exp Eye Res 1991;52(2):167-173.

240. Friedman DS, O'Colmain BJ, Munoz B et al. Prevalence of age-related macular degeneration in the United States. Arch Ophthalmol 2004;122(4):564-572.

241. Risk factors associated with age-related macular degeneration. A case-control study in the age-related eye disease study: Age-Related Eye Disease Study Report Number 3. Ophthalmology 2000;107(12):2224-2232.

242. McCarty CA, Mukesh BN, Fu CL, Mitchell P, Wang JJ, Taylor HR. Risk factors for age-related maculopathy: the Visual Impairment Project. Arch Ophthalmol 2001;119(10):1455-1462.

243. Reichenbach A, Bringmann A. Muller cells in healthy and diseased retina. 1st edition ed. New York: Springer; 2010.

244. Penfold PL, Provis JM. Macular Degeneration. Berlin: Springer; 2005.

245. Provis JM, Penfold PL, Cornish EE, Sandercoe TM, Madigan MC. Anatomy and development of the macula: specialisation and the vulnerability to macular degeneration. Clin Exp Optom 2005;88(5):269-281.

246. Provis JM. Development of the primate retinal vasculature. Prog Retin Eye Res 2001;20(6):799-821.

247. Espaillat A, Aiello LP, Arrigg PG, Villalobos R, Silver PM, Cavicchi RW. Canthaxanthine retinopathy. Arch Ophthalmol 1999;117(3):412-413.

248. Powner MB, Gillies MC, Tretiach M et al. Perifoveal muller cell depletion in a case of macular telangiectasia type 2. Ophthalmology 2010;117(12):2407-2416.

249. Green WR, Quigley HA, De la CZ, Cohen B. Parafoveal retinal telangiectasis. Light and electron microscopy studies. Trans Ophthalmol Soc U K 1980;100(Pt 1):162-170.

250. Eliassi-Rad B, Green WR. Histopathologic study of presumed parafoveal telangiectasis. Retina 1999;19(4):332-335.

251. Charbel Issa P., Berendschot TT, Staurenghi G, Holz FG, Scholl HP. Confocal blue reflectance imaging in type 2 idiopathic macular telangiectasia. Invest Ophthalmol Vis Sci 2008;49(3):1172-1177.

252. Charbel Issa P., van der Veen, Stijfs A, Holz FG, Scholl HP, Berendschot TT. Quantification of reduced macular pigment optical density in the central retina in macular telangiectasia type 2. Exp Eye Res 2009;89(1):25-31.

253. Imai Y, Ibata I, Ito D, Ohsawa K, Kohsaka S. A novel gene iba1 in the major histocompatibility complex class III region encoding an EF hand protein expressed in a monocytic lineage. Biochem Biophys Res Commun 1996;224(3):855-862.

254. Provis JM, Diaz CM, Penfold PL. Microglia in human retina: a heterogeneous population with distinct ontogenies. Perspect Dev Neurobiol 1996;3(3):213-222.

255. Diaz-Araya CM, Provis JM, Penfold PL, Billson FA. Development of microglial topography in human retina. J Comp Neurol 1995;363(1):53-68.

256. Gass JD. Muller cell cone, an overlooked part of the anatomy of the fovea centralis: hypotheses concerning its role in the pathogenesis of macular hole and foveomacualr retinoschisis. Arch Ophthalmol 1999;117(6):821-823.

257. Mizutani M, Gerhardinger C, Lorenzi M. Muller cell changes in human diabetic retinopathy. Diabetes 1998;47(3):445-449.

258. Tuccari G, Trombetta C, Giardinelli MM, Arena F, Barresi G. Distribution of glial fibrillary acidic protein in normal and gliotic human retina. Basic Appl Histochem 1986;30(4):425-432.

259. Penfold PL, Wong JG, Gyory J, Billson FA. Effects of triamcinolone acetonide on microglial morphology and quantitative expression of MHC-II in exudative age-related macular degeneration. Clin Experiment Ophthalmol 2001;29(3):188-192.

260. Penfold PL, Madigan MC, Gillies MC, Provis JM. Immunological and aetiological aspects of macular degeneration. Prog Retin Eye Res 2001;20(3):385-414.

261. Charbel Issa P., Helb HM, Rohrschneider K, Holz FG, Scholl HP. Microperimetric assessment of patients with type 2 idiopathic macular telangiectasia. Invest Ophthalmol Vis Sci 2007;48(8):3788-3795.

262. Clemons TE, Gillies MC, Chew EY et al. The National Eye Institute Visual Function Questionnaire in the Macular Telangiectasia (MacTel) Project. Invest Ophthalmol Vis Sci 2008;49(10):4340-4346.

263. Schmitz-Valckenberg S, Fan K, Nugent A et al. Correlation of functional impairment and morphological alterations in patients with group 2A idiopathic juxtafoveal retinal telangiectasia. Arch Ophthalmol 2008;126(3):330-335.

264. Pichler P, Kocher T, Holzmann J et al. Peptide labeling with isobaric tags yields higher identification rates using iTRAQ 4-plex compared to TMT 6-plex and iTRAQ 8-plex on LTQ Orbitrap. Anal Chem 2010;82(15):6549-6558.

265. Tsacopoulos M, Poitry-Yamate CL, MacLeish PR, Poitry S. Trafficking of molecules and metabolic signals in the retina. Prog Retin Eye Res 1998;17(3):429-442.

266. Winkler BS, Pourcho RG, Starnes C, Slocum J, Slocum N. Metabolic mapping in mammalian retina: a biochemical and 3H-2-deoxyglucose autoradiographic study. Exp Eye Res 2003;77(3):327-337.

267. Poitry-Yamate CL, Poitry S, Tsacopoulos M. Lactate released by Muller glial cells is metabolized by photoreceptors from mammalian retina. J Neurosci 1995;15(7 Pt 2):5179-5191.

268. Charbel Issa P., Helb HM, Holz FG, Scholl HP. Correlation of macular function with retinal thickness in nonproliferative type 2 idiopathic macular telangiectasia. Am J Ophthalmol 2008;145(1):169-175.

269. Charbel Issa P., Finger RP, Holz FG, Scholl HP. Eighteen-month follow-up of intravitreal bevacizumab in type 2 idiopathic macular telangiectasia. Br J Ophthalmol 2008;92(7):941-945.

270. Bringmann A, Pannicke T, Biedermann B et al. Role of retinal glial cells in neurotransmitter uptake and metabolism. Neurochem Int 2009;54(3-4):143-160.

271. Gaudric A, Ducos de LG, Cohen SY, Massin P, Haouchine B. Optical coherence tomography in group 2A idiopathic juxtafoveolar retinal telangiectasis. Arch Ophthalmol 2006;124(10):1410-1419.

272. Charbel Issa P., Scholl HP, Gaudric A et al. Macular full-thickness and lamellar holes in association with type 2 idiopathic macular telangiectasia. Eye 2009;23(2):435-441.

273. Distler C, Weigel H, Hoffmann KP. Glia cells of the monkey retina. I. Astrocytes. J Comp Neurol 1993;333(1):134-147.

274. Gass JD. Histopathologic study of presumed parafoveal telangiectasis. Retina 2000;20(2):226-227.

275. Barber AJ, Antonetti DA. Mapping the blood vessels with paracellular permeability in the retinas of diabetic rats. Invest Ophthalmol Vis Sci 2003;44(12):5410-5416.

276. Hogan MJ, Alvarado JA, Weddell J.E. Blood Supply. Histology of the Human Eye: An Atlas and Textbook. Philadelphia: WB Saunders; 1971:508-519.

277. Powner MB, Scott A, Zhu M et al. Basement membrane changes in capillaries of the ageing human retina. Br J Ophthalmol 2011;95(9):1316-1322.

278. Ashton N. Vascular basement membrane changes in diabetic retinopathy. Montgomery lecture, 1973. Br J Ophthalmol 1974;58(4):344-366.

279. Vracko R, Benditt EP. Capillary basal lamina thickening. Its relationship to endothelial cell death and replacement. J Cell Biol 1970;47(1):281-285.

280. Cai J, Boulton M. The pathogenesis of diabetic retinopathy: old concepts and new questions. Eye (Lond) 2002;16(3):242-260.

281. Tooke JE. Possible pathophysiological mechanisms for diabetic angiopathy in type 2 diabetes. J Diabetes Complications 2000;14(4):197-200.

282. Armulik A, Abramsson A, Betsholtz C. Endothelial/pericyte interactions. Circ Res 2005;97(6):512-523.

283. Hogan MJ, Feeney L. The ultrastructure of the retinal blood vessels. II. The small vessels. J Ultrastruct Res 1963;49:29-46.

284. Hainsworth DP, Katz ML, Sanders DA, Sanders DN, Wright EJ, Sturek M. Retinal capillary basement membrane thickening in a porcine model of diabetes mellitus. Comp Med 2002;52(6):523-529.

285. Stitt AW, Anderson HR, Gardiner TA, Archer DB. Diabetic retinopathy: quantitative variation in capillary basement membrane thickening in arterial or venous environments. Br J Ophthalmol 1994;78(2):133-137.

286. Anderson HR, Stitt AW, Gardiner TA, Archer DB. Diabetic retinopathy: morphometric analysis of basement membrane thickening of capillaries in different retinal layers within arterial and venous environments. Br J Ophthalmol 1995;79(12):1120-1123.

287. Carlson EC. Scanning and transmission electron microscopic studies of normal and diabetic acellular glomerular and retinal microvessel basement membranes. Microsc Res Tech 1994;28(3):165-177.

288. Bloodworth JM, Jr., Molitor DL. Ultrastructural aspects of human and canine diabetic retinopathy. Invest Ophthalmol 1965;4(6):1037-1048.

289. Addison DJ, Garner A, Ashton N. Degeneration of intramural pericytes in diabetic retinopathy. Br Med J 1970;1(5691):264-266.

290. Fiala JC. Reconstruct: a free editor for serial section microscopy. J Microsc 2005;218(Pt 1):52-61.

291. Ishikawa T. Fine structure of retinal vessels in man and the macaque monkey. Invest Ophthalmol 1963;2:1-15.

292. Gardiner TA, Anderson HR, Degenhardt T et al. Prevention of retinal capillary basement membrane thickening in diabetic dogs by a non-steroidal anti-inflammatory drug. Diabetologia 2003;46(9):1269-1275.

293. Mansour SZ, Hatchell DL, Chandler D, Saloupis P, Hatchell MC. Reduction of basement membrane thickening in diabetic cat retina by sulindac. Invest Ophthalmol Vis Sci 1990;31(3):457-463.

294. Stitt AW, Bhaduri T, McMullen CB, Gardiner TA, Archer DB. Advanced glycation end products induce blood-retinal barrier dysfunction in normoglycemic rats. Mol Cell Biol Res Commun 2000;3(6):380-388.

295. Ruberti JW, Curcio CA, Millican CL, Menco BP, Huang JD, Johnson M. Quick-freeze/deep-etch visualization of age-related lipid accumulation in Bruch's membrane. Invest Ophthalmol Vis Sci 2003;44(4):1753-1759.

296. Cusick M, Chew EY, Chan CC, Kruth HS, Murphy RP, Ferris FL, III. Histopathology and regression of retinal hard exudates in diabetic retinopathy after reduction of elevated serum lipid levels. Ophthalmology 2003;110(11):2126-2133.

297. Wangsa-Wirawan ND, Linsenmeier RA. Retinal oxygen: fundamental and clinical aspects. Arch Ophthalmol 2003;121(4):547-557.

298. Kuwabara T, Cogan DG. Studies of retinal vascular patterns. I. Normal architecture. Arch Ophthalmol 1960;64:904-911.

299. Scoles D, Gray DC, Hunter JJ et al. In-vivo imaging of retinal nerve fiber layer vasculature: imaging histology comparison. BMC Ophthalmol 2009;9:9.

300. Povazay B, Hofer B, Torti C et al. Impact of enhanced resolution, speed and penetration on three-dimensional retinal optical coherence tomography. Opt Express 2009;17(5):4134-4150.

301. Baumuller S, Charbel IP, Scholl HP, Schmitz-Valckenberg S, Holz FG. Outer retinal hyperreflective spots on spectral-domain optical coherence tomography in macular telangiectasia type 2. Ophthalmology 2010;117(11):2162-2168.

302. Crabb JW, Miyagi M, Gu X et al. Drusen proteome analysis: an approach to the etiology of age-related macular degeneration. Proc Natl Acad Sci U S A 2002;99(23):14682-14687.

303. Decanini A, Karunadharma PR, Nordgaard CL, Feng X, Olsen TW, Ferrington DA. Human retinal pigment epithelium proteome changes in early diabetes. Diabetologia 2008;51(6):1051-1061.

304. Simo R, Higuera M, Garcia-Ramirez M, Canals F, Garcia-Arumi J, Hernandez C. Elevation of apolipoprotein A-I and apolipoprotein H levels in the vitreous fluid and overexpression in the retina of diabetic patients. Arch Ophthalmol 2008;126(8):1076-1081.

305. Luo C, Yang X, Kain AD, Powell DW, Kuehn MH, Tezel G. Glaucomatous tissue stress and the regulation of immune response through glial Toll-like receptor signaling. Invest Ophthalmol Vis Sci 2010;51(11):5697-5707.

306. Tezel G, Yang X, Luo C et al. Oxidative stress and the regulation of complement activation in human glaucoma. Invest Ophthalmol Vis Sci 2010;51(10):5071-5082.

307. Pierce A, Unwin RD, Evans CA et al. Eight-channel iTRAQ enables comparison of the activity of six leukemogenic tyrosine kinases. Mol Cell Proteomics 2008;7(5):853-863.

308. Griffin TJ, Xie H, Bandhakavi S et al. iTRAQ reagent-based quantitative proteomic analysis on a linear ion trap mass spectrometer. J Proteome Res 2007;6(11):4200-4209.

309. Glen A, Gan CS, Hamdy FC et al. iTRAQ-facilitated proteomic analysis of human prostate cancer cells identifies proteins associated with progression. J Proteome Res 2008;7(3):897-907.

310. Oberg AL, Mahoney DW, Eckel-Passow JE et al. Statistical analysis of relative labeled mass spectrometry data from complex samples using ANOVA. J Proteome Res 2008;7(1):225-233.

311. Griffiths SD, Burthem J, Unwin RD et al. The use of isobaric tag peptide labeling (iTRAQ) and mass spectrometry to examine rare, primitive hematopoietic cells from patients with chronic myeloid leukemia. Mol Biotechnol 2007;36(2):81-89.

312. Fujiki Y, Hubbard AL, Fowler S, Lazarow PB. Isolation of intracellular membranes by means of sodium carbonate treatment: application to endoplasmic reticulum. J Cell Biol 1982;93(1):97-102.

313. Shilov IV, Seymour SL, Patel AA et al. The Paragon Algorithm, a next generation search engine that uses sequence temperature values and feature probabilities to identify peptides from tandem mass spectra. Mol Cell Proteomics 2007;6(9):1638-1655.

314. Song X, Bandow J, Sherman J et al. iTRAQ experimental design for plasma biomarker discovery. J Proteome Res 2008;7(7):2952-2958.

315. Kerns MJ, Darst MA, Olsen TG, Fenster M, Hall P, Grevey S. Shrinkage of cutaneous specimens: formalin or other factors involved? J Cutan Pathol 2008;35(12):1093-1096.

316. Drasdo N, Fowler CW. Non-linear projection of the retinal image in a wide-angle schematic eye. Br J Ophthalmol 1974;58(8):709-714.

317. Bingle L, Bingle CD. Distribution of human PLUNC/BPI fold-containing (BPIF) proteins. Biochem Soc Trans 2011;39(4):1023-1027.

318. Hoang QV, Linsenmeier RA, Chung CK, Curcio CA. Photoreceptor inner segments in monkey and human retina: mitochondrial density, optics, and regional variation. Vis Neurosci 2002;19(4):395-407.

319. Tsacopoulos M, Magistretti PJ. Metabolic coupling between glia and neurons. J Neurosci 1996;16(3):877-885.

320. Bhosale P, Larson AJ, Frederick JM, Southwick K, Thulin CD, Bernstein PS. Identification and characterization of a Pi isoform of glutathione S-transferase (GSTP1) as a zeaxanthin-binding protein in the macula of the human eye. J Biol Chem 2004;279(47):49447-49454.

321. Wu LZ, Huang ZS, Wu DZ, Chan E. Characteristics of the capillary-free zone in the normal human macula. Jpn J Ophthalmol 1985;29(4):406-411.

322. Erickson PA, Feinstein SC, Lewis GP, Fisher SK. Glial fibrillary acidic protein and its mRNA: ultrastructural detection and determination of changes after CNS injury. J Struct Biol 1992;108(2):148-161.

323. Piatigorsky J. Gene sharing, lens crystallins and speculations on an eye/ear evolutionary relationship. Integr Comp Biol 2003;43(4):492-499.

324. Sax CM, Piatigorsky J. Expression of the alpha-crystallin/small heat-shock protein/molecular chaperone genes in the lens and other tissues. Adv Enzymol Relat Areas Mol Biol 1994;69:155-201.

325. Wistow G. Identification of lens crystallins: a model system for gene recruitment. Methods Enzymol 1993;224:563-575.

326. Ingolia TD, Craig EA. Four small Drosophila heat shock proteins are related to each other and to mammalian alpha-crystallin. Proc Natl Acad Sci U S A 1982;79(7):2360-2364.

327. Horwitz J. Alpha-crystallin. Exp Eye Res 2003;76(2):145-153.

328. Ilagan JG, Cvekl A, Kantorow M, Piatigorsky J, Sax CM. Regulation of alphaA-crystallin gene expression. Lens specificity achieved through the differential placement of similar transcriptional control elements in mouse and chicken. J Biol Chem 1999;274(28):19973-19978.

329. de Jong WW, Zweers A, Goodman M. Relationship of aardvark to elephants, hyraxes and sea cows from alpha-crystallin sequences. Nature 1981;292(5823):538-540.

330. de Jong WW, Zweers A, Versteeg M, Nuy-Terwindt EC. Primary structures of the alpha-crystallin A chains of twenty-eight mammalian species, chicken and frog. Eur J Biochem 1984;141(1):131-140.

331. de Jong WW, Leunissen JA, Leenen PJ, Zweers A, Versteeg M. Dogfish alpha-crystallin sequences. Comparison with small heat shock proteins and Schistosoma egg antigen. J Biol Chem 1988;263(11):5141-5149.

332. Horwitz J. Alpha-crystallin can function as a molecular chaperone. Proc Natl Acad Sci U S A 1992;89(21):10449-10453.

333. Cui W, Tomarev SI, Piatigorsky J, Chepelinsky AB, Duncan MK. Mafs, Prox1, and Pax6 can regulate chicken betaB1-crystallin gene expression. J Biol Chem 2004;279(12):11088-11095.

334. Cvekl A, Piatigorsky J. Lens development and crystallin gene expression: many roles for Pax-6. Bioessays 1996;18(8):621-630.

335. Cvekl A, Sax CM, Bresnick EH, Piatigorsky J. A complex array of positive and negative elements regulates the chicken alpha A-crystallin gene: involvement of Pax-6, USF, CREB and/or CREM, and AP-1 proteins. Mol Cell Biol 1994;14(11):7363-7376.

336. Cvekl A, Kashanchi F, Sax CM, Brady JN, Piatigorsky J. Transcriptional regulation of the mouse alpha A-crystallin gene: activation dependent on a cyclic AMP-responsive element (DE1/CRE) and a Pax-6-binding site. Mol Cell Biol 1995;15(2):653-660.

337. Kawauchi S, Takahashi S, Nakajima O et al. Regulation of lens fiber cell differentiation by transcription factor c-Maf. J Biol Chem 1999;274(27):19254-19260.

338. Yang Y, Stopka T, Golestaneh N et al. Regulation of alphaA-crystallin via Pax6, c-Maf, CREB and a broad domain of lens-specific chromatin. EMBO J 2006;25(10):2107-2118.

339. Sax CM, Cvekl A, Piatigorsky J. Transcriptional regulation of the mouse alpha A-crystallin gene: binding of USF to the -7/+5 region. Gene 1997;185(2):209-216.

340. Horwitz J, Emmons T, Takemoto L. The ability of lens alpha crystallin to protect against heat-induced aggregation is age-dependent. Curr Eye Res 1992;11(8):817-822.

341. Andley UP, Mathur S, Griest TA, Petrash JM. Cloning, expression, and chaperone-like activity of human alphaA-crystallin. J Biol Chem 1996;271(50):31973-31980.

342. Bova MP, Ding LL, Horwitz J, Fung BK. Subunit exchange of alphaA-crystallin. J Biol Chem 1997;272(47):29511-29517.

343. Derham BK, van Boekel MA, Muchowski PJ et al. Chaperone function of mutant versions of alpha A- and alpha B-crystallin prepared to pinpoint chaperone binding sites. Eur J Biochem 2001;268(3):713-721.

344. Sun TX, Das BK, Liang JJ. Conformational and functional differences between recombinant human lens alphaA- and alphaB-crystallin. J Biol Chem 1997;272(10):6220-6225.

345. Van MR, Slingsby C, Vierling E. Structure and function of the small heat shock protein/alpha-crystallin family of molecular chaperones. Adv Protein Chem 2001;59:105-156.

346. Lee GJ, Vierling E. A small heat shock protein cooperates with heat shock protein 70 systems to reactivate a heat-denatured protein. Plant Physiol 2000;122(1):189-198.

347. Koteiche HA, McHaourab HS. Mechanism of a hereditary cataract phenotype. Mutations in alphaA-crystallin activate substrate binding. J Biol Chem 2006;281(20):14273-14279.

348. Kamradt MC, Chen F, Cryns VL. The small heat shock protein alpha B-crystallin negatively regulates cytochrome c- and caspase-8-dependent activation of caspase-3 by inhibiting its autoproteolytic maturation. J Biol Chem 2001;276(19):16059-16063.

349. Liu JP, Schlosser R, Ma WY et al. Human alphaA- and alphaB-crystallins prevent UVA-induced apoptosis through regulation of PKCalpha, RAF/MEK/ERK and AKT signaling pathways. Exp Eye Res 2004;79(3):393-403.

350. Mehlen P, Kretz-Remy C, Preville X, Arrigo AP. Human hsp27, Drosophila hsp27 and human alphaB-crystallin expression-mediated increase in glutathione is essential for the protective activity of these proteins against TNFalpha-induced cell death. EMBO J 1996;15(11):2695-2706.

351. Andley UP, Song Z, Wawrousek EF, Bassnett S. The molecular chaperone alphaA-crystallin enhances lens epithelial cell growth and resistance to UVA stress. J Biol Chem 1998;273(47):31252-31261.

352. Andley UP, Song Z, Wawrousek EF, Fleming TP, Bassnett S. Differential protective activity of alpha A- and alphaB-crystallin in lens epithelial cells. J Biol Chem 2000;275(47):36823-36831.

353. Xi J, Farjo R, Yoshida S, Kern TS, Swaroop A, Andley UP. A comprehensive analysis of the expression of crystallins in mouse retina. Mol Vis 2003;9:410-419.

354. Jolly C, Morimoto RI. Role of the heat shock response and molecular chaperones in oncogenesis and cell death. J Natl Cancer Inst 2000;92(19):1564-1572.

355. Boelens WC, Croes Y, de Jong WW. Interaction between alphaB-crystallin and the human 20S proteasomal subunit C8/alpha7. Biochim Biophys Acta 2001;1544(1-2):311-319.

356. Khachik F, Spangler CJ, Smith JC, Jr., Canfield LM, Steck A, Pfander H. Identification, quantification, and relative concentrations of carotenoids and their metabolites in human milk and serum. Anal Chem 1997;69(10):1873-1881.

357. Khachik F, de Moura FF, Zhao DY, Aebischer CP, Bernstein PS. Transformations of selected carotenoids in plasma, liver, and ocular tissues of humans and in nonprimate animal models. Invest Ophthalmol Vis Sci 2002;43(11):3383-3392.

358. Krinsky NI, Landrum JT, Bone RA. Biologic mechanisms of the protective role of lutein and zeaxanthin in the eye. Annu Rev Nutr 2003;23:171-201.

359. Landrum JT, Bone RA. Lutein, zeaxanthin, and the macular pigment. Arch Biochem Biophys 2001;385(1):28-40.

360. Zhao DY, Wintch SW, Ermakov IV, Gellermann W, Bernstein PS. Resonance Raman measurement of macular carotenoids in retinal, choroidal, and macular dystrophies. Arch Ophthalmol 2003;121(7):967-972.

361. Bone RA, Landrum JT, Friedes LM et al. Distribution of lutein and zeaxanthin stereoisomers in the human retina. Exp Eye Res 1997;64(2):211-218.

362. Whitehead AJ, Mares JA, Danis RP. Macular pigment: a review of current knowledge. Arch Ophthalmol 2006;124(7):1038-1045.

363. Davies NP, Morland AB. Macular pigments: their characteristics and putative role. Prog Retin Eye Res 2004;23(5):533-559.

364. Trieschmann M, van Kuijk FJ, Alexander R et al. Macular pigment in the human retina: histological evaluation of localization and distribution. Eye (Lond) 2008;22(1):132-137.

365. Seddon JM, Ajani UA, Sperduto RD et al. Dietary carotenoids, vitamins A, C, and E, and advanced age-related macular degeneration. Eye Disease Case-Control Study Group. JAMA 1994;272(18):1413-1420.

366. Landrum JT, Bone RA, Joa H, Kilburn MD, Moore LL, Sprague KE. A one year study of the macular pigment: the effect of 140 days of a lutein supplement. Exp Eye Res 1997;65(1):57-62.

367. Mares-Perlman JA, Brady WE, Klein R et al. Serum antioxidants and age-related macular degeneration in a population-based case-control study. Arch Ophthalmol 1995;113(12):1518-1523.

368. Yamada E. Some structural features of the fovea centralis in the human retina. Arch Ophthalmol 1969;82(2):151-159.

369. Snodderly DM, Brown PK, Delori FC, Auran JD. The macular pigment. I. Absorbance spectra, localization, and discrimination from other yellow pigments in primate retinas. Invest Ophthalmol Vis Sci 1984;25(6):660-673.

370. Snodderly DM, Auran JD, Delori FC. The macular pigment. II. Spatial distribution in primate retinas. Invest Ophthalmol Vis Sci 1984;25(6):674-685.

371. Li B, Vachali P, Frederick JM, Bernstein PS. Identification of StARD3 as a lutein-binding protein in the macula of the primate retina. Biochemistry 2011;50(13):2541-2549.

372. Kato S, Ishita S, Sugawara K, Mawatari K. Cystine/glutamate antiporter expression in retinal Muller glial cells: implications for DL-alpha-aminoadipate toxicity. Neuroscience 1993;57(2):473-482.

373. Kato S, Sugawara K, Matsukawa T, Negishi K. Gliotoxic effects of alpha-aminoadipic acid isomers on the carp retina: a long term observation. Neuroscience 1990;36(1):145-153.

374. Zimmerman RP, Corfman TP. A comparison of the effects of isomers of alpha-aminoadipic acid and 2-amino-4-phosphonobutyric acid on the light response of the muller glial cell and the electroretinogram. Neuroscience 1984;12(1):77-84.

375. Pow DV. Visualising the activity of the cystine-glutamate antiporter in glial cells using antibodies to aminoadipic acid, a selectively transported substrate. Glia 2001;34(1):27-38.

376. Shen W, Zhang J, Chung SH, Hu Y, Ma Z, Gillies MC. Submacular DL-alpha-aminoadipic acid eradicates primate photoreceptors but does not affect luteal pigment or the retinal vasculature. Invest Ophthalmol Vis Sci 2011;52(1):119-127.

377. Li B, Vachali P, Bernstein PS. Human ocular carotenoid-binding proteins. Photochem Photobiol Sci 2010;9(11):1418-1425.

378. Horwitz J, Bova MP, Ding LL, Haley DA, Stewart PL. Lens alpha-crystallin: function and structure. Eye (Lond) 1999;13 (Pt 3b):403-408.

379. Khachik F, Beecher GR, Goli MB, Lusby WR, Smith JC, Jr. Separation and identification of carotenoids and their oxidation products in the extracts of human plasma. Anal Chem 1992;64(18):2111-2122.

380. Bhosale P, Li B, Sharifzadeh M et al. Purification and partial characterization of a lutein-binding protein from human retina. Biochemistry 2009;48(22):4798-4807.

381. Kaufman MH. Postcranial morphological features of homozygous tetraploid mouse embryos. J Anat 1992;180 (Pt 3):521-534.

382. MANN I. GEOGRAPHIC OPHTHALMOLOGY. A REVIEW OF THE POSSIBILITIES. Arch Ophthalmol 1964;72:632-636.

383. Hirashima M, Kobayashi T, Uchikawa M, Kondoh H, Araki M. Anteroventrally localized activity in the optic vesicle plays a crucial role in the optic development. Dev Biol 2008;317(2):620-631.

384. Kagiyama Y, Gotouda N, Sakagami K, Yasuda K, Mochii M, Araki M. Extraocular dorsal signal affects the developmental fate of the optic vesicle and patterns the optic neuroepithelium. Dev Growth Differ 2005;47(8):523-536.

385. Burmeister M, Novak J, Liang MY et al. Ocular retardation mouse caused by Chx10 homeobox null allele: impaired retinal progenitor proliferation and bipolar cell differentiation. Nat Genet 1996;12(4):376-384.

386. Nguyen M, Arnheiter H. Signaling and transcriptional regulation in early mammalian eye development: a link between FGF and MITF. Development 2000;127(16):3581-3591.

387. Green ES, Stubbs JL, Levine EM. Genetic rescue of cell number in a mouse model of microphthalmia: interactions between Chx10 and G1-phase cell cycle regulators. Development 2003;130(3):539-552.

388. Sigulinsky CL, Green ES, Clark AM, Levine EM. Vsx2/Chx10 ensures the correct timing and magnitude of Hedgehog signaling in the mouse retina. Dev Biol 2008;317(2):560-575.

389. Zuber ME, Gestri G, Viczian AS, Barsacchi G, Harris WA. Specification of the vertebrate eye by a network of eye field transcription factors. Development 2003;130(21):5155-5167.

390. Yun S, Saijoh Y, Hirokawa KE et al. Lhx2 links the intrinsic and extrinsic factors that control optic cup formation. Development 2009;136(23):3895-3906.

391. Bharti K, Nguyen MT, Skuntz S, Bertuzzi S, Arnheiter H. The other pigment cell: specification and development of the pigmented epithelium of the vertebrate eye. Pigment Cell Res 2006;19(5):380-394.

392. Martinez-Morales JR, Rodrigo I, Bovolenta P. Eye development: a view from the retina pigmented epithelium. Bioessays 2004;26(7):766-777.

393. Strauss O. The retinal pigment epithelium in visual function. Physiol Rev 2005;85(3):845-881.

394. Martinez-Morales JR, Signore M, Acampora D, Simeone A, Bovolenta P. Otx genes are required for tissue specification in the developing eye. Development 2001;128(11):2019-2030.

395. Martinez-Morales JR, Dolez V, Rodrigo I et al. OTX2 activates the molecular network underlying retina pigment epithelium differentiation. J Biol Chem 2003;278(24):21721-21731.

396. de IR, McAvoy JW. Spatio-temporal distribution of acidic and basic FGF indicates a role for FGF in rat lens morphogenesis. Dev Dyn 1993;198(3):190-202.

397. Pittack C, Grunwald GB, Reh TA. Fibroblast growth factors are necessary for neural retina but not pigmented epithelium differentiation in chick embryos. Development 1997;124(4):805-816.

398. Hyer J, Mima T, Mikawa T. FGF1 patterns the optic vesicle by directing the placement of the neural retina domain. Development 1998;125(5):869-877.

399. Martinez-Morales JR, Del BF, Nica G, Hammerschmidt M, Bovolenta P, Wittbrodt J. Differentiation of the vertebrate retina is coordinated by an FGF signaling center. Dev Cell 2005;8(4):565-574.

400. McCabe KL, Gunther EC, Reh TA. The development of the pattern of retinal ganglion cells in the chick retina: mechanisms that control differentiation. Development 1999;126(24):5713-5724.

401. Picker A, Brand M. Fgf signals from a novel signaling center determine axial patterning of the prospective neural retina. Development 2005;132(22):4951-4962.

402. Vinothkumar S, Rastegar S, Takamiya M, Ertzer R, Strahle U. Sequential and cooperative action of Fgfs and Shh in the zebrafish retina. Dev Biol 2008;314(1):200-214.

403. Cai Z, Feng GS, Zhang X. Temporal requirement of the protein tyrosine phosphatase Shp2 in establishing the neuronal fate in early retinal development. J Neurosci 2010;30(11):4110-4119.

404. Zhao S, Hung FC, Colvin JS et al. Patterning the optic neuroepithelium by FGF signaling and Ras activation. Development 2001;128(24):5051-5060.

405. Galy A, Neron B, Planque N, Saule S, Eychene A. Activated MAPK/ERK kinase (MEK-1) induces transdifferentiation of pigmented epithelium into neural retina. Dev Biol 2002;248(2):251-264.

406. Guillemot F, Cepko CL. Retinal fate and ganglion cell differentiation are potentiated by acidic FGF in an in vitro assay of early retinal development. Development 1992;114(3):743-754.

407. Mochii M, Mazaki Y, Mizuno N, Hayashi H, Eguchi G. Role of Mitf in differentiation and transdifferentiation of chicken pigmented epithelial cell. Dev Biol 1998;193(1):47-62.

408. Park CM, Hollenberg MJ. Basic fibroblast growth factor induces retinal regeneration in vivo. Dev Biol 1989;134(1):201-205.

409. Pittack C, Jones M, Reh TA. Basic fibroblast growth factor induces retinal pigment epithelium to generate neural retina in vitro. Development 1991;113(2):577-588.

410. Sakaguchi DS, Janick LM, Reh TA. Basic fibroblast growth factor (FGF-2) induced transdifferentiation of retinal pigment epithelium: generation of retinal neurons and glia. Dev Dyn 1997;209(4):387-398.

411. Vogel-Hopker A, Momose T, Rohrer H, Yasuda K, Ishihara L, Rapaport DH. Multiple functions of fibroblast growth factor-8 (FGF-8) in chick eye development. Mech Dev 2000;94(1-2):25-36.

412. Reh TA, Nagy T, Gretton H. Retinal pigmented epithelial cells induced to transdifferentiate to neurons by laminin. Nature 1987;330(6143):68-71.

413. Spence JR, Madhavan M, Aycinena JC, Del Rio-Tsonis K. Retina regeneration in the chick embryo is not induced by spontaneous Mitf downregulation but requires FGF/FGFR/MEK/Erk dependent upregulation of Pax6. Mol Vis 2007;13:57-65.

414. Vergara MN, Del Rio-Tsonis K. Retinal regeneration in the Xenopus laevis tadpole: a new model system. Mol Vis 2009;15:1000-1013.

415. Yoshii C, Ueda Y, Okamoto M, Araki M. Neural retinal regeneration in the anuran amphibian Xenopus laevis post-metamorphosis: transdifferentiation of retinal pigmented epithelium regenerates the neural retina. Dev Biol 2007;303(1):45-56.

416. Zhao S, Thornquist SC, Barnstable CJ. In vitro transdifferentiation of embryonic rat retinal pigment epithelium to neural retina. Brain Res 1995;677(2):300-310.

417. Horsford DJ, Nguyen MT, Sellar GC, Kothary R, Arnheiter H, McInnes RR. Chx10 repression of Mitf is required for the maintenance of mammalian neuroretinal identity. Development 2005;132(1):177-187.

418. Rowan S, Chen CM, Young TL, Fisher DE, Cepko CL. Transdifferentiation of the retina into pigmented cells in ocular retardation mice defines a new function of the homeodomain gene Chx10. Development 2004;131(20):5139-5152.

419. Bharti K, Liu W, Csermely T, Bertuzzi S, Arnheiter H. Alternative promoter use in eye development: the complex role and regulation of the transcription factor MITF. Development 2008;135(6):1169-1178.

420. Morcillo J, Martinez-Morales JR, Trousse F, Fermin Y, Sowden JC, Bovolenta P. Proper patterning of the optic fissure requires the sequential activity of BMP7 and SHH. Development 2006;133(16):3179-3190.

421. Cepko CL, Austin CP, Yang X, Alexiades M, Ezzeddine D. Cell fate determination in the vertebrate retina. Proc Natl Acad Sci U S A 1996;93(2):589-595.

422. Levine EM, Green ES. Cell-intrinsic regulators of proliferation in vertebrate retinal progenitors. Semin Cell Dev Biol 2004;15(1):63-74.

423. Walcott JC, Provis JM. Muller cells express the neuronal progenitor cell marker nestin in both differentiated and undifferentiated human foetal retina. Clin Experiment Ophthalmol 2003;31(3):246-249.

424. Rapaport DH, Rakic P, LaVail MM. Spatiotemporal gradients of cell genesis in the primate retina. Perspect Dev Neurobiol 1996;3(3):147-159.

425. Harman AM, Ferguson J. Morphology and birth dates of horizontal cells in the retina of a marsupial. J Comp Neurol 1994;340(3):392-404.

426. Harman AM, Snell LL, Beazley LD. Cell death in the inner and outer nuclear layers of the developing retina in the wallaby Setonix brachyurus (quokka). J Comp Neurol 1989;289(1):1-10.

427. Belliveau MJ, Young TL, Cepko CL. Late retinal progenitor cells show intrinsic limitations in the production of cell types and the kinetics of opsin synthesis. J Neurosci 2000;20(6):2247-2254.

428. Dutting D, Meyer SU. Transplantations of the chick eye anlage reveal an early determination of nasotemporal polarity. Int J Dev Biol 1995;39(6):921-931.

429. Dutting D, Thanos S. Early determination of nasal-temporal retinotopic specificity in the eye anlage of the chick embryo. Dev Biol 1995;167(1):263-281.

430. Matsuno T, Itasaki N, Ichijo H, Nakamura H. Retinotectal projection after partial ablation of chick optic vesicles. Neurosci Res 1992;15(1-2):96-101.

431. Simon H, Hornbruch A, Lumsden A. Independent assignment of antero-posterior and dorso-ventral positional values in the developing chick hindbrain. Curr Biol 1995;5(2):205-214.

432. Peters MA. Patterning the neural retina. Curr Opin Neurobiol 2002;12(1):43-48.

433. Chambon P. A decade of molecular biology of retinoic acid receptors. FASEB J 1996;10(9):940-954.

434. Mangelsdorf DJ, Evans RM. The RXR heterodimers and orphan receptors. Cell 1995;83(6):841-850.

435. Mori M, Ghyselinck NB, Chambon P, Mark M. Systematic immunolocalization of retinoid receptors in developing and adult mouse eyes. Invest Ophthalmol Vis Sci 2001;42(6):1312-1318.

436. Lohnes D, Kastner P, Dierich A, Mark M, LeMeur M, Chambon P. Function of retinoic acid receptor gamma in the mouse. Cell 1993;73(4):643-658.

437. Lufkin T, Lohnes D, Mark M et al. High postnatal lethality and testis degeneration in retinoic acid receptor alpha mutant mice. Proc Natl Acad Sci U S A 1993;90(15):7225-7229.

438. Iulianella A, Lohnes D. Contribution of retinoic acid receptor gamma to retinoid-induced craniofacial and axial defects. Dev Dyn 1997;209(1):92-104.

439. Lohnes D, Mark M, Mendelsohn C et al. Function of the retinoic acid receptors (RARs) during development (I). Craniofacial and skeletal abnormalities in RAR double mutants. Development 1994;120(10):2723-2748.

440. Hernandez RE, Putzke AP, Myers JP, Margaretha L, Moens CB. Cyp26 enzymes generate the retinoic acid response pattern necessary for hindbrain development. Development 2007;134(1):177-187.

441. Niederreither K, Vermot J, Schuhbaur B, Chambon P, Dolle P. Retinoic acid synthesis and hindbrain patterning in the mouse embryo. Development 2000;127(1):75-85.

442. White JC, Highland M, Clagett-Dame M. Abnormal development of the sinuatrial venous valve and posterior hindbrain may contribute to late fetal resorption of vitamin A-deficient rat embryos. Teratology 2000;62(6):374-384.

443. Begemann G, Schilling TF, Rauch GJ, Geisler R, Ingham PW. The zebrafish neckless mutation reveals a requirement for raldh2 in mesodermal signals that pattern the hindbrain. Development 2001;128(16):3081-3094.

444. Maves L, Kimmel CB. Dynamic and sequential patterning of the zebrafish posterior hindbrain by retinoic acid. Dev Biol 2005;285(2):593-605.

445. Molotkova N, Molotkov A, Sirbu IO, Duester G. Requirement of mesodermal retinoic acid generated by Raldh2 for posterior neural transformation. Mech Dev 2005;122(2):145-155.

446. Begemann G, Marx M, Mebus K, Meyer A, Bastmeyer M. Beyond the neckless phenotype: influence of reduced retinoic acid signaling on motor neuron development in the zebrafish hindbrain. Dev Biol 2004;271(1):119-129.

447. Gale E, Zile M, Maden M. Hindbrain respecification in the retinoid-deficient quail. Mech Dev 1999;89(1-2):43-54.

448. Maden M, Gale E, Kostetskii I, Zile M. Vitamin A-deficient quail embryos have half a hindbrain and other neural defects. Curr Biol 1996;6(4):417-426.

449. Dupe V, Lumsden A. Hindbrain patterning involves graded responses to retinoic acid signalling. Development 2001;128(12):2199-2208.

450. Durston AJ, Timmermans JP, Hage WJ et al. Retinoic acid causes an anteroposterior transformation in the developing central nervous system. Nature 1989;340(6229):140-144.

451. Sive HL, Draper BW, Harland RM, Weintraub H. Identification of a retinoic acid-sensitive period during primary axis formation in Xenopus laevis. Genes Dev 1990;4(6):932-942.

452. Marshall H, Nonchev S, Sham MH, Muchamore I, Lumsden A, Krumlauf R. Retinoic acid alters hindbrain Hox code and induces transformation of rhombomeres 2/3 into a 4/5 identity. Nature 1992;360(6406):737-741.

453. Godsave SF, Koster CH, Getahun A et al. Graded retinoid responses in the developing hindbrain. Dev Dyn 1998;213(1):39-49.

454. Abu-Abed S, Dolle P, Metzger D, Beckett B, Chambon P, Petkovich M. The retinoic acid-metabolizing enzyme, CYP26A1, is essential for normal hindbrain patterning, vertebral identity, and development of posterior structures. Genes Dev 2001;15(2):226-240.

455. Sakai Y, Meno C, Fujii H et al. The retinoic acid-inactivating enzyme CYP26 is essential for establishing an uneven distribution of retinoic acid along the anterio-posterior axis within the mouse embryo. Genes Dev 2001;15(2):213-225.

456. Emoto Y, Wada H, Okamoto H, Kudo A, Imai Y. Retinoic acid-metabolizing enzyme Cyp26a1 is essential for determining territories of hindbrain and spinal cord in zebrafish. Dev Biol 2005;278(2):415-427.

457. Maden M, Ong DE, Summerbell D, Chytil F. Spatial distribution of cellular protein binding to retinoic acid in the chick limb bud. Nature 1988;335(6192):733-735.

458. Boylan JF, Gudas LJ. Overexpression of the cellular retinoic acid binding protein-I (CRABP-I) results in a reduction in differentiation-specific gene expression in F9 teratocarcinoma cells. J Cell Biol 1991;112(5):965-979.

459. Fiorella PD, Napoli JL. Expression of cellular retinoic acid binding protein (CRABP) in Escherichia coli. Characterization and evidence that holo-CRABP is a substrate in retinoic acid metabolism. J Biol Chem 1991;266(25):16572-16579.

460. Balkan W, Colbert M, Bock C, Linney E. Transgenic indicator mice for studying activated retinoic acid receptors during development. Proc Natl Acad Sci U S A 1992;89(8):3347-3351.

461. Enwright JF, III, Grainger RM. Altered retinoid signaling in the heads of small eye mouse embryos. Dev Biol 2000;221(1):10-22.

462. McCaffery P, Drager UC. Retinoic acid synthesis in the developing retina. Adv Exp Med Biol 1993;328:181-190.

463. Rossant J, Zirngibl R, Cado D, Shago M, Giguere V. Expression of a retinoic acid response element-hsplacZ transgene defines specific domains of transcriptional activity during mouse embryogenesis. Genes Dev 1991;5(8):1333-1344.

464. Perz-Edwards A, Hardison NL, Linney E. Retinoic acid-mediated gene expression in transgenic reporter zebrafish. Dev Biol 2001;229(1):89-101.

465. Fan X, Molotkov A, Manabe S et al. Targeted disruption of Aldh1a1 (Raldh1) provides evidence for a complex mechanism of retinoic acid synthesis in the developing retina. Mol Cell Biol 2003;23(13):4637-4648.

466. Sandell LL, Sanderson BW, Moiseyev G et al. RDH10 is essential for synthesis of embryonic retinoic acid and is required for limb, craniofacial, and organ development. Genes Dev 2007;21(9):1113-1124.

467. Molotkov A, Molotkova N, Duester G. Retinoic acid guides eye morphogenetic movements via paracrine signaling but is unnecessary for retinal dorsoventral patterning. Development 2006;133(10):1901-1910.

468. Gage PJ, Suh H, Camper SA. Dosage requirement of Pitx2 for development of multiple organs. Development 1999;126(20):4643-4651.

469. Gage PJ, Zacharias AL. Signaling "cross-talk" is integrated by transcription factors in the development of the anterior segment in the eye. Dev Dyn 2009;238(9):2149-2162.

470. Matt N, Dupe V, Garnier JM et al. Retinoic acid-dependent eye morphogenesis is orchestrated by neural crest cells. Development 2005;132(21):4789-4800.

471. McCaffery P, Lee MO, Wagner MA, Sladek NE, Drager UC. Asymmetrical retinoic acid synthesis in the dorsoventral axis of the retina. Development 1992;115(2):371-382.

472. Marsh-Armstrong N, McCaffery P, Gilbert W, Dowling JE, Drager UC. Retinoic acid is necessary for development of the ventral retina in zebrafish. Proc Natl Acad Sci U S A 1994;91(15):7286-7290.

473. Mey J, McCaffery P, Drager UC. Retinoic acid synthesis in the developing chick retina. J Neurosci 1997;17(19):7441-7449.

474. Sakai Y, Luo T, McCaffery P, Hamada H, Drager UC. CYP26A1 and CYP26C1 cooperate in degrading retinoic acid within the equatorial retina during later eye development. Dev Biol 2004;276(1):143-157.

475. Wagner E, McCaffery P, Drager UC. Retinoic acid in the formation of the dorsoventral retina and its central projections. Dev Biol 2000;222(2):460-470.

476. Hendrickson AE, Yuodelis C. The morphological development of the human fovea. Ophthalmology 1984;91(6):603-612.

477. Bach, Seefelder. ATLAS ZUR ENTWICKLUNGSGESCHICHTE DES MENSCHLICHEN AUGES. Leipzig: Verlang von Wilhelm Engelmann; 1911.

478. O'Brien KM, Schulte D, Hendrickson AE. Expression of photoreceptor-associated molecules during human fetal eye development. Mol Vis 2003;9:401-409.

479. Georges P, Madigan MC, Provis JM. Apoptosis during development of the human retina: relationship to foveal development and retinal synaptogenesis. J Comp Neurol 1999;413(2):198-208.

480. Okada M, Erickson A, Hendrickson A. Light and electron microscopic analysis of synaptic development in Macaca monkey retina as detected by immunocytochemical labeling for the synaptic vesicle protein, SV2. J Comp Neurol 1994;339(4):535-558.

481. Crooks J, Okada M, Hendrickson AE. Quantitative analysis of synaptogenesis in the inner plexiform layer of macaque monkey fovea. J Comp Neurol 1995;360(2):349-362.

482. Linberg KA, Fisher SK. A burst of differentiation in the outer posterior retina of the eleven-week human fetus: an ultrastructural study. Vis Neurosci 1990;5(1):43-60.

483. van DD, Provis JM, Billson FA. Early differentiation of ganglion, amacrine, bipolar, and Muller cells in the developing fovea of human retina. J Comp Neurol 1990;291(2):203-219.

484. Nishimura Y, Rakic P. Synaptogenesis in the primate retina proceeds from the ganglion cells towards the photoreceptors. Neurosci Res Suppl 1987;6:S253-S268.

485. Provis JM, van DD. Retinal development in humans: the roles of differential growth rates, cell migration and naturally occurring cell death. Aust N Z J Ophthalmol 1985;13(2):125-133.

486. La Vail MM, Rapaport DH, Rakic P. Cytogenesis in the monkey retina. J Comp Neurol 1991;309(1):86-114.

487. Peirson SN, Butler JN, Foster RG. Experimental validation of novel and conventional approaches to quantitative real-time PCR data analysis. Nucleic Acids Res 2003;31(14):e73.

488. Poche RA, Furuta Y, Chaboissier MC, Schedl A, Behringer RR. Sox9 is expressed in mouse multipotent retinal progenitor cells and functions in Muller glial cell development. J Comp Neurol 2008;510(3):237-250.

489. Duester G. Retinoic acid synthesis and signaling during early organogenesis. Cell 2008;134(6):921-931.

490. Golz S, Muhleisen T, Schulte D, Mey J. Regulation of RALDH-1, RALDH-3 and CYP26A1 by transcription factors cVax/Vax2 and Tbx5 in the embryonic chick retina. Int J Dev Neurosci 2008;26(5):435-445.

491. Schulte D, Peters MA, Sen J, Cepko CL. The rod photoreceptor pattern is set at the optic vesicle stage and requires spatially restricted cVax expression. J Neurosci 2005;25(11):2823-2831.

492. Alfano G, Conte I, Caramico T et al. Vax2 regulates retinoic acid distribution and cone opsin expression in the vertebrate eye. Development 2011;138(2):261-271.

493. Deeb SS, Liu Y, Hayashi T. Mutually exclusive expression of the L and M pigment genes in the human retinoblastoma cell line WERI: Resetting by cell division. Vis Neurosci 2006;23(3-4):371-378.

494. Fukami M, Nishimura G, Homma K et al. Cytochrome P450 oxidoreductase deficiency: identification and characterization of biallelic mutations and genotype-phenotype correlations in 35 Japanese patients. J Clin Endocrinol Metab 2009;94(5):1723-1731.

495. Liu H, Etter P, Hayes S et al. NeuroD1 regulates expression of thyroid hormone receptor 2 and cone opsins in the developing mouse retina. J Neurosci 2008;28(3):749-756.

496. Ng L, Hurley JB, Dierks B et al. A thyroid hormone receptor that is required for the development of green cone photoreceptors. Nat Genet 2001;27(1):94-98.

497. Raine JC, Hawryshyn CW. Changes in thyroid hormone reception precede SWS1 opsin downregulation in trout retina. J Exp Biol 2009;212(17):2781-2788.

498. Roberts MR, Hendrickson A, McGuire CR, Reh TA. Retinoid X receptor (gamma) is necessary to establish the S-opsin gradient in cone photoreceptors of the developing mouse retina. Invest Ophthalmol Vis Sci 2005;46(8):2897-2904.

499. Srinivas M, Ng L, Liu H, Jia L, Forrest D. Activation of the blue opsin gene in cone photoreceptor development by retinoid-related orphan receptor beta. Mol Endocrinol 2006;20(8):1728-1741.

500. Veldhoen K, Allison WT, Veldhoen N, Anholt BR, Helbing CC, Hawryshyn CW. Spatio-temporal characterization of retinal opsin gene expression during thyroid hormone-induced and natural development of rainbow trout. Vis Neurosci 2006;23(2):169-179.

501. Kelley MW, Turner JK, Reh TA. Retinoic acid promotes differentiation of photoreceptors in vitro. Development 1994;120(8):2091-2102.

502. Stenkamp DL, Adler R. Cell-type- and developmental-stage-specific metabolism and storage of retinoids by embryonic chick retinal cells in culture. Exp Eye Res 1994;58(6):675-687.

503. Kelley MW, Williams RC, Turner JK, Creech-Kraft JM, Reh TA. Retinoic acid promotes rod photoreceptor differentiation in rat retina in vivo. Neuroreport 1999;10(11):2389-2394.

504. Osakada F, Ikeda H, Mandai M et al. Toward the generation of rod and cone photoreceptors from mouse, monkey and human embryonic stem cells. Nat Biotechnol 2008;26(2):215-224.

505. Stevens CB, Cameron DA, Stenkamp DL. Plasticity of photoreceptor-generating retinal progenitors revealed by prolonged retinoic acid exposure. BMC Dev Biol 2011;11(1):51.